# GROUNDWATER STUDY FOR THE REGIONAL GRANADA AQUIFER SYSTEM

## (SOUTHERN SPAIN)
## HYDROCHEMISTRY AND ISOTOPE STUDY

**-DIPLOMA THESIS-**
**-Diplomarbeit-**

# STRUCTURAL AND SEDIMENTOLOGICAL ASPECTS OF BASIN DEPOSITS

**-GEOLOGICAL MAPPING-**
**-Diplomkartierung-**

**Submitted to:**
**Freie Universität Berlin (FUB)**
**Prof. Dr. A. Pekdeger**

**Submitted by:**
**Christoph Sprenger**

**Berlin, May 2006**

# Acknowledgements

## Zusammenfassung (German summary)

Ziel dieser Diplomarbeit ist Herkunft und Fliesswege des Grundwassers zu untersuchen, das in der Nähe von *Granada* (Südspanien) in einem alluvialen Grundwasserleiter (*Vega de Granada*) eines intramontanen Beckens am Fuß der *Sierra Nevada* angetroffen wird. Fragen zur höhenabhängigen Grundwasserneubildung und Herkunftsräume des Grundwassers in der *Vega de Granada* standen dabei im Vordergrund. Weitere Fragen zur Rolle von lateralen und unterirdischen Zuflüssen waren hierfür zu stellen. Dies erforderte eine Anwendung von hydrogeologischer, hydrochemischer und isotopenhydrogeologischer Methoden.

Das Arbeitsgebiet umfaßt weite Teile des Beckens von Granada sowie im wesentlichen die im Osten liegenden *Sierras*, und kann unterteilt werden in einem metamorphen Kernbereich der *Sierra Nevada* (*Nevado-Filabride*), einem karbonatischen Komplex (*Alpujarride*) und die Sedimente des intramontanen Beckens von *Granada* (S.2). Das Arbeitsgebiet in Südspanien ist als semi-arid zu bezeichnen und durch ein mediterranes Klima gekennzeichnet. Im intramontanen Becken von Granada zeigt eine Analyse der vorhandenen Klimadaten daß aufgrund der hohen Temperaturen während der Sommerzeit (Mai – September) der größte Teil der Niederschläge direkt verdunstet oder durch Pflanzenaktivitäten nicht dem Grundwasser zugeführt wird. Während des Winters (Oktober – April) kann in der *Vega de Granada* nur mit einer geringen Grundwasserneubildungsrate gerechnet werden. Wohingegen in der *Sierra Nevada* mit einer ganzjährigen Grundwasserneubildung gerechnet werden kann und dieses Gebiet als Hauptlieferant für die *Vega de Granada* gilt (S.8f).

Im Rahmen dieser Arbeit wurden über 200 Proben von Niederschlag, Oberflächengewässer, Quellen oder Brunnen über einem Zeitraum von einem Jahr (Februar 2004 – März 2005) genommen und ausgewertet. Die Auswertung erfolgte anhand hydrochemischer und isotopengeochemischer Analysen und der im Feld gemessenen Parameter.

Anhand der Hauptelementchemie wurden die Regen-, Oberflächen- und Grundwasserproben in vier Gruppen unterteilt. Zusätzlich wurden Sättigungsindizes (SI) mit PHREEQC 2.11 bezüglich Kalzit, Dolomit, Gips und Anhydrit berechnet und ausgewertet (S.29ff):
• Gering mineralisierte Proben (EC < 100 µS/cm) der Regenereignisse und einem kleinen Bach (*Arroyo*) aus der *Sierra Nevada* sind in der ersten Gruppe zusammengefaßt.
• In der zweiten Gruppe befinden sich Ca-Mg-$HCO_3$- oder Mg-Ca-$HCO_3$ - Wässer aus den Bereichen der *Alpujarride* Sequenz, in denen Kalkgestein ansteht und gute Neubildungsbedingungen bietet. Die wechselnde Dominanz von Ca oder Mg ist charakteristisch für den *Alpujarride* Karst und wird auf veränderliche Anteile von Kalzit und Dolomitgestein zurückgeführt. Die Berechnungen der SI bezogen auf Kalzit und Dolomit zeigen, daß die Proben dieser Gruppe untersättigt oder nahe am Sättigungsgleichgewicht sind.
• Das Grundwasser in den alluvialen Kiesen und Sanden der *Vega de Granada* bildet die dritte Gruppe und zeichnet sich durch eine erhöhte Mineralisierung und eine Dominanz von Ca und

SO$_4$ bei hohen Hydrogenkarbonat-Gehalten aus. Hier wurden Übersättigungen anhand der SI in Bezug auf Kalzit und Dolomit festgestellt.

• Die vierte Gruppe bilden Thermalwässer mit Wassertemperaturen >20°C. Diese wurden anhand der Hauptelementchemie in zwei Untergruppen unterteilt. Die erste Untergruppe ist aufgrund der geringeren Mineralisation und Temperatur eher vom flachen Grundwasserstrom beeinflußt und zeigt eine geochemische Signatur ähnlich der der *Alpujarride* Sequenz ist aber zusätzlich durch erhöhte SO$_4$. Konzentrationen gekennzeichnet. Die zweite Untergruppe zeichnet sich durch eine höhere Mineralisierung und ein ausgeglichenes Verhältnis von Erdalkalien und Alkalien bei hohen Hydrogenkarbonat-Gehalten aus. Die Thermal Quellen dieser Untergruppe sind an einer Störungszone orientiert, welche die Interne Zone von der Externen Zone der Betischen Kordillere trennt.

Eine Analyse des Kalk – Kohlensäure Gleichgewichts in den Proben der Quellen und Brunnen zeigte, das Lösung von Kalzit in einem offenen System unter konstanten CO$_2$ Partialdruck Bedingungen stattfindet. Es konnte gezeigt werden, daß die gelöste Kohlensäure in den Proben der Quellen im Austausch mit atmosphärischen CO$_2$ oder durch erhöhten CO$_2$ Partialdruck in Bereichen verstärkter Bodengenese zustande gekommen ist (S.38f).

Aufgrund der sehr unterschiedlichen Probentypen (Regen, Schnee, Quellen, Thermalquellen, Brunnen und Oberflächenwasser) und des ganzjährigen Probennamezeitraumes (Februar 2004 – März 2005) zeigten die Signaturen der stabilen Isotope des Wassers ($\delta^{18}$O, $\delta$D) eine große Spannweite. Diese Spannweite reichte von extrem abgereicherten, frischen Winterschnee Proben bis hin zu extrem angereicherten Proben aus kleinen abflußlosen Verdunstungs-Becken in den Höhenlagen (> 2200 m.ü.NN) der *Sierra Nevada* (S.39f).

Die im Rahmen dieser Arbeit genommenen Regenproben (n=11) wurden dazu benutzt fundamentale Prozesse der Niederschlagsbildung anhand der stabilen Isotope nachzuvollziehen. Es konnten dabei Mengen-, Temperatur- und Höheneffekte nachgewiesen werde. Jedoch reichte die Probenanzahl bei weitem nicht aus um eine aussagekräftige Lokale Meteorische Wasser Linie (LMWL) oder um lokale Höhengradienten zu berechnen. Aus diesem Grund wurden Niederschlagsmuster aus dem IAEA-GNIP Datenbestand von der Station *Gibraltar* und 1,5 Jahres Zeitreihen aus einer Doktorarbeit (GARRIDO 2003) für *Granada* studiert. Aus diesen Daten konnte eine lokale höhenabhängige Verteilung der Niederschläge berechnet werden und somit konnten mittlere Neubildungshöhen für Quellen und Brunnen abgeleitet werden. Dabei wurden aufgrund der unterschiedlichen räumlichen Verteilungsmuster der Niederschläge unterschiedliche Höhengradienten berechnet. Des Weiteren konnte nachgewiesen werden dass aufgrund der deutlichen Verschiebung zwischen der mittleren gewichteten Isotopen-Zusammensetzung des Niederschlages und des Grundwassers die Neubildung hauptsächlich in den Wintermonaten stattfindet (S.41ff).

Im Rahmen dieser Arbeit wurden über 70 Proben aus Höhenlagen > 2200 m.ü.NN in der *Sierra Nevada* genommen und ausgewertet. Die Ergebnisse der Analyse der Schnee, Schneeschmelz und *Laguna* (kleine Becken in der *Sierra Nevada*) -Proben können wie folgt zusammengefaßt werden (S.45ff):

• *Laguna* (n=39) -Proben zeigen eine extreme Anreicherung, die einer für offene Wasserflächen typischen Verdunstungslinie folgen. Aufgrund der niedrigen Temperaturen (~5 ℃) und der niedrigen Luftfeuchtigkeiten (~30 %) in diesen Höhenlagen, war es möglich für kleine abflußlose Becken ohne konstanten Zufluß maximale Verdunstungsverluste von ~51 % zu berechnen.

• Schnee (n=11) Proben konnten aufgrund ihrer Position auf der Meteorischen Wasser Linie (MWL) in frischen Schnee und bereits alterierten Schnee unterteilt werden. Die frischen Schnee Proben sind bis zu 10 ‰ abgereicherter an $^{18}$O als bereits alterierter Schnee. Die Alteration scheint entlang der MWL zu verlaufen.

• Schneeschmelz (n=25) Proben liegen oft nahe bei der WMMWL (West Mediterrane MWL) und zeigen einen schwachen Verdunstungs-Trend unter hohen Luftfeuchte Bedingungen an. Die Steigung der Verdunstungslinie ist charakteristisch für einen erhöhten Einfluß von Gleichgewichts Bedingungen während der Fraktionierung.

Die im Rahmen dieser Arbeit beprobten Quellen konnten aufgrund der isotopenchemischen Signaturen mittleren Grundwasserneubildungshöhen zugewiesen werden. Aufgrund unterschiedlicher räumlicher Verteilungsmuster der Niederschläge im Arbeitsgebiet mußte zwischen Grundwasserneubildungsgebieten aus der *Sierra Nevada* und Neubildungsgebieten aus der *Sierra de la Peza* unterschieden werden. Es wurde oft festgestellt, daß je tiefer sich eine Quelle befindet, desto höher die Grundwasserneubildung stattfinden muß. Vertikale Unterschiede zwischen den realen Höhen der Quellen und den berechneten mittleren Grundwasserneubildungshöhen von 300–1300 m wurden festgestellt. Anhand von drei schematischen Profilschnitten wurden die räumlichen Fliesspfade von Quellen in der *Sierra Nevada* und der *Sierra de la Peza* aufgezeigt (S.49f, S.58ff).

Die im Rahmen dieser Arbeit beprobten Vorfluter konnten aufgrund fehlender Abflußdaten nicht auf Volumen-Gewichtete δ-Werte normiert werden. Die Proben des *Rio Genil* zeigten an der höchsten Probennamestelle saisonale Variationen und deuten den hohen Einfluß von Oberflächenabfluß innerhalb des *Nevado-Filabride* Komplexes an. Proben aus dem Stausee (*Embalse de Canales*) des *Genil* und direkt am Abfluß des Stausees waren sehr ähnlich und wurden im Beobachtungszeitraum sukzessive schwerer. Dieser Trend reflektiert den sinkenden Wasserstand des Stausees bei einem geringen Zufluß. Anhand der Proben des Stausees *Embalse de Canales* konnte keine eindeutige Verdunstungs-Anreicherung nachgewiesen werden. Proben aus dem Stausee *Embalse de Quentar* aus unterschiedlichen Wassertiefen (2, 5, 10 m) lagen innerhalb des Meßfehlers und erlaubten daher keine Interpretation. Der Einfluß von Bewässerung und anderen anthropogenen Faktoren machte sich im Unterlauf des *Genil* in Form von einer Auslöschung von saisonalen Variationen bemerkbar. Der *Genil* fließt in die *Vega de Granada* mit einen durchschnittlichen δ$^{18}$O Wert von -8.3 ‰ und verlässt die Vega mit einem δ$^{18}$O Wert von -

7.3 ‰. Während des Verlaufes des *Genils* durch die *Vega de Granada* verändert sich das hydraulische Fließverhalten von influenten (wasserverlierender Fluß) zu effluenten (wasseraufnehmeder Fluß) Verhältnissen. Das bedeutet das der *Genil* beim Verlassen der *Vega de Granada* das hydrochemische wie auch isotopenchemische Signal des Grundwassers trägt. Während des Beobachtungszeitraumes zeigte der Zufluss des *Rio Darro* zur *Vega de Granada* ein um 0.2 ‰ schwereres Signal als der *Genil* und spiegelt damit das kleinere und durch niedrigere mittlere Höhen gekennzeichnete Einzugsgebiet wieder. Die mittlere isotopenchemische Signatur des *Darro* am Zufluß zur *Vega de Granada* war signifikant angereicherter an schweren Isotopen als das Grundwasser in der *Vega de Granada*. Dadurch spiegelt sich der geringe Einfluß des *Darro* auf die Grundwasserneubildung durch Flußbett-Infiltration wieder. Die mittlere isotopenchemische Signatur des *Genil* am Zufluß zur *Vega de Granada* war der Zusammensetzung des Grundwassers der *Vega de Granada* sehr ähnlich. Dadurch spiegelt sich der große Einfluß des *Genil* auf die Grundwasserneubildung durch Flußbett-Infiltration wieder. Zuflüsse aus dem im Norden der *Vega de Granada* liegenden und weite Teile der *Sierra Arana* umfassenden Einzugsgebiet des *Rio Cubillas* wurden an drei Stellen einmalig beprobt und zeigten das der Stausee des *Cubillas* (*Embalse de Cubillas*) eine deutliche Verdunstungssignatur trägt. Diese Signatur wird durch den *Cubillas* in die *Vega de Granada* übertragen und dann durch Mischungsprozesse des angereicherten Flußwassers mit dem abgereicherten Grundwasser abgeschwächt. Weitere Oberflächenzuflüsse aus diesem nördlichen Bereich wurden nicht bestimmt und könnten Gegenstand weiterer Studien sein (S.53ff).

Die räumliche Verteilung der stabilen Isotope in Brunnen Proben aus der *Vega de Granada* zeigt deutlich daß im süd-östlichen Bereich die Werte am negativsten sind. In diesem Bereich kann daher mit einem starken lateralen Zustrom von Grundwasser aus den angrenzenden *Sierras* oder mit einer Grundwasserneubildung durch die lokale Vorflut (*Dilar*, *Monachil*, *Genil*) gerechnet werden. Nach Westen hin zeigen die Isotopen eine starke Anreicherung infolge von Verdunstung an. Maximale Verdunstungsverluste konnten anhand der Regressionslinie und den klimatische Rahmenbedingungen in den Proben mit ~20 % berechnet werden. Wasser-Gesteins Wechselwirkungen in der *Vega de Granada* konnte nicht ausgeschlossen werden. Dies könnte Gegenstand weiterer Untersuchungen sein. Des Weiteren zeigte sich daß die *Sierra Elvira* als Grundwasserneubildungsgebiet einem starken Einfluß auf die *Vega de Granada* hat. Brunnen die im südlich der *Sierra Elvira* angrenzenden Bereich liegen zeigten eine abgereicherte isotopenchemische Signatur die einer mittleren Neubildungshöhe von etwa 1500 m.ü.N.N. entsprechen würde. Eine der größten Quellen innerhalb der *Vega de Granada* (*Manantial de la Reina*) mit Schüttungen von etwa 12.000 l/min zeigte ein isotopenchemisches Signal ähnlich zu denen im Norden gelegenen Brunnen und konnte deshalb der *Sierra Elvira* als Neubildungsgebiet zugewiesen werden (S.63ff).

Die Isotopen Signaturen der Thermal Quellen zeigte eine deutliche Abweichung der δ-Werte von der WMMWL. Diese Abweichungen wurden als Wasser-Gesteins Wechselbeziehungen gedeutet. Wie bereits die Betrachtung der Hydrochemie zeigte, konnten die Proben der Thermal Wässer

auch anhand der isotopenchemischen Signaturen in zwei Untergruppen unterteilt werden. Die erste Untergruppe (*Fte.Urquiza*) liegt dabei näher an der WMMWL und zeigt nur geringe Wasser-Gesteins Wechselwirkungen. Die zweite Untergruppe ist stärker alteriert und die Abweichungen der $\delta^{18}$O Werte von der WMMWL liegen bei maximal $\Delta0.5$ ‰ (S.66f).

## Summary

Aim of this thesis (Diplomarbeit) is the investigation of the origin and the flow pattern of groundwater which is found in an alluvial aquifer (*Vega de Granada*) at the foot of the *Sierra Nevada* (southern Spain). Open questions considering altitudes and areas of recharge from the *Vega de Granada* groundwater have been the main task. Furthermore, questions concerning lateral and subsurface groundwater flow were considered. Several hydrogeological, hydrochemical and isotope-hydrochemical methods have been applied to cope with this task.

The study area comprises vast parts of the *Granada* basin and the adjacent *Sierras* in the east. Geologically, the area can be divided into a metamorphic core (*Nevado-Filabride*), a carbonate domain (*Alpujarride*) and the sediments of the intramontaineous basin. As shown by analysis of climate data, the study area in southern Spain is considered to be semi-arid with a mediteranean climate. Due to high temperatures in summer (May-September) most of the precipitation evaporates or is transpired by plants. During winter (October - April) only little to no groundwater recharge in the *Vega de Granada* is expected to occur. The main groundwater recharge area is the *Sierra Nevada* with preferential formation of groundwater during winter.

Within this study more than 200 samples of precipitation (rain, snow), surface water (river, reservoir) and groundwater (springs, wells) over the monitoring time from February 04 to March 05 were taken and analysed. The analysis was made according to the measured hydrochemical and isotopechemical parameters and the in-field measured data.

Four hydrochemical groups can be classified according to the composition of the major constituents. Additionally, saturation indices (SI) were calculated with the software PHREEQC 2.11 in respect to calcite, dolomite, anhydrite and gypsum.
• Low mineralized samples (EC < 100 µS/cm) from precipitation and small streams (*Arroyo*) in the *Sierra Nevada* are summarized in group one.
• Water type of Ca-Mg-HCO$_3$- and Mg-Ca-HCO$_3$ is found in the *Alpujarride* domain, where limestone gives good recharge conditions. Characteristic for this carbonate terrain with dolomite and calcite host-rocks is the changing dominance of Ca and Mg. Calculation of SI of this group show that samples are close to or in equilibrium with calcite and dolomite.
• Groundwater from the alluvial gravel and sands (*Vega de Granada*) is highly mineralized and dominated by Ca and SO$_4$ with high content of hydrogen. In this group oversaturation with respect to calcite and dolomite was observed.

• Thermal water (>20 ˚C) samples were subdivided into two groups. The first subgroup is according to their low mineralization and temperature considered to be influenced by shallow groundwater. The hydrochemical signature is similar to those in the *Alpujarride* domain but is additional characterized by an increased content in hydrogencarbonate. The second subgroup is characterized by increased mineralization and a balanced relation of earthalkalis and alkalis at high hydrogencarbonate content. Thermal springs of this subgroup are associated with a deep-reaching fault zone between the Internal and the External Zone.

The investigation of the carbonate chemistry showed that calcite solution evolves under open-system conditions. Initial $CO_2$ pressures range from atmospheric derived ($pCO_2$ = -3) to increased $CO_2$ content derived from soil air ($pCO_2$ = -2) (p.38).

On the basis of the wide range in sampling types (rain, snow, springs, thermal springs, wells and surface water) and the time of monitoring (February 2004 – March 2005) the signatures of stable isotopes ($\delta^{18}O$, $\delta D$) show a divers range, from depleted winter snow samples ($\delta^{18}O$ = -10 ‰) to enriched and even positive ($\delta^{18}O$ = +3 ‰) samples from small endorheic basins at altitudes >2200 masl in the *Sierra Nevada* (p.39).

Stable isotopes in rain samples were used to examine fundamental processes of rain formation, like amount-, temperature- and altitude effect. Unfortunately, the amount of rain samples was not sufficient for establishing local altitude gradients. Therefore, the pattern in precipitation was studied in samples from the IAEA-GNIP database and from 1.5 year time series from *Granada* (GARRIDO 2003). According to this datasets local altitude gradients were constructed and therefore it was possible to associate groundwater to mean recharge altitudes. Since the *Sierra Nevada* springs and the *Sierra de la Peza springs* are located on different orographic divides of the Betic Cordillera, a spatial shift in $\delta^{18}O$ values is expected to occur. This shift is expressed by different $\delta^{18}O$ / altitude relationship. Furthermore, it was shown that, according to the shift between the mean weighted isotope signature in rain and the mean groundwater composition, recharge will take place mainly during the winter months (p.41).

More than 70 samples taken at altitudes >2200 masl in the *Sierra Nevada* were taken and analysed. The main characteristics of local snow, snowmelt or *laguna* (small basins in the *Sierra Nevada*) samples can be described as:
• *Laguna* (n=39) samples are often enriched in $\delta^{18}O$ following an evaporation trend which is characteristic for open water bodies. According to the low temperature (~ 5 ºC) and the low humidity (~ 30 %) conditions at these altitudes, a maximum evaporative loss of 51 % in small endorheic basins was calculated.
• Snow (n=11) samples can be subdivided in fresh snow and alterated snow according to their position on the MWLs. Fresh snow is depleted up to 10 ‰ in $\delta^{18}O$ compared to snowmelt. The alteration seems to follow the MWL.

• Snowmelt samples are located near to the WMMWL following an evaporative enrichment under high humidity conditions. The slope of the regression line is characteristic for evaporation under increased equilibrium conditions during evaporation (p.49, p.58).

Within the scope of this work isotope signatures of springs were associated to average groundwater recharge altitudes. According to a changing spatial distribution in precipitation it was necessary to distinguish between the *Sierra Nevada* and the *Sierra de la Peza* groundwater recharge areas. It was recognized that the lower the spring is situated, the higher the recharge area is. Vertical discrepancy between actual altitude and estimated recharge altitude (vertical distance) was estimated between 300 – 1300 m. Local groundwater flow was visualized by three isotope cross-sections for the *Sierra Nevada* and the *Sierra de la Peza* (p.49, p.58).

Since no discharge values of rivers were available, it was not possible to calculate volume weighted river values. Samples from the *Emb.de Quentar* were taken from various depths below surface (2, 5, 10 m) and were within the precision in measurement. Therefore no further interpretation was allowed. Seasonal variations in the samples of the highest site from the *Rio Genil* were observed. This indicates the strong influence of surface run-off in the metamorphic *Nevado-Filabride* complex. Samples from the reservoir (*Emb.de Canales*) of the *Genil* and samples from the discharge of this reservoir were very similar and became progressively depleted. This trend reflects the decreasing water table of the reservoir without significant inflow. No evaporation trend was observed in samples from the *Emb.de Canales*. The influence of irrigation and other anthropogenic impacts were observed in the underflow of the *Rio Genil* by attenuated seasonal isotope signatures. The *Rio Genil* is at the inflow to the *Vega de Granada* with $\delta^{18}O$ = -8.3 ‰ one per mill lighter than at the outflow with -7.3 ‰. The hydraulic regime in the *Vega de Granada* changes from influent (losing river) at the inflow of the *Rio Genil* to effluent (gaining river) at its outflow. Thus, the *Genil* carries at the outflow of the *Vega de Granada* the hydrochemical and the isotope signature of the groundwater. The *Rio Darro* showed at the inflow to the *Vega de Granada*, during the time of monitoring, an isotope signature which was 0.2 ‰ heavier than the signature from the *Genil*. This reflects the smaller and the lower mean altitude of the *Rio Darro* catchment area. The mean isotope signature of the *Rio Darro* at the inflow to the *Vega de Granada* was significant enriched compared to the groundwater of the *Vega de Granada*. This is interpreted as a minor influence of the *Darro* for GWR through indirect infiltration. Controversy, the mean isotope signature of the *Rio Genil* at the inflow to the *Vega de Granada* was very similar compared to the groundwater of the *Vega de Granada*. This is interpreted as a strong influence of the *Genil* for GWR through riverbed infiltration. River inflow at the northern border of the *Vega de Granada* by the *Rio Cubillas*, which drains vast parts of the *Sierra Arana,* was sampled once at three sites. A strong evaporative enrichment was observed in the sample from the reservoir of the *Cubillas* (*Emb.de Cubillas*). This enriched signature was transferred by the *Cubillas* to the *Vega de Granada* groundwater and then attenuated by mixing processes with the depleted groundwater from the east. Other river inflow signatures were not sampled and could be subject for further studies (p.53).

It is shown that the spatial distributions of stable isotopes from wells located in the south-eastern part of the *Vega de Granada* were highly depleted. Therefore, this area is considered to be influenced by lateral inflow from the adjacent *Sierras* or indirect recharge by the local rivers (*Genil*, *Monachil*, *Dilar*). In contrast, groundwater from the centre and the western part of the *Vega de Granada* is relatively enriched in both isotopes with a strong enrichment in $\delta^{18}$O indicating evaporation losses. Maximum evaporation losses were calculated, according to the regression line of the well samples and the climatic conditions, with ~20 %. Water-Rock interaction in the *Vega de Granada* alluvial aquifer cannot be excluded and might be subject for further studies. A flow of depleted groundwater is observed south to the *Sierra Elvira* carbonate complex indicating the importance of the *Sierra Elvira* as a local groundwater recharge area. This signature was associated to GWR altitudes around 1500 masl. One of the most important springs in the *Vega de Granada* (*Manantial de la Reina*) with 12.000 l/m runoff was associated, according to the similar isotope signature with groundwater in the north, to groundwater recharge area in the *Sierra Elvira* (p.63).

The isotope signatures of thermal springs are supposed to be influenced by water-rock interactions, due to a shift from the WMMWL. In accordance to the hydrochemical classification, the thermal springs can also be divided by the isotope signatures into two subgroups. Samples which are located near to the WMMWL are supposed to be less influenced by water-rock interactions, while points which are shifted from the WMMWL represent progressively increasing water-rock interaction with the host-rocks of the aquifer under various water temperature conditions. Maximum deviations from the WMMWL are $\Delta$0.5 ‰ (p.66).

Table of content

## List of figures

List of tables

## 1 Introduction

This work is divided in two parts, the diploma thesis and the geological mapping. The work tries to collect existing data as well as it provides new data concerning hydrochemistry and hydrogeology of the aquifer systems in the study area. The main objectives of this work are:

Diploma thesis:

- Taking water samples (springs, wells, surface water and precipitation) for AAS and ICP-MS analysis as well as $\delta^{18}O$ and $\delta^{2}H$.

- Establishing a network of spring- and river-sites at different altitudes for frequent and single sampling.

- Using an ACCESS database to manage the hydrochemical and isotope data.

- Collect and check available data concerning hydrogeology and hydrochemistry.

- Interpretation of hydrochemical data with PHREEQC 2.11.

- Interpretation of isotope data for a better understanding of the groundwater recharge for the *Vega de Granada* aquifer.

- Use of available information of the area for generating a Digital Elevation Model (DEM).

Mapping:

- Description of the stratigraphic sequence, geological formations and structural elements of the mapping area.

- Present a geological map of the formations in scale 1:20 000 (paper copy) generated with ArcGis 8.2.

## 1.2 Regional geological setting

The Betic-Rif mountain belt, located in southern Spain and northern Morocco, form an alpine orocline, which now joins at the strait of Gibraltar. This belt was developed from late Mesozoic to Cenozoic within a convergent stress regime between Africa and Iberia[1]. The cordilleras are separated by the Alboran Sea, which consists of extended Neogene continental crust. The Betic-Rif orogen is, among other Mediteranean mountains, characterised by coeval shortening and extension during late stages of orogenesis. Traditionally, the rocks of the Betic-Rif orogen are divided into three zones: a) Internal Zone, b) External Zone and c) Flysch (Fig. 1.1).

The Internal Zone consists of metamorphed Palaeozoic and Mesozoic rocks separated by several Neogene intramontane basins (e.g. the *Granada* basin). Structually rocks of this zone were grouped, together with other metamorphed belts, behind a north dipping subduction zone (Fig.3.2 top). From early Miocene (23-20 Ma) subduction rollback occurred in the western mediteranean and caused a counterclockwise rotation of this metamorphed belts to their current positions (LONERGAN & WHITE 1997). The Internal Zone can be subdivided into three complexes of variable metamorphic grade. From bottom to top: (a) Nevado-Filabride, (b) Alpujarride and (c) Malaguide[1].

a) this complex crops out in large anticlinar structures that form, among others, the uppermost part of *Sierra Nevada*. It is made up of metamorphic rocks with mainly dark colours and variable lithology, which are micaschists, quarzites, gneisses, marbles, amphibolites, eclogites
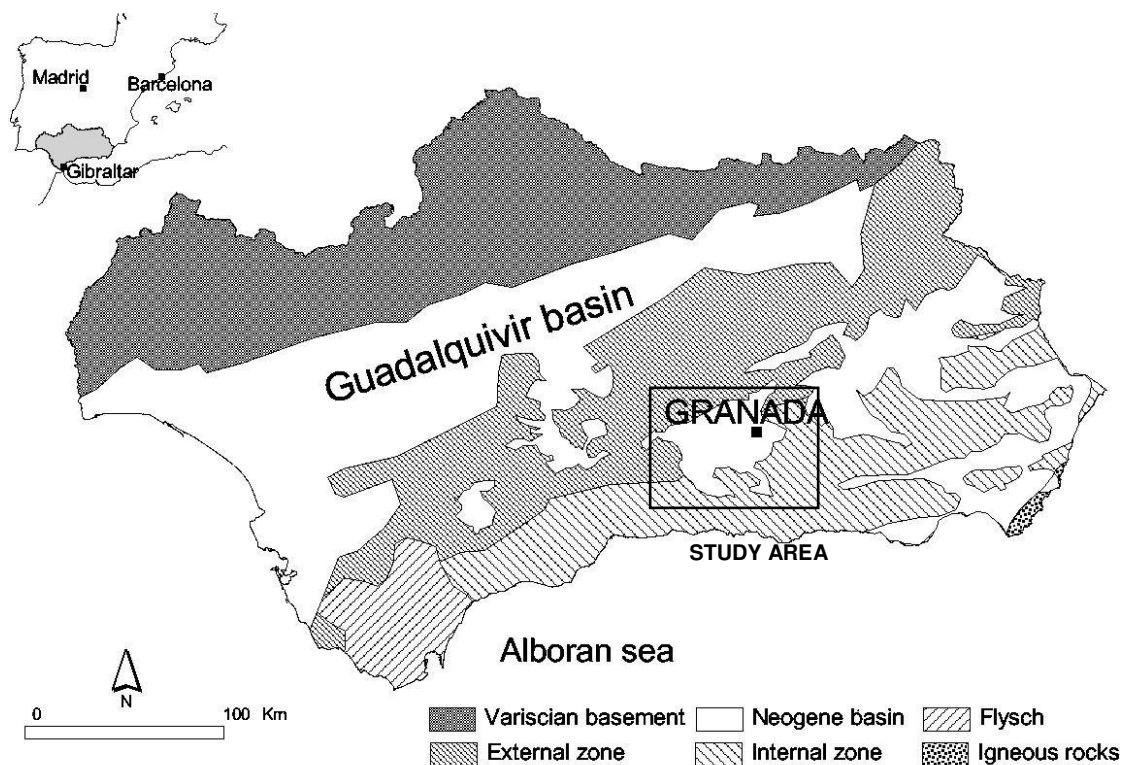


• Figure 1.1 Geological sketch of Andalusia showing the threefold division of the Betic Cordillere (External Zone, Internal Zone, Flysch). The rectangle indicates the study area. Geology simplified from IGME 2002.

---

[1] AZAÑON et al 2002

and serpentinites. This sequence is not good dated but associated to the Paleozoic[1] and builds the metamorphic core.

b) this complex crops out largely around the *Nevado-Filabride* and consists of metapelitic-metapsammitic formations, attributed to the Paleozoic but predominantly of calcareous and dolomitic rocks aged to middle to upper Triassic[1]. The carbonatic rocks are moderate karstified[1]. Most of the spring sites are located within this unit.

c) this complex consists of low-grade metamorphed carbonate and siliciclastic rocks associated to Paleozoic until Palaeogene ages[1]. This unit crops out around *Malaga* and plays no important hydrogeological role in the study area.
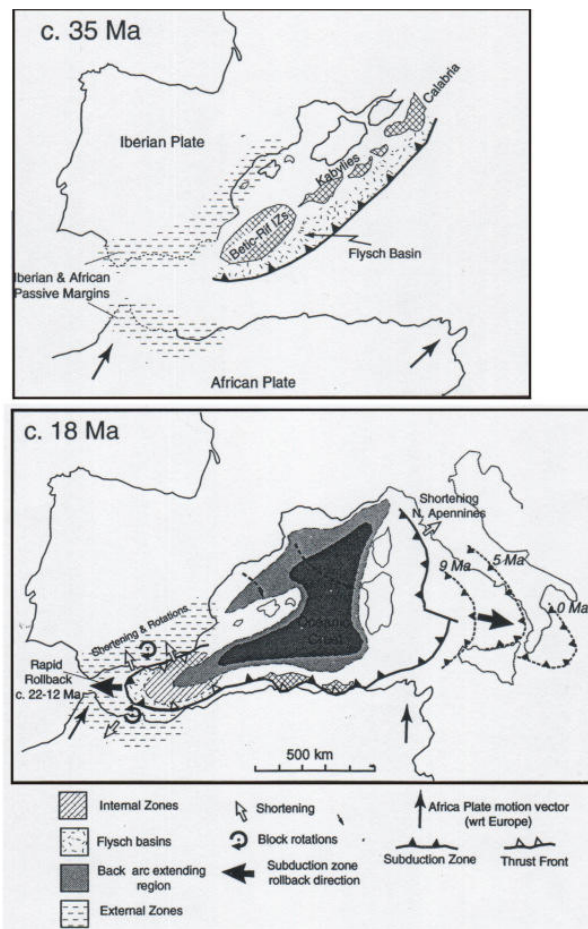


• Figure 1.2 Geologic evolution of the Betic-Rif mountain belt (LONERGAN & WHITE 1997).

The External Zone consists of Mesozoic and Palaeogene sediments, which were deposited in a basinal- (Subbetikum) and a shelf-facies (Prebetikum) on the Iberian and the Maghrebian palaeomargin of the Thetys Ocean (Fig.1.2 top). These rocks were deformed by northwest directed thrusting and folding during early to late Miocene[1]. The Flysch nappes consists of Cretaceous[2] to Miocene deep-water sediments in flysch-facies, now concentrated in the western parts of the Betics (around Gibraltar). The Guadalquivir basin, located to the north of the Betics, is filled with Neogene sediments and is interpreted as the Betic foreland basin[1]. Further to the north the Variscian basement crops out and builds mid-range mountaineous areas known as the Sierra Morena. The Internal/External Zone border is now buried under the sediments of the *Granada* basin. The *Granada* basin is an intramontane depression filled with sediments from early Burdigal (lower Miocene, 20 Ma) to Quaternary[1]. The sedimentary infilling is up to 2km thick. Geophysical data show that the *Granada* basin is a large half-graben structure, thickening northwards and limited by normal faults striking ENE-WSW, NW-SE and dipping to S. In early Tortonian (11.5 Ma) time the Alboran sea covered most of the Betic Cordillera and the area now called "*Granada* basin"(Fig.1.2). Sediments of this period can now be found at >1500masl near *Granada*. During the middle Tortonian (9 Ma) the sedimentary environment became more homogenous towards widespread platform calcareous sandstones and calcarenites (BRAGA et al. 1990). During the upper Tortonian (8 Ma) increasing

---

[1] Azañon et al 2002

geomorphodynamic took place at the eastern and north-eastern margins of the basin (e.g. DABRIO et al. 1978) and form a paleogeography similar to nowadays. Although the basin remains marine influenced and coral reef development is reported (BRAGA et al. 1990). Beginning at the Tortonian-Messinian boundary (7 Ma) the basin was gradually isolated from the sea due to uplift processes in the southern and western edges. At this time the basin was eventually dried up (Messinian salt crisis). Later a period of lacustrine sedimentation (upper Messinian, 6 Ma) took place. Since the Pliocene (5 Ma), the onshore Neogene basins (e.g. Granada basin) underwent rapid uplift, induced by continued convergence stress between Africa and Eurasia and/or slab break-off (LONERGAN & WHITE 1997) and leading later to a stage of detrital continental deposition (Pliocene and Quaternary).

## 1.3 Geomorphology

In general the morphology of the *Granada* region is a product of folding, faulting and erosive processes over geological time. The most dominant morphological feature is a elongated dome named *Sierra Nevada*, with altitudes from 900-3400 m above sea level (masl) and the highest mountain of the Iberian Peninsula named *El Mulhacen* (3482 masl) (Fig.1.3). To the north the *Sierra Arana* builds a shallower mountain range (with altitudes from 800-1800 masl). To the west the relative flat *Granada* basin stretches over a length from N-S ca.40km and E-W ca.55km with altitudes from 500-800 masl. The shallow mountains range *Las Guajaras* with moderate altitudes of 800-1500 masl follows in the south.
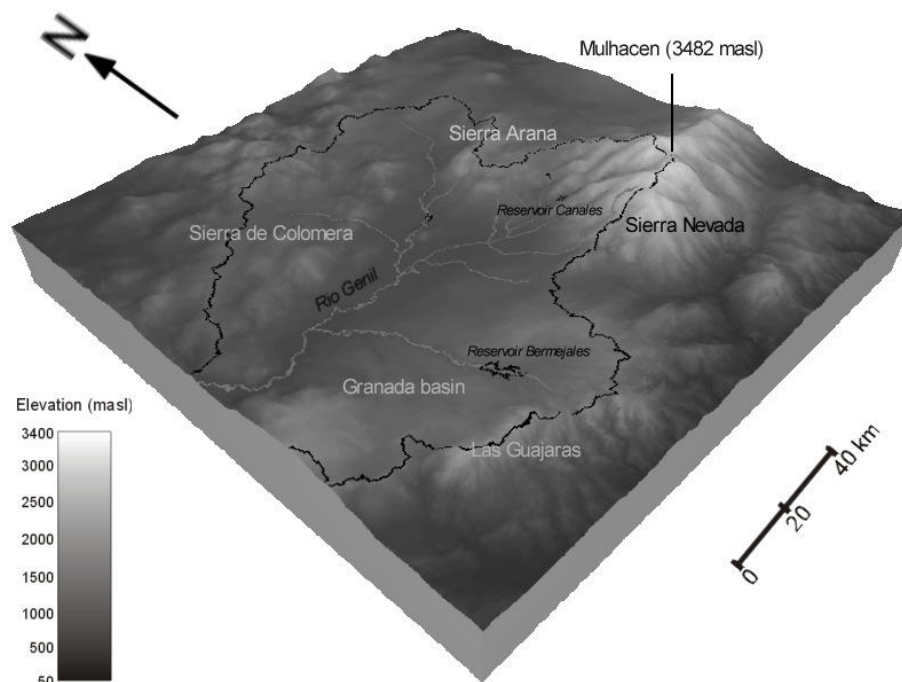


• Figure 1.3 Digital elevation model (DEM) of the *Granada* basin and the surrounding mountain ranges with the catchment area of the *Rio Genil*. (DEM derived from Mapa Digital Andalucia 2002).

From the origin of the *Rio Genil* in the *Sierra Nevada* to the end of the *Granada* basin the river courses over a length of ca. 90km. The *Rio Genil* flows into the river *Guadalquivir* and finally in the Atlantic sea. The entire catchment area of the *Rio Genil* extends largely over the study area and is printed only in parts (Fig.1.3). According to the catchment delineation, only

ca. 23% of the surface of the *Sierra Nevada* is drained by the catchment area of the *Rio Genil*. The catchment area can be subdivided into several sub basins.

## 1.4 Climate, Meteorology

The Granada region has a Mediterranean climate with a slight continental tendency (CASTILLO 1986) following a yearly weather pattern: dry hot season from June to October, and moderate cold wet season from November to May.



**Pinos Puente 594masl (2000-2005)**

**Padul 753masl (2000-2005)**

**Albergue Universitario 2550masl (1960-1997)**
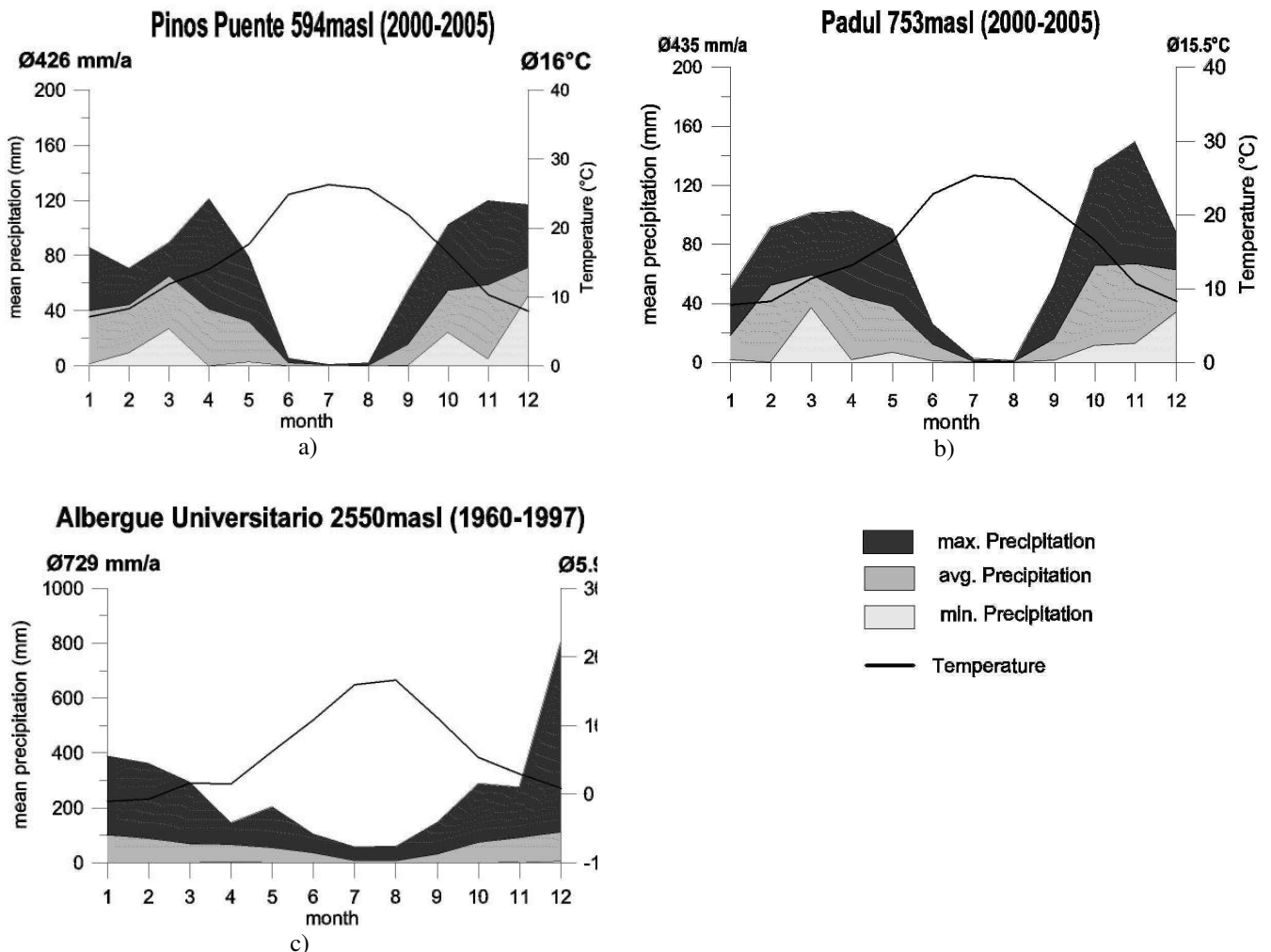
• Figure 1.4 (a-c) Climate diagrams of selected stations. (Data derived from www.juntadeandalucia.es)

The temperature course of all the meteorological stations shows a maximum from Jule-August and a minimum from December-January (Fig.1.4, a-c). The study area is generally characterized by strong variations in the climate. The average temperature, in the *Granada* basin lies between 15 and 16 °C, while in the high regions of the *Sierra Nevada* (*Albergue Universitario* 2550 masl) average temperatures range between 5 – 6 °C. These variations are caused by differences in elevation, spatial position and the environment around the stations. Most of the precipitation (from >20 up to more than 180 mm/month in single months) falls in few heavy rain events in rainy periods (October to March). December is the wettest month, followed by March. The driest period is around July with rainfall less than 10 mm per month, sometimes just 0-5 mm. During a 5-7 month period the potential evapotranspiration exceeds

the monthly amount of precipitation which leads to the definition of a semiarid climate in the *Granada* basin. The average decrease of air temperature with increasing altitude depends both on seasonal and regional variations. In winter, the gradients are (slightly) lower than in summer, because of frequent temperature inversion during cold season. This atmospheric boundary layer (ABL) is the bottom layer of the troposphere that is in contact with the surface of the earth. It is often turbulent and is capped by a statically stable layer of air or temperature inversion. The ABL depth (i.e., the inversion height) is variable in time and space, ranging from tens of meters in strongly statically stable situations, to several kilometres in convective conditions over deserts (STULL 1988).

More than 75% of the precipitation in the *Sierra Nevada* above 2000m falls as snow (CASTILLO 2000). Between December and March a continuous snow cover exists above 2200 masl and even in summer snow patches at shady slopes exist.
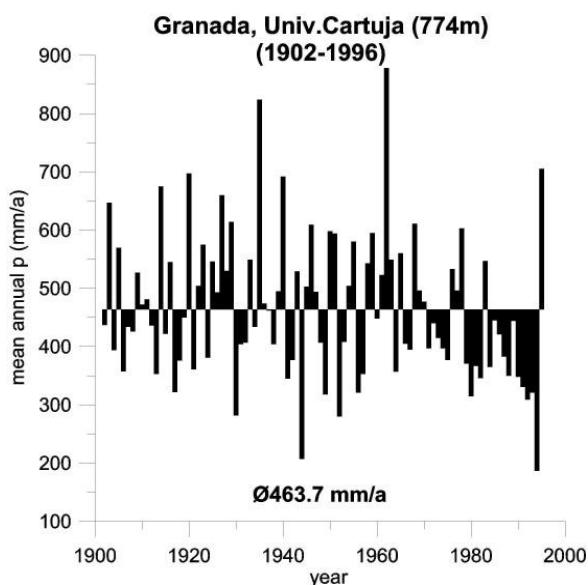


• Figure 1.5 Year to year variations from average annual of annual precipitation in the city of *Granada* (Data derived from IGME 2000).

There are considerable variations in the quantity of the annual rainfall from year to year. The average annual rainfall at *Universitario Cartuja* Meteorological Station in the city of Granada for the period 1902–1997 is 463.7 mm. The maximum recorded annual rainfall was 880 mm in the year 1962, while the minimum was 190 mm in 1994 (Fig.1.5).

The predominately weather situation in the winter months are two high pressure cells over the Azores and Russia and a low pressure cell over the British islands. This produces a circulation, bringing rain bearing air masses from the North Atlantic. In the summer months often a low pressure zone lies over the Iberian Peninsula.

In the *Granada* region, the dominant travel direction of rain bearing air masses is from the west towards the east. Rainfall increases eastwards with elevation, with the maximum rain amount at the peaks in the *Sierra Nevada* (2000-3400 masl). Further, to the east, at the lee side of the mountains, there is a decline in rainfall amounts as air masses are heated, decreasing the relative humidity and resulting in a rain shadow. The Isohyetal map (Fig. 1.6) shows annual precipitation averages of the *Granada* region during different time periods. As shown in figure 1.6 mean annual precipitation amounts in the *Sierra Arana* are in the highest region about 700 - 800 mm. Mean annual precipitation in the *Granada* basin is around 500 mm.
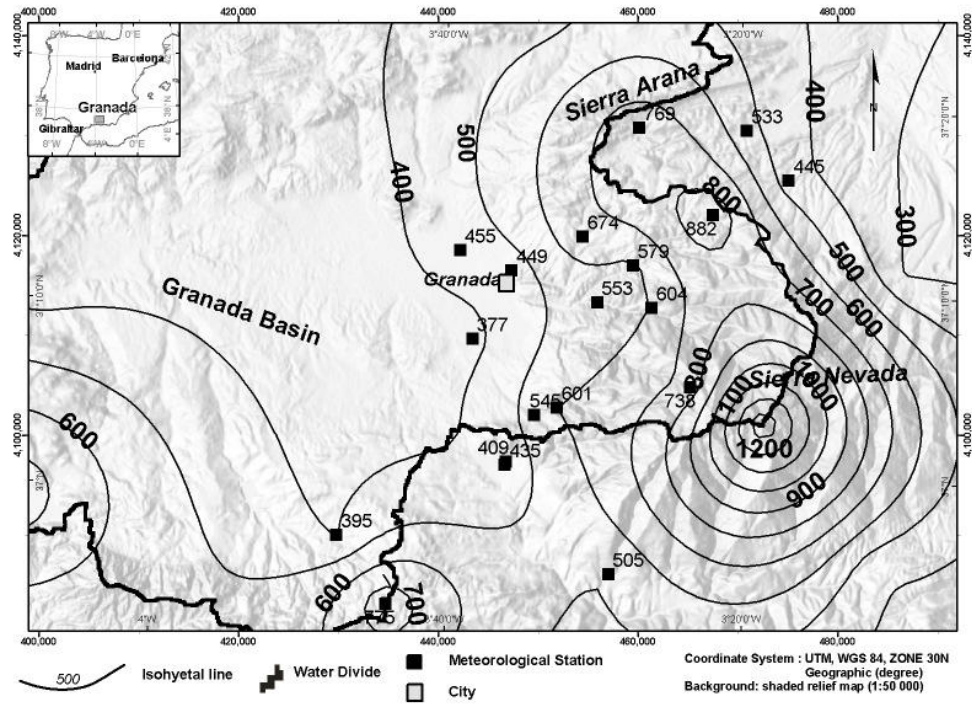


• Figure 1.6 Isohyetal contour map of annual precipitation averages of the *Granada* region calculated with records of the indicated meteorological stations from various time periods (Data shown in Appendix 1, table a1.1)

The isohyetal contour map was calculated according to data shown in appendix 1, table a1.1. Methods are explained in section 3.4.

## 2.1 Groundwater recharge

As expected for a semiarid area with limited precipitation groundwater recharge (GWR) in the *Granada* basin itself is very low and close connected to rainy seasons. Appendix 2 (Table a2.1 - Table a2.6) shows that the actual evapotranspiration (ETA) of 6 climate stations calculated according to Turc (GRAY 1973) and Coutagne (REMENIERAS 1974) equations (for methods see section 3.4.1). Generally Turc provides higher ETA values than Coutagne and results in negative GWR for almost all months and stations. Thus Coutagne equation is used for calculation.
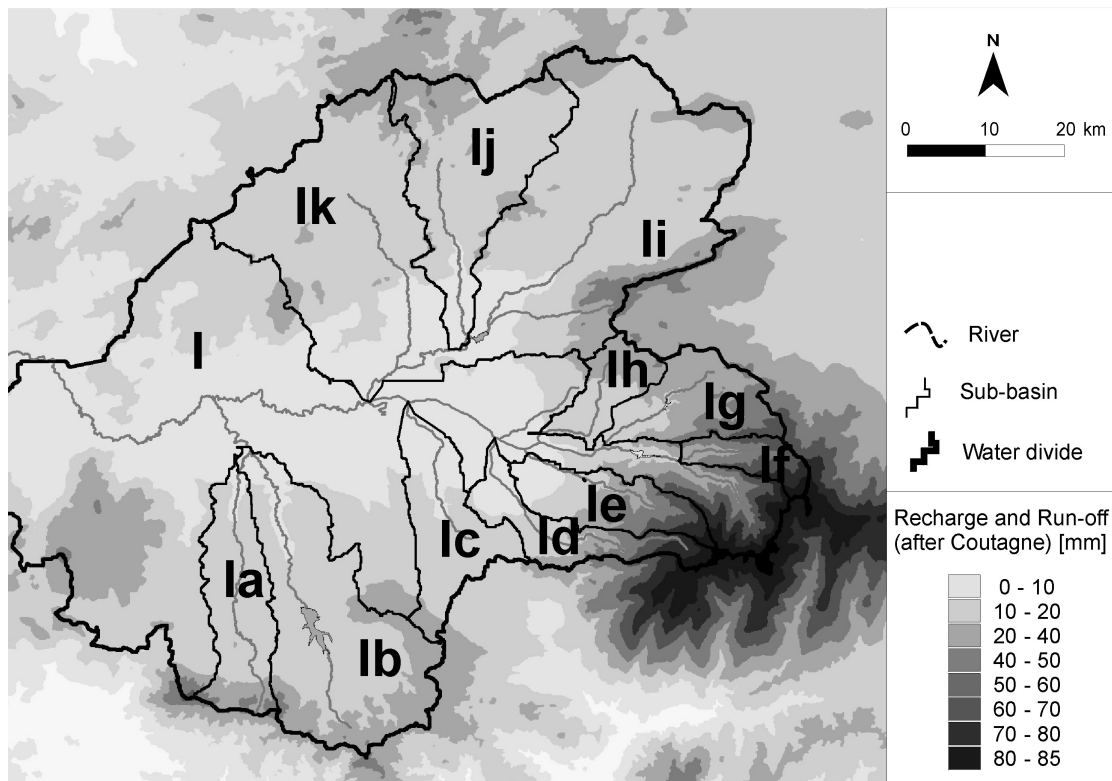


• Figure 2.1 GWR map and extend of the *Rio Genil* catchment area and the tributary sub-basins.

In the basin ETA almost equalled precipitation (97-98%) and only an average of 5-10 mm/a remains for groundwater recharge. In the *Sierra Nevada* GWR is considerable higher (ca. 61.6mm/a) but due to the lack of more meteorological stations no detailed calculations are possible. Main water surplus occurs during rain periods between October to March (maximum in December 3.9 mm/month) in the basin and maximum 15.5 mm/month (January) in the *Sierra Nevada*. During the dry season around June very little to no surplus occurs at all

• Table 1.1 Name, ID and catchment area.

| Name | ID | Area [km$^2$] |
|---|---|---|
| *Rio Genil* | I | 1649.63 |
| *Rio de Alhama* | Ia | 173.73 |
| *Rio Cacin* | Ib | 403.76 |
| *Arroyo del Salado* | Ic | 167.78 |
| *Rio Dilar* | Id | 117.74 |
| *Rio Monachil* | Ie | 124.10 |
| *Rio Maitena* | If | 57.22 |
| *Rio de Aguas Blancas* | Ig | 139.82 |
| *Rio Darro* | Ih | 77.37 |
| *Rio Cubillas* | Ii | 765.5 |
| *Rio de la Colomera* | Ij | 319.27 |
| *Arroyo de la Canada* | Ik | 438.13 |
| **Σ (km$^2$)** | | **4434.05** |

in the basin and little in the *Sierra Nevada*. Taking into consideration the high uncertainty of

the ETA calculations it is only possible to state that the groundwater recharge in the basin is very low, maybe even negative in the dry season while there maybe some minor recharge during the rain season. The main groundwater recharge is supposed to come from the *Sierra Nevada* east of the basin.

## 2.2 Hydrogeology
### 2.2.1 Alluvial aquifer (*Vega de Granada*)

Most of the previous published works is dealing with the hydrogeology of the *Vega de Granada* which is the most important aquifer. This area has been studied intensively (among others CASTILLO & FERNANDEZ-RUBIO 1985, DELGADO et. al 2002). Most of the works are about urgent problems of the aquifer like pollution by nitrates and microbiology, over exploration and vulnerability.

The *Vega de Granada* aquifer consists of alluvial material (Gravel, Sand, Silt, Conglomerates) deposited by the rivers *Monachil*, *Darro*, *Dilar* and, most important *Genil*. The aquifer surface occupies an area of approx. 200 km$^2$ (22 km x 8 km) and in the centre a thickness of approx. 250 m is reported.

Since prehistoric time the *Vega de Granada* is settled and humans favoured this area due to the good fertility (HAARMANN 2001). In the time of Arabian domination (8$^{th}$ – 15$^{th}$ century) an irrigation network (*Acequias*) was designed and installed which is, with minor modifications, still in use until today. The Spanish word *Vega* means cultivated land and irrigation plays an
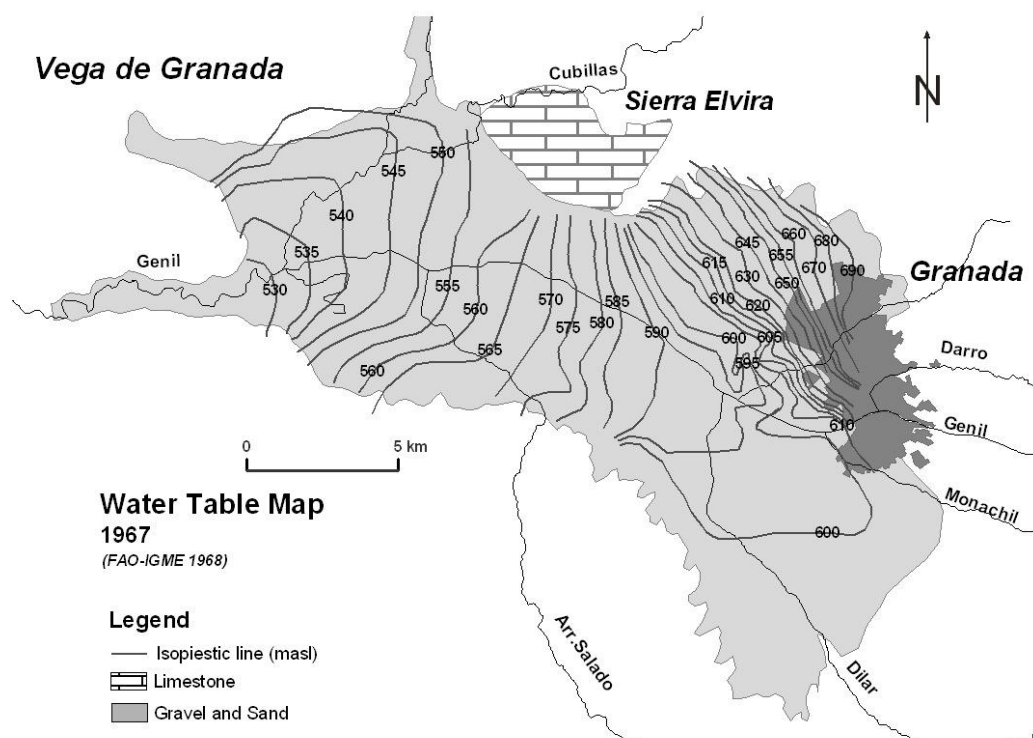


• Figure 2.2 Water table trend map from 1967 (FAO-IGME 1968).

9

important role in the hydraulic balance. Nowadays in the area several plants are cultivated, like tobacco, poplar grove, cereal, corn and vegetables (CASTILLO 1993).
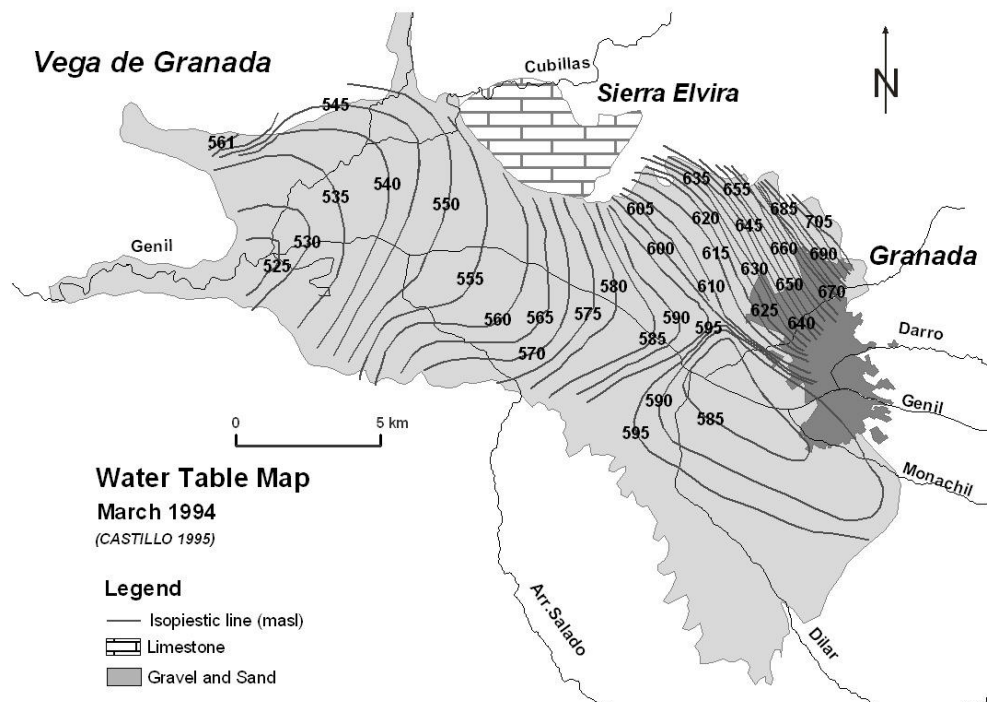


• Figure 2.3 Water table map from March 1994 (CASTILLO 1995).

First groundwater table surface measurement was carried out in 1967 (Fig.2.2, FAO-IGME 1968). It must be considered as a general trend map, since the period of measurement was given for a whole year (1967). This first groundwater table trend contour map represents the hydraulic regime without important anthropogenic impact on the flow system. Main hydraulic characteristics can be recognized: the isopiestic lines are relative close together in the north-eastern part of the *Vega de Granada*, due to low permeabilities of the aquifer (hydraulic gradient 1.5 %). Higher permeabilities are visible in the south-eastern part of the *Vega de Granada* (hydraulic gradient 0.2 – 0.4 %). The groundwater follows the general regional hydraulic gradients indicating an approximated E-W flow direction. The aquifer system underwent important changes in the water balance during the last century. These changes are connected to the building of the reservoirs (Reservoirs of *Quentar* 1973 and *Canales* 1988), changes in the irrigation techniques and the development in urbanisation. Changes are reflected by the groundwater table contour map from March 1994 (Fig.2.3, CASTILLO 1995). Here, in the south-eastern part a groundwater drawdown due to pumping can be observed. A decrease in the water table evolution from 1967 to 2001 is stated in IGME 5.32 2001.

Lateral limits are considered to be open boundaries to the relative low permeable deposits of the Mio-/Pliocene units in the S, E and NE. The horst structure of the *Sierra Elvira* carbonate rocks represents a potential recharge area at the central northern border of the aquifer with open boundary characteristics. General water balance considerations taken from IGME 5.32 2001 are:

Input flow:
- Direct infiltration by rainfall over permeable surface.
- Indirect infiltration by river bed recharge from the (sub-) basins (*Genil*, *Monachil*, *Dilar*, *Darro, Cubillas*).
- Indirect infiltration by the irrigation network (*Acequias*) losses.
- Indirect infiltration from the irrigation network.
- Lateral inflow by surface runoff from less permeable material of the *Mio-/Pliocene* unit.
- Lateral concealed inflow by the *Sierra Elvira* carbonate system.

Outflow:
- Drainage by rivers (*Genil, Cubillas*), irrigation channels (*Acequias*) and springs.
- Pumping stations for irrigation, urban and industrial demands.

Annual GWR is calculated by various authors (e.g. CASTILLO 1995, IGME 5.32 2001) and is considered to be 232 hm$^3$/a total. A publication by CASTILLO 1995 estimates that 70 % of GWR is derived from infiltration of surface runoff water from the *Sierra Nevada*. This results in predominated high quality hydrogencarbonate water facies in the eastern and especially in the south-eastern part of the *Vega de Granada* (compare to section 4.1.2). Other parts of the aquifer are characterised by an increase in salinization (e.g. centre and southern part of the aquifer) (CASTILLO 1986).

## 2.2.2 Mio-/Pliocene basin deposits

This very heterogeneous unit covers most of the area of the *Granada* basin (1350 km$^2$). The geology is divers and can be described as sedimentary sequences of an intramontane basin. These sequences include marine sediments, such as carbonates and evaporates and terrigenous sediments, such as conglomerates and sandstones. Not much data about the hydrogeological units of the Mio-/Pliocene basin sediments is available. In IGME 5.32 2001 considered to have 50 hm$^3$/a GWR derived from rainfall on the area. Additionally, a not quantified flux of lateral and vertical groundwater flow derived from unknown origin was identified.

## 2.2.3 Carbonate terrains (*Sierra de la Peza*, *Sierra de Padul*, *Sierra Arana*, *Sierra Elvira*)

The hydrogeological unit *Sierra de la Peza* and *Sierra de Padul* consists of material from the *Alpujarride* complex which are limestone, dolomite, marble and calcareous schists. The units are moderate fissured and carstified. Within the *Sierra de la Peza* unit minor Jurassic carbonate formations of the *Subbetics* (External Zone) can be found. The carbonate terrains are considered to be unconfined aquifers with high permeabilities due to carstification. Carbonate units of the *Alpujarride* together with formations of the *Subbetics* form the northern limit of the *Sierra de Padul* unit to the *Sierra Arana* unit (IGME 5.30 2001).

Precipitation is the exclusive input for GWR and discharge takes place at the open boundaries.

In the north-eastern part of the *Sierra de la Peza* a strong discharge to the southeast, expressed as high discharge spring, in altitudes at ca. 1100 masl are observed. Important springs in this area are: *Fte.de Nivar* (1080 masl), *Fte.Grande* (1114 masl). Important springs are situated within this unit: e.g. *Nacimiento Rio Darro* situated at the boundary between the *Alpujarride* and postorogene silts (Serravielense). An N-S directed flow is estimated in the sub basin of the *Rio Darro*. No data about the piezometric evolution or exploitable water amounts of this aquifer are available (IGME 5.31 2001).

## 2.2.4 Metamorphic terrains (*Nevado Filabride*)

The metamorphic terrain (*Nevado Filabride*) consists of various schists (micaschists with chloritoids, garnet micaschists with andalusite) and quarzites. The schists are of low permeability, but in the *Nevado-Filabride* glaciogenic alterated material is common. CASTILLO 2001 discusses the "Hydrogeologic behaviour of hard rocks affected by glaciarism and periglaciarism in the Sierra Nevada". Here, high transmissivities of $1.5 - 8 * 10^{-2}$ days$^{-1}$ are reported.

## 2.3 Stable isotopes in hydrogeology

Differences in the stable isotopic signature of snow, rainfall, surface water and groundwater is used to quantify and qualify e.g. groundwater recharge, residence time or groundwater recharge provenances and is a widespread tool in hydrogeology. An introduction of the processes of stable isotopes in hydrogeological systems gives CLARK & FRITZ 1997.

### 2.3.1 Isotope fractionation

Isotopes are atoms of the same element with differences in their number of neutrons. All possible combinations of stable hydrogene ($^1$H, $^2$H or D) with stable oxygene isotopes ($^{16}$O, $^{17}$O, $^{18}$O) occur in natural water, but only $H_2^{18}O$, $HD^{16}O$ and the ordinary $H_2^{16}O$ are due to their natural abundances of analytical relevance (IAEA 2000). All isotope results are reported in $\delta^{18}O$ and $\delta D$ ($\delta^2H$) notation, representing per mil (‰) deviation from the Vienna Standard Mean Ocean Water (VSMOW):

$$\delta_{sample}(‰) = \left( \frac{R_{sample} - R_{reference}}{R_{reference}} \right) \cdot 1000 \quad (e.g.\ R_{H_2O} = \frac{H_2^{18}O}{H_2^{16}O}) \quad (eq.2.1)$$

R is always defined as the ratio of the heavier to the lighter isotope. The VSMOW standard is a mixture of distilled ocean water with small amounts of ocean water (IAEA 2000). The variations of the $^{18}$O and $^2$H concentrations are controlled by fractionation during evaporation and condensation. This phase transition reactions can take place under equilibrium conditions or non-equilibrium (kinetic) conditions.

a) equilibrium fractionation
The variations of $HD^{18}O$ and $H_2^{18}O$ during fractionation are expressed by the ratios of the vapour pressures α.:

$$\alpha = \frac{R_1}{R_2} \qquad e.g.\ \alpha_{water-vapour} = \frac{R_{water}}{R_{vapour}} \qquad (eq.2.2)$$

α expresses the isotope ratio $R_1$ in the reactant phase ($R_1 = (H_2^{18}O)/(H_2O)$ for $^{18}$O or $R_1 = (HD^{18}O)/(H_2O)$ for D) relative to $R_2$ in the product phase. At 20°C, α for $H_2^{16}O/ H_2^{18}O$ is according to KAKIUCHI AND MATSUO 1979 (eq.2.4, eq.2.5) 1.0835, while $\alpha$ for oxygen fractionation between water and vapour at the same temperature is 1.0099. Due to the very little variations in isotopic fractionation the deviation of α from 1 is commonly used. This enrichment factor ε, is defined as ε (‰) = (α − 1) * $10^3$. ε represents the enrichment (ε > 0) or the depletion (ε < 0) of the rare isotope in the reactant with respect to the product. The relationship between α and the δ notation is then:

$$\alpha_{water-vapour} = \frac{\delta_{water} + 1000}{\delta_{vapour} + 1000} \quad (CLARK\ \&\ FRITZ\ 1997) \qquad (eq.2.3)$$

The temperature dependence of α is defined according to KAKIUCHI AND MATSUO 1979 for $\delta^{18}O$:

$$10^3 \ln \alpha = \frac{5.97 \cdot 10^6}{T^2} - \frac{32.80 \cdot 10^3}{T} + 52.22 \qquad \text{(eq.2.4)}$$

and for δD:

$$10^3 \ln \alpha = \frac{2.40 \cdot 10^6}{T^2} + \frac{64.55 \cdot 10^3}{T} - 168 \qquad \text{(eq.2.5)}$$

where T is temperature in kelvins. Vapour evaporating from ocean water, with an defined isotopic composition of 0 ‰ relative to the VSMOW scale, would be only under equilibrium conditions, depending on temperature 8 to 10 ‰ depleted in $^{18}O$ (T = 40 °C, ε = 8.4 ‰; T = 20 °C, ε = 9.9 ‰, eq.2.4;eq.2.5).

The equations 2.4 and 2.5 are useful for calculating the degree of equilibrium exchange from water with vapour. Since vapour evaporated from the ocean show enrichments of around ε = - 12 ‰ a second process, the non-equilibrium or kinetic fractionation must be considered. Isotopic fractionation between a liquid and vapour is an equilibrium process **only** when the vapour is saturated with respect to the liquid. Fractionation caused by evaporation in natural processes can be considered as a non-equilibrium process, while only weak indications of kinetic isotope effects were observed in condensation processes (DANSGAARD 1964).

b) <u>non-equilibrium fractionation (kinetic)</u>

Kinetic fractionation results from a "one way" physical or chemical reaction, e.g. evaporation of water with instant withdrawal of the vapour and therefore avoiding further contact to the water. Kinetic fractionation is influenced by the surface temperature, wind speed, salinity, and most important: humidity. At lower humidity, water-vapour exchange is minimized, and evaporation becomes an increasingly non-equilibrium process. This inverse kinetic isotope effect occurs most commonly in reactions involving hydrogen atoms (BIGELEISEN & WOLFSBERG 1958) and results in evaporation lines which differ in the slope to the GMWL. GONFIANTINI 1986 describes the kinetic fractionation in relation to humidity with the following equations:

$$\varepsilon\,^{18}O_{kinetic} = 14.2\,(1-h)\ (\times 10^3 ‰) \qquad \text{(eq.2.6)}$$

$$\varepsilon\,^2H_{kinetic} = 12.5\,(1-h)\ (\times 10^3 ‰) \qquad \text{(eq.2.7)}$$

where h is the humidity (100% = 1). The total fractionation between the water body and the open air is then the sum of the fractionation factor for equilibrium water-vapour exchange ($\varepsilon_{equilibrium}$) and the kinetic factor ($\varepsilon_{kinetic}$). For $\delta^{18}O$ according to:

$$\delta^{18}O_l - \delta^{18}O_v = \varepsilon^{18}O_{equilibrium} + \varepsilon^{18}O_{kinetic} = \varepsilon^{18}O_{total} \qquad \text{(eq.2.8)}$$

The indices l and v are for liquid and vapour, respectively. Since atmospheric water forms under about 85 % humidity a displacement of the evaporation line towards a d-excess (or intercept) is observable. If now evaporation rates are high due to high temperatures and low

relative humidity in the atmosphere at the initial formation of water vapour, a strong kinetic effect takes place and the d-excess is high (JOUZEL & MERLIVAT 1984).

Evaporation rates were calculated, according to a Rayleigh enrichment, in relation to temperature and humidity and plotted in $\delta^{18}O$ vs. $\delta D$ diagrams (Fig.2.5), according to CLARK & FRITZ 1997:

$$\delta = \delta_o + \Delta\varepsilon_{total} * \ln(f) \hspace{3cm} (eq.2.9)$$

where $\delta_0$ is the initial value (here $\delta^{18}O$= -8 ‰; $\delta D$= -54 ‰) and $\delta$ is the resulting value. The resulting graphs (Fig.2.5) are useful to estimate the conditions during evaporation and the proportion of fractionation with factors $f$ from 1 to 0.1. According to the above mentioned equations (eq.2.9) strong kinetic fractionation, due to low humidity (h = 0.2) and high temperatures (T = 20 °C), result in more shallow slopes around 4.3. Higher humidity (h = 0.8) and lower temperatures (T = 5 °C) results in evaporation lines which are closer to the GMWL and have slopes around 6.8.
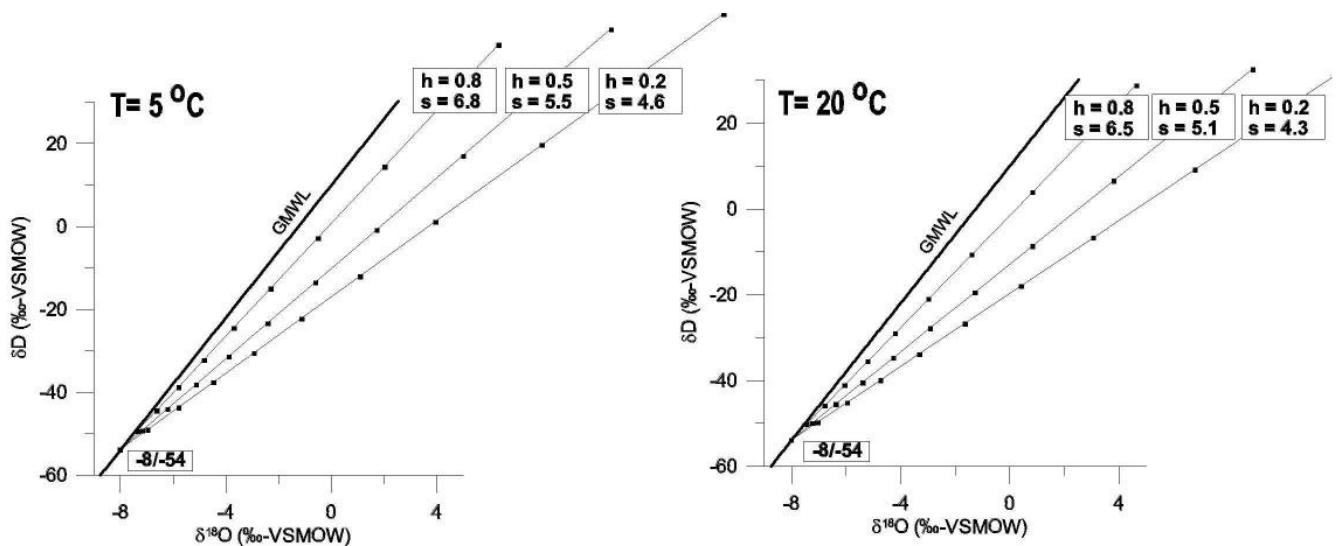


• Figure 2.5: Differences in evaporation rates in relation to humidity (h) in a $\delta^{18}O$ vs. $\delta D$ (‰-VSMOW) diagram for 5°C and 20°C. showing the predominating exchange fractionation process at values for *f* from 1 to 0.1. (s = slope of evaporation line, Calculated according equation 2.9)

The strong correlation between temperature and $\delta^{18}O$–$\delta^2H$ controls the position of precipitation on the meteoric water line. From this correlation it is possible to distinguish isotope effects due to season, altitude, amount and continentality — the basis of isotope hydrogeology.

_temperature effect_ – with decreasing $\delta^{18}O$ values for precipitation with decreasing temperature. Temperature has the strongest effect on the isotopic composition due to the strong temperature dependence on the fractionation between vapour and liquid (CLARK & FRITZ 1997).

_seasonal effect_ – often a seasonal change of the stable isotope ratios is observed as a result of temperature effects, different trajectories of air masses, and varying fractionation processes in the source area of atmospheric moisture, with more negative $\delta^{18}O$ values during winter (CLARK & FRITZ 1997).

altitude effect – often more depleted values of precipitation are observed at higher altitudes (Fig.2.6). This is the combined result of temperature effects and repeated rain-out.
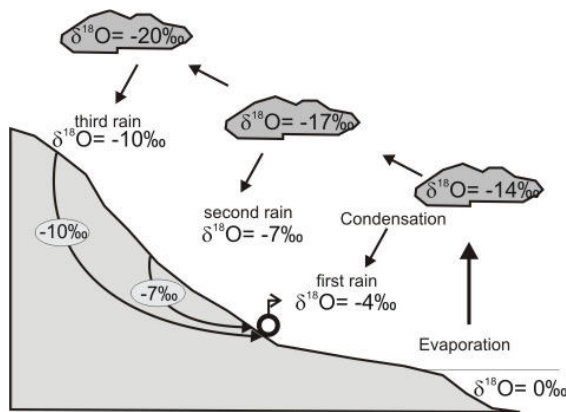


• Figure 2.6: Altitude effect and mixing of groundwater in the spring water (modified after www.IAEA.org).

Equilibrium fractionation increases with lower temperatures, making fractionation more efficient at higher altitudes. Repeated rain-out during uplift of air masses causes a Rayleigh-type distillation process (CLARK & FRITZ 1997). The magnitude of this effect depends on local climate and topography. Gradients for the _Sierra Nevada_ are between -0.2 and –1.3 ‰ ($\delta^{18}O$/100m) and –1 and –9 ‰ ($\delta D$/100m) (GARRIDO 2003).

_amount effect_ - small amounts of rain are often enriched in heavy isotopes. No amount effect is observed in rain out events which exceed 20 mm/month (IAEA 2000). The factors that lead to a relationship between the amount of rainfall and the relative delta values are e.g.:

• with low amount of precipitation the degree of cooling below the cloud mass will be minimal. Because the below-cloud air temperature is high, there will be a significant amount of evaporation below the clouds. The light isotopes preferentially are incorporated into the vapour, leading in isotopically heavy rain (DANSGAARD1964).

## 2.3.2 The meteoric water lines

As shown in the previous section the forming of precipitation due to condensation can be described as an equilibrium process. Within the hydrological cycle, the $^{18}O$ and D stable isotopes of precipitation and fresh surface water correlate on a global scale. This linear correlation, as a best-fit line termed Global Meteoric Water Line (GMWL), is expressed as:

$$\delta^2H = 8 * \delta^{18}O + 10 \text{ (CRAIG 1961)} \qquad \text{(eq.2.10)}$$

This line is an average of many local or regional meteoric water lines, which vary from the global line due to different climatic and geographic parameters. Rain which condensates from water vapour at 20 °C, only under equilibrium conditions would be enriched by the factor ε $^{18}O$ = -9.9 ‰ / ε D = -80 ‰. By calculating the ratio between ε D/ ε D we yield 8.1, which is close to the slope of the GMWL with s=8. The independent term of the equation 2.8 is a value for the deuterium excess (d-excess), which is therefore defined by:

$$\text{d-excess} = \delta^2H - 8 * \delta^{18}O \text{ (DANSGAARD 1964)} \qquad \text{(eq.2.11)}$$

Values for deuterium intercept (d-excess) range from 0 to 20 ‰ but can vary regionally due to variations in humidity, wind speed and sea surface temperature during primary evaporation (CLARK & FRITZ 1997). The d-excess is considered to be conservative and therefore useful for identifying the vapour source area. Air masses originated from the Mediterranean Sea have, due to low relative humidity and high temperatures, relative high d-excess value at about 14‰. While air masses from the Atlantic show d-excess values around 10‰. Values lower than 10 ‰ may be indicative of secondary evaporation processes, e.g. the evaporation of falling raindrops in a warm and dry atmosphere (ARAGUAS - ARAGUAS et al. 2000) which is characteristic for summer rain. The Western Mediterranean Meteoric Water Line (WMMWL) is equal in the slope but differ in the intercept to the GMWL according to:

$$\delta^2H = 8 * \delta^{18}O + 13.7 \text{ (CELLE-JENATON 2001)} \qquad \text{(eq.2.12)}$$

Local or regional meteoric water lines (LMWL) are presented by GARRIDO 2003 derived from rain samples for *Granada* city as:

$$\delta^2H = 6.5 * \delta^{18}O - 1 \text{ } (Granada) \qquad \text{(eq.2.13)}$$

and for the *Sierra Nevada* derived from snow samples taken between 1200 – 2800 masl as:

$$\delta^2H = 7.4 * \delta^{18}O + 8 \text{ } (Sierra Nevada) \qquad \text{(eq.2.14)}$$

These equations representing the $^2H$ and $^{18}O$ relation in the study area for comparable short time periods, and are discussed in section 2.4.

In general, groundwater values of $\delta^{18}O$ from wells in the *Vega de Granada* reflect the volume-weighted mean of recharge precipitation. The local groundwater average of well samples ($\delta^{18}O$=-8.13; $\delta D$=-55.3 (‰-VSMOW)) from the *Vega de Granada* (see section 4.2.5, table 4.7) plots on the intersection of the WMMWL with the LMWLs (eq.2.13, eq.2.14). These regression lines are considered as Local Meteoric Water Line (LMWL), but the WMMWL is a good average of these lines as indicated in Fig. 2.7.
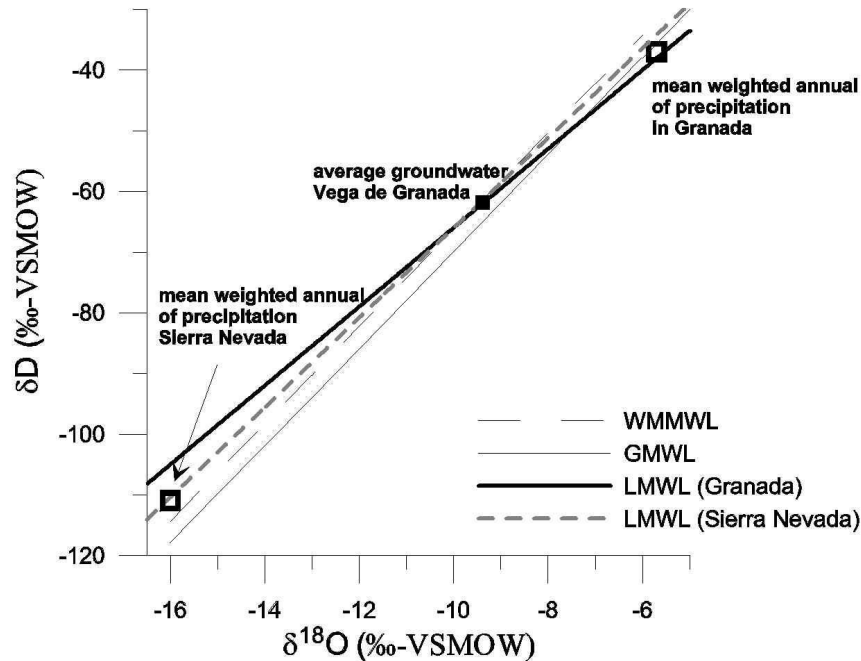


• Figure 2.7 GMWL (Global Meteoric Water Line), WMMWL (Western Mediterranean Meteoric Water Line) and LMWL (Local Meteoric Water Line) for *Granada* (eq. 2.11) and *Sierra Nevada* (eq. 2.12) with the mean groundwater signature from the alluvial aquifer (*Vega de Granada*).

## 2.4 Previous isotope studies relevant for the study area

The seasonal plot of $\delta^{18}O$ from three IAEA precipitation series is plotted in Fig. 2.8 (IAEA-GNIP 2004). The Gibraltar and the Barcelona graphs are quite similar due to their position near at a shore ($\delta^{18}O$ ±3‰), while the Madrid samples show a continental effect ($\delta^{18}O$ ±6‰). IAEA-GNIP data from Spain and Portugal (including samples from the Azores island) is discussed in detail by BEDMAR 1994, and most striking findings are summarised here.
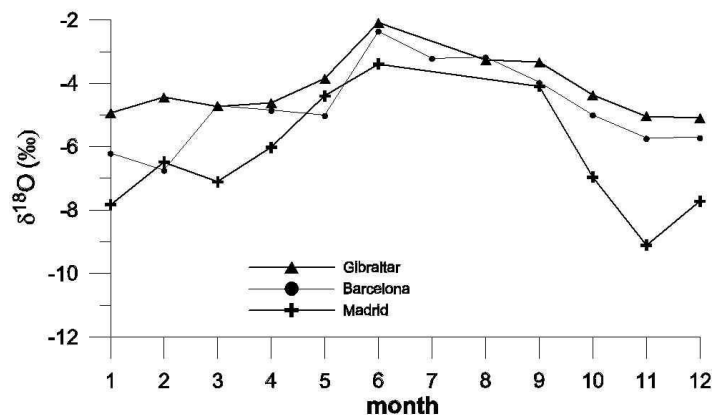


• Figure 2.8 Seasonal variations of $\delta^{18}O$ in Iberian precipitation from IAEA stations based on the monthly means from 1985-1991 (Barcelona), 1988-2001 (Madrid), 1962-2001 (Gibraltar) (all data IAEA-GNIP 2004).

The precipitation-weighted average of $\delta^{18}O$ at Gibraltar is –3.9 ‰ and the monthly average varies between –4.7 and –2.1 ‰. D-excess shows the lowest values in the summer months, with variations from 4.3 (June) to 13 (November). The low d-excess for the summer data suggest high humidity conditions during primary evaporation. The regression line of $\delta^{18}O$ vs. $\delta D$ in the Gibraltar samples is described as (IAEA-GNIP 2004):

$$\delta D = 6.19 * \delta^{18}O + 3 \qquad\qquad (eq.2.15)$$
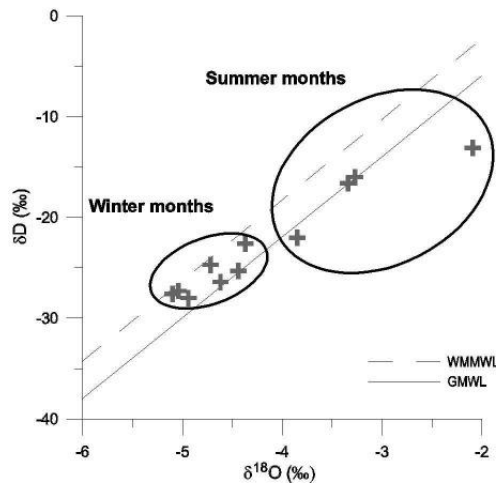


• Figure 2.9 $\delta^{18}O$ - $\delta D$ diagram of IAEA-GNIP data at Gibraltar between 1961 and 2001 with regression trend line (dashed-dotted), GMWL (solid) and LMWL (dashed).

The $\delta^{18}O$ against $\delta D$ values of the Gibraltar samples plot **along** or **below** of the GMWL in the summer months and **between** the WMMWL and the GMWL in winter months (Fig.2.9). Samples of precipitation with heavier (higher) $\delta^{18}O$ and $\delta D$ values tend to fall **below** the GMWL. Considering the climatic conditions at Gibraltar during the summer months (high temperatures) and the sampling method (samples from few and small rain events), this effect could be caused by evaporation in the atmosphere or during sampling.

During the hydrological summer (April – October) the highest amount of precipitation and the most depleted $\delta^{18}O$ values are observed (Fig.2.9). For June a weighted mean value of –2.09 ‰ $\delta^{18}O$ was obtained. Rainfall at the beginning of the rainy season in October has a relatively light isotopic signature of $\delta^{18}O$ with a minimum weighted mean around –5.1 ‰ in December. At the end of the rainy season a general return to heavier (higher) $\delta^{18}O$ and lower d-excess values are observed. Due to the position of Gibraltar at the strait between Atlantic and Mediteranean Sea, it is expected that isotope signatures from precipitation show both climatic influences.

BEDMAR 1994 discusses the stable isotope composition of ca. 800 samples taken from springs and wells and ca. 900 samples from precipitation collected during the last 30 years from Spain and Portugal. In this study a local meteoric water line for the Iberian Peninsula was calculated according to $\delta^2H = (6.84 +/-0.09)\delta^{18}O + (4.35 +/-4.6)$. The deviations from the global meteoric water line are discussed in this paper in detail. Additionally, vapour source analyse were made to distinguish between Atlantic and Mediterranean origin. A contour map of the $\delta^{18}O$ distribution is useful to interpretate local isotope data but in the *Granada* area unfortunately not the necessary precision due to the lack of a sampling network is given (e.g. no $\delta^{18}O$ vs. altitude correlation in the *Sierra Nevada* is visible). Variations of $\delta^{18}O$ - $\delta^2H$ correlation over time from groundwater and precipitation provides information about groundwater recharge processes.

The doctoral thesis from GARRIDO 2003 is about the general composition of stable isotopes ($\delta^{18}$O, $\delta^2$H) of the vapour in the atmosphere and the precipitation in the *Granada* province. This work is used to validate the mean weighted precipitation values in the study area. GARRIDO 2003 calculates here the average value in $\delta^{18}$O for precipitation (rain) in *Granada* with –5.7 ‰ ($\delta$D = -37 ‰), while the average values snow in the *Sierra Nevada* are $\delta^{18}$O = -16 ‰ ($\delta$D = -111 ‰). Analyses of the d-excess in precipitation confirm that the major part of rain bearing air masses for the *Granada* Region is according to GARRIDO 2003 originated from the Atlantic ocean (d-excess ~ 10 ‰). The author found out that isotope composition of atmospheric water vapour show altitude gradients for the *Sierra Nevada* between -0.2 and –1.3 ‰ (for $\delta^{18}$O/100m) and –1 and –9 ‰ (for $\delta$D/100m). Since the formation of vapour in the atmosphere and the formation of rain shows similar altitude dependencies (CLARK & FRITZ 1997), it possible to adapt vapour derived gradients on recharge rain. Regression lines calculated from snow samples taken in the *Sierra Nevada* in altitudes from 1000 – 3000 (masl) vary from $\delta$D = 7.1 * $\delta^{18}$O + 5 in January 2003 and $\delta$D = 7.4 * $\delta^{18}$O + 8 in November 2001. Regression lines from precipitation taken in *Granada* city vary from $\delta$D = 6.9 * $\delta^{18}$O + 2 to $\delta$D = 6.5 * $\delta^{18}$O – 1, while regression line from the *Sierra Nevada* vary seasonal between $\delta$D = 7.4 * $\delta^{18}$O + 8 in January and $\delta$D = 7.1 * $\delta^{18}$O + 5 in March. These calculations can be considered as the local meteoric water lines (LMWL, see eq.2.13 and eq.2.14)).

# 3 Methods
## 3.1 Sampling strategy

Adapted to the objectives (section 1.1), the sampling strategy of this combined study of hydrogeochemistry (major and minor ions) and stable isotope data ($\delta^{18}O$, $\delta D$) was to estimate GWR altitudes and areas for springs and wells. According to this purpose it is necessary to detect possible isotope end-members. To detect the precipitation end-members composition of isotope signatures rainwater, snow or snowmelt were sampled. Rain samples were sampled on different altitudes in order to calculate the local $\delta$-value vs. altitude relation. Sampling strategy directed towards a dense network of springs in the assumed recharge areas (*Sierra Nevada, Sierra de la Peza*) to get a detailed insight on the local isotopic composition. Springs from different altitudes were chosen to detect the altitude effect in isotope signatures and selected sites were sampled frequently to discover temporal variations. The Neogene infilling of the *Granada* depression was sampled widely to get an idea of possible end member composition. Since groundwater of the *Vega de Granada* was supposed to be more or less time constant, a network of wells was sampled once in order to detect spatial differences. Observation wells and pumping wells distributed in the *Vega of Granada* should show representative isotopic signature of this important aquifer. Surface water (rivers, reservoirs etc.) and groundwater from springs show often seasonal variations and were sampled frequently. Additionally, time series at two rivers (*Rio Genil, Rio Darro*) were run with a sampling period of two or three weeks. Important reservoirs (*Quentar, Canales* and *Cubillas*) were also sampled.

## 3.2 Sampling campaigns

Water samples were collected for stable isotope studies ($\delta^{18}O$, $\delta D$), major ($Ca^{2+}$, $Mg^{2+}$, $Na^{+}$, $K^{+}$, $Cl^{-}$, $SO_4^{2-}$, $NO_3^{-}$) and minor ion ($Fe^{2+}$, $Mn^{2+}$, $Sr^{2+}$) analysis in the *Granada* region. Sites within the Neogene sediments of the *Granada* basin and the adjacent eastern mountains (*Sierra Nevada, Sierra Arana, Sierra Padul-La Peza, Las Guajaras*) were sampled. Site locations are shown in Figure 4.15. Sampling campaigns were carried out by the cooperation partners and by the author as listed in chronological order in Tab. 3.1. Each sampling campaign is document Ted in appendix 3 with all in field measured parameters, type of sampled site, location, operating person, laboratory analyses and the internal IGME and FUB declaration.

• Table 3.1 Overview of sampling campaigns in chronological order and measured parameters (further explanation see text)

| Number of samples | Date | Parameters | Institution | sampled site types |
|---|---|---|---|---|
| 13 | Feb 04 | Isotopes/Ions | FUB | springs/snow or snowmelt |
| 4 | May 04 | Isotopes | UGR | springs |
| 73 | June 04 - Sept 04 | Isotopes | UJA | snow or snowmelt |
| 10 | Nov 04 | Isotopes | IGME | observation wells |
| 5 | Dec 04 | Isotopes | IGME | rainwater |
| 3 | Feb 05 | Isotopes | AWI | snow |
| 13 | Feb 05 | Isotopes/Ions | FUB | wells/springs/surface water |
| 105 | Oct 04 - March 05 | Isotopes/Ions | FUB | surface water/ precipation |

The first sampling campaign was carried out in February 2004 by Prof.Dr.Pekdeger (FUB) and Dr.Kohfahl (FUB). They took samples from 12 springs (*Sierra Nevada, Sierra La Peza-Padul*, Neogene basin). Additionally, one snow sample (*Sierra Nevada*) were taken. EC and water temperature were measured with WTW Microprocessor Conductivity Meter LF 196 device. The samples were stored in polypropylene bottles (50ml) with watertight caps. All spring samples were collected for stable isotope studies and ion analysis. For detailed information see appendix 3, tab.a3.1.

Four samples from springs were taken by Prof.Dr.Benavente (UGR) in the Neogene basin and the *Sierra Nevada* yet again. The samples were stored in polypropylene bottles (50ml), for isotopic analysis, and sealed with parafilm to avoid evaporation. EC, pH and water temperature have been measured with unknown devices (appendix 3, tab. a3.2).

During June to September 2004 snow and snowmelt samples were sampled by Dr.Hidalgo (UJA) in high regions (>2200masl) of the *Sierra Nevada*. The samples were taken from small lakes (Spanish: *laguna*), snowmelt or snow. EC and water temperature were measured in field with WTW Conductivity device. The samples were stored in polypropylene bottles (50ml), for isotopic analysis, and sealed with parafilm to avoid evaporation (see Photo 1-4). For detailed information see appendix 3, tab.a3.3. Selected sites are documented with the photos 1-4.

Ten samples of ground water from observation wells and wells in the *Vega de Granada* were drawn in November 2004 at depths right below the water table using a plastic ladle from the IGME staff. Water temperature and E.C. were measured in field with unknown devices (appendix 3, Tab. a3.4).

Five rain samples at different altitudes (670, 1310, 1500, 1550masl) were collected in December 2004 by the IGME. The samples were stored in polypropylene bottles (50ml), for isotopic analysis, and sealed with parafilm to avoid evaporation. No physical parameters were measured in field. Only isotopic analysis were made (appendix 3, tab. a3.5).

Three snow samples were collected by Dr. H. Meyer (AWI) at different altitudes. SP-GR-235 was sampled from a thin snowmelt crust at a snow patch and SP-GR-236 was sampled right below of that melt crust. The samples were stored in double density polypropylene bottles (25ml), for isotopic analysis, and sealed with parafilm to avoid evaporation. No physical parameters were measured in field. Only isotopic analysis were made (appendix 3, tab. a3.6).

13 samples were collected at the 18.2.2005 mainly in the *Vega de Granada*, with logistic support from Prof. Dr. J. Benavente, by the author. Six wells, four springs and three river samples were taken. EC and water temperature were measured in field with a WTW LF196 microprocessor conductivity meter standardised to 20 °C. The pH was measured on site with a combined In gold pH electrode and WTW pH 330/SET hand-held pH/mV meter frequently calibrated using two standard buffers (appendix 3, tab. a3.7).

• Photo 1 *Laguna de los Machos* (X 468241 Y 4100417 Z 2919)



• Photo 2 Snowpatch *Barr. de San Juan Nac. Rio Genil* (X 4103799 Y 467193 Z 2718).



• Photo 3 *Laguna Mula* (X 463052 Y 4101813 Z 2495).



• Photo 4 *Laguna Aguas Verdes* (X 467372 Y 4100518 Z 3059).

Surface and precipitation samples were collected between October 2004 and March 2005 by the author. Five sites at the *Rio Darro* and *Rio Genil* have been sampled every 2 to 3 weeks. Other river sites were sampled only one time. Additionally, three reservoirs (Spanish: *embalse*) were sampled (*Emb.de Quentar*, *Canales*, *Cubillas*). Reservoir and river water samples were filtered on site with 0.2 mm acetate cellulose filters. Rainwater was sampled in March 2005 at two sites (appendix 3, tab.a3.8).

Between October 2004 and March 2005 21 springs in the eastern mountains of *Granada* were sampled to establish a network and to run time series at selected springs. Nine springs were sampled three to five times. EC and water temperature were measured in field with a Multiline P4 (WTW) microprocessor conductivity meter standardised to $20^{o}$C (Tab.5.11). The pH was measured on site with a combined Ingold pH electrode and WTW pH 330/SET hand-held pH/mV meter frequently calibrated using two standard buffers. Eh and $O_2$ measurements sometimes took a long time and might be incorrect. It was tried to measure total alkalinity (referred to as HCO3-) in field but the available time not being sufficient to do so, the

measurements were postponed to the home laboratory (kitchen) upon return. Usually HCl titration was used in the field for the determination of the HCO3$^-$ species. Spring water samples were not filtered. All samples were stored in precleaned polypropylene bottles (50ml). The samples for cation measurements were acidified to pH 2 with ultrapure $HNO_3$, and one bottle of each sample (not acidified) was kept for anion determination. For detailed information see appendix 3, tab.a3.8 and tab.a3.9.

## 3.3 Analysis
3.3.1 Ions

Major ion analysis ($Ca^{2+}$, $Mg^{2+}$, $Na^+$, $K^+$, $Cl^-$, $SO_4^{2-}$, $NO_3^-$) and minor ion analysis ($Fe^{2+}$, $Mn^{2+}$, $Sr^{2+}$) data was conducted at the Hydrogeology Laboratory for AMS and ICP measurement at the FUB. For precision of measurement, analytical method and measurement devices see appendix 3, tab. a3.10 and tab.a3.11.

3.3.2 Stable isotopes analysis

$\delta D$ and $\delta^{18}O$ were measured by the AWI (Dr. H. Meyer) mass spectrometer using the equilibrium method (MEYER et al 2003). Analyses were done on carbon dioxide that has equilibrated with the water sample at a constant temperature (18 ±0.01 $^o$C). Only 5 ml water were added to reaction vessels, then evacuated by pumping and connected to the mass spectrometer. This technique was improved to fully automated procedures and both species can be measured in one run. The precision of measurement is approx. 0.1 ‰ for $\delta^{18}O$ and 0.8 ‰ for $\delta^2H$, but is in most cases significant smaller. The precision in isotope measurement ranges between 0.02 ‰ and 0.09 ‰ in $\delta^{18}O$ and between 0.1 ‰ and 0.4 ‰ in $\delta D$. Each laboratory is using its own standards, which are calibrated against the VSMOW standard (appendix 3, tab.a3.10).

## 3.4 Climate

The calculations of the groundwater recharge are based on a database provided by the IGME and Junta de Andalucia website (www.juntadeandalucia.es). The data contains monthly and daily measurements with different time periods (oldest one 1/1902 *Observatorio Cartuja*) for 28 stations within and around the study area (appendix 3, Tab.3.14). Due to the lack of more meteorological stations in the Sierra Nevada (only one available) precipitation (P) was extrapolated according to the western slope gradient in mean annual precipitation, which is 70mm/100m (CASTILLO 2000). Thus maximum P is approximately 1330 mm/a in 3400 masl, which corresponds to the lowest estimation of previous works (e.g. CASTILLO 1985). At lower altitudes more meteorological stations are available and measured data was used to interpolate an isohyetal map. Temperature gradients for the Sierra Nevada are given by DELGADO CALVO-FLORES et.al 1989 as: T (°C) = 18.457-0.0061 * Altitude (masl). An ACCESS climate database was set up with all the above mentioned data to handle the different parameters.

To avoid mistakes, e.g. variable time periods, trend graphs were calculated. As shown in Fig3.1 (a-d) no significant trend is observable. From this data, the yearly average was calculated and an isohyetal map was calculated by using the software Surfer 7.0 with the kriging interpolation method. The variogram settings were modelled with Surfer 7.0 and applied. The map was imported to ArcView 3.2 and converted to a raster by using a linear minimum curvature (Fig.1.6).



a)

b)

c)

d)
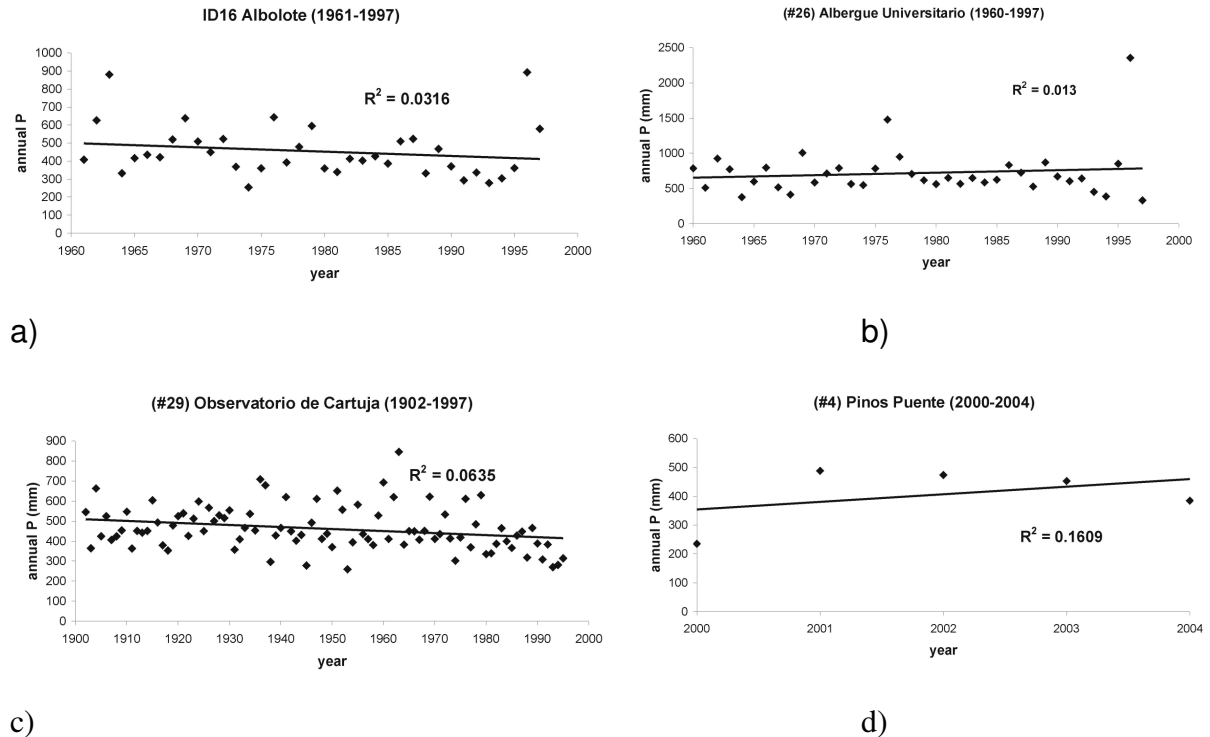
• Figure 3.1 (a-d): Trend analysis of different time periods and stations within the study area.

## 3.4.1 Climatic groundwater recharge potential

Groundwater recharge (GWR) for the study area was calculated according to the general equation P = ETA + R + GWR (P = precipitation, ETA = actual evapotranspiration, R = runoff). Climate information from 6 different meteorological stations in the study area was used (appendix 2, tab. a2.1 – a2.6).

Unfortunately no data about soil moisture, soil moisture changes over time and soil depths were available. Thus soil moisture storage and its change over time was not taken into account. Only one data set from stations located in the *Sierra Nevada* east of the basin (the potential recharge area) could be obtained. For that reason the climatic parameters for a "virtual" station were extrapolated.

Since it was not possible to quantify surface runoff (R), it was put together with the groundwater recharge (GWR). Actual evapotranspiration was calculated according to TURC (GRAY 1973) and COUTAGNE (REMENIERAS 1974).

.
TURC: $ETA = P / [0.9 + (P/J)^2]^{0.5}$ $J = 300 + 25*T + 0.05*T^3$
with P = mean annual precipitation [mm]; T = mean annual temperature [°C]

COUTAGNE: $ETA = P - \lambda * P^2$ $\qquad\qquad \lambda = 1 / (0.8 + 0.14 * T)$

with P = mean annual precipitation [m]; T = mean annual temperature [°C]
(valid for 1/8 $\lambda$< P [m/a]< ½ $\lambda$)

For calculations with more complicate equations like HAUDE or SCHROEDER & WYRNICH (MEYER & TESMER 2000) equation the necessary parameters were missing or not suitable for semiarid regions.

Generally the ETA values obtained with the TURC equation were lower, for all 13 stations leading to positive GWR. With the Coutagne equation higher amounts of GWR were calculated. It should be considered that the calculations were simplifications of natural processes and due to the semi-empirical character of the equations a deviation of about ±15-20% was assumed.

Using the salt balance method for the calculation of the groundwater recharge was impossible, since intensive agricultural use in the *Granada* basin and geogene salt modify chloride concentrations in the ground water.

## 3.5 Digital elevation map

A digital elevation map (DEM) was derived from a contour line shapefile (*Mapa Digital de Andalucia*). The shapefile was transferred to ASCII format by using a modified avenue script in ArcGis 3. With Surfer 7.0 the txt-file is converted to a 100x100m cell size grid using the kriging interpolation method with the adapted variogram settings. The software Global Mapper 6.0 was used to convert the surfer grid to USGS DEM format. Now the DEM can be used for spatial analysis (catchment delineation, climate etc.) in ArcGis 3.2. With the DEM and the ArcGis Hydro extensional tool catchment delineation calculations were made.

## 4 Results and Discussion

4.1 Hydrochemistry

In this section graphical and statistical methods were used to classify the water samples into groups with similar geochemical characteristics. First a reliability check was made to confirm the validity of the measured sample data. Electrical balance and total dissolved solids (TDS) vs. Electrical conductivity (EC) was used to perform this reliability check.

4.1.1 Reliability check

The amount of positive ions and complexes with consideration of their valency and the amount of negative ions and complexes must be equal. The hydrochemical analysis, given in mg/l, were transformed to mmol(eq)/l [(meq/l)] and the electrical balance was calculated according to (DVWK 1992):

$$balance\,(\%) = \frac{\sum Cations - \sum Anions}{\left(\sum Cations + \sum Anions\right) \cdot 0.5} \cdot 100 \qquad (eq.4.1)$$

According to equation 4.1 analyses higher than 5% were considered as failed. Figure 4.1 shows that only two of the measured samples (n = 54) are out of the tolerance limit and therefore not used for further calculations.
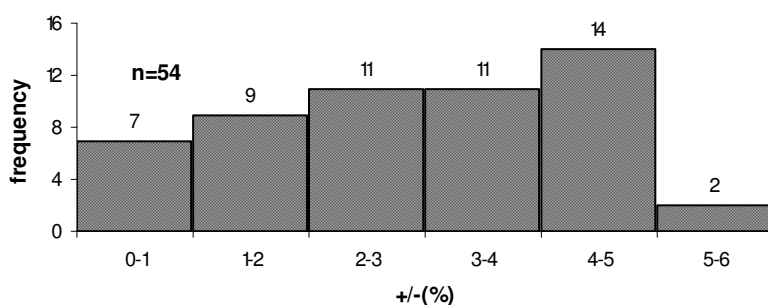


• Figure 4.1 Electrical balances vs. frequency of measured samples.

TDS are the salts of calcium, sodium, potassium, magnesium, hydrogencarbonat, chlorides and sulphates, additional minor amounts if organic solvents. TDS is calculated using the equation:

$$TDS\,(mg/l) = Ca^{2+} + Mg^{2+} + Na^{+} + K^{+} + SO_4^{2-} + Cl^{-} + NO_3^{-} + HCO_3^{-} \qquad (eq.4.2)$$

The results of the calculations were shown in appendix 4, tab.a4.1. TDS values for the precipitation samples range from 7 – 16 mg/l, springs showed variations between 33 – 540 mg/l while the thermal springs had values between 2000 – 3500 mg/l. The pumping well samples values vary between 300 – 1900 mg/l. Values between 68 – 280 mg/l were calculated

for surface water in the mountains, while river samples in the *Vega de Granada* were between 910 – 9900 mg/l. The highest TDS value (9900 mg/l) was calculated from a river sample (*Arroyo de Salado*), which drains the southern part of the Granada basin.

EC is the measurement of the total dissolved salts based on current flow. EC, measured in μS/cm or mS/cm, is the reciprocal value of electrical resistivity. EC is positive proportional to the amount of total dissolved salts.

The EC measurements made in this work, ranged in the precipitation samples from 13 - 125 μS/cm. Springs showed values from 77 – 850 μS/cm, while the thermal springs had values between 750 – 3500 μS/cm. Pumping well samples vary between 820 – 1700 μS/cm. Values between 130 – 440 μS/cm are measured for surface water in the mountains, while river samples in the *Vega de Granada* alluvial aquifer showed variations between 1500 – 15600 μS/cm.

EC and TDS are both parameters for the total dissolved amount of salts in a water solution. Therefore, they must be directly proportional to each other. Figure 4.2 shows the correlation between EC and TDS with the mathematical approximation of:

$$TDS = 0.57 \cdot EC \qquad \text{(eq.4.3)}$$

The best fit to the regression line is between 150 – 500 μS/cm. Low (<150 μS/cm) show minor deviation from the regression line due to high dilution.
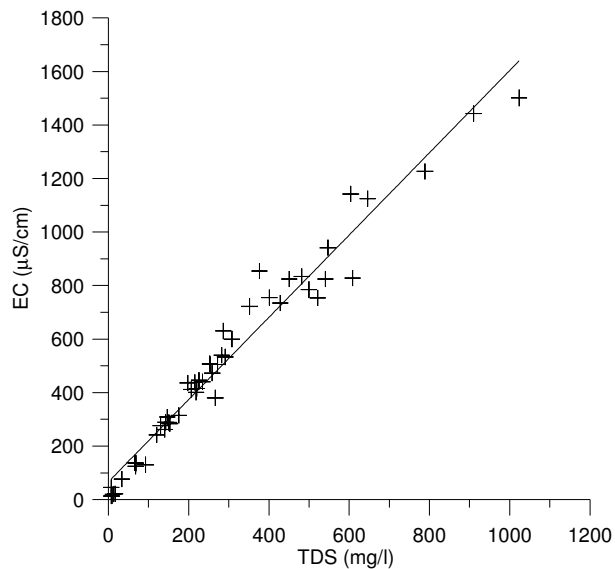


• Figure 4.2 Linear relation between EC and TDS of measured samples.

28

## 4.1.2 Classification and characterisation of water samples

With the software Aquachem 4.0 chemical analysis were plotted in piper, stiff and schoeller diagrams to visualise general chemical characteristics. The spatial distribution of major chemical constituents, presented as stiff diagrams is shown in connection to a simplified geologic map. Additionally, saturation indices (SI) were calculated and carbonate chemistry was modelled with the software PHREEQC 2.11.

For a given reaction ( $a \cdot A + b \cdot B \Leftrightarrow c \cdot C + d \cdot D$ ) the degree of saturation, the solubility product ($K_s$) of a mineral phase in aqueous solution is compared to the product of ion activities $[A]_{sample}$ and $[B]_{sample}$ (IAP) described by:

$$K_s = \frac{[C]^c \cdot [D]^d}{[A]^a \cdot [B]^b} \qquad (eq.4.4) \qquad IAP = [A]^a \cdot [B]^b \qquad (eq.4.5)$$

The ratio between the ion activity product and solubility product $K_s$ is the saturation state with respect to a certain mineral. In general, the logarithm of the saturation state is used, according to:

$$SI = \log \frac{IAP}{K_s} \qquad (eq.4.6)$$

The SI is a calculation of how much a certain mineral phase has dissolved in groundwater relative to the amount it can potentially solve. Negative values indicate an undersaturation with respect to the considered mineral phase, while positive values indicate an oversaturation. Because of the logarithmic scale of the SI a value of +1 means that the sample is 10 times oversaturated. In praxis a SI of ± 0.2 (2 times over- or undersaturation) is treated to be in equilibrium with the mineral phase. Since no pH and alkalinity was determined for samples taken before September 2004, calculation of SI was made for only for spring, well and surface water samples taken between October 2004 and March 2005.

The piper plot (Fig.4.3) shows all measured samples, which were classified according to their major chemical composition. 4 main groups and one single sample (brine) can be distinguished. Most samples were classified as earth alkaline waters with prevailing bicarbonates (group 1) or prevailing sulphate (group 2). Group 3 members (thermal springs) can be subdivided into earth alkaline water with prevailing sulphate (*Fte. Urquiza*) and earth alkaline water with increased alkalis and prevailing sulphate and chlorides (baths or Spanish: *baños*). The low mineralized samples (group 4) are earth alkaline water with prevailing bicarbonates. The brine sample from the *Arroyo Salado* can be described as alkaline water with prevailing sulphate and chloride.
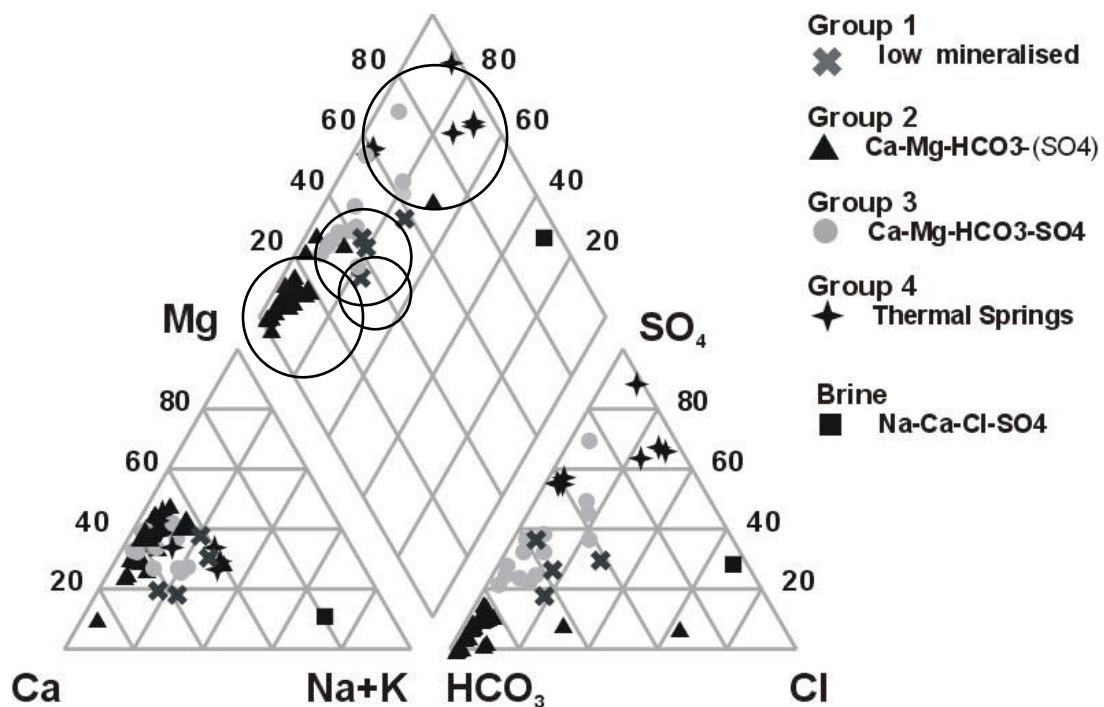


• Figure 4.3 Piper plots of all hydrochemical analysis.

## Group 1 (low mineralized, EC<100µS/cm)

Group 1 members have electrical conductivities <100 µS/cm. These low mineralized samples consisting of 3 rain water samples (*Granada* city) and 1 sample (*Arr. Caballo*) from a stream (ephemeral river) in the *Nevado-Filabride* metamorphic domain which was taken during snowmelt period. Due to the high dilution of these samples watertype declaration is not expressive and therefore not made. Locations are shown in fig. 4.15 together with all sites for isotope sampling. A calculation of saturation indices makes no sense for group 1 members. Stiff diagrams are constructed by plotting the 4 major anions and major cations (in meq/l) as indicated in figure 4.5. Stiff plots are used to evaluate the change in water composition as the water flows through different geological formations. First priority in precipitation samples is the study of isotope signatures.
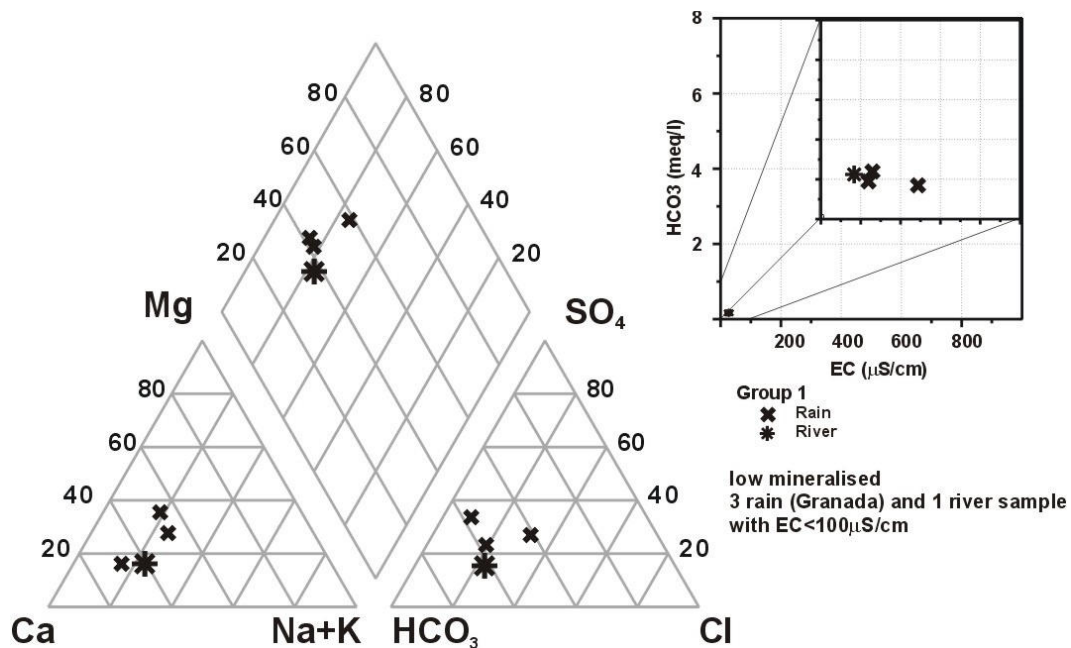


• Figure 4.4 Piper plot and EC vs. HCO₃ scatter of group 1 members.
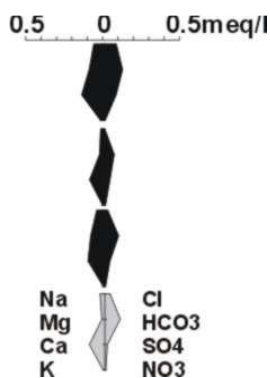


• Figure 4.5 Stiff plot of river (grey) and rain (black) samples (group 1).

## Group 2 (Ground- and surfacewater of Ca-Mg-HCO3-(SO4) type)

The samples of group 2 members were taken from 15 springs located in the units of the *Alpujarride* carbonate complex, 3 sites situated (*Fte. Alta, Barr. de San Juan, Arr.Caballo*) in the *Nevado-Filabride* metamorphic complex, 5 samples (*Fte.Palmones, Fte. Molinos, Fte. de Vita, Rio Genil2, Rio Darro2*) located in the basin sediments (Mio-/Pliocene) and 1 sample (*Alhencira*) located in the *Vega de Granada* alluvial aquifer (Quaternary). Site locations and stiff diagrams are shown in connection to a simplified geological map in figure 4.7. Between the Feb.04 and subsequently taken samples no or very little variations over time were observed, therefore only one stiff diagram per site is printed.

*Barr. de San Juan* (*Rio Genil 1*), *Rio Genil 2* and *Arr. Caballo* are samples from rivers or streams and classified as Ca-Mg-HCO3-SO4 type. These samples are due to their low mineralization and high bicarbonate concentration also group 2 members. The well sample (*Alhencira*) represents rather the composition of the carbonate springs than wells and is therefore classified as group 2 members.

Group 2 members have electrical conductivity ranging between 77 and 854 µS/cm and containing between 0.36 and 7.03 (∅3.6) mmol/l $HCO_3$. All samples lie in a relative narrow pH range between 7.2 and 8.1 (Tab.4.1). Within this pH range the dissolved inorganic carbon exists almost entirely as $HCO_3$ species and suggests that open-system conditions dominate (FREEZE & CHERRY 1979). The scatter diagram of EC vs. $HCO_3$ (Fig.4.6) shows the geochemical

• Table 4.1 Summary of group 2 physical parameters and saturation indices.

| n=33 | T | pH | E.C. | SI Calcite | SI Dolomite | SI Anhydrite | SI Gypsum |
|---|---|---|---|---|---|---|---|
| Min | 6.00 | 7.2 | 125 | -2.24 | -4.83 | -4.29 | -4.03 |
| Max | 17.10 | 8.1 | 854 | 0.76 | 1.16 | -1.77 | -1.52 |
| Med | 11.47 | | 417 | -0.35 | -0.98 | -2.85 | -2.59 |

evolution of springwater from low mineralized water (*Fte. Alta)* in the metamorphic core (*Nevado-Filabride*) to higher mineralized springwater in the *Alpujarride* carbonate complex.

A parameter determining differences in carbonate geochemistry of the host-rock area is the molar $Ca^{2+}:Mg^{2+}$ ratio. Geochemical modelling was made for a PHREEQC input file (appendix 4, tab. a4.2), with rainwater (taken in *Granada* city) as the initial water which was equilibrated $CO_2$ (log $pCO_2$=-2) and then equilibrated to calcite and dolomite separately and in sequence. These calculations show that dominant calcite dissolution results in a high molar $Ca^{2+}:Mg^{2+}$ ratio (far above 2), while dolomite dissolution shows a theoretically stochiometric 1:1 relation. This finding is due to the higher solubility of calcite, which is a reason for the fact that hardly no carstification in dolomite rocks is found. However, in the study area it is more common that dolomite and calcite coexists (Fig.4.7) and this results in ratios which are around 1.4. These geochemical fingerprints can be recognized in Piper diagrams (e.g. Fig.4.6).

Cations of group 2 members are mainly composed of Ca and Mg, with a ratio between 0.9 and 7.0 with an average ratio of 2.1 (appendix 4, tab.a4.4). As indicated by calculations with PHREEQC these ratios are typical for dolomite dissolution (1.0) or dolomite dissolution in

the presence of calcite (1.4). It is obvious that springs show a positive trend in mineralization from the metamorphic core (*Nevado-Filabride*) to the carbonate domain (*Alpujarride*), reflecting the assumed flowpath from the recharge area to adjacent areas (Fig.4.6). The trend in the molar $Ca^{2+}$:$Mg^{2+}$ ratio develops analogous.
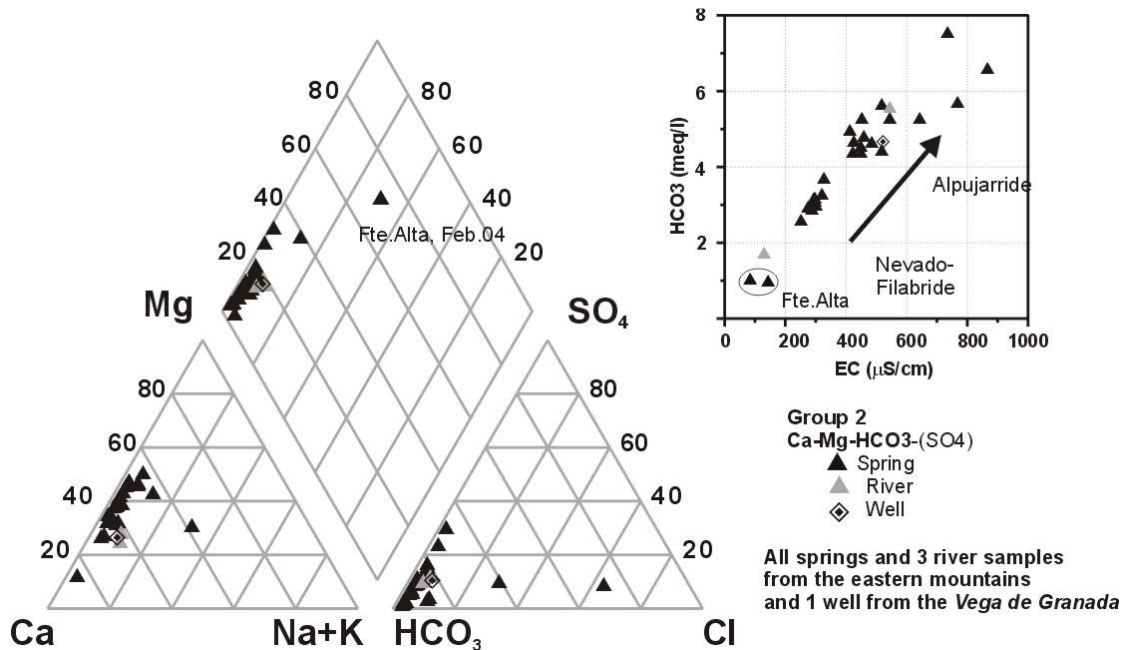


• Figure 4.6 Piper plot and EC vs. HCO₃ scatter of group 2 samples.

Unlike within group 3 sulphate concentrations are low ($\varnothing SI_{CaSO4}$= -2.59, $\varnothing SI_{CaSO4*2H2O}$ = -2.14) (compare Tab.4.1 to Tab.4.2). The predominant ions are Ca, Mg and $HCO_3$ and the percentage of alkali elements Na and K is low. Only *Fte.Savina* shows an exceptional high content in $SO_4$.

*Fte. Alta* is located at a road to a ski resort and the February 04 (Fig.4.6) sample shows an increased content in Na and Cl. This was probably caused by contamination from road-salt during the ski season. The sample, taken in Oct.04 can be considered as less influenced by anthropogenic impacts.

*Fte. Grande* samples show an exceptional high content in hydrogencarbonat (ca. 260 mg/l) and a pH = 7.7 which is significant above the average. This sample is classified as $HCO_3$ type. As shown by the simplified geological map (Fig.4.7) the spring is situated in carbonate rocks belonging to the *Alpujarride* domain.

According to the geological map (Fig.4.7) a spatial coincidence between the distribution of calcite/dolomite host-rocks and the molar $Ca^{2+}:Mg^{2+}$ ratio around 1.4 is given in most of the cases. The geochemical calculation of saturation indices shows that almost all springs are undersaturated or close to the equilibrium with respect to dolomite and calcite.
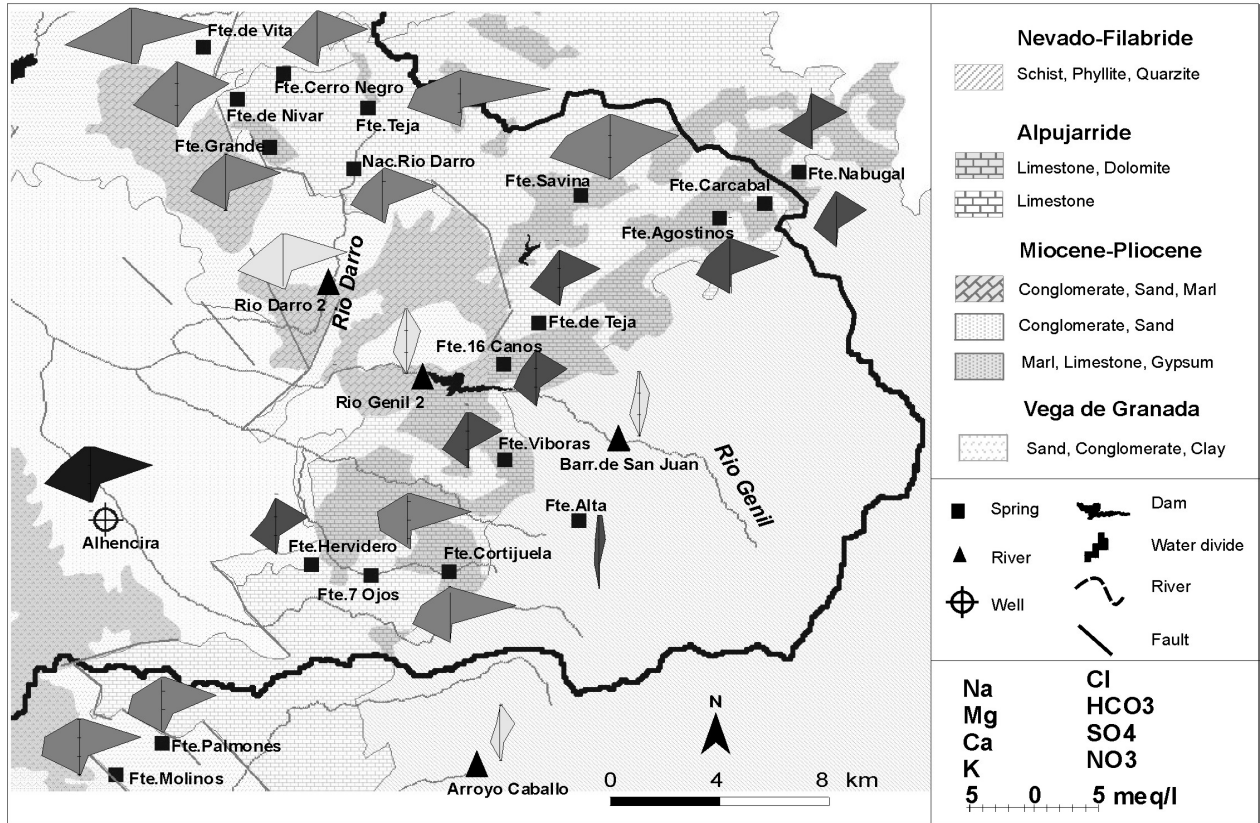


• Figure 4.7 Location map of group 2 members, simplified geology and stiff diagrams of spring (grey), river (light grey) and well (black). Geology simplified from IGME 2002.

## Group 3 (Ground- and surfacewater from the *Granada* basin of Ca-Mg-HCO3-SO4-type)

Group 3 members have electrical conductivities ranging between 380 and 1710 µS/cm and containing between 3.45 and 7.24 $HCO_3$ ($\varnothing$ 5.4 mmol/l). The high Ca concentrations of this

group (61-240 mg/l) leads to an over saturation of calcite (appendix 4, tab.a4.5). The summary in tab.4.2 shows that group 3 members are over or close to the equilibrium with gypsum ($SI_{CaSO4*2H2O}$ = -0.37 to 1.14), while Anhydrite is still undersaturated.

• Table 4.2 Summary of group 3 physical parameters and saturation indices.

| n=10 | T | pH | E.C. | SI Calcite | SI Dolomite | SI Anhydrite | SI Gybsum |
|---|---|---|---|---|---|---|---|
| Min | 11.5 | 7.03 | 380 | 0.05 | -0.04 | -2.07 | -1.82 |
| Max | 15.7 | 8.10 | 1701 | 0.72 | 1.14 | -0.82 | -0.57 |
| Med | 14.1 | | 990 | 0.27 | 0.35 | -1.48 | -1.23 |

The samples of group 3 members were taken from 5 wells, 2 surface water sites and 1 spring located in the *Vega de Granada* alluvial aquifer (Quaternary), 2 samples were taken from a spring (*Fte. los Fagailos* ) and surface water site (*Rio Genil 3*) located in the basin sediments (Mio-/Pliocene) (Fig.4.9). The samples are classified as Ca-Mg-HCO3-SO4 water types, except for *Rio Genil 3* classified as Ca-Mg-HCO3-Cl-SO4 type.
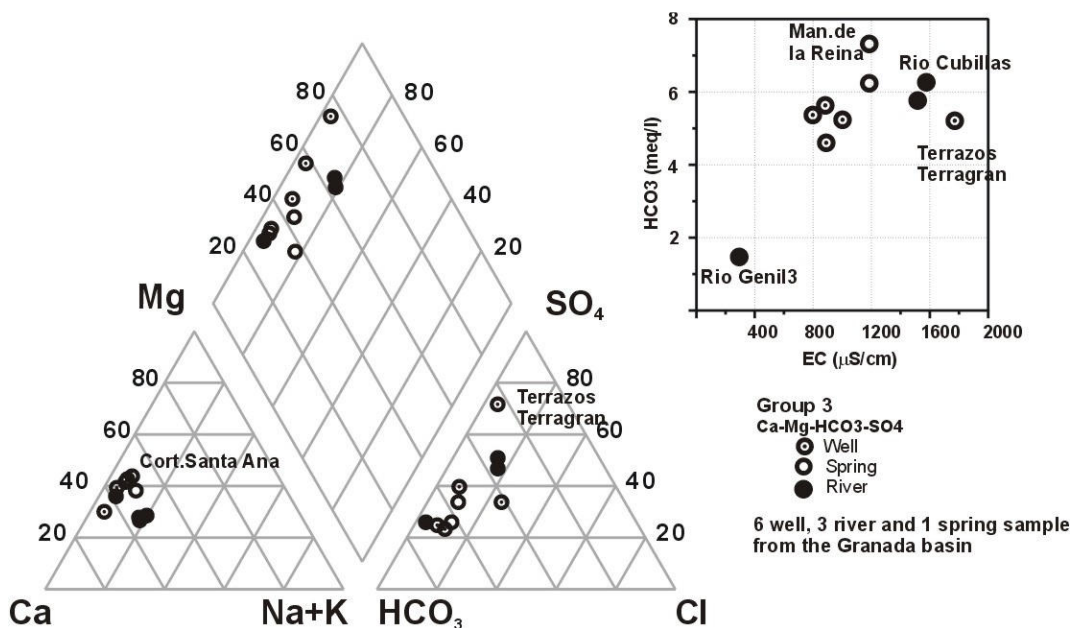


• Figure 4.8 Piper plot and EC vs. $HCO_3$ scatter of group 3 members.

The chemical composition of the well sample (*Cortijo de Santa Ana*) shows the typical features of a carbonate influenced groundwater which is dominated by Ca, Mg, $HCO_3$ and minor amounts of K, Cl, and $SO_4$. On the basis of this chemical signature the water sample from is supposed to be influenced by water derived from the *Sierra Elvira* carbonate rocks.
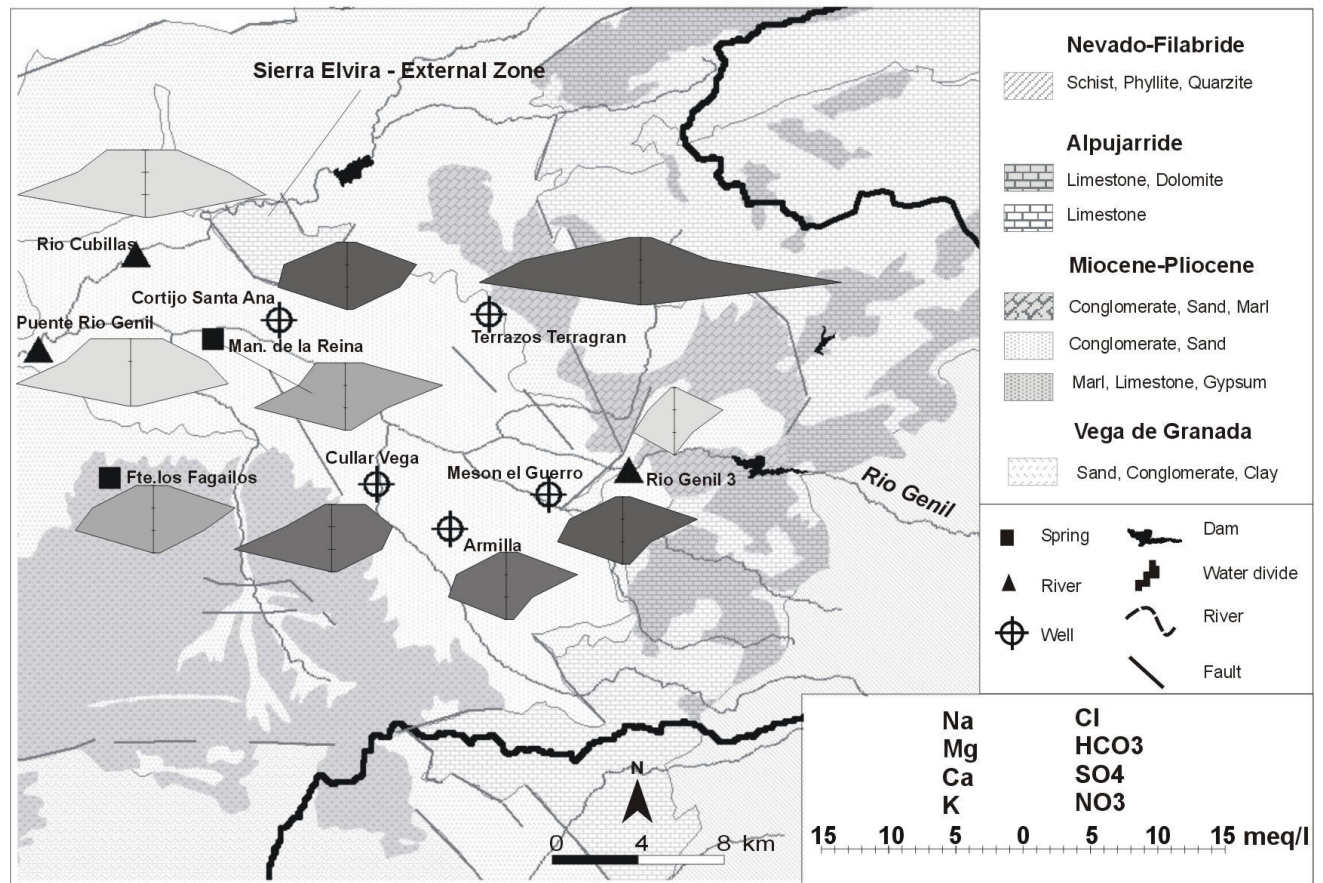
• Figure 4.9 Location map of group 3 members, simplified geology and stiff diagrams of well (dark grey), river (light) and spring (grey) samples. Geology simplified from IGME 2002.

Samples from the south-eastern part of the *Vega de Granada* showing a chemical composition very similar to springwater classified as group 2, but are due to their high content in sulphate group 3 members. Approximately at *Man. de la Reina* the former influent groundwater flow regime (*Rio Genil-Vega de Granada)* becomes effluent, and the chemical composition represents the shallow groundwater chemistry.

The water sample from *Terrazos Terragren* shows a very unique composition. This sample was higher mineralized than all other groundwater samples (EC=1600μS/cm). Dominant ions are Ca and SO4, followed by Mg and HCO3. This industrial well shows a very high content in CaSO4 (Gypsum), which cannot be explained by local geology and is therefore probably contaminated by the industrial plant itself.

All samples have Nitrate concentrations below 50mg/l, though the *Vega de Granada* is considered to be one of the highest polluted aquifers in Andalusia. The effect of dispersion in the unsaturated zone is likely to eliminate the seasonal input of nitrate due to fertilizers. It is possible that the nitrate front which migrates slowly downwards with maybe 0.5 m/a has not yet arrived the groundwater table.

## Group 4 (Thermal springs in the *Granada* basin)

Group 4 samples have water temperatures >20 ºC and are according to HÖLTING 1997 classified as thermal water. The sample sites are located in the *Vega de Granada* alluvial aquifer (Quaternary) (*Baños de Sierra Elvira*) and in the marine/terrigenous basin sediments (Mio-/Pliocene). Locations are shown in figure 4.15. Group 4 members show two subgroups with respect to EC values and general chemical composition:

• 4a - ∅ EC = 800 µS/cm with prevailing sulphate (*Fte.Urquiza*)

• 4b - EC>2600 µS/cm with increased alkalis and prevailing sulphate and chlorides (*Baños de la Malah, Baños de Santa Fe, Baños de Sierra Elvira*).
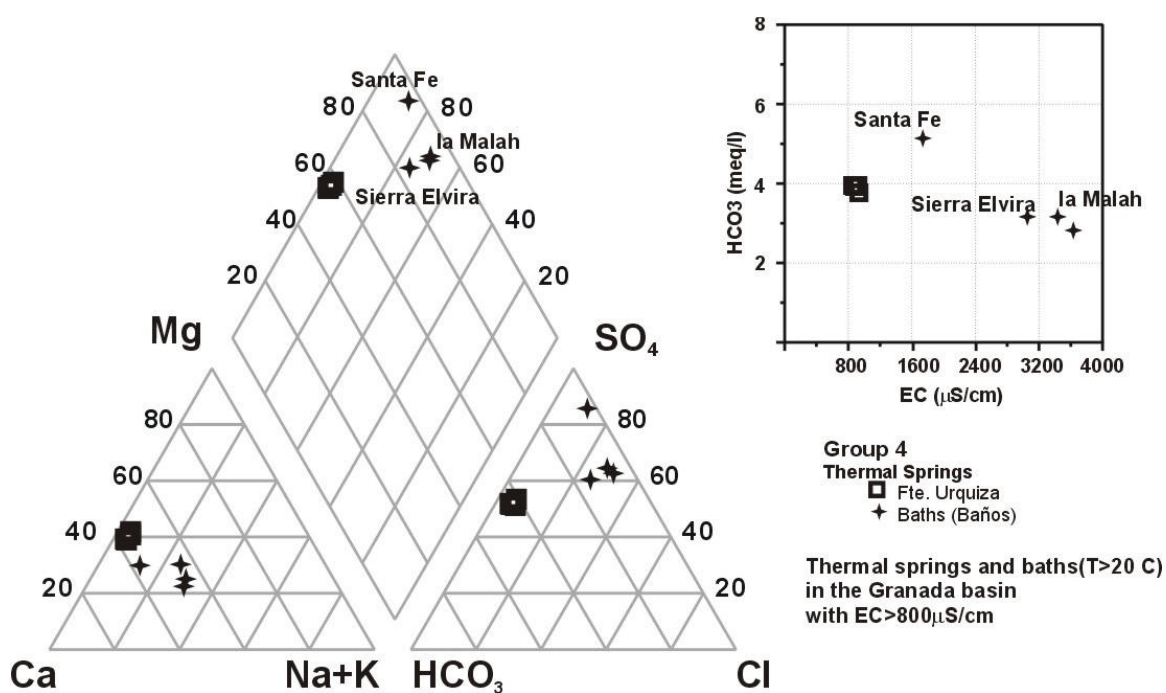


• Fig.4.10 Piper plot and EC vs. HCO3 scatter of group 4 members.

Subgroup 4a samples (*Fte. Urquiza*) were taken from a double tube spring with water temperatures around 25 ºC. Both tubes show a very similar chemical composition to each other and over time. *Fte.Urquiza* is used by the local population for medical purposes and classified as Ca-Mg-SO4-HCO3 type. The low mineralization, the low temperature and the low content in alkalis and earthalkalis indicates that this spring is more influenced by shallow groundwater derived from the eastern mountains compared to the other thermal springs (Fig.4.11). The increased sulphate (∅ 226 mg/l) and calcium concentration (∅ 100 mg/l) indicating gypsum bearing host-rocks on the flow path of this spring (e.g. Messinian evaporites). The dominant ions are Mg, Ca and $HCO_3$ indicating calcite bearing host-rocks on the flow path (e.g. *Alpujarride*).

Subgroup 4b samples (n=4) were taken from thermal springs termed *Baños* (baths). Samples were classified as Ca-Na-Mg-(Cl)-(SO4) or Ca-Mg-SO4-type. These samples are characterized by relative low pH values (7.1 – 7.3). *Baños Sierra Elvira* and *Baños Santa Fe* are located on a virtual line from the southwest of the *Granada* basin (*Alhama de Granada*) to the northeast (*Sierra Elvira*). This line coincides with the External/Internal zone boundary (see chapter 5, Fig.5.13). This fact leads to the assumption that the occurrence of thermal springs is close connected to deep reaching tectonic fault zones. *Fte.Urquiza* and *Baños de la Malah* are located on a fault system which is perpendicular to External/Internal and strikes from northeast to the southeast (compare chapter 5, Geological Mapping). This approximately NE-SW striking fault system is related to extensional tectonical motions (LOPEZ-CHICANO et al. 2001).
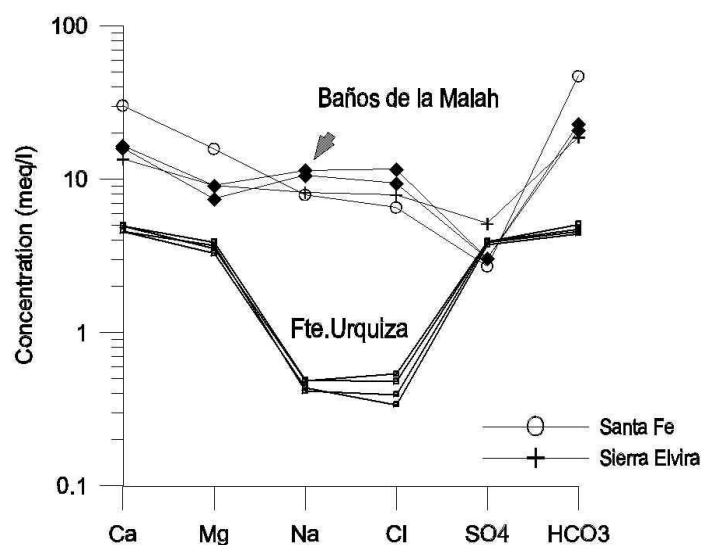


• Figure 4.11 Schoeller diagram of thermal springs (group 4).

Chemical characteristics of group 4 members are visualised by a semi logarithmic plot of concentration (meq/l) vs. major constituent, termed as Schoeller diagrams. The semi logarithmic scale allows visualising a wide range of concentration and mixing effects are expressed in vertical shifts of the lines without a change in shape. Different water types will be displayed by crossing lines. The hydrochemical differences between the two subgroups are illustrated in figure 4.11.

• Table 4.3 Summary of group 4 physical parameters and saturation indices.

| n=8 | T | pH | E.C. | SI Calcite | SI Dolomite | SI Anhydrite | SI Gybsum |
|---|---|---|---|---|---|---|---|
| Min | 21.0 | 7.0 | 754 | -0.269 | -0.585 | -1.502 | -1.273 |
| Max | 36.6 | 7.6 | 3700 | 0.393 | 0.733 | -0.184 | -0.023 |
| Med | 25.2 | | 1926 | 0.006 | -0.068 | -1.046 | -0.830 |

## Single sample (Brine from the river *Arroyo Salado*)

The brine sample was taken from the river *Arroyo de Salado*, which drains an area of approx. 170 km$^2$ in the southern part of *Granada* basin (Tab.1.1). In this part of the basin marine
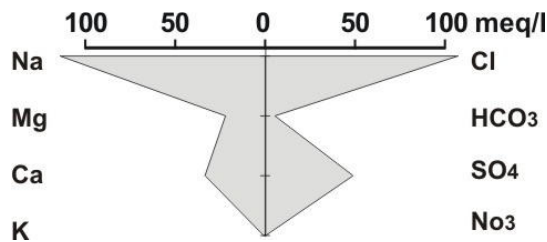


• Fig.4.12 Stiff diagram of brine sample (*Arr.Salado*).

evaporites, like gypsum and halite, are largely cropping out. The high alkali content with prevailing sulphate and chloride leads to the classification as Na-Ca-Cl-SO4. Geochemical calculations of this high mineralized sample (EC=15 500μS/cm) shows that Ca- and Mg-Carbonate minerals are strong oversaturated (e.g. $SI_{calcite}$= 1.51, $SI_{Dolomite}$ = 2.69, $SI_{Aragonite}$=1.35). Gypsum is saturated with $SI_{CaSO4*2H2O}$ =-0.05, while Anhydrite is still undersaturated $SI_{CaSO4}$ = -0.31. The high Sr concentration of 14 500 ppb leads to saturation of Sr sulphate minerals ($SI_{Coelestin}$= 0.0). This might be explained by intense Coelestine mining in the south-eastern part of the Mio/Pliocene basin formations. Iron oxides are also highly oversaturated $SI_{Fe(OH)3}$= 4, $SI_{Goethite}$= 9.

It is important to recognise, that the geochemical calculation of SI are based only on the analysed ions as shown in section 3.3.1 and do not account for silicate minerals.

## 4.1.3 Carbonate chemistry

In the study area dissolution and precipitation of carbonate minerals plays an important hydrochemical role because of the widespread distribution of calcite and dolomite host-rocks. The amount of calcium carbonate that recharge water can dissolve is controlled by temperature, pH and pCO$_2$ conditions in the soil zone. The higher the CO$_2$ concentration (expressed as carbonic acid, H$_2$CO$_3$) of the water, the lower its pH and the more aggressively the water dissolve carbonate minerals, according to:

$$CaCO_3 + H_2CO_3 \rightarrow Ca^{2+} + 2HCO_3^- \qquad \text{(eq.4.7)}$$
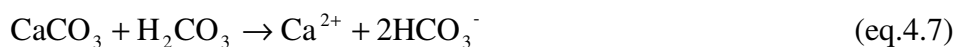
According to the equilibrium concept water from precipitation that flow through carbonate rocks dissolves calcite and dolomite to the point of saturation. As the water now encounters carbonate minerals in the saturated zone, carbonate specie H$_2$CO$_3$ is converted to HCO$_3$, decreasing H$_2$CO$_3$ content and partial CO$_2$ pressure (FREEZE AND CHERRY 1997). If this dissolution takes place in the unsaturated zone where abundant CO$_2$ is present this geochemical environment is termed as open-system condition (pCO$_2$ = const.). Controversy, closed-system conditions means that no delivery of atmospheric or soil CO$_2$ from the gas phase occurs, and the CO$_2$ will be consumed. Therefore, the equilibrium with Carbonate minerals is much sooner reached under closed-system conditions.

Calculations for calcite dissolution under closed- and open-system conditions were made with PHREEQC 2.1. The line of CaCO$_3$ saturation in pure water (for input file see in appendix 4, tab.a4.7) was calculated with T=10°C and pCO$_2$ = -2. A second input file calculates the molar

concentrations of dissolved $Ca^2$ in relation to $pCO_2$ under closed- and open-system conditions (input file in appendix 4, tab.a4.8). This file uses as an initial solution a rain sample from *Granada* city which was equilibrated with two $CO_2$ pressures representing atmospheric ($pCO_2$ = -3.5) or soil $CO_2$ ($pCO_2$ = -2) and equilibrated to either $CaCO_3$ without replenishing $CO_2$ (closed-system) or $CaCO_3$ with constant $pCO_2$ (open-system) conditions. By plotting the molar concentrations of dissolved $Ca^{2+}$ in the ground water (springs, wells) against $pCO_2$ and then considering where the data lie relative to theoretical carbonate trajectories it should be possible to associate the samples to the assumed open or closed-system system conditions.

The semilogarithmic plot of $CO_2$ (mol/l) against Ca (mol/l) shows the spring samples (group 2) and well (group 3) members with consideration of possible hydrochemical evolution pattern (Fig.4.13). Vertical lines indicate open-system dissolution with different initial $pCO_2$ values (-2 and –3), while closed-system dissolution will evolve on curvature lines. The line of saturation (SI=0) with respect to calcite divides the samples taken from wells and springs. Spring samples (group 2) almost always plot below the line of saturation, indicating the geochemical evolution from recharge water in high regions with atmospheric $CO_2$ ($pCO_2$ = -3.5) and recharged water with increased soil development ($pCO_2$ = -2). Well samples (group 3) almost always plot above the line the saturation, indicating that still calcite dissolution takes place in the alluvial aquifer *Vega de Granada*. Most spring samples are plotting along vertical trajectories with variable initial $pCO_2$ content indicating open-system conditions.

It is important to recognize that the theoretical calculations are based only on calcite equilibrium and do not account for silicate weathering, complexation, cation exchange or any other biogeochemical process that may affect $Ca^{2+}$ activities in the aquifer.
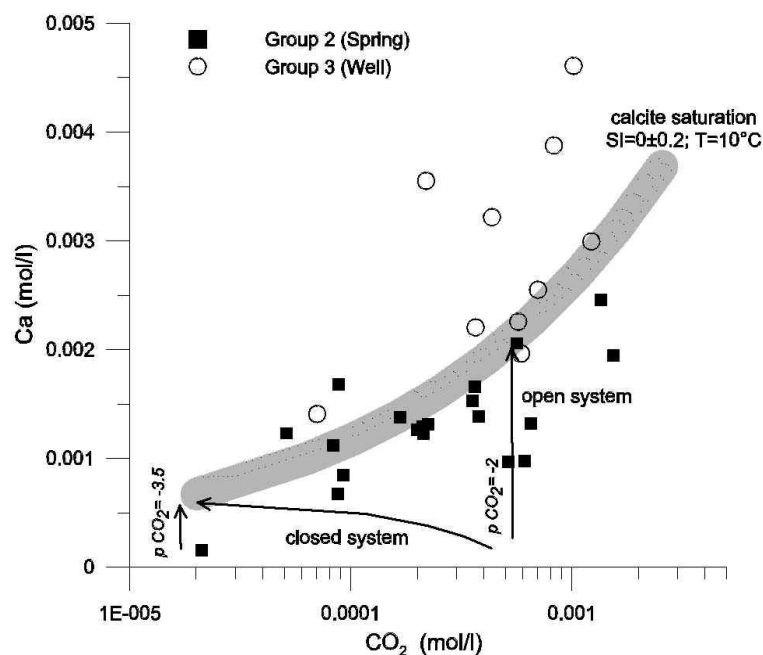


• Figure 4.13 Open and closed system trajectories for calcite dissolution of group 2 and group 3 members.

## 4.2 Stable isotopes of water ($\delta^{18}$O, $\delta^2$H)

In this section the signatures in the isotopic composition of water were studied in precipitation, springs, reservoirs, rivers and thermal springs in the *Granada* region. In arid and semiarid areas stable isotopes of water ($^{18}$O, $^2$H) are important investigative tools for hydrogeological studies (VERHAGEN et al. 1991). Groundwater provenances, mechanisms of groundwater recharge (indirect, direct) and recharge conditions (altitude, degree of evaporative enrichment) can be identified by the variations in the isotopic composition. All site locations are shown in fig.4.15, for detailed information about the sampling campaigns see section 3.2.

Results are presented in $\delta^{18}$O vs. $\delta$D diagrams to visualise the isotopic characteristics. Local $\delta$-value against altitude relationship in precipitation is constructed by data from GARRIDO 2003 and is used to calculate recharge altitudes for groundwater from springs and wells as discussed in section 2.4. Additionally, geomorphologic profiles, derived from the digital elevation model, are used to display the spatial pattern of selected springs, rivers and reservoir sites.

A schematic $\delta^{18}$O vs. $\delta$D diagram (Fig.4.14) was plotted in order to give an overview of variations and general distribution. Because of the similar content in isotopes samples of rain and surface water are not displayed in Fig. 4.14. The samples are grouped according to their site type in rain samples (n=11), snow and snowmelt samples (n=77), spring samples (n=68), river samples (n=41), reservoir samples (n=8) and thermal spring samples (n=14). Each group shows characteristic isotopic signatures and are discussed in the following sections.
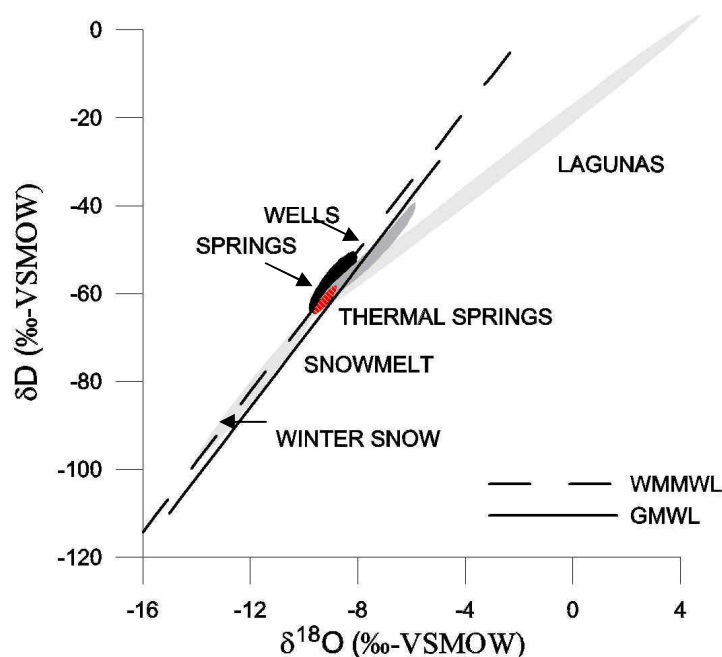


• Figure 4.14 Schematic overview of $\delta$D and $\delta^{18}$O relationship of all samples with the GMWL and the WMMWL as reference.
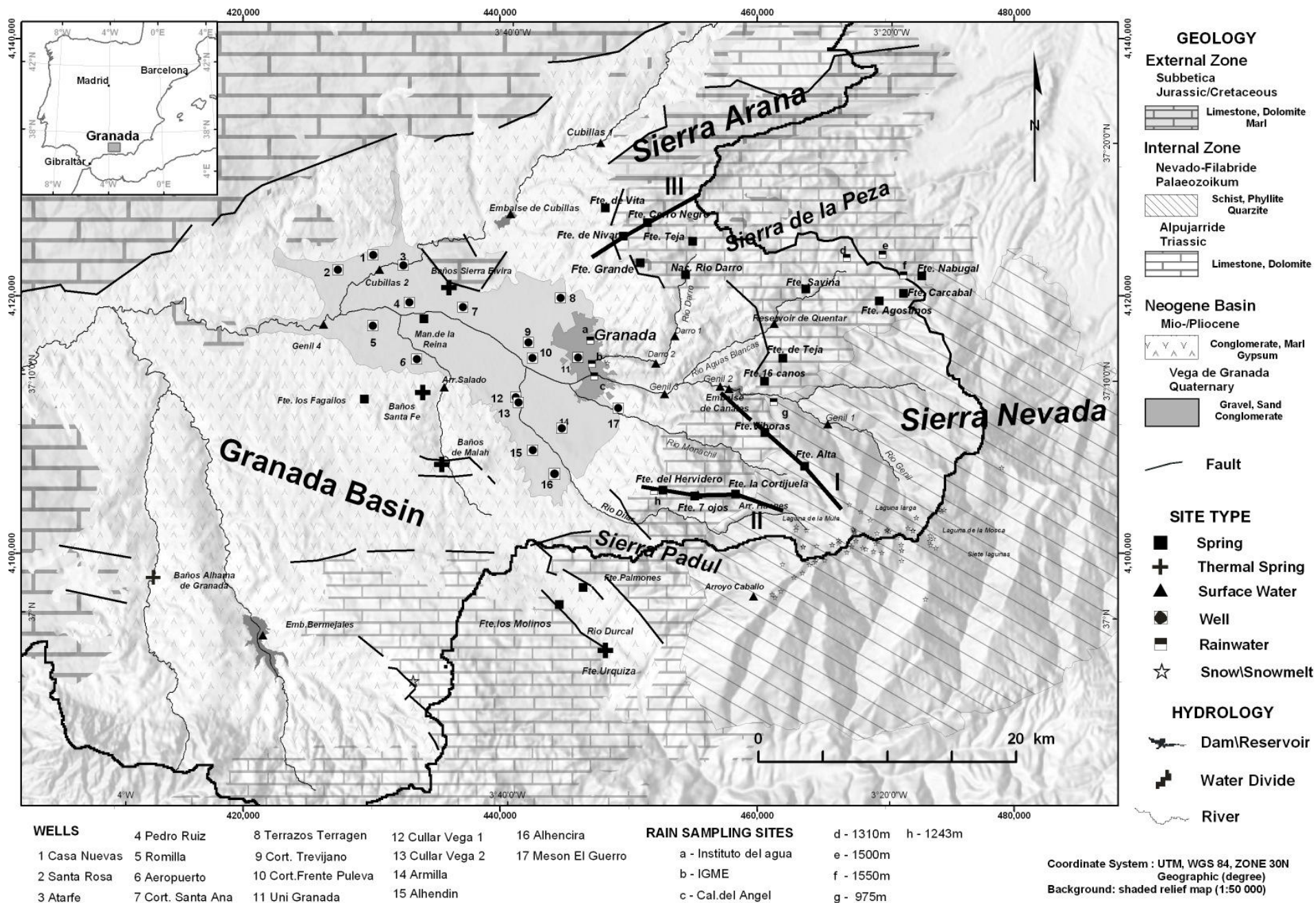
• Figure 4.15 Location map of sample sites for stable isotope analysis and isotope transects I, II, III. Geology simplified from IGME 2002.

## 4.2.1 Precipitation

Precipitation is the only input source for groundwater recharge within the study area. Therefore, the understanding of the isotopic composition from rain- and snowfall is essential for hydrogeological studies. This section deals with the isotopic data provided by the GNIP (Global Network of Isotopes in Precipitation) database of the IAEA (International Atomic Energy Agency) for one station on the Iberian peninsula (*Gibraltar*) and rain samples taken from GARRIDO 2003 near *Granada* (*Generalife*). These samples are presented together with few rain samples (n=11) from the *Granada* basin and samples from various altitudes in the *Sierra Nevada*. Additionally snow, snowmelt and *laguna* samples taken in the *Sierra Nevada* in altitudes >2200 masl are presented. For sampling locations see Fig.4.15.

## 4.2.1.1 Rainwater

Due to the position of Gibraltar at the strait between the Atlantic and the Mediterranean Sea, it is expected that isotope signatures of precipitation shows Atlantic and Mediteranean climatic influences.

The IAEA δ-values of rain are showing certain seasonal variations on the Iberian Peninsula (BEDMAR 1994) and are controlled by temperature, humidity and water vapour. Because of the higher temperature differences in winter between the source of air-vapour and the area of precipitation, more water vapour can be removed from the air masses on their trajectory, making the high altitude precipitation isotopic depleted in D and $^{18}$O in winter.

• Table 4.4 Mean weighted $\delta^{18}$O and δD values for the hydrological year, - winter and –summer at *Gibraltar* station (1962-2001). IAEA-GNIP 2004 data.

| Gibraltar 5 masl | mean weighted $\delta^{18}$O (‰) | mean weighted δD (‰) |
|---|---|---|
| Hydrological year | **-4.2** | **-22.7** |
| Sommer (may-oct) | -3.9 | -18.1 |
| Winter (nov-apr) | ***-4.8*** | ***-26.6*** |

That means that in general, the δ values are higher in summer and lower in winter and averaging rain water samples from different seasons lead to false estimations of groundwater recharge. Since only winter rain-events have the climatic potential to recharge the groundwater the seasonal variation in the stable isotope compositions must be considered. Therefore, samples are grouped in the hydrological winter (Nov.-Apr.) and the hydrological summer (May-Oct.). The mean volume weighted difference of $\delta^{18}$O between summer and winter rain in Gibraltar is 0.9 ‰ (Table 4.4).

The seasonal distributions of the mean weighted values of $\delta^{18}O$ and d-excess of precipitation, air temperature and mean precipitation values for the IAEA-GNIP station *Gibraltar* (Fig.4.16) and for the station *Granada* (*Generalife*) (Fig.4.17) were plotted for each month. Samples from the station in *Generalife* represent a three-year period while samples from the station in *Gibraltar* represent a 39-year period. Therefore, the graphs from the *Generalife* station have more uncertainties, but are considered to be sufficient for the purposes of this study.
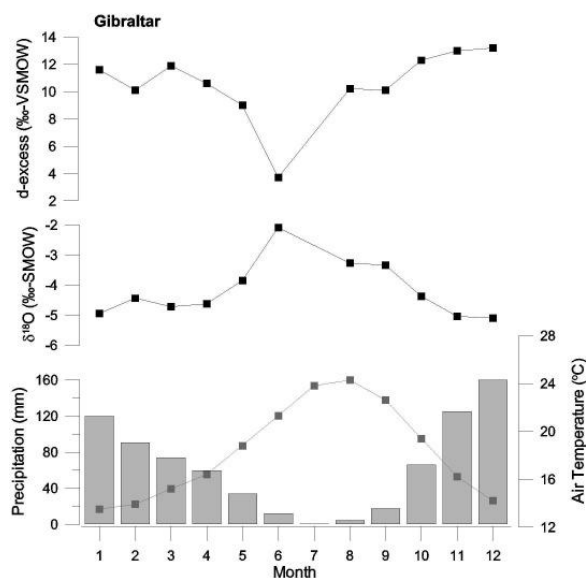


• Figure 4.16 Seasonal distribution of mean weighted $\delta^{18}O$ measured in precipitation at *Gibraltar* station (1962-2001), air temperature (right y-axis) and d-excess (‰ VS.MOW). The bars indicate mean monthly amounts of precipitation scaled to the left y-axis. IAEA–GNIP 2004
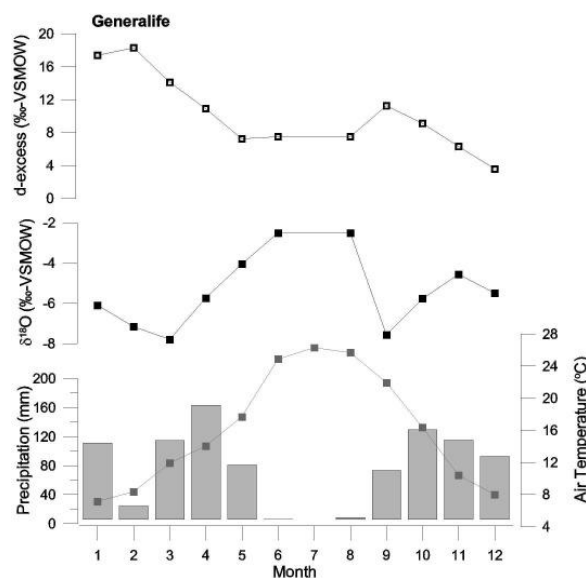
• Figure 4.17 Seasonal distribution of mean weighted $\delta^{18}O$ measured in precipitation at *Generalife* station (Dec.1999-Nov.2002), air temperature (right y-axis) from *Padul* station and d-excess (‰ VS.MOW). The bars indicate mean monthly amounts of precipitation. GARRIDO 2003

Both stations show correlation of low $\delta^{18}O$ with high monthly amounts of rainfall. During the hydrological summer (May – October) the most enriched $\delta^{18}O$ values are observed, with $\delta^{18}O= -3.9 ‰$ for *Gibraltar* (Tab.4.4) and $\delta^{18}O= -4.5 ‰$ for *Generalife* (Tab.4.5). For June both stations show weighted mean values in $\delta^{18}O$ of around $-2 ‰$. Rainfall, at the beginning of the rainy season in October, has a relatively light isotopic signature of $\delta^{18}O$ which evolves to a weighted mean in December around $-5 ‰$ for *Gibraltar* and $\delta^{18}O= -6 ‰$ for *Generalife*. At the end of the rainy season (April) a general return to heavier (higher) $\delta^{18}O$ and lower d-excess values is observed in *Gibraltar* and *Generalife* samples. During the hydrological winter (November - April) the most depleted $\delta^{18}O$ values were observed, with $\delta^{18}O= -4.8 ‰$ for *Gibraltar* (Tab.4.4) and $\delta^{18}O= -6.1 ‰$ for *Generalife* (Tab.4.5). These differences are caused by continental- and altitude effects.

The mean volume weighted difference of $\delta^{18}O$ between summer and winter rain in *Generalife* is 1.6 ‰ (Tab.4.5).

• Table 4.5 Mean weighted $\delta^{18}O$ and $\delta D$ values for the hydrological year, - winter and –summer at *Generalife* station (Dec.1999-Nov.2002). GARRIDO 2003 data.

| *Generalife 845 masl* | mean weighted $\delta^{18}O$ (‰) | mean weighted $\delta D$ (‰) |
|---|---|---|
| Hydrological year | **-5.4** | **-32.9** |
| Sommer (may-oct) | -4.5 | -27.4 |
| Winter (nov-apr) | **-6.1** | **-37.5** |

44

The distributions of $\delta^{18}O$ values of rain samples taken at various locations in the *Granada* basin and in the adjacent *Sierras* was plotted with meteorological data (air temperature (ºC), precipitation (mm)) from the *Padul* meteorological station for the time of monitoring from February 2004 to March 2005 (Fig.4.16) (all measured values are shown appendix 4, tab.a4.8 – tab.a4.11).

It is expected that rain samples show variation in the isotopic content due to amount, altitude and seasonality and the range in $\delta^{18}O$ between –18.6 and –2.1 ‰ is reflecting these effects. No clear correlation between altitude and δ-values can be observed in these samples. Rain samples from low amount rain events seem to tend to have enriched δ-values. Since no precise amount of the rain event is available, no exact volume weighted values can be applied. Four rain events have been sampled in four different methods (n=11) and are described in chronological order as:

• (1) first low amount rain event (20. – 25. February 04) with max. 8.8 mm was sampled only one time in *Granada* city ($\delta^{18}O$ = -7.83 ‰, δD = -59.2 ‰, d-excess = 1.84 ‰). This rain sample seems to be affected by evaporation as it plots below of the GMWL (Fig.4.19). Furthermore, it is considered to be shifted towards more enriched values according to the amount effect.

• (2) second rain event (28.November - 6.December 04) with total amount of rainwater of 74.4 mm (max. 32.6 mm) was sampled on the 2.December cumulative on four different altitudes (670, 1310, 1500, 1550 masl). Characteristic of this event is, after a long dry period in summer, that the first rain event which falls through a dry atmosphere is altered. This alteration can be described as evaporation processes during rain fall. The rain sample taken at the lowest site (670 masl) shows the most depleted values ($\delta^{18}O$ = -7.08 ‰, δD= -24.3 ‰) and rain taken at highest site (1550 masl) shows the second most depleted values ($\delta^{18}O$ = -6.87 ‰, δD= -29.7 ‰). Therefore, no positive correlation can be observed between altitude and δ-values. Furthermore, the high d-excess (19.7 – 26.2‰) leads to a shift of δD above the WMMWL and cannot be explained (Fig.4.19).
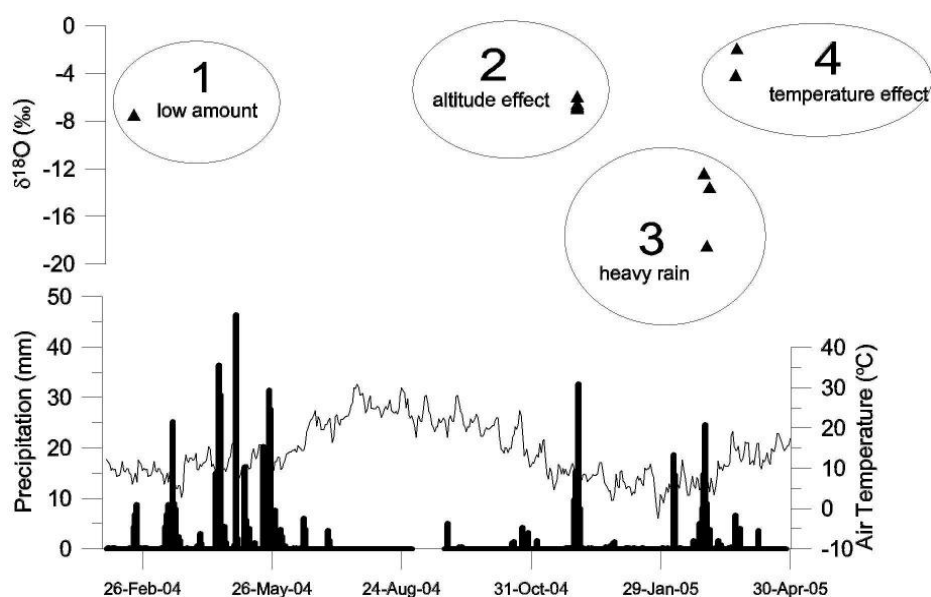


• Figure 4.18 Precipitation (mm) and air temperature (ºC) at *Padul* station between 01.02.2004 and 30.04.2005, $\delta^{18}O$ (‰-VSMOW) of measured rain samples.

45

• (3) third rain event (27. February - 5. March 05) with total amount of 63 mm (max. 24.6 mm) was sampled in *Granada* city altitudes (650 masl) in three single samples. A strong temperature correlation is observed. These samples show the most depleted δ-values and are interpreted as high amount rain event at low temperatures (reverse amount effect).

• (4) fourth rain event (23./24. March 05) with total low amount of rainwater of 6.6 mm was sampled in *Granada* city (650 masl) and in 1295 masl in two single samples. The altitude gradient in $\delta^{18}$O is -0.34 ‰/100 m.

It is shown that local precipitation varies due to a change in altitude, temperature, season and amount. The variations in precipitation isotopes observed in the study area suggests that, in regions with highly variable microclimates and rainfall conditions, a detailed precipitation sampling network is necessary to avoid misinterpretations for temporal and spatial mean weighted precipitation.

The $\delta^{18}$O vs. δD (‰-VSMOW) diagram shows all rain samples taken within this study. The numbers refer to the rain events introduced in the section above (Fig.4.19). Due to the lack of sufficient enough precipitation events during the time of monitoring, data from GARRIDO 2003 was used to understand local precipitation pattern.
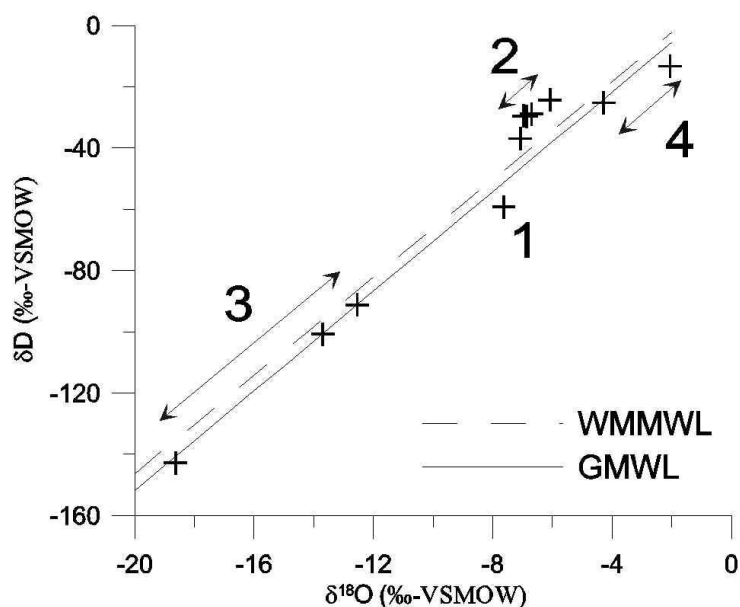


• Figure 4.19 $\delta^{18}$O (‰-VSMOW) - δD(‰-VSMOW)  diagram of rain samples.

## 4.2.1.2 Snow and snowmelt samples

In this section more than 70 samples classified as snow, snowmelt or *laguna* (mountainous lakes in the *Sierra Nevada*) site types are presented in $\delta^{18}O$ vs. $\delta D$ diagrams. The isotopic alteration of snow and the influence of this alteration on runoff and GWR were examined by many studies (e.g., MOSER & STICHLER 1974, 1980).

Snowmelt samples are often located **near** or **below** to the WMMWL. The regression line calculated with snowmelt samples is $\delta D = 5.66 * \delta^{18}O-10.36$. Compared to the *laguna* samples, the slope of almost 6 is reflecting the increased equilibrium exchange processes, between the melt water and the vapour within the snowpack. Assuming that the average value of snowmelt samples is represented by the intersection of the regression line with the WMMWL ($\delta^{18}O = -10$ ‰; $\delta D=-66.3$‰), the maximum enrichment can be estimated by up to 2 ‰ in $\delta^{18}O$ (Fig.4.20).

Since signatures of melt water and fresh snow can differ, the isotope signature of fresh snow is not appropriate for the use as an end member. By determining the magnitude of alteration from snow to snowmelt in the *Sierra Nevada* it is possible to show how this alteration can influence the estimation of the importance of snowmelt as a source of groundwater recharge. Snow and snowmelt samples data show that infiltration resulting from snowmelt in the *Sierra Nevada* can be enriched in $\delta^{18}O$ and $\delta D$ compared to the signature of fresh snow. The alteration in isotope signature tends to have a slope close to that of the MWL, so even highly altered samples plot near the MWL.

By comparing the signatures of snowmelt and winter rain precipitation to a local spring water signature, it is possible to calculate the proportions of snowmelt and rain in local groundwater
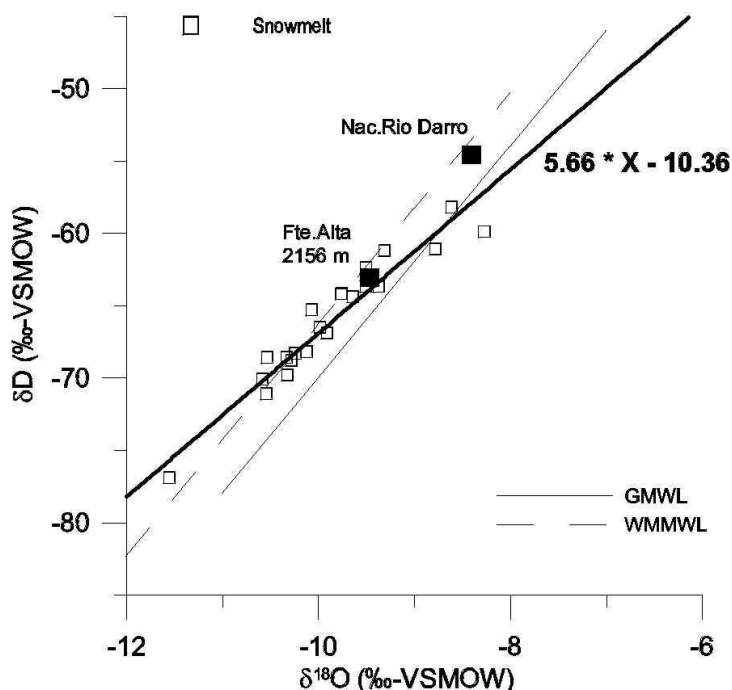


• Figure 4.20 $\delta^{18}O$ - $\delta D$ diagram of snowmelt samples from the *Sierra Nevada* with average value of *Fte.Alta* and *Nac. Rio Darro*.

recharge. Since average snowmelt signature and average spring water signature of *Fte.Alta* ($\delta^{18}O$ = -9.5 ‰) samples is very similar, it is possible to state that *FteAlta* seems to be dominated by snowmelt derived from high altitudes in the *Sierra Nevada* (Fig.4.20).

If snowmelt takes place during spring thawn due to rain, then the runoff will be a mixture of the rain and the snowmelt that has re-equilibrated with the remaining snowpack. The $\delta^{18}O$ value of the runoff will depend on the amount of rain, and the amount of melting, but will evolve towards the isotopic composition of the rain. Rain water at 2300 masl with a winter average of $\delta^{18}O$ = -9 ‰ (see Calculating recharge altitudes) and snowmelt with $\delta^{18}O$ = -10 ‰ shows that snowmelt and rain is found to be responsible for both 50% of the recharge during spring thawn. This seasonal variation can be seen in samples from *Fte. Alta.* Here the winter-sample (February $\delta^{18}O$ = -9.5 ‰) is more depleted than the summer-sample (October $\delta^{18}O$ = -9.4 ‰) and the variance of 0.1 ‰ is greater than the precision in measurement (measurement precision = 0.03 ‰). Other spring samples, e.g. *Nac.Rio Darro*, show signatures which seem to be not influenced by recharge water from snowmelt (Fig.4.20).

The *lagunas* samples show, in contrast to snowmelt samples, strong evaporative enrichment. Samples taken from *lagunas* are highly altered and even positive isotope ratios occur (e.g. *Laguna Mula* $\delta^{18}O$ = +3.8). The regression line calculated with *laguna* samples is $\delta D = 4.97 * \delta^{18}O - 17.3$ (n=39; $r^2$=0.96). A slope of less than 5 is typical for evaporation from open water surfaces (CLARK & FRITZ 1997), such as *lagunas*. Compared to the regression-slope of the snowmelt samples, the slope of the regression-line from *laguna* samples is shallower. This reflects the increasing influence of kinetic fractionation processes (Fig.4.22).

By taking the average temperature (~5 °C) from the meteorological station *Albergue Universitario* (see section 1.4), the slope of the regression line (s = 4.97) allows to approximate the relative humidity according to GONFIANTINI 1986 with around *h* = 0.3 (= 30 %). Now it is possible to determine the kinetic fractionation factors using Gonfiantini's equations (section 2.7), giving $\varepsilon^{18}O_{kinetic}$ = –9.94 ‰. The total enrichment ($\varepsilon_{total} = \varepsilon_{equilibrium} + \varepsilon_{kinetic}$) for evaporation under these conditions with the mean temperature of 5 °C in 2500 masl ($\varepsilon_{equilibrium}$ = -10.8 ‰) is then $\varepsilon_{total}$ = -20.74 ‰. The intersection of the regression line with the WMMWL is considered as the initial isotope ratio without evaporative impact ($\delta^{18}O_{initial}$ ~ -10.7 ‰). The sample taken from *Laguna Martin* shows the most enriched value and represents the maximum evaporative enrichment ($\delta^{18}O_{sample}$ = 3.8 ‰). The total enrichment of this samples can then be calculated with maximum $\Delta\delta^{18}O = \delta^{18}O_{initial} - \delta^{18}O_{sample}$ = 14.5 ‰. The fractional water loss from evaporation can then be modelled according to a Rayleigh distillation. For $\delta^{18}O$, the evaporative enrichment is up to 14.5 ‰. According to equation 2.9.:

$$\varepsilon_{total}(\delta^{18}O) * \ln f = 14.5 ‰$$

yielding a residual water fraction *f* of 0.49 and so a maximum evaporative loss in the sample of *Laguna Martin* of 51 %. These values must be considered as maximum evaporation losses in small endorheic basins without constant inflow, e.g. *Laguna Martin*, *Laguna de la Mula* (see photo 4).
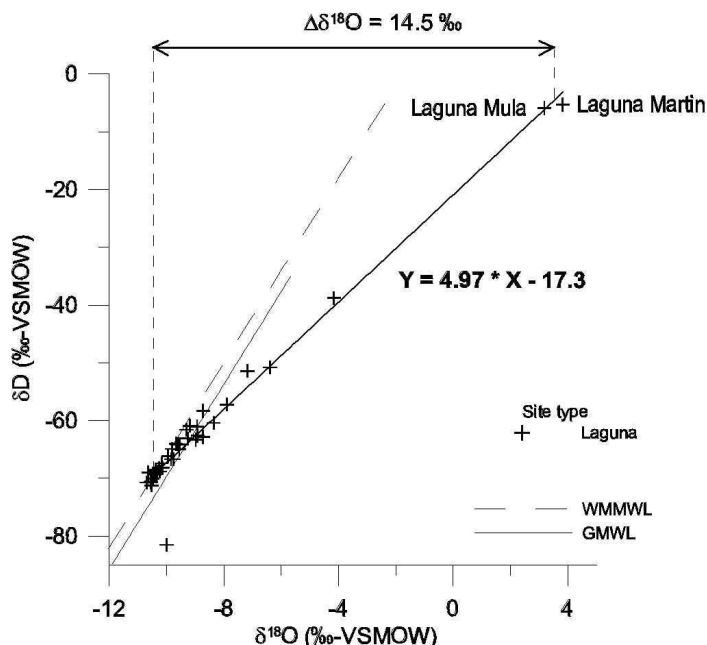
• Figure 4.22 $\delta^{18}O$ - $\delta D$ diagram of *laguna* samples from the *Sierra Nevada*. Meteoric water lines as reference.

A correction of $\delta^{18}O$ from evaporative enrichment was applied, in order to establish a precipitation vs. altitude correlation. The corrected values indicate the isotopic composition without enrichment by evaporation. As the corrected value marks the intersection of the evaporation line (regression line) with the LMWL (WMMWL), it is defined by simple linear algebra according to:

$$\delta^{18}O_{corrected} = \frac{i_{LMWL} - (s_{evaporation} \times \delta^{18}O_{measured}) - \delta D_{measured}}{s_{evaporation} - s_{LMWL}} \qquad (eq.4.9)$$

where *s* corresponds to the slope of the evaporation line determined in equation above as 4.97 or $s_{LMWL}$ with 8, and *i* is the intercept of the WMMWL, with *i* = +13.7 ‰. In the study area the variability of this corrected $\delta^{18}O$ in snow meltwater is assumed to reflect mainly different rain-out altitudes and seasonality. Corrected $\delta^{18}O$ values are presented in appendix 4, tab.a4.13.
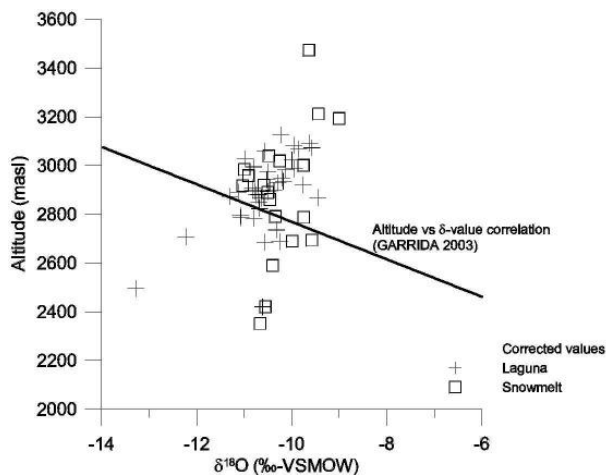


• Figure 4.23 Corrected $\delta^{18}O$ (‰-VSMOW) vs. Altitude (masl) of snowmelt and *laguna* samples.

Figure 4.23 shows the distribution of evaporative-enrichment corrected $\delta^{18}O$-values vs. the altitude (masl). No clear correlation between altitude and $\delta^{18}O$ is observable. Considering the fact that all samples have been taken in the dry season (April-September), it indicates that these samples reflect mainly different rain events in the wet season (October-March) before and alteration processes during storage.

49

## 4.2.2 Estimation recharge altitudes

Recharge elevations for each spring and well were estimated by calculating a $\delta^{18}O$ vs. altitude relationship in precipitation. By taking the mean weighted winter value from *Generalife* (-6.1 ‰) as a end member and interpolating a gradient according to GARRIDO 2003 with –0.2 ‰/100 m for altitudes between 700 - 2200 masl. Only $\delta^{18}O$ was used for this analysis; the deuterium patterns were similar. The easy assumption in this case is that the average $\delta$-value in groundwater represents an average elevation of recharge. By plotting $\delta^{18}O$ vs. altitude (masl) of both spring and rain sample, it is possible to estimate the recharge altitude. Therefore, the mean recharge altitude of a sample can be seen as the matching point of the intersection of a vertical line from the groundwater sample with the interpolated line of precipitation. For ground water sites that were sampled frequently, the average isotopic composition was used to determine recharge altitude.

According to the two groundwater provenances distinguished in section 4.2.4, also two groundwater recharge areas must be distinguished. Since the *Sierra Nevada* springs and the *Sierra de la Peza springs* are located on different orographic divides of the Betic Cordillera, a spatial shift in $\delta^{18}O$ values is expected to occur. This shift is expressed by different $\delta^{18}O$ / altitude relationship (Fig.4.24).
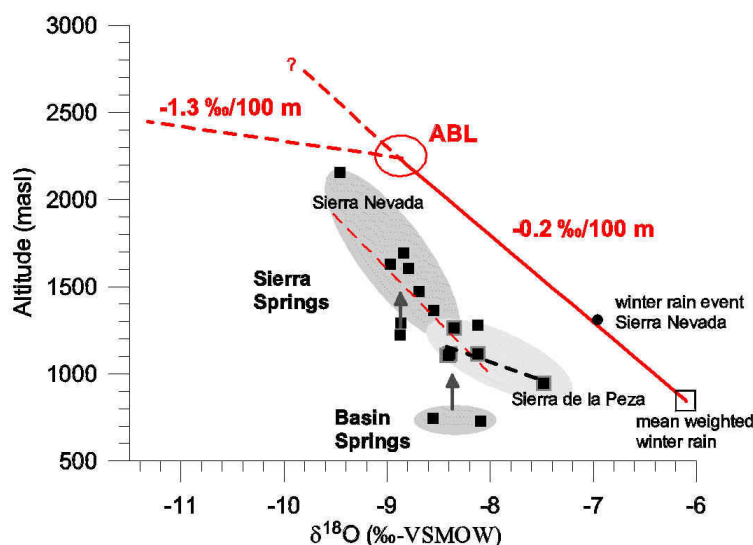


• Figure 4.24 Average $\delta^{18}O$ values of springs (squares) vs. Altitude (masl). Regression lines in spring samples calculated for the *Sierra Nevada* (red dashed line) and *Sierra de la Peza* (black dashed line). Interpolated precipitation line (red line) taken from GARRIDO 2003 is representing mean recharge altitudes. Mean weighted winter rain in the *Granada* basin (open square). ABL=atmospheric boundary layer.

The mean weighted $\delta^{18}O$ from the station *Generalife* (845 masl) within the hydrological winter 2001/02 (Nov-Apr.) seems to be a good approximation for winter rain in the *Granada* basin (see section 4.2.1.1). The $\delta^{18}O$ / Altitude gradients, taken from GARRIDO 2003 were compared with local springwater. GARRIDO 2003 divided the gradients into a low and a high altitude gradient. The separation is caused by the atmospheric boundary layer (ABL) (see section 1.4 Climate). The altitude vs. $\delta^{18}O$ gradient (-0.2 ‰/100 m, eq.4.10) is valid for 800-2200 masl. Above 2200

masl the ABL causing a stable atmospheric stratification with a temperature inversion in which temperature increases with altitude in winter. In summer the atmosphere is more turbulent and the temperature gradient is normal. Based on a best-fit linear correlation of the relationship between the interpolated $\delta^{18}O$ of precipitation vs. altitude of figure 4.24 exhibits equations, which can be used to estimate recharge altitudes according to:

| *Sierra Nevada* | **Equation** | **Altitude range** | **Gradient** | |
|---|---|---|---|---|
| Altitude (masl) = -500 * $\delta^{18}O$ – 2205 | | 800 – 2200 masl | -0.2 ‰/ 100 m | (eq.4.10) |
| Altitude (masl) = -76.9 * $\delta^{18}O$ + 1522 | | 2200 – 3400 masl | -1.3 ‰/ 100 m | (eq.4.11) |

According to these equations the reconstruction of groundwater recharge areas was approximated by $\delta^{18}O$ concentration of -0.2 ‰ with an increase of 100 m altitude in the *Sierra Nevada* below 2200 masl and of –1.3 ‰ / 100 m above 2200 masl for winter precipitation. GARRIDO 2003 calculated regression lines between the altitude and δ-values for $\Delta\delta^{18}O$ = -1.3 ‰/100 m and for $\Delta D$ = -9 ‰/100 m for dependencies valid for altitudes between 2200 – 3200 masl.

The actual altitude of each spring sample site was then subtracted from the precipitation derived recharge altitude. The discrepancy between actual altitude and estimated recharge altitude (vertical distance) was used to indicate sources of water. Average recharge altitudes and vertical distances for the *Sierra Nevada* and *Granada* basin springs were calculated as shown in tab.4.6. The vertical distance for the *Sierra Nevada* springs ranges between 370 and 1000 m, only basin springs have values far above 1000 m (1100; 1300 m). The basin springs (*Fte.Palmones*, *Fte.Molinos*) and the *Sierra* springs have similar $\delta^{18}O$ values (arrow in Fig.4.24). Thus the recharge altitudes must be similar. Also high vertical distance can be found in three *Sierra Nevada* springs (*Fte. de los 16 canos*, *Fte. del Hervidero*, *Fte. 7 ojos*) as indicated with the arrow in figure 4.24.

The resolution of mean recharge calculations is defined by the precision in isotope measurement and the local altitude gradient. The altitude effect of –0.2 ‰/100 m (–0.002 ‰/m or 500 m/‰), with a precision of measurement of ± 0.1 ‰ on the $\delta^{18}O$ of the groundwater, leads to a maximum resolution of 500 * 0.1 = ± 50 m. If the precision is higher, e.g. 0.04 ‰, the maximum resolution for establishing recharge altitude is 500 * 0.04 = ± 20m. The precision in isotope measurement ranges between 0.02 ‰ and 0.09 ‰ in $\delta^{18}O$ and between 0.1 ‰ and 0.4 ‰ in δD.

• Table 4.6 Average δ^{18}O values, maximum error and average recharge altitude for *Sierra Nevada* springs and *Granada* basin springs (*cursive*).

| Site | Altitude (masl) | Ø δ$^{18}$O (‰) | δ$^{18}$O error (‰) | Ø recharge Altitude (masl) | vertical distance (m) |
|---|---|---|---|---|---|
| Fte. Alta | 2156 | -9.46 | 0.04 | 2522 (+/-20) | 366 |
| Fte. las Viboras | 1629 | -8.97 | 0.06 | 2277 (+/-30) | 648 |
| Fte. del Hervidero | 1292 | -8.87 | 0.05 | 2229 (+/-25) | 937 |
| Fte. la Cortijuela | 1695 | -8.84 | 0.07 | 2214 (+/-35) | 519 |
| Fte. de los 16 canos | 1222 | -8.87 | 0.06 | 2231 (+/-30) | 1009 |
| Fte. de Teja | 1278 | -8.12 | 0.03 | 1855 (+/-15) | 577 |
| *Fte. Palmones* | *745* | *-8.56* | *0.04* | *2072 (+/-20)* | *1327* |
| *Fte. los Molinos* | *730* | *-8.09* | *0.06* | *1841 (+/-30)* | *1111* |
| Fte. Savina | 1113 | -8.10 | 0.10 | 1845 (+/-50) | 732 |
| Fte. Agostinos | 1362 | -8.55 | 0.05 | 2070 (+/-25) | 708 |
| Fte. Carcabal | 1605 | -8.79 | 0.07 | 2190 (+/-35) | 585 |
| Fte. Nabugal | 1471 | -8.69 | 0.04 | 2140 (+/-20) | 669 |
| Fte. 7 ojos | 1411 | -8.97 | 0.02 | 2280 (+/-10) | 869 |
| **min** | **730** | **-9.46** | **0.02** | **1841** | **366** |
| **max** | **2156** | **-8.09** | **0.10** | **2522** | **1327** |
| **average** | **1362** | **-8.68** | **0.05** | **2135** | **774** |

The groundwater flow direction from NE to SW in the *Sierra de la Peza* carbonate aquifer indicates the strong influence of the *Sierra Arana* as the recharge area for the *Sierra de la Peza* springs. Compared to the climatic conditions in the *Sierra Nevada*, the relative low decrease in temperatures with altitude in the *Sierra Arana* must produce a shallower δ$^{18}$O/altitude gradient. That means that rainfall at similar altitudes is in the *Sierra Arana* more depleted than in the *Sierra Nevada*. This difference in local precipitation pattern is reflected by the shallower regression between spring samples from the *Sierra de la Peza* aquifer (section 4.2.4). Since no data about isotopes in precipitation in this area is available, local gradients must be approximated according to general isotope/altitude relationship. The gradient for the *Sierra de la Peza* springs have been applied to the local geomorphology (derived from the DEM) in order to achieve reasonable recharge altitudes. Average recharge altitudes and vertical distances for the *Sierra de la Peza* spings were calculated as shown in tab.4.7.

| *Sierra de la Peza* | **Equation** | **Altitude range** | **Gradient** | |
|---|---|---|---|---|
| | Altitude (masl) = -332* δ$^{18}$O – 1190 | 800 – 2200 masl | -0.3 ‰/ 100 m | (eq.4.12) |

• Table 4.7 Average δ^{18}O values, maximum error and average recharge altitude for *Sierra de la Peza* springs.

| Site | Altitude (masl) | Ø δ$^{18}$O (‰) | δ$^{18}$O error (‰) | Ø recharge Altitude (masl) | vertical distance (m) |
|---|---|---|---|---|---|
| Fte. Grande | 1114 | -8.40 | 0.02 | 1597 (+/- 7) | 483 |
| Fte. de Nivar | 1108 | -8.41 | 0.04 | 1600 (+/-13) | 492 |
| Fte. Cerro Negro | 1115 | -8.12 | 0.08 | 1505 (+/-27) | 390 |
| Nac. Rio Darro | 1106 | -8.42 | 0.06 | 1605 (+/- 20) | 499 |
| Fte. de Vita | 944 | -7.48 | 0.04 | 1293 (+/-13) | 349 |
| Fte. Teja | 1262 | -8.35 | 0.02 | 1582 (+/-7) | 320 |
| **min** | **944** | **-8.42** | **0.02** | **1293** | **320** |
| **max** | **1262** | **-7.48** | **0.08** | **1605** | **499** |
| **average** | **1108** | **-8.19** | **0.04** | **1531** | **422** |

The vertical distance for the *Sierra de la Peza* springs are low (average=422 m) and ranges between 320-499 m.

It is important to recognize that several factors may modify the above mentioned equations (eq.4.10, 4.11, 4.12). Calculations are based only on a relative small time period of monitoring of 1.5 years (eq.4.10, 4.11) or were estimated (eq.4.12). The equations should be considered as rough estimations, which can vary seasonally and spatially. As shown in section 1.4 the year to year change in precipitation is highly variable and therefore a detailed knowledge of isotopes in local precipitation is necessary. Furthermore, one could expect that $\delta^{18}O$ vs. altitude in spring samples and $\delta^{18}O$ vs. altitude in precipitation samples are parallel. This is not the case. Therefore, the above equation may overestimate recharge elevations especially in lower altitudes and the groundwater recharge altitude equation appears to be dominated by high altitude rainfall (lower $\delta^{18}O$) infiltration.

## 4.2.3 Surface water samples

In this section surface water samples from streams (*Arroyo, Barranco*), rivers (*Rio*) and reservoirs (*Embalse*) are presented. Rivers were sampled frequently on different altitudes in order to discover seasonal variations and recharge conditions in the *Rio Genil* and the *Rio Darro*. Additionally, single samples were taken from the *Rio Cubillas* and the reservoirs *Canales*, *Cubillas* and *Quentar* were sampled.

### 4.2.3.1 Rio Genil

The *Rio Genil* is the most important river in the study area and is considered to be a main source for indirect recharge to the alluvial aquifer *Vega de Granada*. The river sites are described from the highest point at 1180 masl (*Barr.de San Juan*) downstream to the lowest site in the *Vega de Granada* at 650 masl. D-excess and $\delta^{18}O$ (‰-VSMOW) against time is plotted in the left diagram in order to visualize seasonal effects. The right diagram shows the $\delta D$ and Altitude (masl) against $\delta^{18}O$ (‰-VSMOW) diagrams of *Genil* samples in order to visualize possible evaporation processes (Fig.4.25). Site locations are shown in figure 4.15.

Seasonal variations in isotopes can be observed in the high altitude site (*Barr. de San Juan* or *Genil 1*), located in the metamorphic core *Nevado-Filabride*. Due to the low permeabilities in this terrain it is expected that surface runoff dominates the discharge. The variations in the isotopes will follow the course of a hydrograph derived from river discharge measurements. High rates of discharge are expressed as low $\delta$ - values. Therefore, samples taken between September to November (no rainfall) represent the base flow of the river, while the January sample is slightly shifted towards lighter isotopes due to snowfall and the March sample shows a strong peak towards lighter isotopes due to snow thawn. Especially the March sample represents the isotopic composition right after rainfall event.
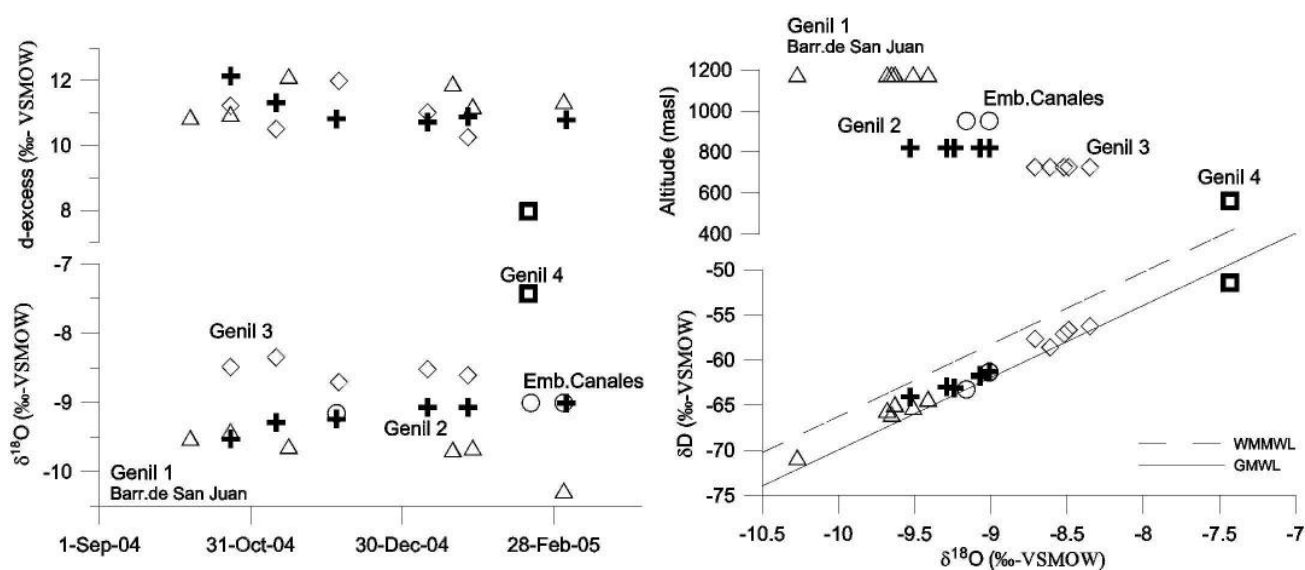


• Figure 4.25 $\delta^{18}O$ with d-excess vs. time diagrams (left) and $\delta D$ with Altitude (masl) vs. $\delta^{18}O$ (‰-VSMOW) diagrams (right) of *Genil* samples.

Following the course of the *Genil* downstream the next site is situated in the reservoir (*Emb.de Canales*) of the *Genil*. The reservoir was build between 1975 - 1989 and stretches over a length of 340 m with a maximum storage capacity of 7.248 m$^3$ and a maximum depth of 156 m (*Ministerio de Medio Ambiente, Embalse de Canales* 2001). Samples taken from the reservoir itself and at the discharge (*Genil 2*) showing a very similar isotope composition. No samples from depth below surface were taken, since stratification within the water column was not expected and may only occur during summer, when strong sun radiation warms up the upper surface water layer. Therefore the reservoir is considered to be a well mixed water body with minor changes in the isotopic composition in relation to the water depth. Seasonal variations are attenuated in the reservoir due to fast internal mixing relative to the residence time in the reservoir. Minor to none evaporative enrichment can be observed. Nevertheless, over the time period of monitoring the isotope signature in the reservoir follows a successive trend from relative light δ-values to more positive values. This trend reflects the decreasing water table within the reservoir due to minor input flow.

Following the course of the *Genil* further downstream the next site is situated in the Mio-/Pliocene basin fillings (*Genil 3*). This site is situated after the inflow of the river *Aguas Blancas* into the *Genil*. Samples from the river *Aguas Blancas* (*Emb.de Quentar*) show a significant heavier isotopic composition with $\delta^{18}O$ = -7.8 ‰ and δD = - 52 ‰ compared to samples from site *Genil 3*. This reflects the lower altitudes where surface runoff takes place in the catchment area of the river *Aguas Blancas*. A more detailed discussion is presented in the following sections. Samples of the *Genil 3* site showing a subparallel shift along the MWLs towards heavier isotopes (max. +1‰ in $\delta^{18}O$) composition compared to upstream samples from the reservoir *Canales*. Assuming a binary mixture from water of the *Genil* with water from the *Aguas Blancas* it is possible to calculate the degree of mixture with simple algebra according to:

$$\delta_{sample} = d \cdot \delta_A + (1-d) \cdot \delta_B \qquad\qquad (eq.4.13)$$

where d is the degree or proportion of mixture of the mixed sample (*Genil* 3) from sample A (*Genil 2*) with sample B (*Quentar*). This leads to a calculated proportion of mixture of d = 0.58 and so a water surplus of 42 % by the river *Aguas Blancas* to the river *Genil*. This calculation may overestimate the influence of the river *Aguas Blancas* as it neglects other sources of water such as irrigation. However, it is obvious that the relative light isotopic composition of the *Genil* is significantly influenced by the relative heavy signature from the *Aguas Blancas* river.

The sample *Genil 4*, taken from the western part of the *Vega de Granada* shows a very strong isotopic enrichment, shifting the isotopic composition of the groundwater away from the local meteoric line along an evaporation line. This tendency could be driven by the re-use of waters mainly for irrigation purposes in combination with mixing processes with already enriched water. A more detailed discussion is presented in section 4.2.7 Wells. D-excess values provide no useful information. A trend in the δD vs. $\delta^{18}O$ from the high altitude site (*Barr.de San Juan*) downstream which courses not exactly parallel to the MWLs (Fig.4.25).

## 4.2.3.2 Rio Darro

The *Rio Darro* is a tributary to the *Genil* and both rivers intersect in the city of *Granada*. The sampling sites of the *Rio Darro* are described from the highest site at 1106 masl downstream to the lowest site at 820 masl. For site location see figure 4.15. D-excess and $\delta^{18}O$ (‰-VSMOW) against time is plotted in the left diagram in order to visualize seasonal effects. The right diagram shows the $\delta D$ and Altitude (masl) against $\delta^{18}O$ (‰-VSMOW) in order to visualize possible evaporation processes (Fig.4.26).

Samples from the highest site (*Nacimiento Rio Darro* 1106 masl) (open triangles), showing a quite constant course of $\delta$-values over the time of monitoring, with a maximum deviation of $\Delta 0.12$ ‰ in the $\delta^{18}O$ values between the November 04 and March 05 sample. This low deviation reflects the relative wide catchment area, where seasonal variations are attenuated by mixing processes. The isotopic most depleted sample taken in March 05 indicates the recharge water derived from precipitation probably from the winter 04/05.

Following the course of the river downstream the next site is *Darro 2* (crosses). This site is situated in the N-S stretching valley of the *Darro* at an altitude of 875 masl. Comparing *Darro 2* samples with samples from *Nac.Rio Darro* taken at the same time often a shift in $\delta^{18}O$ values to the spring is $\Delta 0.2$ ‰, which is significant above the error in measurement. Since variations in $\delta^{18}O$ ($\Delta 0.16$ ‰) are significant above the error in measurement (0.03 ‰), seasonal variations were observed.

Following the course of the *Darro* further downstream the next site (*Darro 3*) is situated in conglomeratic sediments termed as *Alhambra* formation. A typical sinusoidal course of $\delta^{18}O$ can be observed in the temporal plot of *Darro 3* samples. The fact that these seasonal variations are stronger compared to samples from *Darro 2* leads to the assumption that anthropogenic impacts (irrigation) may cause these variations.
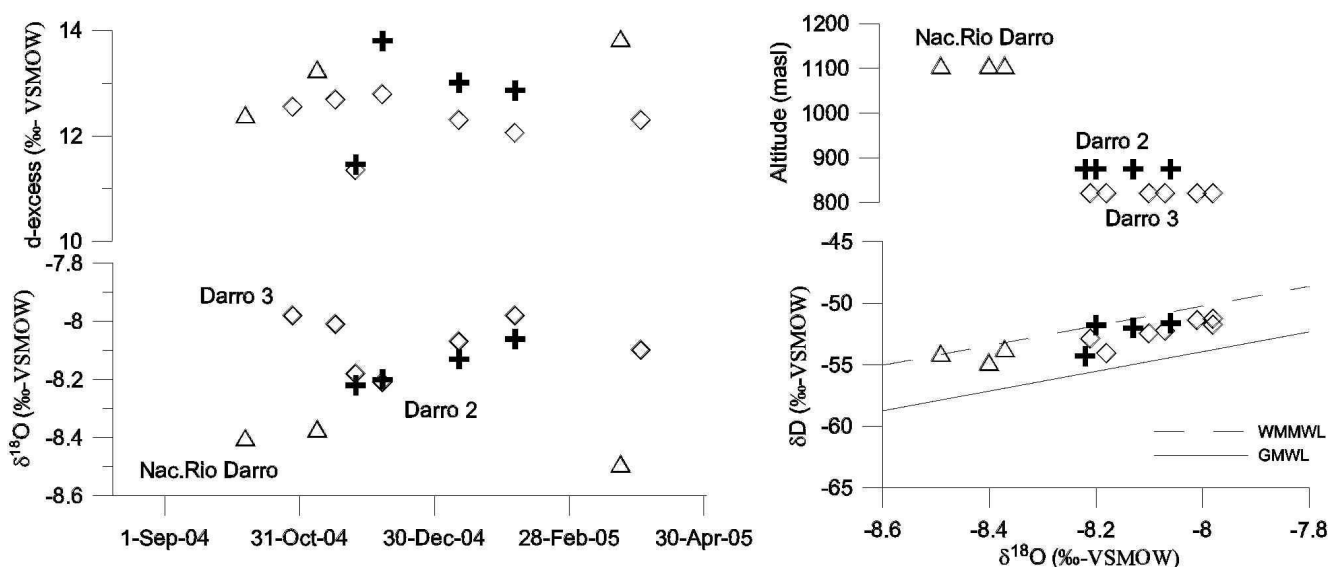


• Figure 4.26 $\delta^{18}O$ with d-excess vs. time diagrams (right) and $\delta D$ with Altitude (masl) vs. $\delta^{18}O$ (‰-VSMOW) diagrams (left) of *Darro* samples.

## 4.2.3.3 Rio Cubillas

Fig.4.27 shows all samples taken from the river *Cubillas* (*Rio Cubillas*), which is a tributary to the *Genil*. Both rivers intersect in the western part of the *Vega de Granada*, as shown in figure 4.15. Compared to river samples from the *Darro* or *Genil* the pattern of the isotopes is very different according to the large catchment area with low average elevation.

The site *Cubillas 1* is situated in the Mio-/Pliocene basin sediments in altitudes of 693 masl and exhibits the most depleted value of all *Cubillas* samples. Since *Cubillas 1* sample plots below the MWL evaporative enrichment cannot be excluded.

The sample from the reservoir (*Embalse de Cubillas*) shows strong evaporative enrichment, but cannot be quantified due to the lack of the end-member compositions. The reservoir was build between 1939 - 1963 and stretches over a length of 370 m with a maximum storage capacity of 600 000 m$^3$ and a maximum depth of 52 m (*Ministerio de Medio Ambiente, Embalse de Cubillas* 2001).

The site *Cubillas* 2 is situated in the *Vega de Granada* and is plotting between the reservoir and the *Cubillas 1* sample. In this area of the *Vega de Granada* aquifer the hydraulic behaviour is considered to be influent (gaining river). Therefore, the sample from *Cubillas 2* could be interpreted as mixing between strong enriched river water from the *Cubillas* with less enriched groundwater of the *Vega de Granada* at the north-western part of the *Vega*.
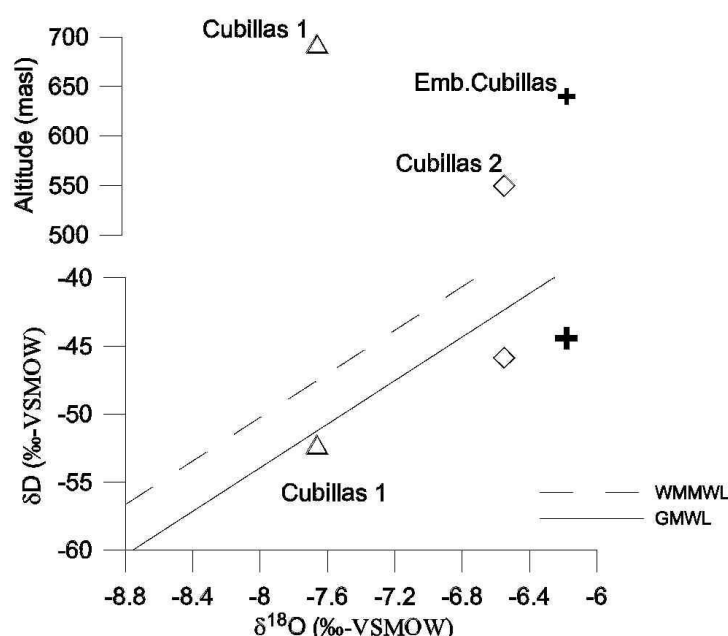


• Figure 4.27 δ$^{18}$O (‰-VSMOW) vs. δD (‰-VSMOW) and δD (‰-VSMOW) vs. Altitude (masl) diagrams of river Cubillas samples.

## 4.2.3.4 *Embalse de Quentar*

The reservoir (*Emb.de Quentar*) is situated near the village *Quentar*, which is situated in the north-eastern part of the study area. This reservoir is fed by the river *Aguas Blancas*, which is a tributary to the *Genil*. The catchment area of the river *Aguas Blancas* is ca. 140 km$^2$ with altitudes from 800–2300 masl (mean altitude = 2500 masl). The reservoir was build between 1971 - 1975 and stretches over a length of 200 m with a maximum storage capacity of 277 000 m$^3$ and a maximum depth of 133m (*Ministerio de Medio Ambiente, Embalse de Quentar* 2001).

The samples were taken from three different depth below surface (-2, -5, -10 m) as shown in fig.4.28. Variations in the $\delta^{18}O$ content in relation to sample depth are within tolerance of measurement precision, thus no trend can be observed. This confirms the assumption that large water bodies like reservoirs can be, at least in winter, considered as a non stratified water column. The $\delta$-values of these samples are located on or slightly over the GMWL. This suggests that may evaporation occurred in the reservoir, but are due to the lack of further samples not quantifiable.
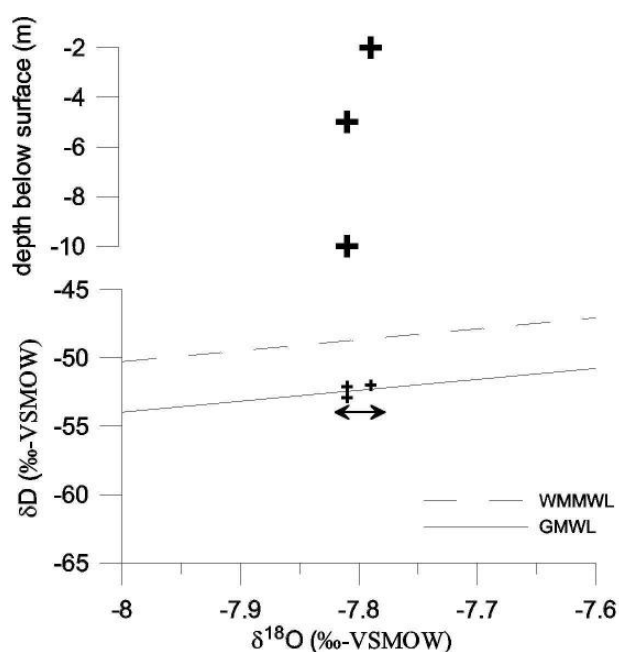


• Figure 4.28 $\delta^{18}O$ (‰-VSMOW) vs. $\delta D$ (‰-VSMOW) of samples from the reservoir *Quentar* and depth below surface (arrow indicates the range of precision in $\delta^{18}O$ measurement).

## 4.2.4 Springs

Groundwater derived from a spring must be considered as a mixture from different altitudes. Thus the mean $\delta^{18}O$ or $\delta D$ value of each sampling location gives an approximation of the spatial and temporal mean elevation of upland recharge. The interpretation of the recharge area for groundwater also includes consideration of the geologic structure, the recharge patterns and the sample type.

According to their $\delta^{18}O$ vs. $\delta D$ relationship, the spring samples show a spectrum of $\delta^{18}O$ from – 9.5 to -8 (‰-VSMOW). D-excess ranges between 10 ‰ and 17 ‰ and confirms the sources of rain bearing air masses from the Atlantic (d-excess = 10 ‰) or the Mediteranean Sea (d-excess = 14 ‰). The position of the spring samples **along** the water lines is used to characterise groundwater recharge provenances. Two main groundwater provenances can be distinguished: a) *Sierra Nevada* and b) *Sierra de la Peza*. Most of the $\delta D$ and $\delta^{18}O$ values plot parallel to the WMMWL, but especially in the *Sierra de la Peza* group several samples plot below of the WMMWL (Fig.4.29). This fact indicates the different climatic conditions and therefore different isotope signature as discussed in section 4.2.2, where the $\delta^{18}O$ composition of precipitation was used to estimate the source area of recharge to springs.

*Sierra Nevada* springs show the most depleted $\delta$-values with –9.5 - -8.5 ‰ and can be subdivided by the spatial location in springs from the metamorphic core of the *Nevado-Filabride* and springs in the *Alpujarride* carbonate complex. Springs located in the north-eastern part of the study area in the *Sierra de la Peza* are considered to be fed by water from the *Sierra Arana* and are significant heavier (-8.5 - -8 ‰-VSMOW).

Springs, surface water and selected precipitation sites are discussed more detailed together with profiles in order to visualise the local recharge pattern.
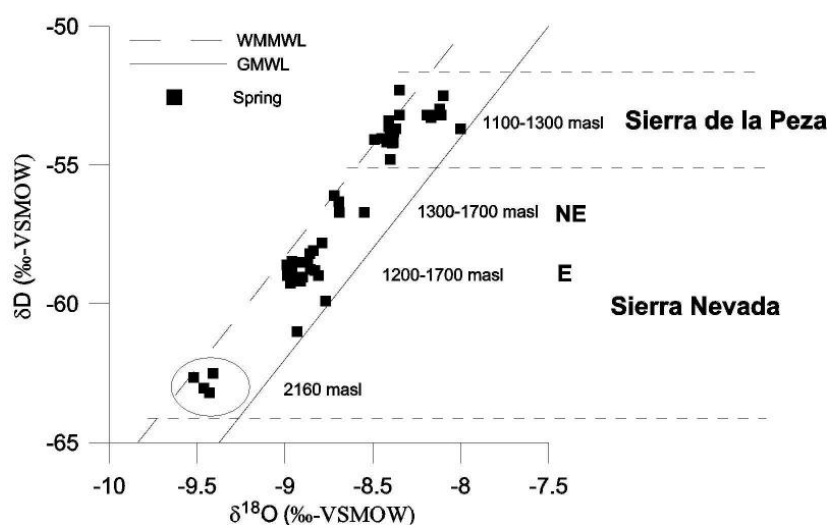


• Figure 4.29 $\delta^{18}O$ vs. $\delta D$ (‰-VSMOW) diagram of spring samples from different *Sierras* in the study area.

Because isotope partitioning at least correlates with temperature and the geomorphology in the study area shows strong temperature gradients, the composition of the groundwater isotope composition depends indirectly on altitude. By plotting the $\delta^{18}O$ value against altitude of the site it is possible to detect local altitude effects.

The regression line calculated with the average values from *Sierra Nevada* springs is defined as: Altitude (masl) = -571.43 * $\delta^{18}O$ - 3522.91 (n = 11; $r^2$ = 0.58), thus the mean altitude gradient is -0.17 ‰ / 100m, which is very close to the gradients from GARRIDO 2003 with 0.2 ‰ / 100 m. The regression line calculated with the average values from *Sierra de la Peza* springs is defined as: Altitude (masl) = -209.04 * $\delta^{18}O$ - 604.81 (n = 6; $r^2$ = 0.58  ), thus the mean altitude gradient is shallower -0.48 ‰ / 100m. Local $\delta^{18}O$ / altitude gradients in the literature vary from -0.2/100 m to -0.5/100 m (CLARK & FRITZ 1997). As shown in figure 4.30 springs which are located on altitudes around 1200 masl with $\delta^{18}O$ values around -9 ‰ (*Fte. Hervidero*, *Fte. 16 Canos*, *Fte. 7 Ojos*) are isotopical equal to springs located on altitudes around 1600 masl. This means that these low elevation springs are fed from the same altitudes as springs on the higher elevation. This increased flowpath should be seen in increased SI values since residence time and therefore reaction time will increase (see transect III).
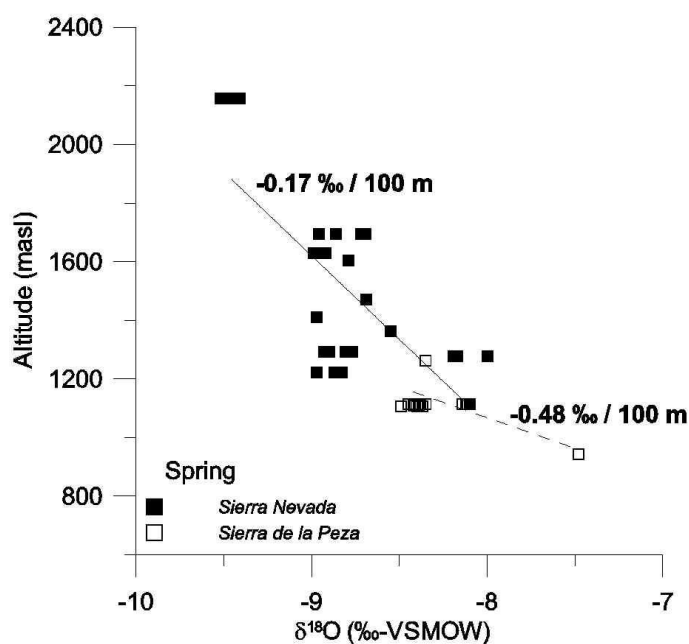


• Figure 4.30 Average $\delta^{18}O$ (‰-VSMOW) vs. Altitude (masl) of all *Sierra*

Mean recharge elevation in transect I and II (Fig.4.31; Fig.4.32) were calculated with the *Sierra Nevada* equation, valid for altitudes between 800 – 2200 masl and introduced in section 4.2.2 (tab.4.6). The rectangles in the isotope profiles for each sampling site shows the mean $\delta^{18}O$, $\delta D$ and d-excess values together with the standard deviation for frequently measured sites. The water table heights are considered to be a subdued copy of the topographic relief, which was derived from the DEM. All isotope transects provide information about local flow paths.

In fig.4.31 the highest sampling site shown is a snow sample taken at the peak of *El Mulhacen* during summer. This signature is characteristic for summer snowmelt as discussed in previous section. The spring located at the highest elevation (*Fte.Alta*) exhibits the most depleted mean $\delta^{18}O$ composition (-9.5 ‰), which represents groundwater recharge provenances in the *Nevado-Filabride* metamorphic core at altitudes >2156 masl. Standard deviation of $\delta^{18}O$ and $\delta D$ is low (0.04 and 0.3 respectively, equal to maximum error in measurement) and reflects that seasonal variations are attenuated. Mean recharge elevation is calculated with 2522 masl (+/-20), giving a relative low difference between real altitude and mean recharge altitude with 367 m. This relative low vertical deviation is confirmed by low run off (6 l/min) and small surface catchment area (ca.10 km$^2$).

*Fte.las Viboras* located in altitudes at 1629 masl (*Alpujarride*) shows mean isotopic composition of $\delta^{18}O$ = -8.97 ‰ and represents groundwater recharge provenances at the border between the *Nevado-Filabride* metamorphic core and the *Alpujarride* carbonate complex. No groundwater flow between the *Alpujarride* carbonate complex and the *Nevado-Filabride* metamorphic core can be observed and confirms the closed boundary conditions. Exchange between these units may be dominated by surface runoff.
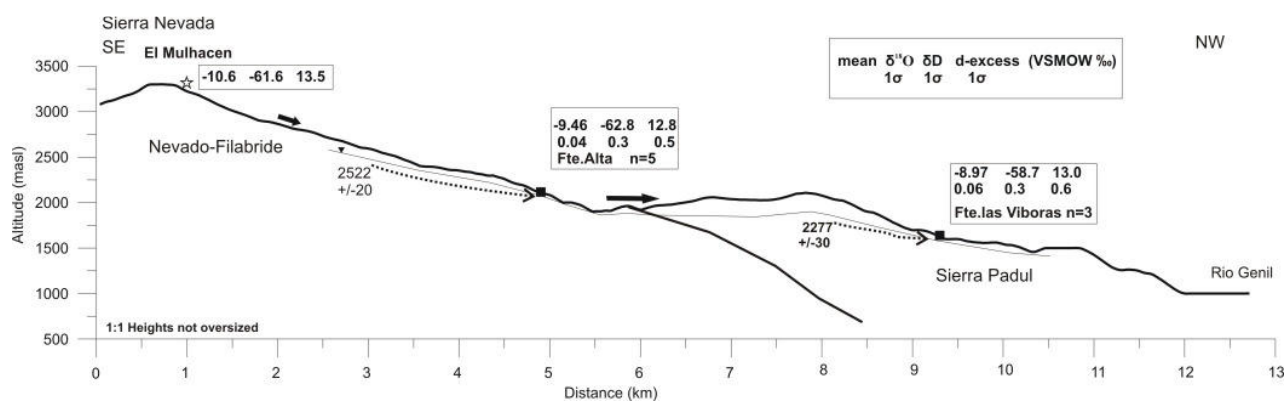


• Figure 4.31 Isotope transect I: High altitude springs and snow samples in the *Sierra Nevada*. Mean recharge altitudes and precision of calculation. Black solid arrows indicate surface runoff, dotted arrows indicate flowpaths, thin line indicate water table. Altitude/distance relation is given in lower left corner.

*Fte.Cortijuela* located in altitude of 1695 masl shows mean isotopic composition of $\delta^{18}O$ = -8.8 and $\delta D$ = -57.6 ‰ with standard deviation of 0.1 and 1.1 respectively. The relative high standard deviation is above the maximum measurement error with 0.07 and therefore seasonal variations are observed in this low runoff (0.8 l/min) and relative small catchment area spring (fig.4.32).

*Fte.del Hervidero* located in altitudes at 1292 masl shows mean isotopic composition of $\delta^{18}O$ = -8.87 ‰. The mean composition is relative light and the mean recharge elevation is calculated with 2229 masl. The high difference between real and calculated mean recharge altitude is 937 m and the calculated undersaturation with respect to calcite and dolomite ($SI_{Cc}$= - 0.7; $SI_{Do}$= -1.9) may be indicative for high flow velocities with minor dissolution of calcite host-rocks.

*Fte.7 Ojos* located in altitudes at 1411 masl shows isotopic composition of $\delta^{18}O$ = -8.97 ‰ and $\delta D$ = -59.2 ‰. This single measurement sample was taken during snowmelt period and might be misleading for calculating the mean recharge elevation since seasonal event is reflected in the *Arr. Huenes* is heavier than the *Fte.7 Ojos* sample and suggest that catchment area of the stream is smaller compared to the catchment area of the spring. No correlation between SI values and vertical deviation between real and mean recharge altitude is observed.
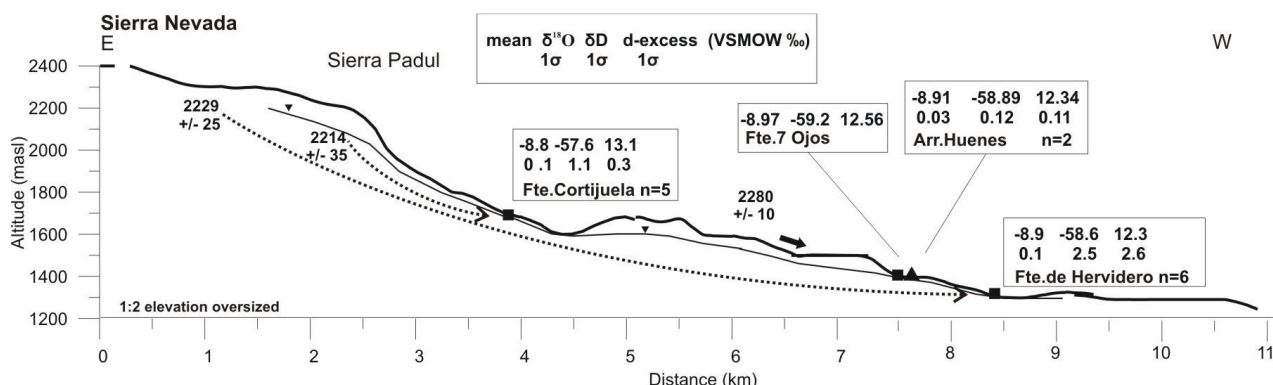


• Figure 4.32 Isotope transect II: High altitude springs and river samples in the *Sierra Nevada*. Mean recharge altitudes and precision of calculation. Black solid arrows indicate surface runoff, dotted arrows indicate flowpaths, thin line indicate water table. Altitude – distance relation is given in lower left corner.

Mean recharge elevation in transect III (Fig.4.33) is calculated with the *Sierra de la Peza* equation (eq.4.12) introduced in section 4.2.5. Mean recharge altitude calculations for springs located in the *Sierra de la Peza* are shown in tab.4.7.

*Fte.Cerro Negro* located in altitude of 1115 masl shows mean isotopic composition of $\delta^{18}O = -8.12$ and $\delta D = -53.0$ ‰ with standard deviation of 0.01 and 0.3, respectively. Mean recharge elevation is calculated with 1505 masl (+/-27), giving a relative low vertical discrepancy of 390 m. Samples from this spring are undersaturated with respect to calcite and dolomite (SI $_{Cc}$ = -0.34; SI $_{Do}$ = -1.03).

*Fte.de Nivar* located in altitude of 1108 masl shows mean isotopic composition of $\delta^{18}O = -8.41$ and $\delta D = -53.9$ ‰ with standard deviation of 0.01 and 0.3 respectively. Calculations of SI confirms the increased flowpath by increased saturation with respect to calcite and dolomite (SI $_{Cc}$ = -0.02; SI $_{Do}$ = -0.37). Spring samples visualised in the isotope transect III show positive correlation between SI values and vertical discrepancy between actual and recharge altitude.

It was recognized that groundwater from low altitude springs must be derived from higher altitudes compared to springs which are situated above. Therefore, the lower the spring is situated the longer the flowpath and the higher the recharge area is.
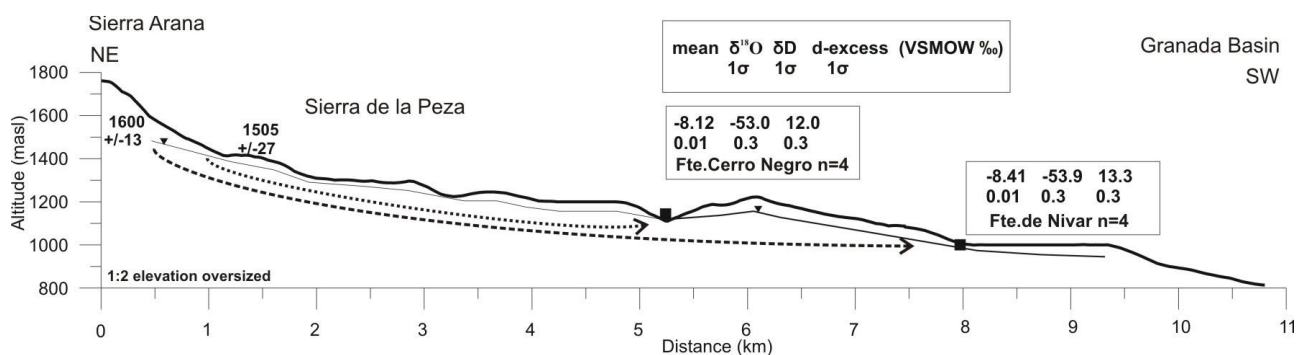


• Figure 4.33 Isotope transect III: Springs and river samples in the *Sierra de la Peza*. Mean recharge altitudes and precision of calculation. Black solid arrows indicate surface runoff, dotted arrows indicate flowpaths, thin line indicate water table. Altitude – distance relation is given in lower left corner.

## 4.2.5 Wells in the *Vega de Granada*

Groundwater samples from wells in the *Vega de Granada* plot **below** of the WMMWL and show variations in $\delta^{18}O$ from –9.2 ‰ to –6.92 ‰ with a preferential enrichment in $\delta^{18}O$ indicating evaporation losses are observed (Fig.4.34). The numbers refer to wells documented in location map figure 4.15.

Samples from wells located in the **south-eastern** part of the *Vega de Granada*, at the beginning of the flowpath (e.g. *Alhencira* (16)) through the alluvial aquifer, plot near to the WMMWL. These samples are considered to be not affected by evaporation but still a displacement to the WMMWL is observed (e.g. *Cullar Vega 1*). This displacement to the WMMWL may implies minor water-rock interactions from the groundwater with the host rocks on its flowpath. Therefore, assuming attenuated seasonal effects, the mean isotopic composition of groundwater in this area can be estimated by drawing a line parallel to $\delta^{18}O$ axis until it intersects with the WMMWL. This results in local mean groundwater compositions in $\delta^{18}O$ of ~ -9.3 ‰. In contrast, groundwater from the **centre** and the **western** part of the *Vega de Granada* is relative enriched in both isotopes with a strong enrichment in $\delta^{18}O$ indicating evaporation losses. The regression line fitted to the 17 well samples is defined as:

$$\delta D = 6.07 * \delta^{18}O - 5.88 \ (n=17, r^2=0.98) \quad\quad\quad (eq.4.14)$$

By taking the annual average temperature (~15°C) from the *Granada* basin (see section 1.4), the slope of the regression line (s = 6.07) allows to approximate the relative humidity according to GONFIANTINI 1986 with around *h* = 0.8 (=80 %). Now it is possible to determine the kinetic fractionation factors using Gonfiantini's equations (section 2.7), giving $\varepsilon^{18}O_{kinetic}$ = -2.84 ‰. The
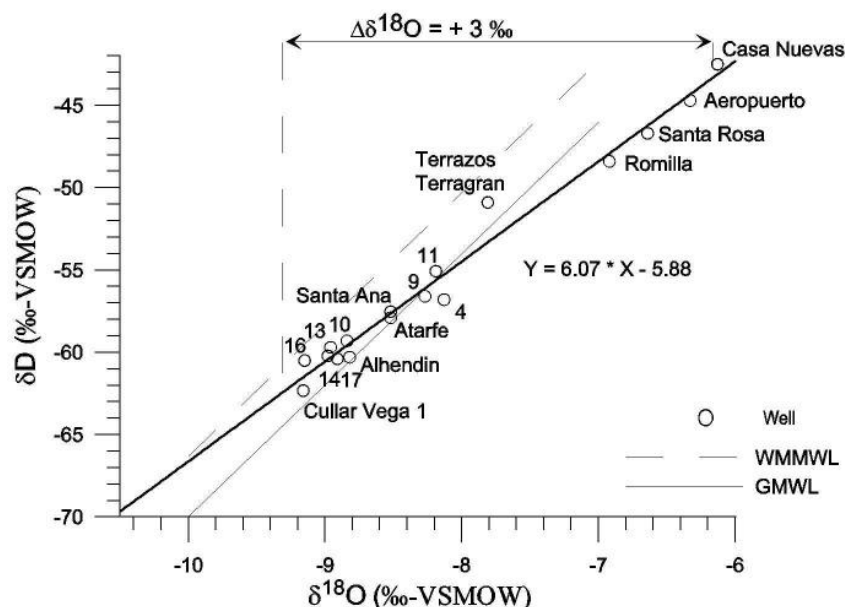


• Figure 4.34 $\delta^{18}O$ vs. $\delta D$ in groundwater from wells in the *Vega de Granada* alluvial aquifer. MWLs as reference. Numbers refer to wells documented in location map (Fig.4.15).

total enrichment ($\varepsilon_{total} = \varepsilon_{equilibrium} + \varepsilon_{kinetic}$) for evaporation under these conditions with the mean temperature of 15 °C in the *Granada* basin ($\varepsilon_{equilibrium}$ = -10.3 ‰) is then $\varepsilon_{total}$ = -13.14 ‰. The intersection of the regression line with the WMMWL is considered as the initial isotope ratio without evaporative impact ($\delta^{18}O_{initial}$ ~ -9.2 ‰). The sample taken from *Casa Nuevas* shows the most enriched value and represents the maximum evaporative enrichment ($\delta^{18}O_{sample}$ = -6 ‰). The total enrichment of this samples can then be calculated with maximum $\Delta\delta^{18}O = \delta^{18}O_{initial} - \delta^{18}O_{sample}$ = 3.2 ‰. The fractional water loss from evaporation can then be modelled according to a Rayleigh distillation. For $\delta^{18}O$, the evaporative enrichment is up to 3.2 ‰. According to equation 2.9.:

$$\varepsilon_{total}(\delta^{18}O) * \ln f = 3.2 \text{ ‰}$$

yielding a residual water fraction *f* of 0.78 and so an maximum evaporative loss in the sample of *Casa Nuevas* of 22 %.

For identifying the source area a correction of $\delta^{18}O$ for evaporative enrichment was applied. Corrected values indicate the isotopic composition without enrichment by evaporation. As the corrected value marks the intersection of the evaporation line with the LMWL (WMMWL), it is defined by equation 4.9, where *s* corresponds to the slope of the evaporation line determined in equation above (eq.4.14) as 6.07, and *i* is the intercept of the WMMWL, with *i*= +13.7 ‰. In the study area the variability of corrected $\delta^{18}O$ in groundwater is assumed to reflect mainly different recharge altitudes. The mean isotopic composition of corrected $\delta^{18}O$-values is -10.16 ‰, while uncorrected $\delta^{18}O$-values lead to an average of -8.13 ‰ (Tab.4.8). This exceptional low mean isotopic composition of corrected $\delta$-values leads to the assumption that either the regression line is false due to wrong measurements or other processes like water-rock interaction might shift the $\delta$-values. Examination of this assumption might be subject to further studies.

• Table 4.8 Sites, type, date of sampling, $\delta^{18}O$, $\delta D$ (‰-VSMOW), corrected values without evaporative enrichment for $\delta^{18}O$ (‰-VSMOW) in wells and observation wells and the resulting evaporative enrichment.

| Site name | Type | Sampling date | $\delta^{18}O$ (‰) | $\delta D$ (‰) | $\delta^{18}O$ (‰) corrected | $\delta^{18}O$ (‰) enrichment |
|---|---|---|---|---|---|---|
| Aeropuerto | Observation well | 25. Nov 04 | -6.33 | -44.7 | -10.35 | 4.02 |
| Alhencira | Well | 18. Feb 05 | -9.15 | -60.5 | -9.67 | 0.52 |
| Alhendin | Observation well | 08. Nov 04 | -8.82 | -60.3 | -10.6 | 1.78 |
| Armilla | Well | 18. Feb 05 | -8.98 | -60.2 | -10.06 | 1.08 |
| Atarfe | Observation well | 17. Nov 04 | -8.52 | -57.9 | -10.3 | 1.78 |
| Camino frente Puleva | Observation well | 16. Nov 04 | -8.84 | -59.3 | -10.02 | 1.18 |
| Casa Nuevas | Well | 22. Nov 04 | -6.13 | -42.5 | -9.84 | 3.71 |
| Cort. Santa Ana | Well | 18. Feb 05 | -8.52 | -57.5 | -10.11 | 1.59 |
| Cort. Trevijano | Observation well | 26. Nov 04 | -8.27 | -56.6 | -10.42 | 2.15 |
| Cullar Vega 1 | Observation well | 09. Nov 04 | -8.96 | -59.7 | -9.85 | 0.89 |
| Cullar Vega 2 | Well | 18. Feb 05 | -9.16 | -62.3 | -10.58 | 1.42 |
| Meson El Guerro | Well | 18. Feb 05 | -8.91 | -60.4 | -10.37 | 1.46 |
| Pedro Ruiz | Observation well | 12. Nov 04 | -8.13 | -56.8 | -10.96 | 2.83 |
| Romilla | Observation well | 05. Nov 04 | -6.92 | -48.4 | -10.41 | 3.49 |
| Santa Rosa | Well | 10. Nov 04 | -6.64 | -46.7 | -10.41 | 3.77 |
| Terrazos Terragran | Well | 18. Feb 05 | -7.81 | -50.9 | -8.91 | 1.1 |
| UGR, Facultad de Ciencias | Well | 09. Mrz 05 | -8.19 | -55.1 | -9.87 | 1.68 |
| | **min** | | **-9.16** | **-62.3** | **-10.96** | **0.52** |
| | **max** | | **-6.13** | **-42.5** | **-8.91** | **4.02** |
| | **mean** | | **-8.13** | **-55.28** | **-10.16** | **2.03** |

The spatial distribution of the measured $\delta^{18}O$ - values of groundwater from well samples and one spring sample (*Man.de la Reina*) from the *Vega de Granada* (without thermal springs) is used for interpolation with Surfer 7.0 using the kriging method, after fitting the data set to a spherical variogram. The resulting grid was converted a shapefile format and imported to ArcGis 8.3.

Figure 4.35 shows the spatial distribution of $\delta^{18}O$ values in groundwater from the *Vega de Granada* with the average δ-values of sampled rivers. Highly depleted δ-values can be found in the central **northern** and the **south-eastern** part of the *Vega de Granada* alluvial aquifer, while enriched δ-values are found in the **western** part of the *Vega de Granada*.

The *Rio Genil* is at the inflow to the *Vega de Granada* with $\delta^{18}O$ = -8.3 ‰ one per mill lighter than at the outflow with -7.3 ‰. The hydraulic regime in the *Vega de Granada* changes from influent (losing river) at the inflow of the *Rio Genil* to effluent (gaining river) at its outflow. Thus, the *Genil* carries at the outflow of the *Vega de Granada* the hydrochemical and the isotope signature of the groundwater. In the **south-eastern** part of the *Vega de Granada* the most depleted values can be found in the sample from the well *Cullar Vega 1* ($\delta^{18}O$ = -9.12 ‰), in the depth below surface of 110 m. In this area the under-surface depth of the wells is between 50 – 110 m and isotope stratification may be evident. Shallow groundwater is more enriched in δ-values compared to groundwater below. This fact indicated low vertical mixing of groundwater. The mean isotope signature of the *Rio Darro* at the inflow to the *Vega de Granada* was significant enriched compared to the groundwater of the *Vega de Granada*. This is interpreted as a minor influence of the *Darro* for GWR through indirect infiltration.
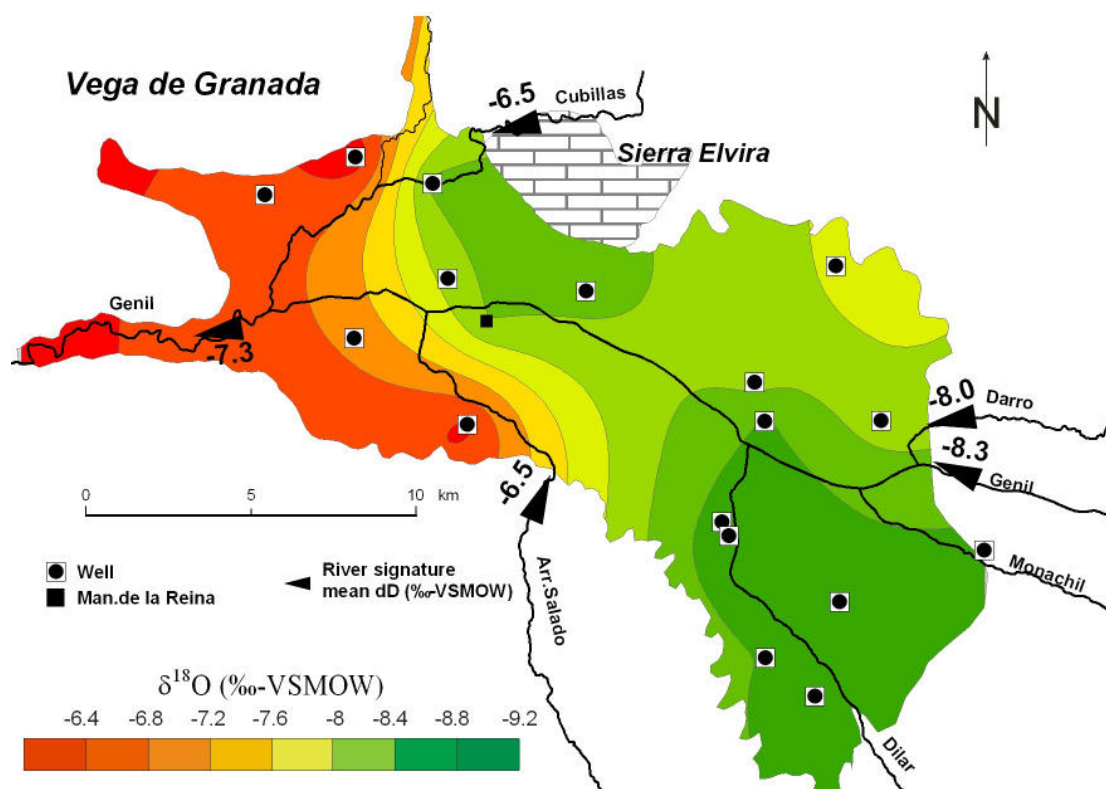


• Figure 4.35 Spatial distributions of $\delta^{18}O$ values in the alluvial aquifer *Vega de Granada* with mean $\delta^{18}O$ values of sampled rivers.

Controversy, the mean isotope signature of the *Rio Genil* at the inflow to the *Vega de Granada* was very similar compared to the groundwater of the *Vega de Granada*. This is interpreted as a strong influence of the *Genil* for GWR through riverbed infiltration.

The high depletion in the **south-eastern** part of the *Vega de Granada* indicates a strong groundwater flow derived from high altitudes in the *Sierra Nevada* (>2200 masl). The groundwater recharge may take place by indirect infiltration. Unfortunately, no samples were taken from the *Rio Dilar*. This river might play an important role in the recharge dynamics in the **south-eastern** part of the *Vega de Granada*.

A flow of depleted groundwater is observed south to the *Sierra Elvira* carbonate complex in the central **northern** part of the *Vega de Granada*. Groundwater in this area is in $\delta^{18}O$ around -8.4 ‰ and indicates the importance of the *Sierra Elvira* carbonate complex as a local groundwater recharge area. One of the most important springs in the *Vega de Granada* (*Manantial de la Reina*) with 12.000 l/m runoff can be associated, according to the similar isotope signature with groundwater from wells in the north (*Cort. Santa Ana*, *Atarfe*), to groundwater recharge area in the *Sierra Elvira*.

The **north-eastern** part of the *Vega de Granada* was sampled only at one well-site (*Terrazos Terragren*) and shows an moderate isotope signature, which is not affected by evaporation ($\delta^{18}O$ = -7.81 ‰; $\delta D$ = -50.9 ‰).

The river *Arr. de Salado* was sampled once at the **southern** inflow to the *Vega de Granada*. The $\delta^{18}O$ value of -6.5 ‰ ($\delta D$ = -48.24 ‰) is significant lighter than the interpolated isotope distribution of the groundwater with -7.2 – -7.6 ‰. According to the $\delta^{18}O$ vs. $\delta D$ distribution this sample is shifted from the WMMWL. The very unique hydrochemical composition (see section 4.1.2) of this brine

Samples from the *Rio Cubillas* at the **north-western** inflow to the *Vega de Granada* plot below of the WMMWL and show a preferential enrichment in $\delta^{18}O$ indicating evaporation losses (section 4.2.3.3). The high evaporative enrichment in the **western** part of the *Vega de Granada* could be explained by mixing processes of enriched surface water derived from the rivers (*Cubillas*, *Arr. Salado*) with depleted groundwater derived from eastern part of the *Vega*. The degree of this enrichment signature might be emphasized by recycling of groundwater due to irrigation use, leading to the observed evaporative enrichment signature in groundwater samples.

It is important to recognize that GWR dynamics for the *Vega de Granada* is close connected to river-groundwater interactions and a detailed sampling of this interface may be subject for further studies.

Since groundwater signature is more depleted than mean volume weighted precipitation no propriate water surplus from the *Vega* itself can be observed. Only heavy winter rain events may be able to potentially recharge the *Vega de Granada* alluvial aquifer.

## 4.2.6 Thermal Springs

All thermal springs are considered to be of meteoric origin and are influenced by hydrothermal activity in the Betic Cordillera. In accordance to the hydrochemical classification (section 4.1.2), the thermal springs can also be divided by the isotope signatures in two subgroups. Samples which are located **near** to the WMMWL are supposed to be less influenced by water-rock interactions, while points which are **shifted** from the WMMWL represent progressively increasing water-rock interaction with the host-rocks of the aquifer under various water temperature conditions.

The $\delta^{18}O$ vs. $\delta D$ distribution of thermal spring samples is shown in figure 4.36. The *Fte.Urquiza* samples are the most depleted of all thermal springs and are located **near** to the WMMWL with a subparallel shift to the $\delta^{18}O$ axis of $\Delta 0.3$ ‰. This subparallel shift could be interpreted as water-rock interaction from the thermal water with calcite host-rocks under low temperature conditions (water temperature = 22.5 ºC). As expected for water-rock interaction, the $\delta D$ values were not or only slightly altered and the d-excess is quite constant (around +13 ‰). The low deviation in $\delta D$ values of the *Fte.Urquiza* spring samples can be explained by a wide catchment area where seasonal variations are attenuated. The samples from this double tube spring shows the most depleted $\delta$-values with $\delta^{18}O = -8.8$ ‰ and can be associated to recharge altitudes from 2200-2300 masl (see section 4.2.2).

Samples from *Baños* (*Baños de la Malah*, *Baños Santa Fe*, *Baños Alhama de Granada*, *Baños Sierra Elvira*) are **shifted** from the WMMWL. Assuming a similar subparallel shift for the *Baños* samples it is possible, by calculating the matching point from the regression line with the WMMWL, to estimate the initial isotopic signature. The regression line calculated only with *Fte.Urquiza* samples may be indicative for water-rock interaction with calcite host-rocks described by:

$$\delta D = 1.88 * \delta^{18}O - 41.46 \qquad\qquad (eq.4.15)$$
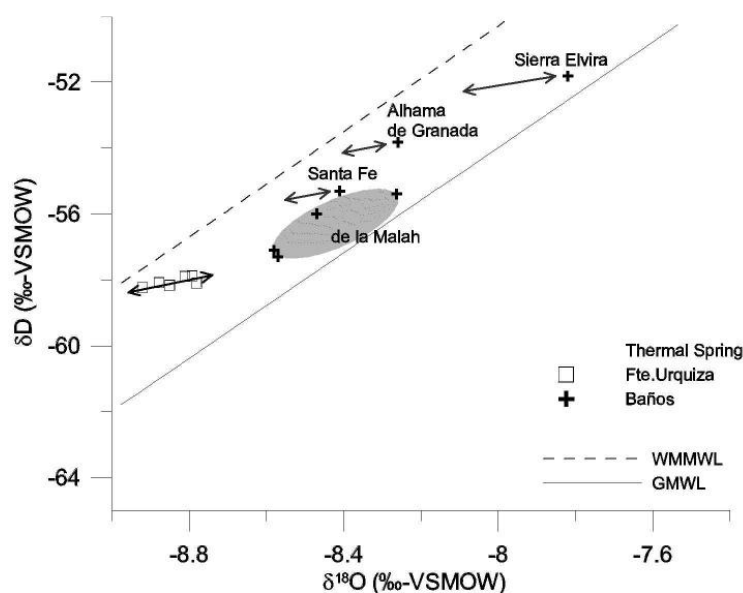


• Figure 4.36 $\delta^{18}O$ (‰-VSMOW) vs. $\delta D$ (‰-VSMOW) diagram of thermal springs.

By calculating corrected $\delta^{18}O$ values and subtracting these values from the measured it is possible to plot the deviation in $\delta^{18}O$ from the WMMWL against water temperature. These corrected $\delta^{18}O$ values are considered to be representative for the initial composition of the thermal waters and therefore indicative for mean recharge elevation (Tab.4.9). Samples taken from sites called Baños are considered to be shifted subparallel to the $\delta^{18}O$ axis according to the trend in *Fte.Urquiza* samples.

• Table 4.9 Sites, Altitude (masl), date of sampling, δ $^{18}$O, δ $^{18}$O error (‰) and mean recharge elevation (masl) for thermal springs.

| site | Altitude (masl) | date | $\delta^{18}O$ (‰) | $\delta^{18}O$ error (‰) | $\delta^{18}O$ corrected (‰) | mean recharge Altitude (masl) |
|---|---|---|---|---|---|---|
| Fte. de Urquiza | 650 | 05. Feb 04 | -8.79 | 0.03 | -9 | 2293 (+/-15) |
| Fte. de Urquiza | 650 | 16-Oct-04 | -8.81 | 0.03 | -8.99 | 2291 (+/-15) |
| Fte. de Urquiza | 650 | 10-Mar-05 | -8.92 | 0.02 | -9.01 | 2302 (+/-10) |
| Fte. de Urquiza left | 650 | 05. Feb 04 | -8.88 | 0.04 | -9 | 2297 (+/-20) |
| Fte. de Urquiza left | 650 | 16-Oct-04 | -8.78 | 0.03 | -9.03 | 2312 (+/-15) |
| Fte. de Urquiza left | 650 | 10-Mar-05 | -8.85 | 0.01 | -9.02 | 2307 (+/-5) |
| Baños de la Malah | 752 | 06. Feb 04 | -8.26 | 0.02 | -8.75 | 2170 (+/-10) |
| Baños de la Malah | 752 | 16-Oct-04 | -8.47 | 0.03 | -8.79 | 2188 (+/-15) |
| Baños de la Malah | 752 | 22. Nov 04 | -8.57 | 0.02 | -8.97 | 2279 (+/-10) |
| Baños de la Malah | 752 | 5-Mar-05 | -8.58 | 0.01 | -8.93 | 2261 (+/-5) |
| Baños de Sierra Elvira | 571 | 18. Feb 05 | -7.82 | 0.02 | -8.3 | 1946 (+/-10) |
| Baños Santa Fe | 840 | 18. Feb 05 | -8.41 | 0.02 | -8.69 | 2141 (+/-10) |
| Baños Alhama de Granada | 760 | 10-Mar-05 | -8.26 | 0.02 | -8.5 | 2042 (+/-10) |

LOPEZ-CHICANO et al. 2001 reported of recharge areas for the *Alhama de Granada* thermal springs in the *Sierra Tejeda* located in the *Alpujarride* domain. LOPEZ-CHICANO et al. 2001 also used several geothermometers (Ab, Qz, An) for calculating equilibrium temperatures and reports of maximum water temperatures in the under surface reservoir of 110 ºC. By using a normal geothermal gradient (~3 °C/100 m) it is possible to calculate the subsurface reservoir depth with ca. 3.6 km. Since the *Granada* region is expected to be a terrain with high geothermal gradients, the reservoir depth must be considered shallower.

The deviation in $\delta^{18}O$ from the WMMWL provides information about the degree of water-rock interaction. Since water-rock interaction is driven by the local carbonate content in the host-rocks on the flowpath and temperature, spring which are situated in carbonates are more deviated than springs which are located in the siliciclastic basin formations. Thermal springs which are located rather in the central part of the *Granada* basin are, despite of their high water temperatures, less deviated than springs which are located at the margins of the basin. In general, no clear correlation between deviation in $\delta^{18}O$ from the WMMWL and temperature can be observed. Only the samples from *Baños de la Malah* show a positive correlation between the water temperature and the high deviation from WMMWL. The high variance in the samples from *Baños de la Malah* may be indicative for mixing processes from deep thermal water with shallow groundwater (Fig.4.37).
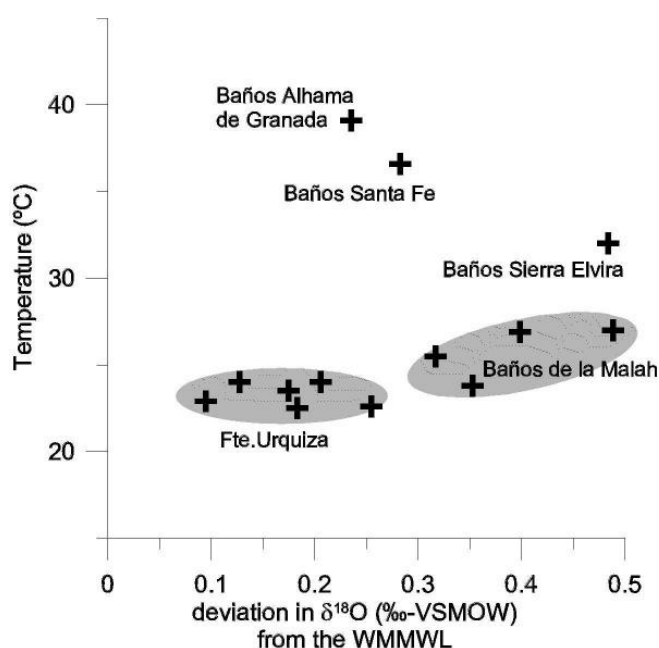


• Figure 4.37 Deviation in $\delta^{18}O$ (‰-VSMOW) from the WMMWL vs. water temperature (°C) of thermal springs samples.

# 5 GEOLOGICAL MAPPING
## 5.1 Introduction

The mapping area is situated near to the town of *Granada*, in southern Spain in the province of Andalusia. The rectangular area occupies an area of approximately 24 km$^2$ (ca. 4x6 km). The corner coordinates are (UTM, WGS84, Zone 30N):

NW : 446 994 / 4 117 167          NE : 453 277 / 4 117 167

SW : 446 994 / 4 113 105          SE : 453 277 / 4 113 105

The topographic data basis maps were the "Hojas 1009; 1026 (1:50 000)" and the geological base maps were the "Mapa Geologia (IGME 1985): *Mapa Geologico-Minero de Andalucia* (1:400 000) (*Junta de Andalucia* 1985)".

The field work was done between November 2004 and February 2005 during an `Erasmus` semester at the *Universidad de Granada* (UGR).

The highest point within the mapping area is a mountain peak in the NE corner with 1083.5 masl. From this point the elevation heights are decreasing in topographic steps to the southwest. Two main rivers are situated in the mapping area: (1) the *Rio Darro*, entering the area in the NE corner and after a sharp bend it courses E-W right in the middle of the mapping area and (2) the *Rio Genil* in the southern part. The *Rio Genil* is considered to be the approximately southern limit of the mapping area.

The mapping area is located in the Neogene fillings of the *Granada* basin. The formations in the mapping area are showing stratigraphic ranges from upper Miocene to Quaternary (Tab.5.1). The youngest formation is the alluvial deposit and river terraces of the *Rio Darro*. Most of the mapping area (70 %) is covered by the formation called "*Conglomerados de la Alhambra*" which is mainly composed of conglomerates and sand. This formation is dated as Villafranchian by using paleontological evidence (AGUIRRE 1957). Within this formation several (paleo-) soils can be found. Below of the *Alhambra* conglomerates a minor formation of red Sandstones is found. This formation is considered to be of middle Pliocene age. To the east older sequences of siltstones and conglomerates are lying under the *Alhambra* conglomerates termed as *Cenes de Lancha* formation. The oldest formation (*Pinos de Genil*) comprises of grey, calcareous siltstones and can be found in the very eastern part of the mapping area. For the stratigraphic ranges of the formations see table 5.1.

• Table 5.1 Neogene stratigraphy with stage ages from 2004 (IUGS 2004) and stage ages from 1975 and stratigraphic ranges of the formations in the mapping area.

| Era Erathem | System Period | Series Epoch | | Stage Age (2004) | Age Ma | Stage Age (1975) | Formations |
|---|---|---|---|---|---|---|---|
| Cenozoic | Neogene | Holocene | | | 0.0115 | Oldenburgian | Alhambra Conglomerates red Siltstones Cenes de Lancha Pinos Genil |
| | | Pleistocene | Upper | | 0.126 | Biharian | |
| | | | Middle | | 0.781 | | |
| | | | Lower | | 1.806 | Villafranchian | |
| | | Pliocene | Gelasian | | 2.588 | | |
| | | | Piacenzian | | 3.600 | | |
| | | | Zanclean | | 5.332 | Ruscinian | |
| | | Miocene | Messinian | | 7.246 | Turolian | |
| | | | Tortonian | | 11.608 | Vallesian | |
| | | | Serravallian | | 13.65 | Maremmian | |
| | | | Langhian | | 15.97 | Vindobonian | |
| | | | Burdigalian | | 20.43 | Burdigalian | |
| | | | Aquitanian | | 23.03 | Aquitanian | |

Aim of this work is to make a geological map, by practising field methods, interpreting the data and presenting these in the form of maps, diagrams and text. The geological map is in scale 1:20 000 and presented as paper copy at the end of this work. Prof. Dr. J. Azañon (UGR) supervised the field work and gave the initial idea, which was to get a more detailed sight on the tectonic structures. In the work "Small-scale faulting, topographic steps and seismic ruptures in the Alhambra (*Granada*, southeast Spain)" AZAÑON et al 2004, the author postulates a direct relationship between cracks in the 14th century old monument of the *Alhambra* and seismic induced ruptures in the underlying sediments. The authors are describing in this work the main faults and corresponding cracks in walls or towers in the *Alhambra* monument (AZAÑON et al 2004, Figure 5.4).

This geological mapping tries to amplify the view on the geological structures to the surrounding areas. The idea was to map the tectonic structures of the sediments around the *Alhambra* monument with the main focus on active tectonic structures and their relation to the recent stressfield. Additional, sedimentary structures and morphological features were used to determine the geological history of the mapping area. According to AZAÑON 2004 the *Alhambra* building underwent important tectonic impacts during their existence. These impacts are today visible in cracks within the walls and towers, small scale faults and cm to meter scale displacements of paleosoils. Within the mapping area several historical monuments are situated, witnessing the rich historical past of the *Alhambra* and the city of *Granada*. From the time of the Roman Empire gold mining is well documented in the *Granada* area. The Romans' gold mining technique

involved undermining entire mountains, using a method called „Ruina Montium". By feeding vast quantities of water, along hydraulic systems and then inducing man-made landslides (MARTIN 2000). Then, slaves panned and picked up the gold. Remains of such works still can be seen in the imposing gold mine near *Cenes de Lancha* (Photo 5.1). Later, between the years 1875 and 1877 a French gold mining company runned the gold mine again and gained an average gold content of $0.5g/m^3$. They dismantled the gold-bearing conglomerate by using a powerful water stream and separated the gold by amalgation with mercury (MARTIN 2000).



• Photo 5.1 Panoramic view of open gold mine near *Lancha de Cenes*
(*Mina de Oro* X 450 867 Y 4 113 962 viewpoint NNE).

The geological evolution of the *Granada* basin is described in chapter 1. Figure 5.2 shows the schematic geological development of the eastern border of the *Granada* basin with emphasising the corresponding conglomeratic units, like the *Alhambra* formation. The sketch in figure 5.2 makes clear that the *Alhambra* formation is derived from the *Alpujarride* and the metamorphic units (*Mulhacen, Veleta*) during stages of extensional tectonic motions.
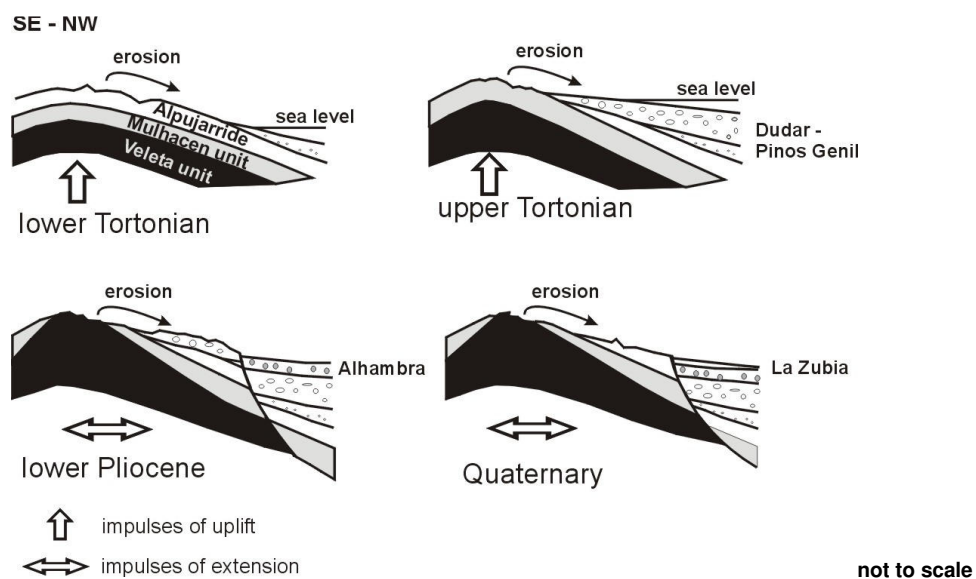


• Figure 5.2 Sketch of the geological history of the eastern border of the *Granada* basin and the *Sierra Nevada* showing the stratigraphic architecture of the corresponding conglomerate units. (modified after MARTIN & BRAGA 1997).

73

Several caves can be found in the mapping area. The caves were excavated in the unconsolidated rocks of the *Alhambra* formation. The *Granada* city district *Sacromonte*, in the northwestern part of the mapping area is famous for its house caves. Other caves, most of them uninhabited, are situated in the southern hillsides (photo 5.3).

• Photo 5.3 Uninhabited cave dwelled in the unconsolidated *Alhambra* formation.
(X 450 540 Y 4 113 864)
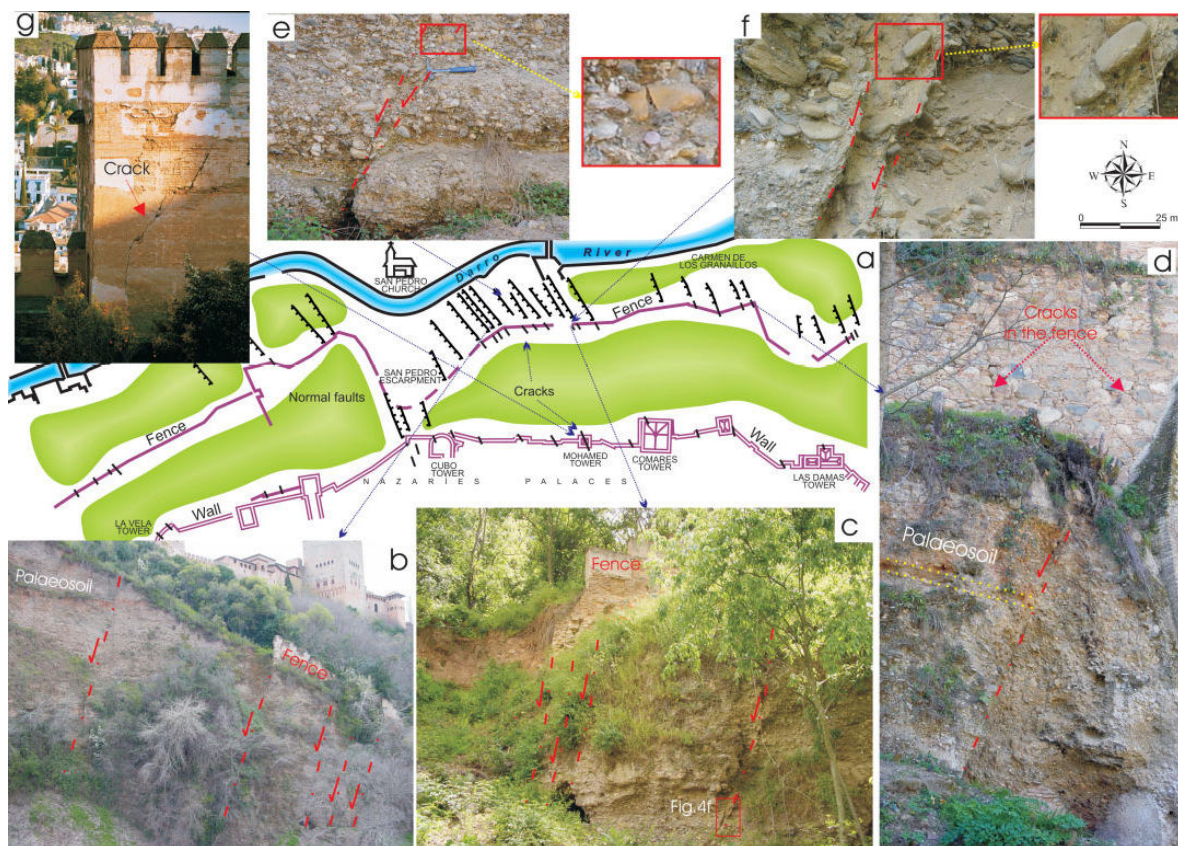


Figure 5.4 (a) Sketch of the northern hillslope of the Alhambra showing the small-scale faults (saw-shaped black lines) observed in the field, as well as the main cracks (black lines) in the fence and wall. (b) Decametrescale faults affecting a palaeosoil. Displacement of these faults is approximately 50 cm. (c) Three decametre-scale faults underlying the fence of the Alhambra. The fence is collapsed in relation to one of these faults. (d) Cracks in the fence of the Alhambra situated just over a metre-scale fault in the conglomerate. Note palaeosol rotated in the hanging wall of the fault. (e) Metre-scale fault in the Alhambra conglomerate. Note the fractured clast in the upper part of the fault zone (red rectangle and magnification to the right). (f) Decimetre-large fault zone with a broken and displaced clast (red rectangle and magnification to the right). Clast is approximately 5 cm long. (g) Crack in the Mohamed tower. (AZAÑON et al 2004)

## 5.2 Methods

According to the aims of this work the collection of field data concerned primarily sedimentological and structural aspects. Classical methods were applied and information was recorded at outcrops within the sedimentary formations. Tools and aids used are simple, and include hammer and compass (with clinometer), 10% hydrochloric acid, hand lens, penknife, folding rule, digital camera and binocular. The main aspects of sedimentary rocks recorded in field are:

-Lithology: mineralogy/composition and colour
-Texture: grain size, grain shape, sorting and fabric
-Beds: bed thickness, contacts between beds, bed geometry
-Sedimentary structures: internal structures of beds, larger scale structures

Clasts in the conglomerates are measured within $1m^2$ at selected locations using three geometric factors.

   a) max. length
   b) max. width, perpendicular to a)
   c) max. thickness, perpendicular to a) and b)
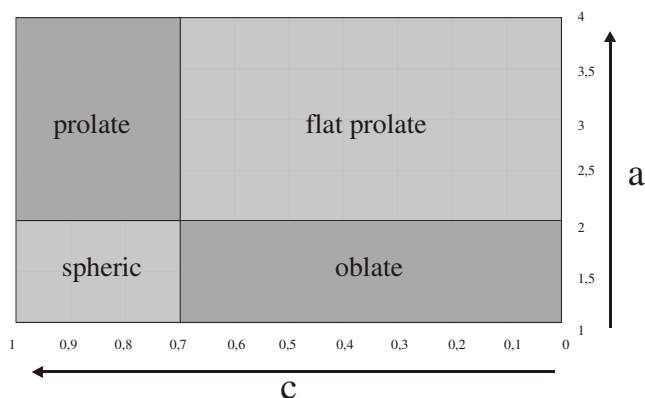


• Figure 5.5 Relationship between shape and lithology (after VALLETON 1955)

The geometric factor b was set to 1 and a and b were plotted as shown in Fig. 5.5. Further information about lithology and grade of roundness has been recorded. Derived from this data it is possible to show the relationship between lithology and shape.

Stereographic plots were done with the freeware StereoNet. Various geographical information systems (GIS) (ArcView 3.2, ArcGis 8.2) were used for generating and presenting maps.

## 5.3 Structural data

The mapping area lies in the Neogene intramontane *Granada* basin. The basin is, according to the seismographic record, one of the most seismically active zones in the whole Iberian Peninsula. Some authors try to estimate the time period in which large earthquakes will occur and SANZ DE GALDEANO et al. 2003 suggest a period of 500 years for earthquakes of magnitude 6. The recent stress field can be described as NW-SE striking compressive and a NE-SW striking extensional vector (GIL 2002) (Fig. 5.6).
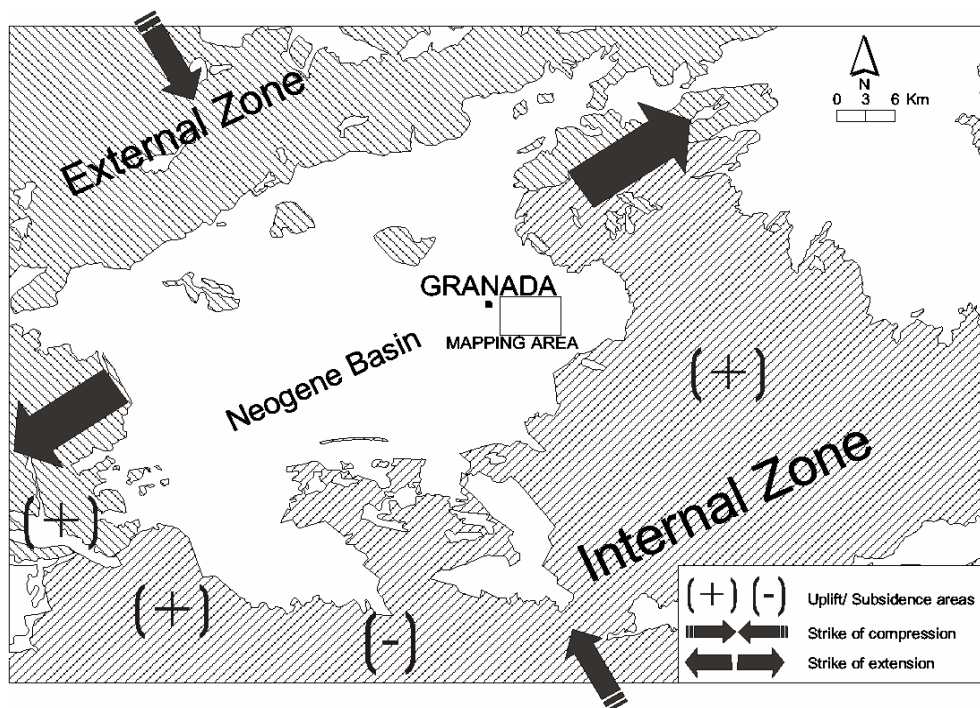


• Figure 5.6 Recent stressfield in the Granada basin. Crosses indicate uplift, minus indicate subsidence (modified after GIL 2002). Geology simplified from IGME 2002.

The Granada basin is affected by at least two sets of important faults. The faults of N 70E to E-W direction form the first set. They are the longest and oldest because many of them moved during the early and middle Miocene (SANZ DE GALDEANO 2003). Recent stress field of the Betic Cordillera can be described as an approximate NNW-SSE compression, combined with a near perpendicular extension (Fig.5.6). At the same time, the region was rising up (crosses), while other parts underwent subsidence (minus) (GIL 2002). The approximate NW-SE faults form the second set. These faults are also present in the eastern sector of the basin as well as in its interior, affecting areas such as *Sierra Elvira*, *Granada*, *Padul* etc. They basically move as normal faults, locally very important and, as in the previous set, moved from the late Miocene to the present. Some of them show a constant and noticeable microseismicity. The second set is considered to be very active and is made responsible for many earthquakes affecting the central and eastern sectors of the basin. The trend of the faults of its two sets facilitates the extension, generally producing small to moderate earthquakes (SANZ DE GALDEANO 2003).

Strike and dip of faults and bedding was measured in field and average values are presented in the geological map. In the mapping area a set of NW-SE orientated normal faults can be found (e.g. Photo 5.7). Most of them show dip-slip kinematics as observed in listric sheer plains at *Barranco de Teatino* (section 5.4.3). Sometimes, weak strike-slip components cannot be excluded, and a wide range of displacement from cm to several m scales is observed. Most of these faults can be considered as extensional features, parallel to the slip vector between Africa and Iberia.
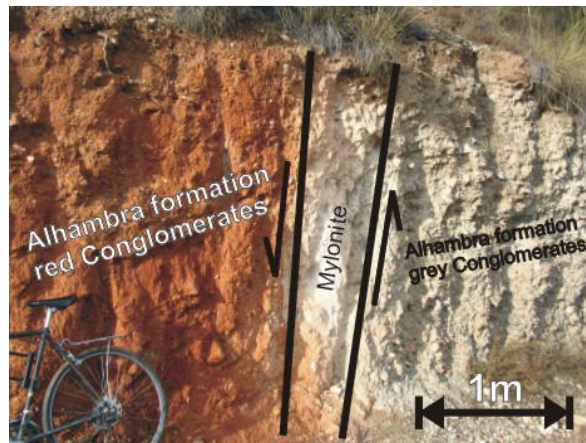


• Photo 5.7: Red and grey conglomerates from the Alhambra formation and
normal fault with strike NW – SE and dip 80° to SW (at 449 500 / 4 114 490).

The distribution of the dip orientations of faults is shown as a rose diagram in figure 5.8. Generally, most of the faults have NW–SE orientations with dip degrees about 60-80. In the mapping area huge amounts of small-scale faults (0.4 m to 2 m length and a displacement of mm to cm) and several main faults (2 m to 5 m visible length and displacement of hectometre to kilometre) can be observed. Photo 5.7 shows an important outcrop for the typical normal NW-SE faults. This fault is considered to be responsible for recent tectonic motions (AZAÑON et al 2004). Clasts at the fault zone are often reoriented parallel to the fault boundary (e.g. Photo 5.13). Sometimes broken clasts (Photo 5.14) or even fault-gauges can be observed. Small scale thrusts with cm displacement are visible in the mapping area (Photo 5.2). Reactivated faults with 2 or more Calcites crusts within the crack can be observed close



• Figure 5.8 Rose diagramm showing the dip direction of the
measured faults.

to the *Silla de Moro* (seat of the moors). The *Silla de Moro* is an ancient arabian ruin, very close

in the north to the *Alhambra* monument. Here, also NE dipping faults considered as not active were observed.

In the south of the mapping area the bedding of the Alhambra formation is often dipped with ca. 20 ° to SW. The dip direction is perpendicular to the second set of faults in the mapping area. Most of the faults crop out at the northern side to the *Alhambra* hill. Broken clasts or paleosoils are observed and have been used as markers to estimate displacement (Photo 5.9). In other cases striaes on fault plains were used to determine the direction of motion.



• Photo 5.9 Small scale thrust (at 448 488 / 4 114 700) with cm
scale displacement. (Hammer length 35 cm).

Especially north to the *Rio Darro* topographic steps are visible separated by normal faults (Photo 5.10). One of these faults is striking NW-SE and separates the hills of *Cerro de San Miguel* and the south to the *Rio Darro* situated *Alhambra* hill. The stairway geometry of the topography is associated from AZAÑON et al 2004 to perpendicular striking normal faults dipping to the SW. The geomorphology and the geometry of the drainage network are strongly indicating the tectonic origin of these steps. The mapping area can be described as fault-bounded graben-horst structure.
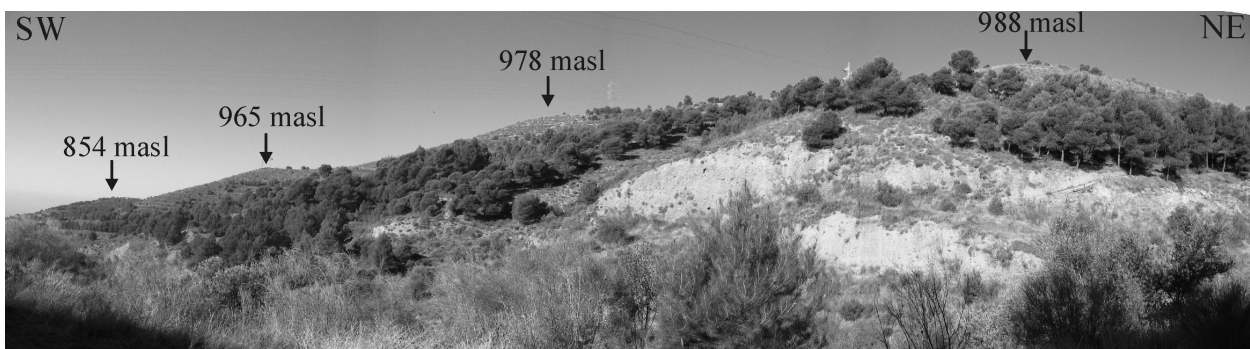


• Photo 5.10 Toppgraphic steps in the *Alhambra* Formation (at 449 694/4 115 920, viewpoint to NW)

## 5.4.1 Alluvial deposits
### Holocene

The youngest formations of the mapping area are Holocene alluvial deposits of the river *Darro*, which can be found in the centre of the mapping area, in the valley of the *Darro*. The *Rio Genil* is channelled and urbanised in the mapping area and no outcrops can be found. The level of the alluvial deposit of the *Rio Darro* is few meters above today's level. The lithology is characteristic for fluviatile deposits.

## 5.4.2 Conglomerates and Sandstones (´*Conglomerados de la Alhambra*´)
### Plio-/Pleistocene

The ´Alhambra Formation´ crops out largely in the eastern sector of *Granada* city. It is deposited discordant over the red Sandstone formation (5.4.3), which can be observed in *Barranco del Teatino*, or above *Cenes de Lancha* formation (5.4.4) with erosional contact. The `*Conglomerados de la Alhambra*` are stratigraphically younger than the Pleistocene sediments (MORENO et al. 1988), and have been dated as Villafranchian using paleontological evidence (AGUIRRE 1957). The Formation is considered to be a redeposit of a conglomerate of Miocene age. The origins of these sediments are connected to tectonic uplift and erosion of the surrounding *Sierras* and are interpreted as coalescent alluvial fan deposits. A geological profile taken from selected outcrops in the valley of the *Rio Darro* is used to present main sedimentological features. The profile description can be found at the end of the section. The typical features of debris flow are summarized in table 5.2.

• Tab.5.2 Main features of debris flows (modified after Füchtbauer 1989)

| Name of massflow | Behaviour | Transportmechanism | Material | Sedimentary structures |
|---|---|---|---|---|
| Debris flow | Plastic | Particles "floating" due to Cohesion and uplift by clay minerals | Clay to Gravel | Matrix supported unsorted to weak graded may show coarse-tail or inverse grading concordent base contacts |
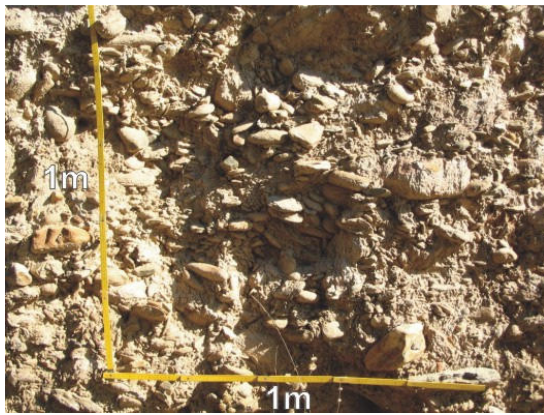
• Photo 5.11 1m² of the *Alhambra formation*.
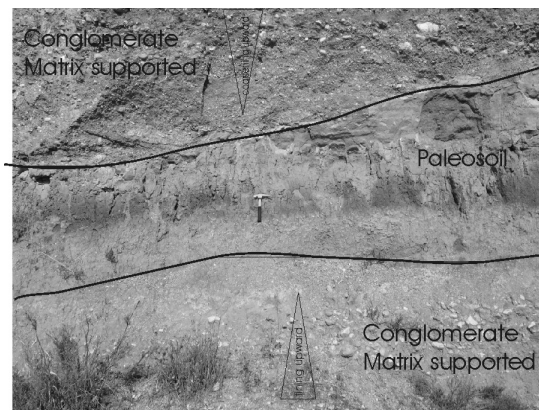


• Photo 5.12 Sedimentological development from coarse conglomerates to soil and, divided by erosional contact, again coarse grained conglomerates. *Alhambra* formation(Hammer lenght ca. 35cm).



• Photo 5.13 Tractive deformation of the *Alhambra* formation (Hammer lenght ca. 35cm).
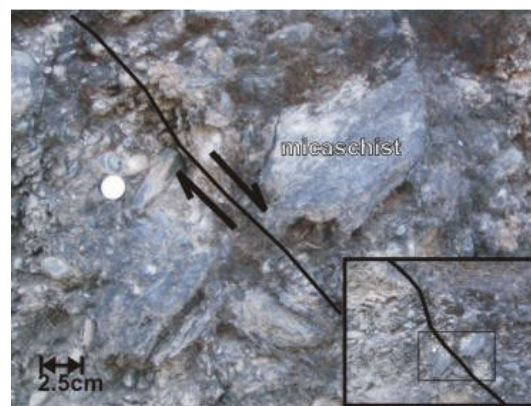


• Photo 5.14 Broken micaschist clast in the *Alhambra* formation.

The usual debris flow consists of grains with very wide ranges in size. The debris flow deposits, found in the mapping area consist of medium to fine grained matrix and varying proportion of matrix-supported clasts. This debrite is rich in clasts of different size and lack any bedding phenomena. A debris flow event shows thickness of 2-3m and at the top reverse grading with boulders.

The clasts are in most cases matrix-supported, which can be secondary calcified. Clast supported conglomerates can also be observed, but are rare.

The distribution of quarzites, schists and carbonates within $1m^2$ for clast analysis in the *Alhambra* formation is shown in Photo 5.11. Clast analysis was made at 5 site locations as shown in the geological map. The lithology of the clasts is very heterogeneous: e.g. various micaschists, quarzites, gneisses, gypsum, marbles, calcites, dolomites, serpentinite etc. According to the clast analysis most of the detritus is shaped like oblates, though spheroid and flat prolate figures occur.

The shape is closely connected to the petrological nature of the clasts, e.g. quarzites show due to their high resistivity mostly spheroid figures, micaschists due to their good cleavage mostly oblate shapes.

By plotting the geometric factors a and b it is possible to visualize the relationship between lithology and shape. Most of the quarzites plot in the lower right part of the diagram and represents a rather spherical shape. The schists show a wide spectrum, but are concentrated in lower left part of the diagram, which represents oblate shapes. The carbonates can be found in the diagram and cannot be associated to a certain shape (Fig. 5.15).
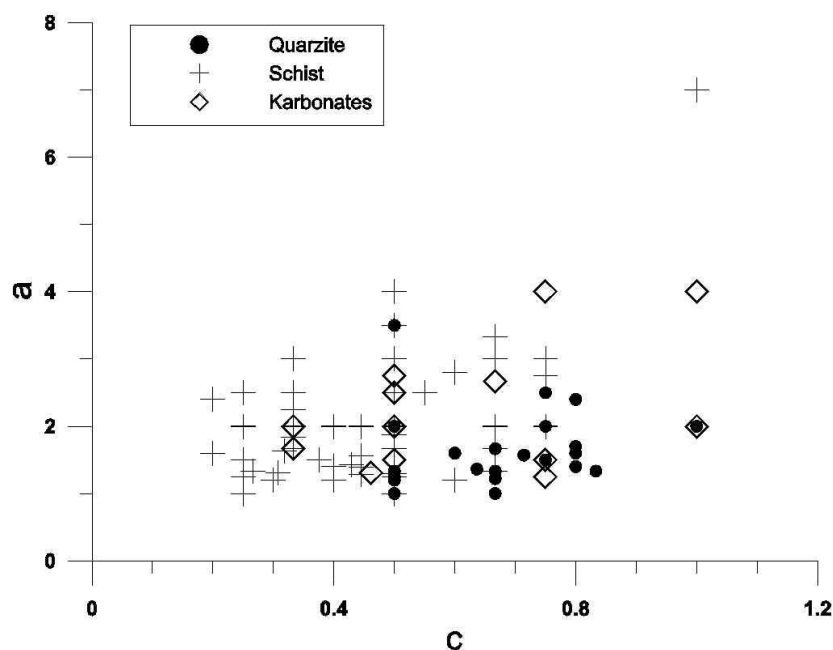


• Figure  5.15 Relationship between lithology and shape of clasts in the *Alhambra* formation (after VALLETON 1955)

At least two source areas can be, according to clast analyses, distinguished. The northern part is mainly fed by rocks from the *Sierra Arana* (predominately calcites and quarzites) and the southern area by rocks from the *Nevado-Filabride* (predominately various micaschists).

## 5.4.3 Red Sandstones/Siltstones and conglomerates middle Pliocene

This formation crops out around the *Barranco de Teatino* and is tilted with angles between 40 and 45° to SW and strikes NW-SE. In *Barr. de Teatino* listric fault plains, which dip in the above conglomerates between 60 and 70° and using the sedimentary surface of the sandstones as a sheer plain, can be observed. On this sheer plains several striaes can be measured and confirm SW movements (Photo 5.16). NW-SE faults with listric geometry could be originated in crustal or shallower detachment. Angular discordance between the overlaying *Alhambra* formation and the underlying red Sandstones is visible in *Barr.de Teatino*, located in the centre of the mapping area. Especially at the northern escarpment of the *Barranco* spectacular outcrops are visible (Fig.5.17).
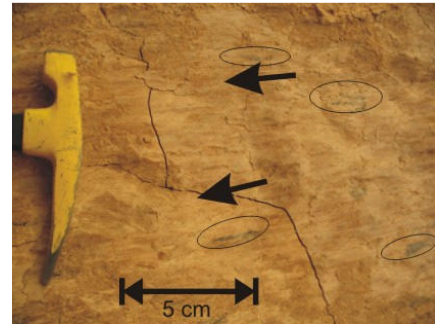


Photo 5.16 Striaes on sedimentary surface on listric fault plains, red Sandstones formation  (X 450 643; Y 4 115 537)
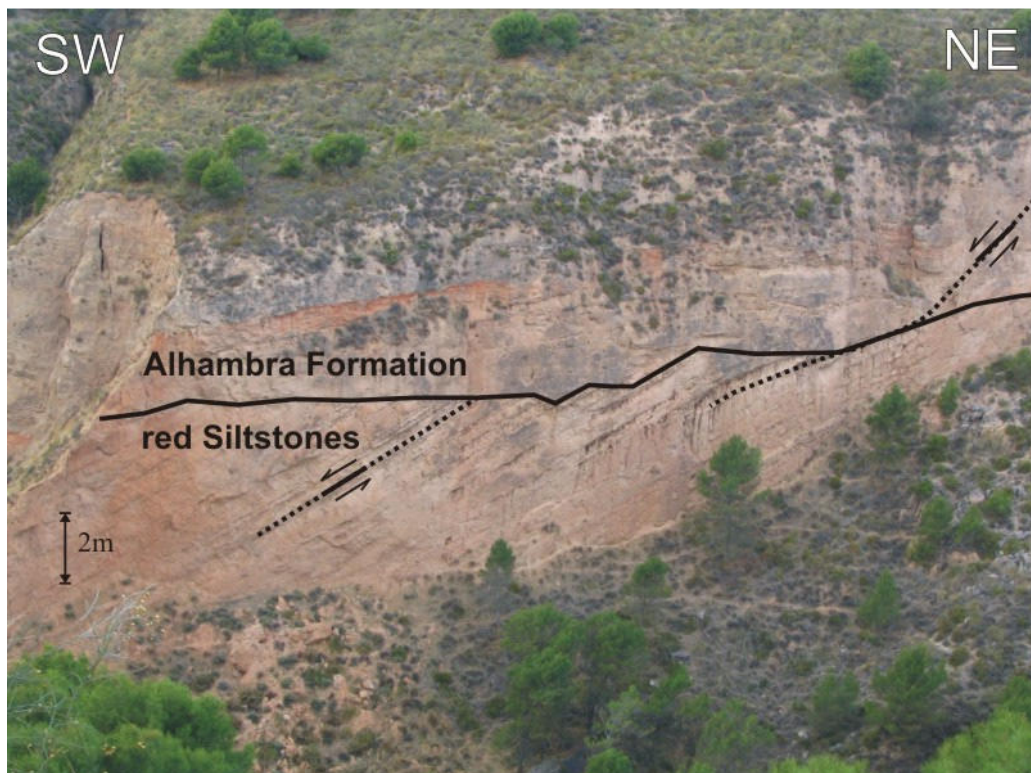


• Figure 5.17 Angular discordance and normal faults at *Barr. de Teatino* (at 450 794/4 115 740, viewpoint to NW)

### 5.4.4 Siltstones with micas, Sandstones and gravel (´Cenes de Lancha´) Messinian

This formation crops out in the eastern part of the mapping area and forms gentle slopes. It is characterized by bright greyish colours. Especially the sandstones show wide cross-bedding. In this formation various fossils are being described (e.g. DABRIO et al. 1978). Within this formation landslides are very common and can be observed in the mapping area. The sedimentological facies can be described as lacustrin.

### 5.4.5 Conglomerates and Sandstones (´Pinos Genil´) Tortonian

This Formation crops out in the eastern most part of the mapping area. It consists of conglomerates with mainly metamorphic (micaschists, gneisses and quarzites) and carbonatic (limestones and dolomites) clasts, which are approx. 2-15cm in diametra. The clasts are not good rounded, in opposite to the ´Alhambra Formation´. The Matrix is silt/sand with high content of micas. Horizons of Sand- and Siltstones appear. Visible thickness is about 200m, though the base contact to lower formations is not cropping out in the mapping area. No evidence of marine sedimentation can be found. It is interpreted as a lacustrine environment deposit.

## 5.5 Profiles

The profile starts with the red Sandstone formation of upper Miocene age at the angular discordance between the *Alhambra* formation and the red Sandstones. A total thickness of 80 m is being described in terms of age, lithology, sedimentological trends and general descriptions. A correlation between geological markers like paleosoils between adjacent areas was not possible.

Most sedimentological trends must be described as fining upward sequences. At the end of most of the fining upward trends (paleo-) soils marking stages of low geomorphological dynamic. At the bottom of the *Alhambra* formation less but thick paleosoils can be found, while at the top of the formation several but thin paleosoils were observed. The *Alhambra* conglomerates are often disorganized, without any bedding.

Within the ´Alhambra Formation´ fining upward sequences, from well-rounded clasts over sand to silty clay are common. At the top Paleosoils, marking stages of low geomorphodynamic activity, can be observed (Photo 5.12). In general soil formation can only take place in periods of geomorphodynamic stability, while active periods produce erosion/sedimentation. In the mapping area several horizons of paleosoils in the *Alhambra* Formation can be found. At the bottom of this formation few amounts but thick paleosoils have been developed, while towards the top the amount is increasing and thickness decreasing. The colours range from strong red over reddish to brownish, depending on the quantity of hematite content. In the Alhambra formation main soil forming processes are clay illuviation and calcification.

Stratigraphic and sedimentological profile



Age Formation | Lithology | Trends | Description

**Left column (0–20 m):**

Alhambra Formation Plio-/Pleistocene

fining upward — sandstone conglomeratic gebankt

paleosoil brownish

fining upward — siltstone conglomeratic

clay lenses

red conglomerates sandy matrix weak imbrication terrestrial

erosional horizon angular discordance

u' Miocene — red siltstones fluviatil dipped

**Right column (20–40 m):**

Alhambra Formation Plio-/Pleistocene

coarsening upward — conglomerates desorganized matrix supported with channels at top coarse tail

sandstone clay lenses

erosional horizon siltstone clay

fining upward — conglomerate desorganized

• Figure 5.18 Profile Ia: *Rio Darro* stratigraphic and sedimentological profile (0-40 m).

Stratigraphic and sedimentological profile
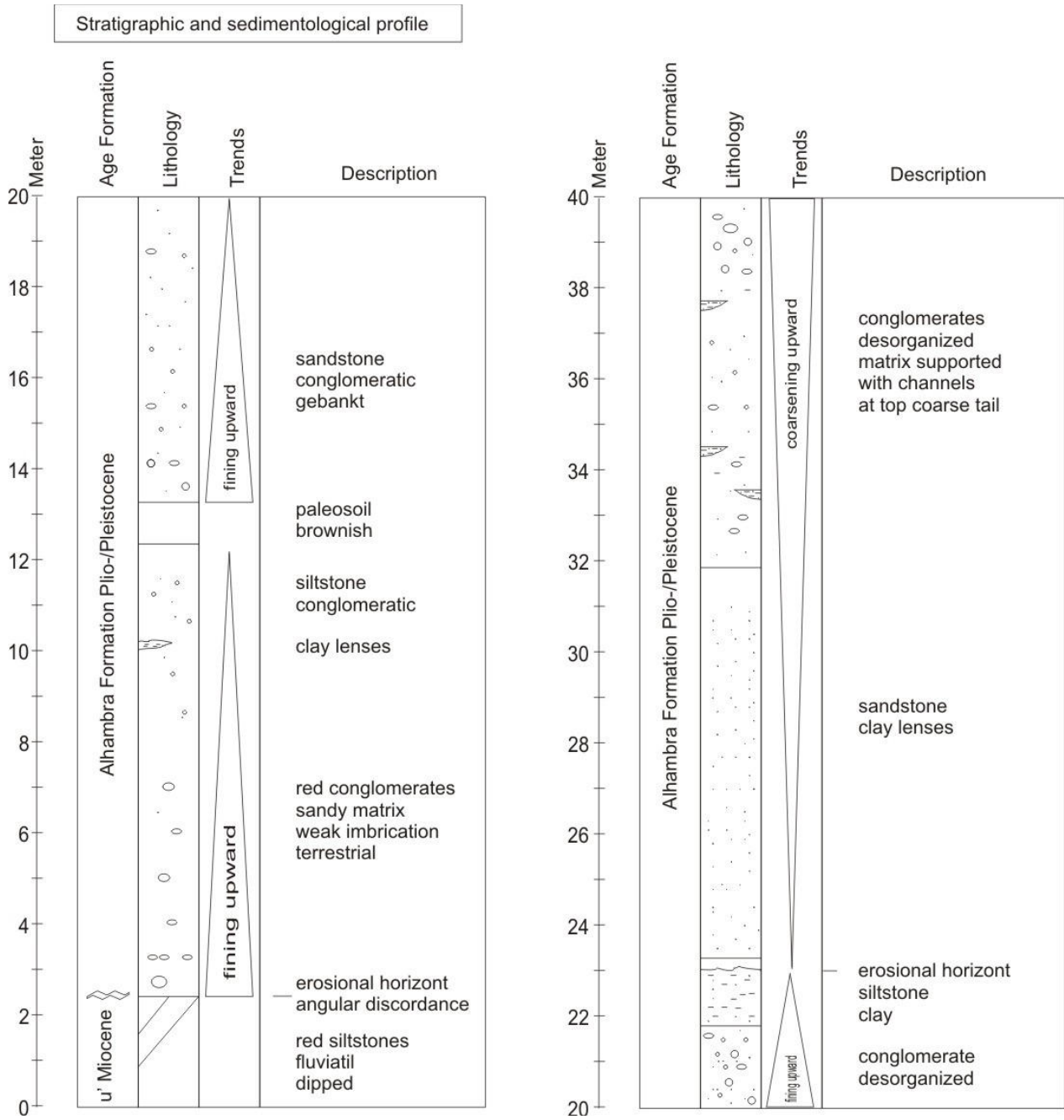


• Figure 5.19 Profile Ib: *Rio Darro* stratigraphic and sedimentological profile (40-80 m).

## Abbreviations

| | |
|---|---|
| ° | degree |
| °C | degree centigrade (Celsius scale) |
| ‰ | per mil |
| 2H | D or Deuterium |
| AAS | Atomic Absorption Spectroscopy |
| ABL | Atmospheric Boundary Layer |
| approx. | approximately |
| Arr. | Arroyo (stream) |
| avg. | average |
| Barr. | Barranco (creek, valley) |
| D | $^2$H or Deuterium |
| d-excess | deuterium excess |
| Emb. | Embalse (reservoir) |
| ETA | actual evapotranspiration |
| Fte. | Fuente (spring) |
| FUB | Freie Universität Berlin |
| GMWL | Global Meteoric Water Line |
| GWR | groundwater recharge |
| ICP | Inductively Coupled Plasma |
| IGME | Instituto Geologico y Minero España |
| Man. | Manantial (spring) |
| masl | meter above sea level |
| max. | maximum |
| min. | minimum |
| MWL | Meteoric Water Line |
| Nac. | Nacimiento (source) |
| SI | saturation index |
| UGR | Universidad Granada |
| UJA | Universidad Jaen |
| vs. | versus |
| VSMOW | Vienna Standard Mean Ocean Water |
| WMMWL | Western Mediteranean Meteoric Water Line |

AGUIRRE, E., (1957). UNA PRUEBA PALEOMASTOLOGICA DE LA EDAD CUATERNARIA DE LOS CONGLOMERADOS DE LA ALHAMBRA (GRANADA). ESTUDIOS GEOLOGICOS 13, 135 - 140.

ALLERTON, S., LONERGAN, L., PLATT, J.P., PLATZMAN E.S. AND McCLELLAND E., (1993) PALAEOMAGNETIC ROTATIONS IN THE EASTERN BETIC CORDILLERE, SOUTHERN SPAIN, EARTH PLANET, SCI. LETT, 119, 225-241.

ARAGUAS-ARAGUAS, L., FROEHLICH, K. AND ROZANSKI, K., (2000). DEUTERIUM AND OXYGEN-18 ISOTOPE COMPOSITION OF PRECIPITATION AND ATMOSPHERIC MOISTURE. HYDROLOGICAL PROCESSES, 14(8): 1341-1355.

AZAÑON, J.M., GALINDO-ZALDIVAR, J., GARCIA-DUENAS, V. JABALOY, A.(2002) THE GEOLOGY OF SPAIN, ALPINE TECTONICS II: BETIC CORDILLERA AND THE BALEARIC ISLANDS GIBBONS, WES, MORENO, T., THE GEOLOGY OF SPAIN, CARDIFF THE GEOLOGICAL SOCIETY LONDON.

AZAÑON, J. M. ,AZOR, A.,BOOTH-REA AND TORCAL, FR (2004) SMALL-SCALE FAULTING, TOPOGRAPHIC STEPS AND SEISMIC RUPTURES IN THE ALHAMBRA (GRANADA, SOUTHEAST SPAIN) 2004, JOURNAL OF QUATERNARY SCIENCE 19(3) 219–227.

BEDMAR, A.P. (1994) COMPOSICION ISOTOPICA DE LAS PRECIPITACIONES Y AGUAS SUBTERRANEAS DE LA PENINSULA IBERICA, CENTRO DE ESTUDIOS DE TECNICAS APLICADAS, P138:

BIGELEISEN, J., AND M. WOLFSBERG, (1958) THEORETICAL AND EXPERIMENTAL ASPECTS OF ISOTOPE EFFECTS IN CHEMICAL KINETICS, ADV. CHEM. PHYS., 1, 15-76.

BRAGA, J.C., MARTIN, J.M., ALCALA, B., (1990) CORAL REEF IN COARSE-TERROGENOUS SEDIMENTARY ENVIRONMENT (UPPER TORTONIAN, GRANADA BASIN, SOUTHERN SPAIN) SEDIMENTARY GEOLOGY, 66: 135 – 150.

CASTILLO, A. FERNANDEZ-RUBIO, R. (1985) "APLICACIÓN DE FERTILIZANTES QUIMICOS EN LA VEGA DE GRANADA. REPERCUSION EN LA CALIDAD DE LAS AGUAS SUBTERRANEAS" I CONGRESO DE GEOQUIMICA. 57-58.

CASTILLO, A. (1986) "LAS AGUAS SUPERFICIALES Y SUBTERRANEAS EN SIERRA NEVADA (GRANADA Y ALMERIA)" EN "SIERRA NEVADA". ED. ANDALUCIA, S.A. DL: GR/694-1985. 145-169.

CASTILLO, A. (1993) "CALIDAD AGRONÓMICA DE LAS AGUAS DE RIEGO DE LA VEGA DE GRANADA" NATURALIA BAÉTICA: 5, 91-103

CASTILLO, A. (1995). EL EMBALSE SUBTERRANEO DE LA VEGA DE GRANADA, UNO DE LOS MAS IMPORTANTES DE ANDALUCIA. TIERRA Y TECONOLOG.A, 9, 37-42.

CASTILLO, A. (2000) - PARQUE NACIONAL DE SIERRA NEVADA, DE CANSECO EDITORES. 2000 PARQUE NACIONAL DE SIERRA NEVADA - CLIMA E HIDROLOGIA - HIDROGEÓLOGO. INVESTIGADOR DEL C.S.I.C. INSTITUTO DEL AGUA (UNIVERSIDAD DE GRANADA).

CELLE-JEANTON, H., TRAVI, Y., BLAVOUX B (2001), ISOTOPIC TYPOLOGY OF PRECIPITATION IN THE WESTERN MEDITERRANEAN REGION AT THREE DIFFERENT TIME SCALES, GEOPHYSICAL RESEARCH LETTERS 28, 1215–1218.

CLARK, I. AND FRITZ, P., (1999). ENVIRONMENTAL ISOTOPES IN HYDROGEOLOGY. LEWIS PUBLISHERS. Boca Raton, 328pp

CRAIG, H. (1961): ISOTOPIC VARIATIONS IN METEORIC WATERS. SCIENCE, 133: 1702-1703.

COUTAGNE, A.(1948): ETUDE GENERALE DES VARIATIONS DE DEBITS EN FONCTION DES FACTUERS QUI LES CONDITIONNENT. 2ŠME PARTIE: LES VARIATIONS DE DEBIT EN PERIODE NON INFLUENCEE PAR LES PRECIPITATION. LA HOULLE BLANCHE, SEPT.-OCT. 1948

DABRIO, J.C., VERA, J.A. (1978) CHARACTERISTICAS SEDIMENTARIAS DEL JURASICO SUBBETICO EN LA REGION DE ALGARINEJO – RUTE. ACT. GEOL. HISP. I – V, 8-11.

DANSGAARD, W. (1964). STABLE ISOTOPES IN PRECIPITATION. TELLUS 16, 436-468.

DELGADO CALVO-FLORES R, DELAGADO FLORES G, PARRAGA MARTINEZ-J, GAMIZ MARTIN-E, SANCHEZ MARANON-M, TENORIO URRIOS-MA, (1989). PROYECTO LUCDERNE. MAPA DE SUELOS. GUEJAR SIERRA. –ICONA. MINESTERIO DE AGRICULTURA, PESCA Y ALIMENTACION. UNIVERSIDAD DE GRANADA.

DELGADO, L; SANCHEZ, L.; CASTILLO, A.; BAEZ, M.E. Y PEÑA, A. (2002) "ESTUDIO DEL IMPACTO DEL HERBICIDA BENSULFURON-METILO EN ENSAYOS DE CAMPO EN LA VEGA DE GRANADA" XIII CONGRESO NACIONAL FARMACÉUTICO

DVWK REGELN 128 (1992): ENTNAHME UND UNTERSUCHUNGSUMFANG VON GRUNDWASSERPROBEN. VERLAG PAUL PAREY

FAO-IGME. (1968). PROYECTO DE INVESTIGACIÓN HIDROGEOLÓGICA DE LA CUENCA DEL GUADALQUIVIR. PNUD.

FEDOROFF, N., (1997). CLAY ILLUVIATION IN RED MEDITERRANEAN SOILS. CATENA 28, 171 – 189.

FÜCHTBAUER, H. (1998) (EDITOR), SEDIMENTE UND SEDIMENTGESTEINE, SCHWEIZERBART'SCHE VERLAGSBUCHHANDLUNG, S.1141.

FREEZE, R.A. AND CHERRY, J.A. (1979): GROUND WATER. PRENTIC HALL INC., NEW JERSEY.

GARRIDO, J.R. (2003) COMPOSICION ISOTOPICA DEL VAPOR DE AGUA ATMOSFERICO EN EL SURESTE DE LA PENINSULA IBERICA, DEPARTAMENTO DE CIENCIAS DE LA TIERRA Y QUIMICA AMBIENTAL, TESIS DOCTORAL, 418

GRAY, D.M. (1973): HANDBOOK OF PRINCIPLES IN HYDROGEOLOGY.- WATER INFORMATION CENTER INC. HUNTINGTON, N.Y.

GÜNSTER, N., SKOWRONEK, A. (2001) SEDIMENT - SOIL SEQUENCES IN THE GRANADA BASIN AS EVIDENCE FOR LONG- AND SHORT-TERM CLIMATIC CHANGES DURING THE PLIOCENE AND QUATERNARY IN THE WESTERN MEDITERRANEAN, QUATERNARY INTERNATIONAL 78, 17 - 32

GONFIANTINI R. (1986). ENVIRONMENTAL ISOTOPES IN LAKE STUDIES. IN HANDBOOK OF ENVIRONMENTAL ISOTOPE GEOCHEMISTRY A., VOL. 1 (ED. P. FRITZ AND J. C. FONTES), PP. 113-168. ELSEVIER.

HAARMANN, U. (2001) : GESCHICHTE DER ARABISCHEN WELT. C.H. BECK MÜNCHEN, 786

IAEA (2000) MEBUS GEYH NIEDERSÄCHSISCHES LANDESAMT FÜR BODENFORSCHUNG HANNOVER ENVIRONMENTAL ISOTOPES IN THE HYDROLOGICAL CYCLE PRINCIPLES AND APPLICATIONS VOLUME IV: GROUNDWATER (WWW.IAEA.ORG)

IAEA-GNIP (2004) GLOBAL NETWORK OF ISOTOPES IN PRECIPITATION. INTERNATIONAL ATOMIC ENERGY AGENCY, VIENNA. URL: HTTP://ISOHIS.IAEA.ORG/. ACCESSED IN OCTOBER 2004.

IGME (2000) PLUVIOMETRIA EN EL OBSERVATORIO DE CARTUJA - 774M – GRANADA, INTERNAL PAPER

IGME (1985) MAPA GEOLOGIA, MAPA GEOLOGICO – MINERO DE ANDALUCIA (1:400 000), JUNTA DE ANDALUCIA

IGME 5.30 (2001) NORMA DE EXPLOTACION DE LA UNIDAD HIDROGEOLOGICA 5.30 (SIERRA ARANA), INTERNAL PAPER

IGME 5.31 (2001) NORMA DE EXPLOTACION DE LA UNIDAD HIDROGEOLOGICA 5.31 (LA PEZA) , INTERNAL PAPER

IGME 5.32 (2001) NORMA DE EXPLOTACION DE LA UNIDAD HIDROGEOLOGICA 5.32 (DEPRESSION DE GRANADA) , INTERNAL PAPER

IGME (2002) MODELO DE DATOS MAPA GEOLÓGICO-MINERO DE ANDALUCÍA ESCALA 1:400.000 (3ª VERSIÓN), E00-FILES.

JOUZEL, J., MERLIVAT, L., (1984). DEUTERIUM AND OXYGEN-18 IN PRECIPITATION: MODELLING OF THE ISOTOPE EFFECTS DURING SNOW FORMATION. JOURNAL OF GEOPHYSICAL RESEARCH 89, 11749–11757.

KAKIUCHI, M. AND MATSUO, S. (1979) DIRECT MEASUREMENTS OF D/H AND 18O/16O FRACTIONATION FACTORS BETWEEN VAPOR AND LIQUID WATER IN THE TEMPERATURE RANGEFROM 10 TO 40°C. GEOCHEM. J. 13, 307–311.

LOPEZ-CHICANO, J.C CERON, A.VALLEJOS, A. PULIDO-BOSCH, (2001) GEOCHEMISTRY OF THERMAL SPRING, ALHAMA DE GRANADA (SOUTHERN SPAIN), APPLIED GEOCHEMISTRY (16) 2001, 1153-1163

MARTIN, J.M. & BRAGA, J.C. (1997). SIERRA NEVADA: HISTORIA DEL LEVANTAMIENTO DE UN RELIEVE DEDUCIDA DE LAS UNIDADES CONGLOMERATICAS DE SU BORDE. CALVO, J.P. & MORALES (ED.), AVANCES EN EL CONOCIMIENTO DEL TERCIARIO IBERICO, 117 – 120

MARTIN, J.M. (2000) GEOLOGIA E HISTORIA DEL ORO DE GRANADA. BOLETIN GEOLOGICO Y MINERO. VOL 111-2 Y 3, 47-60.

MAPA DIGITAL DE ANDALUCÍA 1:100.000 (1999). SEVILLA: CONSEJERIA DE OBRAS PUBLICAS Y TRANSPORTES, INSTITUTO DE CARTOGRAFÍA DE ANDALUCÍA.

MEYER T., TESMER M. (2000): ERMITTLUNG DER FLÄCHENDIFFERENZIERTEN GRUNDWASSERNEUBILDUNG IN SÜDOST-HOLSTEIN NACH VERSCHIEDENEN VERFAHREN UNTER VERWENDUNG EINES GIS, INAUGURAL DISSERTATION, FUB

MEYER, H. SCHÖNICKE, L. WAND, U. HUBBERTEN, H.-W. & FRIDRICHSEN, H. (2000). ISOTOPE STUDIES OF HYDROGEN AND OXYGEN IN GROUND ICE. –EXPERIENCES WITH THE EQUILIBRATION TECHNIQUE. – ISOTPES ENVIRON. HEALTH STUD. 36 P., 133-149.

MINISTERIO DE MEDIO AMBIENTE, EMBALSE DE CANALES (2001),CONFEDERACIÓN HIDROGRÁFICA DEL GUADALQUIVIR ZONA DE GRANADA EMBALSE DE CANALES. P: 1-2

MINISTERIO DE MEDIO AMBIENTE, EMBALSE DE CUBILLAS (2001),CONFEDERACIÓN HIDROGRÁFICA DEL GUADALQUIVIR ZONA DE GRANADA EMBALSE DE CUBILLAS. P: 1-2

MINISTERIO DE MEDIO AMBIENTE, EMBALSE DE QUENTAR (2001),CONFEDERACIÓN HIDROGRÁFICA DEL GUADALQUIVIR ZONA DE GRANADA EMBALSE DE QUÉNTAR- P: 1-2

MORENO, E., SORIA MINGORANCE, J., 1988. MAPA Y MEMORIA EXPLICATIVA DE LA HOJA 1009 (GRANADA) DEL MAPA GEOLOGICO DE ESPANA A ESCALA 1 : 50.000. MADRID, 73 PP.

MOSER, H., AND STICHLER, W., (1974), DEUTERIUM AND OXYGEN-18 CONTENTS AS AN
     INDEX OF THE PROPERTIES OF SNOW COVERS, IN INTERNATIONAL SYMPOSIUM ON SNOW MECHANICS,
     VOLUME 114: GRINDELWALD, SWITZERLAND, INTERNATIONAL ASSOCIATION OF HYDROLOGICAL
     SCIENCES, P. 122–135.

MOSER, H., AND STICHLER, W., (1980), ENVIRONMENTAL ISOTOPES IN ICE AND SNOW, IN
     FONTES, J.C., AND FRITZ, P., EDS., HANDBOOK OF ENVIRONMENTAL ISOTOPEGEOCHEMISTRY, VOLUME
     1A: NEW YORK, ELSEVIER, P. 141–178.

REMENIERAS G. (1974): TRATADO DE HIDROLOGÍA APLICADA. BARCELONA; ESPANA.

SANZ DE GALDEANO, C., PELAZ-MONTILLA, JA, LOPEZ-CASADO, C. (2003) SEISMIC POTENTIAL OF THE MAIN
     ACTIVE FAULTS IN GRANADA BASIN (SOUTHERN SPAIN), PURE AND APPLIED GEOPHYSICS 160, 1537-
     1556.

STULL, R. B. (1988): AN INTRODUCTION TO BOUNDARY LAYER METEOROLOGY, 666 PP.

TURC, L. (1954): CALCUL DU BILAN DE L'EAU EVALUATION EN FUNCTION DES
     PRECIPITATIONS ET DES TEMPERATURES. PUBL. NO. 37 DES L/ASSOCIATION INTERNATIONAL
     D'HYDROLOGY, ASSEMBLÉE GÉNERALE DE ROME, TOME III, 188-202

VANDENSCHRICK, G., B. VAN WESEMAELA, E. FROTA, A. PULIDO-BOSCHB, L. MOLINAB,
     M. STIE´VENARDC, R. SOUCHEZD (2002) USING STABLE ISOTOPE ANALYSIS (D D–D 18O) TO
     CHARACTERISE THE REGIONAL HYDROLOGY OF THE SIERRA DE GADOR, SOUTH EAST SPAIN" JOURNAL OF
     HYDROLOGY 265 43–55.

VERHAGEN B. TH., GEYH M., FRÖHLICH K. & WITH K. (1991): ISOTOPE
     HYDROLOGICAL METHODS FOR THE QUANTITATIVE EVALUATION OF GROUND WATER RESOURCES IN
     ARID AND SEMI-ARID AREAS - DEVELOPMENT OF A METHODOLOGY. RESEARCH REPORTS OF THE
     MINISTRY FOR ECONOMIC COOPERATION OF THE FED. REP. OF GERMANY, 164 P.

VISERAS, C. CALVACHE ML, SORIA JM, FERNADEZ, J.,(2003), DIFFERENTIAL FEATURES OF
     ALLUVIAL FANS CONTROLLED BY TECTONIC OR EUSTATIC ACCOMODATION SPACE. EXAMPLES FROM BETIC
     CORDILLERA, SPAIN. GEOMORPHOLOGY 50, PP 181-202.

WWW.JUNTADEANDALUCIA.ES (2005), CLIMATE DATA
     HTTP://WWW.JUNTADEANDALUCIA.ES/AGRICULTURAYPESCA/PORTAL/OPENCMS/PORTAL/PORTADA.JSP

# APPENDIX 1 (Introduction)

• Table a1.1 : List of meteorological stations, data source, data time period  and mean annual precipitation.

| Station ID | Station Name | X | Y | Z | Data Source | mean annual P | Time period |
|---|---|---|---|---|---|---|---|
| 1 | Baza | 520628 | 4157712 | 814 | Junta Andalucia | 303.1 | 2000-2005 |
| 3 | Loja | 399051 | 4114478 | 487 | Junta Andalucia | 364.4 | 2000-2005 |
| 4 | Pinos Puente | 431534 | 4124395 | 594 | Junta Andalucia | 354.5 | 2000-2005 |
| 5 | Iznalloz | 451312 | 4141428 | 935 | Junta Andalucia | 475.1 | 2000-2005 |
| 6 | Jerez | 486806 | 4116224 | 1212 | Junta Andalucia | 287.7 | 2000-2005 |
| 7 | Cadiar | 483724 | 4086564 | 950 | Junta Andalucia | 426.9 | 2000-2005 |
| 8 | Zafaraya | 397421 | 4094617 | 905 | Junta Andalucia | 773.8 | 2000-2005 |
| 9 | Almunecar | 439612 | 4066365 | 49 | Junta Andalucia | 366.1 | 2000-2005 |
| 10 | Padul | 444684 | 4097558 | 753 | IGME 2000 | 409.3 | 1961-1997 |
| 11 | La Peza | 475063 | 4125456 | 1085 | IGME 2000 | 445.3 | 1961-1997 |
| 12 | Diezma | 470862 | 4130415 | 1233 | IGME 2000 | 532.6 | 1961-1997 |
| 13 | Huetor Santillan | 460117 | 4130759 | 1200 | IGME 2000 | 769 | 1961-1997 |
| 14 | Quentar Tocon | 467479 | 4121993 | 1200 | IGME 2000 | 882.2 | 1961-1997 |
| 15 | Pantano de | 459484 | 4116968 | 975 | IGME 2000 | 579.3 | 1961-1997 |
| 16 | Albolote | 442158 | 4118474 | 654 | IGME 2000 | 454.9 | 1961-1997 |
| 17 | Dilar | 449558 | 4101990 | 990 | IGME 2000 | 545.3 | 1961-1997 |
| 18 | Dilar - Central | 451862 | 4102743 | 980 | IGME 2000 | 600.5 | 1961-1997 |
| 19 | Padul - Agu | 446633 | 4097027 | 740 | IGME 2000 | 434.9 | 1961-1997 |
| 21 | Lanjaron | 457003 | 4086037 | 710 | IGME 2000 | 504.7 | 1961-1997 |
| 22 | Jayena | 429750 | 4090025 | 970 | IGME 2000 | 395.1 | 1961-1997 |
| 23 | Granada - Base Area | 443398 | 4109612 | 685 | IGME 2000 | 376.6 | 1961-1997 |
| 24 | Albunuelas | 434660 | 4083124 | 1120 | IGME 2000 | 775 | 1961-1997 |
| 25 | Pinos Genil | 455902 | 4113285 | 774 | IGME 2000 | 552.9 | 1961-1997 |
| 26 | Albergue Universitario | 465226 | 4104772 | 2550 | IGME 2000 | 738.4 | 1960-1997 |
| 27 | Huetor Santillan | 454443 | 4119852 | 1022 | IGME 2000 | 674.3 | 1961-1997 |
| 28 | Guejar Sierra | 461335 | 4112718 | 1084 | IGME 2000 | 604.3 | 1961-1997 |
| 29 | Observatorio Cartuja | 447308 | 4116447 | 774 | IGME 2000 | 449 | 1902-1997 |
| 38 | Velez Malaga | 399138 | 4073067 | 49 | Junta Andalucia | 395.2 | 2000-2005 |

# APPENDIX 2 (Background)

• Table a2.1 GWR and runoff calculation for the meteorological station Iznalloz (X 451312 Y 4141428 Z 935)

| month | precipitation | temperature | ETA | runoff & recharge | ETA | runoff & recharge |
|---|---|---|---|---|---|---|
| | [mm] | [℃] | TURC | TURC | COUTAGNE | COUTAGNE |
| 1 | 67.64 | 6.40 | 70.50 | -2.86 | 64.94 | 2.70 |
| 2 | 49.56 | 6.98 | 51.95 | -2.39 | 48.18 | 1.38 |
| 3 | 82.24 | 10.16 | 85.82 | -3.58 | 79.20 | 3.04 |
| 4 | 60.12 | 12.14 | 63.11 | -2.99 | 58.67 | 1.45 |
| 5 | 49.72 | 15.76 | 52.32 | -2.60 | 48.90 | 0.82 |
| 6 | 8.15 | 23.45 | 8.59 | -0.44 | 8.13 | 0.02 |
| 7 | 0.65 | 25.16 | 0.69 | -0.04 | 0.65 | 0.00 |
| 8 | 0.24 | 24.52 | 0.25 | -0.01 | 0.24 | 0.00 |
| 9 | 15.80 | 20.49 | 16.65 | -0.85 | 15.73 | 0.07 |
| 10 | 76.44 | 14.86 | 80.20 | -3.76 | 74.41 | 2.03 |
| 11 | 77.80 | 8.93 | 81.14 | -3.34 | 74.85 | 2.95 |
| 12 | 83.52 | 7.05 | 86.67 | -3.15 | 79.62 | 3.90 |
| year | 571.88 | 14.66 | 597.89 | -26.01 | 553.52 | 18.36 |

• Table a2.2 GWR and runoff calculation for the meteorological station *Observatorio de Cartuja* (X 447308 Y 4116447 Z 774)

| month | precipitation | temperature | ETA | runoff & recharge | ETA | runoff & recharge |
|---|---|---|---|---|---|---|
| | [mm] | [℃] | TURC | TURC | COUTAGNE | COUTAGNE |
| 1 | 46.21 | 7.34 | 54.48 | -2.52 | 50.57 | 1.39 |
| 2 | 51.96 | 8.12 | 62.28 | -2.95 | 57.90 | 1.43 |
| 3 | 59.33 | 11.89 | 54.21 | -2.67 | 50.60 | 0.94 |
| 4 | 51.54 | 14.52 | 40.92 | -2.07 | 38.38 | 0.48 |
| 5 | 38.86 | 16.96 | 18.42 | -0.94 | 17.40 | 0.07 |
| 6 | 17.48 | 23.95 | 3.58 | -0.18 | 3.39 | 0.00 |
| 7 | 3.39 | 26.52 | 4.12 | -0.21 | 3.91 | 0.00 |
| 8 | 3.91 | 24.36 | 26.33 | -1.35 | 24.81 | 0.17 |
| 9 | 24.98 | 20.41 | 52.18 | -2.60 | 48.78 | 0.80 |
| 10 | 49.58 | 16.12 | 58.53 | -2.74 | 54.38 | 1.40 |
| 11 | 55.78 | 10.15 | 61.45 | -2.70 | 56.83 | 1.91 |
| 12 | 58.75 | 7.16 | 18.96 | -0.96 | 17.83 | 0.17 |
| year | 461.77 | 15.63 | 455.45 | -21.89 | 424.78 | 8.78 |

• Table a2.3 GWR and runoff calculation for the meteorological station *Padul* (X 444683 Y 4097327 Z 753)

| month | precipitation | temperature | ETA | runoff & recharge | ETA | runoff & recharge |
|---|---|---|---|---|---|---|
| | [mm] | [℃] | TURC | TURC | COUTAGNE | COUTAGNE |
| 1 | 18.00 | 7.76 | 54.65 | -2.53 | 50.73 | 1.39 |
| 2 | 52.12 | 8.26 | 62.13 | -2.93 | 57.74 | 1.46 |
| 3 | 59.20 | 11.42 | 47.04 | -2.32 | 43.96 | 0.76 |
| 4 | 44.72 | 13.19 | 39.72 | -2.00 | 37.26 | 0.46 |
| 5 | 37.72 | 16.46 | 12.81 | -0.66 | 12.11 | 0.04 |
| 6 | 12.15 | 22.84 | 0.69 | -0.04 | 0.65 | 0.00 |
| 7 | 0.65 | 25.39 | 0.37 | -0.02 | 0.35 | 0.00 |
| 8 | 0.35 | 24.82 | 16.76 | -0.86 | 15.83 | 0.07 |
| 9 | 15.90 | 20.81 | 68.80 | -3.35 | 64.07 | 1.38 |
| 10 | 65.45 | 16.51 | 69.67 | -3.17 | 64.58 | 1.92 |
| 11 | 66.50 | 10.76 | 65.39 | -2.89 | 60.51 | 1.99 |
| 12 | 62.50 | 8.32 | 41.85 | -2.01 | 38.96 | 0.88 |
| year | 435.26 | 15.55 | 479.87 | -22.77 | 446.77 | 10.33 |

• Table a2.4 GWR and runoff calculation for the meteorological station *Pinos Puente* (X 431534 Y 4124395 Z 594)

| month | precipitation | temperature | ETA | runoff & recharge | ETA | runoff & recharge |
|---|---|---|---|---|---|---|
| | [mm] | [°C] | TURC | TURC | COUTAGNE | COUTAGNE |
| 1 | 39.84 | 7.11 | 46.50 | -2.22 | 43.28 | 1.00 |
| 2 | 44.28 | 8.32 | 68.25 | -3.17 | 63.36 | 1.72 |
| 3 | 65.08 | 11.88 | 43.28 | -2.16 | 40.51 | 0.61 |
| 4 | 41.12 | 14.02 | 33.71 | -1.71 | 31.69 | 0.31 |
| 5 | 32.00 | 17.66 | 2.42 | -0.12 | 2.30 | 0.00 |
| 6 | 2.30 | 24.85 | 0.53 | -0.03 | 0.50 | 0.00 |
| 7 | 0.50 | 26.27 | 0.46 | -0.02 | 0.44 | 0.00 |
| 8 | 0.44 | 25.66 | 16.44 | -0.84 | 15.54 | 0.06 |
| 9 | 15.60 | 21.91 | 57.53 | -2.85 | 53.71 | 0.97 |
| 10 | 54.68 | 16.32 | 61.63 | -2.87 | 57.23 | 1.53 |
| 11 | 58.76 | 10.35 | 74.46 | -3.10 | 68.70 | 2.66 |
| 12 | 71.36 | 7.96 | 41.01 | -1.93 | 38.08 | 1.00 |
| year | 425.96 | 16.03 | 446.23 | -21.03 | 415.33 | 9.87 |

• Table a2.5 GWR and runoff calculation for the meteorological station *Puebla de Don Fadrique* (X 554482 Y 4192456 Z 1110)

| month | precipitation | temperature | ETA | runoff & recharge | ETA | runoff & recharge |
|---|---|---|---|---|---|---|
| | [mm] | [°C] | TURC | TURC | COUTAGNE | COUTAGNE |
| 1 | 15.56 | 4.02 | 22.90 | -1.14 | 21.43 | 0.33 |
| 2 | 21.76 | 4.68 | 38.90 | -1.90 | 36.31 | 0.69 |
| 3 | 37.00 | 8.44 | 32.21 | -1.61 | 30.19 | 0.41 |
| 4 | 30.60 | 10.62 | 38.07 | -1.91 | 35.69 | 0.47 |
| 5 | 36.16 | 14.11 | 12.28 | -0.63 | 11.61 | 0.04 |
| 6 | 11.65 | 21.35 | 2.74 | -0.14 | 2.60 | 0.00 |
| 7 | 2.60 | 23.17 | 15.73 | -0.81 | 14.86 | 0.06 |
| 8 | 14.92 | 22.76 | 23.94 | -1.22 | 22.57 | 0.15 |
| 9 | 22.72 | 18.39 | 48.22 | -2.38 | 45.05 | 0.79 |
| 10 | 45.84 | 13.32 | 31.90 | -1.58 | 29.82 | 0.50 |
| 11 | 30.32 | 7.54 | 42.64 | -2.00 | 39.60 | 1.04 |
| 12 | 40.64 | 5.58 | 33.79 | -1.67 | 31.57 | 0.55 |
| year | 309.77 | 12.83 | 343.32 | -16.99 | 321.31 | 5.02 |

• Table a2.6 GWR and runoff calculation for the meteorological station *Cadiar* (X 483724 Y 4086564 Z 950)

| month | precipitation | temperature | ETA | runoff & recharge | ETA | runoff & recharge |
|---|---|---|---|---|---|---|
| | [mm] | [°C] | TURC | TURC | COUTAGNE | COUTAGNE |
| 1 | 24.56 | 7.36 | 59.63 | -2.67 | 55.21 | 1.75 |
| 2 | 56.96 | 7.50 | 75.91 | -3.35 | 70.23 | 2.33 |
| 3 | 72.56 | 10.46 | 53.31 | -2.59 | 49.70 | 1.02 |
| 4 | 50.72 | 12.25 | 35.64 | -1.80 | 33.46 | 0.38 |
| 5 | 33.84 | 15.68 | 4.69 | -0.24 | 4.45 | 0.00 |
| 6 | 4.45 | 23.08 | 3.37 | -0.17 | 3.20 | 0.00 |
| 7 | 3.20 | 24.75 | 0.84 | -0.04 | 0.80 | 0.00 |
| 8 | 0.80 | 24.51 | 24.37 | -1.25 | 22.97 | 0.15 |
| 9 | 23.12 | 20.14 | 76.32 | -3.64 | 70.90 | 1.78 |
| 10 | 72.68 | 15.45 | 66.03 | -2.99 | 61.20 | 1.84 |
| 11 | 63.04 | 9.69 | 111.19 | -3.19 | 101.83 | 6.17 |
| 12 | 108.00 | 7.80 | 29.80 | -1.48 | 27.86 | 0.46 |
| year | 513.93 | 14.89 | 541.09 | -23.40 | 501.80 | 15.89 |

# APPENDIX 3 (Methods)

List of all measured parameters, site types, operating persons and date of sampling.

• Table a3.1 Site information and measured parameters of Feb.04 campaign (Dr.Kohfahl/Prof.Pekdeger).

| Site ID | Site name | Type | Village | IGME declaration | Sampling date | Measured parameters |
|---|---|---|---|---|---|---|
| SP-GR-022 | Fte. Alta | spring | Sierra Nevada | | | |
| SP-GR-023 | Fte. las Viboras | | Fuente las viboras | | | |
| SP-GR-024 | Fte. del Hervidero | | La Zubia | | | |
| SP-GR-025 | Fte. la Cortijuela | | | | | |
| SP-GR-026 | Fte. de los 16 canos | | Guejar Sierra | | 05. Feb 04 | T,EC,Ions, D, 18O |
| SP-GR-027 | Fte. de Teja | | | | | |
| SP-GR-028 | Fte. de Urquiza | Thermal spring | Durcal right tube from spectators view | | | |
| SP-GR-029 | Fte. de Urquiza left | | Durcal left tube from spectators view | | | |
| SP-GR-030 | Fte. y Alberca de Palmones | spring | Padul | | | |
| SP-GR-031 | Fte. los Molinos | | | 1942.6.073 | | T,EC,Ions, D, 18O, runoff |
| SP-GR-032 | Banos de la Malah | Thermal spring | La Mahala | 1942.6.007 | 06. Feb 04 | |
| SP-GR-033 | Fte. Grande | spring | Alfacar | | | T,EC,Ions, D, 18O |
| SP-GR-022 | Fte. Alta | | Sierra Nevada | 1941.8.002 | | |

• Tab.a3.2 Site information and measured parameters of May 04/Feb.04 (Prof.Benavente) campaign.

| Site ID | Site name | Type | Village | IGME declaration | Sampling date | Measured parameters |
|---|---|---|---|---|---|---|
| SP-GR-022 | Fte. Alta | Spring | Sierra Nevada | | 12-Mai-04 | T, EC, pH, D, 18O |
| SP-GR-023 | Fte. las Viboras | | | - | | T, EC, pH, D, 18O, runoff |
| SP-GR-032 | Banos de la Malah | Thermal spring | La Mahala | | | T, EC, pH, D, 18O |
| SP-GR-051 | Instituto del agua | Rain | Agua Lluvia Instituto del Agua | | 20-Feb-04 | |

• Table a3.3 Site information and measured parameters of June – Sept. 04 campaigns (Dr.Hidalgo)

| Site ID | Site name | Type | Location | Sampling date | Measured parameters |
|---|---|---|---|---|---|
| SP-GR-038 | Laguna del Majano | snowmelt | desagüe en margen izq de la Laguna del Majano | | |
| SP-GR-039 | desde Pico del Goteron | | Chorrera ladera Este (desde P. del Goterón) | | |
| SP-GR-040 | Laguna de la Mosca | laguna | Laguna de la Mosca | 27-Jun-04 | |
| SP-GR-041 | Collado del Ciervo | | Agua de fusión hacia el collado del Ciervo (3122 m.) | | |
| SP-GR-042 | Ladera SO Mulhacen | | Agua de fusión en Nevero de ladera SO Mulhacén | | |
| SP-GR-043 | Cumbre del Muhacen | snowmelt | Agua de fusión en Nevero cumbre del Mulhacén | | T, EC, D, 18O |
| SP-GR-044 | Circo del Veleta | | Cuenca del Guarnón 1ª chorrera (más oriental) del Circo del Veleta (escombrera de las minas de siderita) | | |
| SP-GR-045 | Laguna Larga (oeste) | laguna | Nieve fundiendo en el interior de la Laguna Larga (oeste) | 04-Jul-04 | |
| SP-GR-046 | Laguna Larguilla | | Nevero fundiendo al Sur de la Laguna Larguilla | | |
| SP-GR-047 | 7ª chorrera del Corra | snowmelt | Agua de fusión cayendo por unas roquillas | | |

-continued- • Table a3.3

| Site ID | Site name | Type | Location | Sampling date | Measured parameters |
|---|---|---|---|---|---|
| SP-GR-048 | Tajos del Campanario | rio | 2ª Chorrerilla por debajo de los Tajos del Campanario de las tres chorrerillas (Río Guarnón individualizado) | 04-Jul-04 | T, EC, D, 18O |
| SP-GR-049 | Fusión nieve | snowmelt | Fusión nieve | 22-Jun-04 | D, 18O |
| SP-GR-053 | Corral del Veleta | | 7ª chorrera del Corral del Veleta (SP47*) | 04-Jul-04 | |
| SP-GR-054 | Nevero Río Mulhacén | snow | Penúltimo nevero Río Mulhacén | 27-Jun-04 | |
| SP-GR-055 | Ladera SE R. Chico | snowmelt | Vereda El Chorrillo-Trevelez. Agua de fusión de nevero (ladera SE R. Chico) | | |
| SP-GR-056 | Margen izq | | desagüe en margen izq | | |
| SP-GR-057 | Laguna de la Caldereta | laguna | Laguna de la Caldereta, nieve fundiendo en la lagunilla | | |
| SP-GR-180 | Collado de la Carigüela | snowmelt | Collado de la Carigüela (cara S) agua de fusión del nevero | 10-Jul-04 | |
| SP-GR-181 | Laguna de Aguas Verdes (algo de nieve) | laguna | Laguna de Aguas Verdes (algo de nieve) | | |
| SP-GR-182 | Lagunillos de los Machos | snowmelt | Único aliviadero del arroyo de los 3 Lagunillos de los Machos | | |
| SP-GR-183 | Laguna de los Machos | laguna | Laguna de los Machos | | |
| SP-GR-184 | Deagüe del Laguneto de la chorrera | snowmelt | Deagüe del Laguneto de la chorrera occidental de R. Seco (3) | | |
| SP-GR-185 | Laguna de Río Seco (5) | laguna | Laguna de Río Seco (5) | | |
| SP-GR-186 | San Juan, margen dcha. (nevero) | snow | San Juan, margen dcha. (nevero) | 17-Jul-04 | |
| SP-GR-187 | Lagunillo de Juego de Bolos | | Lagunillo de Juego de Bolos (sin salida) | | T, EC, D, 18O |
| SP-GR-188 | Laguna de la Caldera | | Laguna de la Caldera | | |
| SP-GR-189 | Lagunillo de la Virgen  5 | | Lagunillo de la Virgen  5 | 21-Jul-04 | |
| SP-GR-190 | Lagunillos de la Virgen 2 | laguna | Lagunillos de la Virgen 2 | | |
| SP-GR-191 | Lagunillos de la Virgen 4 | | Lagunillos de la Virgen 4 | | |
| SP-GR-192 | Lagunillos del Fraile de Capileira 2 | | Lagunillos del Fraile de Capileira 2 | | |
| SP-GR-193 | Lagunillos del Fraile | | Aliviadero del Lagunillos del Fraile de Capileira 1. Aporte principal de un gran cono de derrubios | | |
| SP-GR-194 | Chorrera del Molinillo | Rio Dilar | Río Dílar por debajo de la Chorrera del Molinillo | 28-Jul-04 | |
| SP-GR-195 | Lagunillos de la Mula (S) casi estancada | laguna | Lagunillos de la Mula (S) casi estancada | 28-Jul-04 | |
| SP-GR-196 | Laguna de la Mula | | Laguna de la Mula. No está aliviando, algo excavada. Muy llena de algas | 28-Jul-04 | |
| SP-GR-197 | Nacimiento del Alhorí | nac.alhori | Nacimiento del Alhorí | 31-Jul-04 | |
| SP-GR-198 | Laguna de Juntillas | | Laguna de Juntillas (suelta muy poco agua por el aliviadero) | | |
| SP-GR-199 | Laguna de Vacares | laguna | Laguna de Vacares (restos de nevero) | | |
| SP-GR-200 | Lagunillos de las Calderetas | | Lagunillos de las Calderetas 3  (ver esquema) | | |
| SP-GR-201 | Nacimiento del Río Lanjarón | Nac.Rio Lanjaron | Nacimiento del Río Lanjarón | 05-Aug-04 | |
| SP-GR-202 | Laguna de Lanjarón | | Laguna de Lanjarón. No desagua actualmente pero esta filtrando bastante agua unos 8 m abajo | | |
| SP-GR-203 | Laguna de las Tres Puertas | laguna | Laguna de las Tres Puertas. Entra un hilillo de derrubios | | |
| SP-GR-204 | Siete Lagunas (2). | | Siete Lagunas (2). | 11-Sep-04 | |

-continued- • Table a3.3

| Site ID | Site name | Type | Location | Sampling date | Measured parameters |
|---|---|---|---|---|---|
| SP-GR-205 | Siete Lagunas (1). | laguna | Siete Lagunas (1). | 11-Sep-04 | T, EC, D, 18O |
| SP-GR-206 | Siete Lagunas (7). | | Siete Lagunas (7). | | |
| SP-GR-207 | Siete Lagunas (8). | | Siete Lagunas (8). | | |
| SP-GR-208 | Siete Lagunas 10. Laguna Hondera | | Siete Lagunas 10. Laguna Hondera | | |
| SP-GR-209 | Charquilla debajo de la parte alta de los Borreguiles del Puerto | | Charquilla debajo de la parte alta de los Borreguiles del Puerto | 17-Sep-04 | |
| SP-GR-210 | Laguna de Charca Palo. Aliviando agua y muy clara | | - | 05-Aug-04 | |
| SP-GR-211 | Laguna Bolaños | | | | |
| SP-GR-212 | Laguna Cuadrada | | | | |
| SP-GR-213 | Laguna de Najera grande | | | | |
| SP-GR-214 | Saliente de Lavadero Reina | | | | |
| SP-GR-215 | Laguna del Caballo | | | | |
| SP-GR-216 | Laguna del Carnero | | | | |
| SP-GR-217 | Laguna del Cartujo | | | | |
| SP-GR-218 | Laguna de las Cabras | | | 14-Aug-04 | |
| SP-GR-219 | Lagunillos de Río Seco | | | | |
| SP-GR-220 | Lagunillo del Veleta | | | | |
| SP-GR-221 | Laguneto del Veleta | | Laguneto del Veleta (fusión, colgado, aguas claras). | 22-Aug-04 | |
| SP-GR-222 | Laguneto del Veleta 2 | | Laguneto del Veleta 2 (fusión, colgado, muy turbio). | | |
| SP-GR-223 | Laguneto del Veleta 3 | | Laguneto del Veleta 3 (colgado, muy turbio, fuertemente excavado). | | |
| SP-GR-224 | Laguneto del Puntal de Loma Pua | snowmelt | Laguneto del Puntal de Loma Pua | | |
| SP-GR-225 | Laguna Martín. | laguna | Laguna Martín. Con muchas algas. Estancada. | | |
| SP-GR-226 | Nacimiento de la laguna Martín. | nac. Laguna | Nacimiento de la laguna Martín. | | |
| SP-GR-227 | Laguna 3 del Corral | laguna | Laguna 3 del Corral. Ha bajado más de 1 m. Muy turbia y verdosa. | 25-Sep-04 | |
| SP-GR-228 | Laguna chica Vald. Borreguil. Sale poco agua. | laguna | Laguna chica Vald. Borreguil. Sale poco agua. | | |
| SP-GR-229 | Laguna Larguilla (Gabata) | | Laguna Larguilla (Gabata). Ha bajado casi 1 metro. Desagua poco. | | |
| SP-GR-230 | Laguna Larga. | | Laguna Larga. Ha bajado más de 2 m. de nivel. | | |
| SP-GR-231 | Laguna de la Mosca | Snow or snowmelt | Laguna de la Mosca. No ha bajado mucho de nivel. | | |
| SP-GR-232 | Laguna más alta de las Calderetas | Snow or snowmelt | Laguna más alta de las Calderetas.Sin entrada visible. Ha bajado 10 cm. Cristalina, poca salida. | | |
| SP-GR-233 | | Snow or snowmelt | | | |
| SP-GR-038 | Laguna del Majano | Snow or snowmelt | desagüe en margen izq de la Laguna del Majano | 27-Jun-04 | |
| SP-GR-039 | desde Pico del Goteron | Snow or snowmelt | Chorrera ladera Este (desde P. del Goterón) | | |

• Table a3.4 sites, type, persons, date and measured parameters of November 04 campaign (IGME staff).

| Site ID | Site name | Type | Village | IGME declaration | Sampling date | Measured parameters |
|---|---|---|---|---|---|---|
| SP-GR-081 | Camino frente Puleva | Observation well | Granada Vega | 1941.7.265 | 16-Nov-04 | T, EC,watertable, D, 18O |
| SP-GR-082 | Romilla | | | 1941.5.205 | 05-Nov-04 | |
| SP-GR-083 | Atarfe | | | 1941.6.217 | 17-Nov-04 | |
| SP-GR-084 | Pedro Ruiz | | | 1941.6.221 | 12-Nov-04 | |
| SP-GR-085 | Aeropuerto | | | 1941.6.218 | 25-Nov-04 | |
| SP-GR-086 | Alhendin | | | 1942.3.240 | 08-Nov-04 | |
| SP-GR-087 | Cullar Vega | | | 1942.3.072 | 09-Nov-04 | |
| SP-GR-088 | Casa Nuevas | Well | | 1941.5.090 | 22-Nov-04 | |
| SP-GR-089 | Santa Rosa | | | 1941.5.085 | 10-Nov-04 | |
| SP-GR-090 | Cort. Trevijano | Observation well | | 1941.7.157 | 26-Nov-04 | |

• Table a3.5 Sites, type, persons, date and measured parameters of Dec. 04 rainwater (Fernandez, IGME)

| Site ID | Site name | Type | Village | IGME declaration | Sampling date | Measured parameters |
|---|---|---|---|---|---|---|
| SP-GR-091 | Rain 975m | Rain | Guejar Sierra | - | 02-Dez-04 | D, 18O |
| SP-GR-092 | Rain 1310m | | | - | | |
| SP-GR-093 | Rain 1500m | | | - | | |
| SP-GR-094 | Rain 1550m | | | - | | |
| SP-GR-095 | Rain 670m | | Puerta oficina IGME | - | | |

• Table a3.6 Sites, type, persons, date and measured parameters of Feb.05 campaign (Dr.Meyer, AWI).

| Site ID | Site name | Type | Description | Sampling date | Measured parameters |
|---|---|---|---|---|---|
| SP-GR-235 | Snowpatch 1 | Snow | Schnee, Schmelzkruste; Schneefleck Ende des Winters; vermutl. Evapo+Sublim.; Kiefernwald, NE-Hang; Nevado Filabride | 19. Feb 05 | D, 18O |
| SP-GR-236 | Snowpatch 2 | | Schnee, unterhalb Schmelzkruste; vermutl. Evapo+Sublim.; Kiefernwald, NE-Hang; Nevado Filabride | 19. Feb 05 | D, 18O |
| SP-GR-237 | Snowpatch 3 | | Schnee; N-Hang; in Kurve B. Viboras; Fte. de las Viboras (SP 23) nicht gefunden; Schneegrenze ~1400m | 19. Feb 05 | D, 18O |

• Table a3.7 Sites, types, persons, date and measured parameters of *Vega* sampling campaign feb 05.

| Site ID | Site name | Type | Village | IGME declaration | Sampling date | Measured parameters |
|---|---|---|---|---|---|---|
| SP-GR-130 | Armilla Vivero Dip | Well | Armilla | - | 18-Feb-05 | T, EC, pH, runoff, alcalinity, Ions, D, 18O |
| SP-GR-131 | Cullar Vega | | Cullar Vega | | | |
| SP-GR-132 | Alhencira | | Alhendin | | | |
| SP-GR-133 | Terrazos Terragran | | Pulianas | | | T, EC, pH, alcalinity, Ions, D, 18O |
| SP-GR-134 | Cort. Santa Ana | | Sierra Elvira | | | |
| SP-GR-135 | Banos de Sierra Elvira | Thermal Spring | | | | T, EC, pH, runoff, alcalinity, Ions, D, 18O |
| SP-GR-136 | Meson El Guerro | Well | Huetor de Vega | | | T, EC, pH, alcalinity, Ions, D, 18O |
| SP-GR-137 | Manantial de la Reina | Spring | Santa Fe | | | T, EC, pH, runoff, alcalinity, Ions, D, 18O |
| SP-GR-138 | Arroyo de salado | Surface water | | | | T, EC, pH, alcalinity, Ions, D, 18O |
| SP-GR-139 | Banos Santa Fe | Thermal Spring | Santa Fe, aeropuerto | | | |
| SP-GR-140 | Los Fagailos | Spring | Fuente Vaquelos | | | T, EC, pH, runoff, alcalinity, Ions, D, 18O |
| SP-GR-141 | Rio Cubillas | Surface water | Cubillas | | | T, EC, pH, alcalinity, Ions, D, 18O |
| SP-GR-142 | Puente Rio Genil | | Lachar | | | |

• Table a3.8 Sites, type, persons, date and measured parameters of surface and precipitation.

| Site ID | Site name | Type | Village | Sampling date | Measured parameters |
|---|---|---|---|---|---|
| SP-GR-037 | Rio Genil | Surface water | Rio Genil Barranco de San Juan | 07-Okt-04 | T, EC, pH, alcalinity, ions, D, 18O |
| SP-GR-067 | Rio Durcal | | Durcal | 16-Okt-04 | T, EC, pH, D, 18O |
| SP-GR-068 | Rio Genil 2 | | Pinos de Genil | 23-Okt-04 | |
| SP-GR-069 | Rio Genil 3 | | Granada, at Car Bridge | | T, EC, pH, Eh, O2, D, 18O |
| SP-GR-037 | Rio Genil | | Rio Genil Barranco de San Juan | | T, EC, pH, D, 18O |
| SP-GR-076 | Rio Darro | | Cortijo Jesus del Valle (Granada) | 28-Okt-04 | T, EC, pH, alcalinity, ions, D, 18O |
| SP-GR-069 | Rio Genil 3 | | Granada, at Car Bridge | 10-Nov-04 | T, EC, pH, Eh, D, 18O |
| SP-GR-068 | Rio Genil 2 | | Pinos de Genil | | T, EC, pH, D, 18O |
| SP-GR-037 | Rio Genil | | Rio Genil Barranco de San Juan | 15-Nov-04 | |
| SP-GR-076 | Rio Darro | | Cortijo Jesus del Valle (Granada) | 16-Nov-04 | |
| SP-GR-097 | Embalse de Quentar | | | | T, EC, pH, Eh, D, 18O |
| SP-GR-076 | Rio Darro | | Cortijo Jesus del Valle (Granada) | 25-Nov-04 | T, EC, pH, Eh, alcalinity, ions, D, 18O |
| SP-GR-078 | Rio Darro 2 | | Granada | | T, EC, pH, D, 18O |
| SP-GR-069 | Rio Genil 3 | | Granada, at Car Bridge | 04-Dez-04 | |
| SP-GR-068 | Rio Genil 2 | | Pinos de Genil | | |
| SP-GR-079 | Embalse de Canales | | Granada | | T, EC, pH, Eh, O2, D, 18O |
| SP-GR-078 | Rio Darro 2 | | | 07-Dez-04 | T, EC, pH, alcalinity, ions, D, 18O |
| SP-GR-076 | Rio Darro | | Cortijo Jesus del Valle (Granada) | | T, EC, pH, D, 18O |
| SP-GR-069 | Rio Genil 3 | | Granada, at Car Bridge | 09-Jan-05 | T, EC, pH, Eh, O2, D, 18O |
| SP-GR-068 | Rio Genil 2 | | Pinos de Genil | | T, EC, pH, D, 18O |

• Table a3.8 continued

| Site ID | Site name | Type | Village | Sampling date | Measured parameters |
|---------|-----------|------|---------|---------------|---------------------|
| SP-GR-076 | Rio Darro | Surface water | Cortijo Jesus del Valle (Granada) | 10-Jan-05 | T, EC, pH, D, 18O |
| SP-GR-078 | Rio Darro 2 | | Granada | | |
| SP-GR-037 | Rio Genil | | Rio Genil Barranco de San Juan | 19 Jan 05 | T, EC, pH, alcalinity, ions, D, 18O |
| SP GR 069 | Rio Genil 3 | | Granada, at Car Bridge | 25 Jan 05 | T, EC, pH, D, 18O |
| SP GR 068 | Rio Genil 2 | | Pinos de Genil | | T, EC, pH, Eh, O2, D, 18O |
| SP GR 037 | Rio Genil | | Rio Genil Barranco de San Juan | 27 Jan 05 | T, EC, pH, D, 18O |
| SP GR 076 | Rio Darro | | Cortijo Jesus del Valle (Granada) | 04 Feb 05 | T, EC, pH, alcalinity, ions, D, 18O |
| SP GR 078 | Rio Darro 2 | | Granada | | T, EC, pH, D, 18O |
| SP GR 096 | Arroyo de Huenes | | Fuente siete ojos | 05 Feb 05 | |
| SP GR 098 | Arroyo Caballo | | Pico de Caballo | 13 Feb 05 | |
| SP GR 141 | Rio Cubillas | | Cubillas | 18 Feb 05 | |
| SP GR 142 | Puente Rio Genil | | Lachar | | |
| SP GR 138 | Arroyo de salado | | | | |
| SP GR 079 | Embalse de Canales | | Granada | 19 Feb 05 | |
| SP GR 179 | Callejon del Angel | Rain | Granada   Zaidin | 28 Feb 05 | |
| SP GR 179 | Callejon del Angel | | | 02 Mrz 05 | |
| SP GR 037 | Rio Genil | Surface water | Rio Genil Barranco de San Juan | 05 Mrz 05 | |
| SP GR 079 | Embalse de Canales | | Granada | | |
| SP GR 179 | Callejon del Angel | Rain | Granata Zaidin | | |
| SP GR 068 | Rio Genil 2 | Surface water | Pinos de Genil | 06 Mrz 05 | |
| SP GR 177 | Rio Cubillas | | Deifontes | 08 Mrz 05 | |
| SP GR 178 | Embalse de Cubillas | | Los Cortijos | | |
| SP GR 172 | Oberlauf Alhama de Granada | | Alhama de Granada | 10 Mrz 05 | |
| SP GR 173 | Unterlauf Alhama de Granada | | | | |
| SP GR 171 | Zulauf Hotel Alhama de Granada | | | | |
| SP GR 170 | Embalse Bermejales | | | | |

APPENDIX

• Table a3.9 Sites, types, persons, date and measured parameters of spring and thermal spring samples.

| Site ID | Site name | Type | Village | IGME declaration | Sampling date | Measured parameters |
|---|---|---|---|---|---|---|
| SP-GR-022 | Fte. Alta | | Sierra Nevada | | | T, EC, pH, runoff, alcalinity, ions, D, 18O |
| SP-GR-023 | Fte. las Viboras | | Fuente las viboras | | | T, EC, pH, runoff, D, 18O |
| SP-GR-024 | Fte. del Hervidero | | La Zubia | - | | T, EC, pH, Eh, alcalinity, ions, D, 18O |
| SP-GR-025 | Fte. la Cortijuela | | Fuente la cartijuela (la zubia) | | | T, EC, pH, Eh, O2, runoff, alcalinity, ions, D, 18O |
| SP-GR-026 | Fte. de los 16 canos | | Guejar Sierra | | 07-Okt-04 | T, EC, pH, alcalinity, ions, D, 18O |
| SP-GR-033 | Fte. Grande | | Alfacar | 1941.8.002 | | T, EC, pH, Eh, O2, runoff, alcalinity, ions, D, 18O |
| SP-GR-034 | Fte. de Nivar | | Nivar | 1941.4.002 | | T, EC, pH, runoff, D, 18O |
| SP-GR-035 | Fte. Cerro Negro | | | 1941.3.039 | | T, EC, pH, D, 18O |
| SP-GR-036 | Nacimiento Rio Darro | | Colmenar | 2041.5.018 | | |
| SP-GR-028 | Fte. de Urquiza | | Durcal right tube from spectators view | | | T, EC, pH, alcalinity, ions, D, 18O |
| SP-GR-029 | Fte. de Urquiza left | | Durcal left tube from spectators view | - | | T, EC, pH, alcalinity, ions, D, 18O |
| SP-GR-030 | Fte. y Alberca de Palmones | | Padul | 1942.6.073 | 16-Okt-04 | T, EC, pH, Eh, O2, alcalinity, ions, D, 18O |
| SP-GR-031 | Fte. los Molinos | | | 1942.6.007 | | |
| SP-GR-032 | Banos de la Malah | | La Mahala | - | | T, EC, pH, Eh, O2, runoff, alcalinity, ions, D, 18O |
| SP-GR-033 | Fte. Grande | Spring | Alfacar | 1941.8.002 | | T, EC, pH, runoff, D, 18O |
| SP-GR-034 | Fte. de Nivar | | Nivar | 1941.4.002 | | T, EC, pH, D, 18O |
| SP-GR-035 | Fte. Cerro Negro | | | 1941.3.039 | 08-Nov-04 | T, EC, pH, runoff, D, 18O |
| SP-GR-036 | Nacimiento Rio Darro | | Colmenar | 2041.5.018 | | T, EC, pH, D, 18O |
| SP-GR-070 | Fte. de Vita | | Cogollos Vega | | | |
| SP-GR-071 | Fte. Teja | | Alfacar | | | |
| SP-GR-072 | Fte. Savina | | Beas de Granada | | | T, EC, pH, O2, runoff, D, 18O |
| SP-GR-073 | Fte. Agostinos | | Cortijo de los Agostinos | | 09-Nov-04 | |
| SP-GR-074 | Fte. Carcabal | | La Peza | | | |
| SP-GR-075 | Fte. Nabugal | | | | | T, EC, pH, O2, D, 18O |
| SP-GR-022 | Fte. Alta | | Sierra Nevada | - | | T, EC, pH, runoff, D, 18O |
| SP-GR-023 | Fte. las Viboras | | Fuente las viboras | | 15-Nov-04 | |
| SP-GR-026 | Fte. de los 16 canos | | Guejar Sierra | | | T, EC, pH, D, 18O |
| SP-GR-027 | Fte. de Teja | | | | | T, EC, pH, runoff, D, 18O |
| SP-GR-024 | Fte. del Hervidero | | La Zubia | | | T, EC, pH, Eh, D, 18O |
| SP-GR-025 | Fte. la Cortijuela | | Fuente la cartijuela (la zubia) | | | T, EC, pH, Eh, runoff, D, 18O |
| SP-GR-030 | Fte. y Alberca de Palmones | | Padul | 1942.6.073 | 22-Nov-04 | T, EC, pH, runoff, D, 18O |
| SP-GR-031 | Fte. los Molinos | | | 1942.6.007 | | |
| SP-GR-032 | Banos de la Malah | | La Mahala | | | T, EC, pH, D, 18O |
| SP-GR-077 | Fte. 7 ojos | | La Zubia | | | T, EC, pH, Eh, D, 18O |
| SP-GR-024 | Fte. del Hervidero | | | - | 05-Feb-05 | T, EC, pH, Eh, O2, D, 18O |
| SP-GR-025 | Fte. la Cortijuela | | Fuente la cartijuela (la zubia) | | | T, EC, pH, Eh, D, 18O |
| SP-GR-135 | Banos de Sierra Elvira | | Sierra Elvira | | 18-Feb-05 | T, EC, pH, runoff, D, 18O |

• Table a3.9 continued

| Site ID | Site name | Type | Village | IGME declaration | Sampling date | Measured parameters |
|---------|-----------|------|---------|------------------|---------------|---------------------|
| SP-GR-137 | Manantial de la Reina | Spring | Santa Fe | - | 18-Feb-05 | T, EC, pH, runoff, D, 18O |
| SP-GR-139 | Banos Santa Fe | | Santa Fe, aeropuerto | | | T, EC, pH, D, 18O |
| SP-GR-140 | Los Fagailos | | Fuente Vaquelos | | | T, EC, pH, runoff, D, 18O |
| SP-GR-022 | Fte. Alta | | Sierra Nevada | | 19-Feb-05 | T, EC, pH, D, 18O |
| SP-GR-026 | Fte. de los 16 canos | | Guejar Sierra | | | |
| SP-GR-027 | Fte. de Teja | | | | | T, EC, pH, runoff, D, 18O |
| SP-GR-033 | Fte. Grande | | Alfacar | 1941.8.002 | | |
| SP-GR-034 | Fte. de Nivar | | Nivar | 1941.4.002 | | T, EC, pH, D, 18O |
| SP-GR-035 | Fte. Cerro Negro | | | 1941.3.039 | | T, EC, pH, runoff, D, 18O |
| SP-GR-024 | Fte. del Hervidero | | La Zubia | - | 26-Feb-05 | T, EC, pH, D, 18O |
| SP-GR-026 | Fte. de los 16 canos | | Guejar Sierra | | 05-Mrz-05 | T, EC, pH, runoff, D, 18O |
| SP-GR-030 | Fte. y Alberca de Palmones | | Padul | 1942.6.073 | | T, EC, pH, D, 18O |
| SP-GR-032 | Banos de la Malah | | La Mahala | | | T, EC, pH, runoff, D, 18O |
| SP-GR-033 | Fte. Grande | | Alfacar | 1941.8.002 | 08-Mrz-05 | T, EC, pH, D, 18O |
| SP-GR-028 | Fte. de Urquiza | | Durcal right tube from spectators view | - | 10-Mrz-05 | T, EC, pH, runoff, D, 18O |
| SP-GR-029 | Fte. de Urquiza left | | Durcal left tube from spectators view | | | T, EC, pH, D, 18O |
| SP-GR-174 | Banos Alhama de Granada | | Alhama de Granada | | | T, EC, pH, Eh, runoff, D, 18O |
| SP-GR-025 | Fte. la Cortijuela | | Fuente la cartijuela (la zubia) | | 22-Mrz-05 | T, EC, pH, runoff, D, 18O |

• Table a3.10 Methods, devices and detection limits of hydrochemical analysis.

| Ion | Method | Device | Detection limit |
|-----|--------|--------|-----------------|
| $Ca^{2+}$ | AAS | Perkin Elmer 5000 | 0.05 [mg/l] |
| $Cl$ | photometric | Technicon Autoanalyser | 1.0 [mg/l] |
| $Fe^{2+}$ | AAS | Perkin Elmer 5000 | 0.1 [mg/l] |
| $K^+$ | Flamefotometer | Eppendorf Elex 6361r | 0.1 [mg/l] |
| $Li^+$ | AAS | Perkin Elmer 5000 | 0.05 [mg/l] |
| $Mg^{2+}$ | AAS | Perkin Elmer 5000 | 0.05 [mg/l] |
| $Mn^{2+}$ | AAS | Perkin Elmer 5000 | 0.05 [mg/l] |
| $Na^+$ | Flamefotometer | Eppendorf Elex 6361r | 1.0 [mg/l] |
| $NO_3$ | photometric | Technicon Autoanalyser | 0.05 [mg/l] |
| $SO_4^2$ | photometric | Technicon Autoanalyser | 0.05 [mg/l] |
| $Sr^{2+}$ | ICP | Leemans | 0.05 [mg/l] |
| $δ^{18}O$ | $H_2$ Equilibrium | Delta S Massenspektrometer Finigan | $\pm$ 0.8 ‰ |
| $ΔD$ | $CO_2$ Equilibrium | Delta S Massenspektrometer Finigan | $\pm$ 0.1 ‰ |

• Table a3.11: Determination of physical/chemical parameters and analysis methods in field.

| Parameter | Method | Device |
|---|---|---|
| Temperature | electrometric | Multiline P4 (Fa. WTW); Temperatursonde integrated in pH Sonde SenTIX 41 |
| pH Value (pH1  pH13) | potentiometric with automatic temperature compensation | Multiline P4 + pH Sonde SenTIX 41 (Fa. WTW) |
| Electrical conductivity (10 – 10 000 µS/cm) | elektrometric with automatic temperature compensation (25 °C) | Multiline P4 + LF Sonde TetraCon 325 (Fa. WTW) |
| Oxigen saturation (1   100%) | polarographic | Multiline P4 + Sauerstoffsonde CellOx 325 + Kalibriergefäß OxiCal Sl (Fa. WTW) |
| Redoxpotential ( 200 – 1000 mV) | potentiometric (Ag/AgCl Bezugselektrode) | Multiline P4 (Fa. WTW) + Eh Sonde Pt 4805 (Fa. Ingold) |
| Carbonate species | in field measurement, titration with 0,1 N HCl to pH 4,3 or with 0,1 N NaOH to pH 8,2 | Vollpipette (100 ml) Feldbürette, pH Meter, Becherglas |
| $NO_2$ (0,005 – 0,1 mg/l) | in field measurement: colorimetric | Schnelltest: Aquaquant 1.4408(Fa. Merck) |
| $NH_4^+$ (0,05 – 0,8 mg/l) | in field measurement: colorimetric | Schnelltest: Aquaquant 1.4400.001 (Fa. Merck) |

# APPENDIX 4 (Results and discussion)

• Table a4.1 Reliability check, electrical balance and TDS values.

| site | date | cations meq/l | anions meq/l | balance meq/l | balance % | EC µS/cm | TDS |
|---|---|---|---|---|---|---|---|
| Fte. Alta | 05 Feb 04 | 1.26 | 1.21 | 0.05 | 3.76 | 138 | 65.3 |
| Fte. Alta | 07 Okt 04 | 0.67 | 0.68 | 0.01 | 0.83 | 77 | 33.8 |
| Fte. las Viboras | 05 Feb 04 | 3.21 | 3.08 | 0.13 | 4.07 | 284 | 153.2 |
| Fte. las Viboras | 07 Okt 04 | 3.17 | 3.06 | 0.12 | 3.72 | 288 | 151.0 |
| Fte. del Hervidero | 05 Feb 04 | 3.17 | 3.02 | 0.15 | 4.70 | 286 | 151.5 |
| Fte. del Hervidero | 07 Okt 04 | 2.87 | 2.90 | 0.04 | 1.26 | 289 | 142.9 |
| Fte. la Cortijuela | 05 Feb 04 | 4.54 | 4.66 | 0.11 | 2.47 | 401 | 218.7 |
| Fte. la Cortijuela | 07 Okt 04 | 5.12 | 4.91 | 0.21 | 4.01 | 440 | 234.4 |
| Fte. de los 16 canos | 05 Feb 04 | 2.91 | 2.82 | 0.09 | 3.14 | 262 | 140.2 |
| Fte. de los 16 canos | 07 Okt 04 | 2.40 | 2.46 | 0.06 | 2.66 | 242 | 120.4 |
| Fte. de Teja | 05 Feb 04 | 3.46 | 3.60 | 0.14 | 4.13 | 315 | 175.2 |
| Fte. de Urquiza | 05 Feb 04 | 9.35 | 9.52 | 0.17 | 1.84 | 824 | 540.9 |
| Fte. de Urquiza | 16 Okt 04 | 9.01 | 9.24 | 0.23 | 2.54 | 754 | 521.8 |
| Fte. de Urquiza left | 05 Feb 04 | 8.71 | 8.87 | 0.16 | 1.84 | 785 | 499.7 |
| Fte. de Urquiza left | 16 Okt 04 | 8.32 | 8.63 | 0.32 | 3.79 | 834 | 481.6 |
| Fte. y Alberca de Palmones | 06 Feb 04 | 5.42 | 5.16 | 0.26 | 4.79 | 473 | 258.8 |
| Fte. y Alberca de Palmones | 16 Okt 04 | 5.24 | 5.11 | 0.14 | 2.62 | 505 | 253.5 |
| Fte. los Molinos | 06 Feb 04 | 6.06 | 5.89 | 0.18 | 2.90 | 533 | 291.0 |
| Fte. los Molinos | 16 Okt 04 | 5.95 | 5.83 | 0.13 | 2.12 | 630 | 286.6 |
| Banos de la Malah | 06 Feb 04 | 36.87 | 37.51 | 0.64 | 1.74 | 3090 | 2307.6 |
| Banos de la Malah | 16 Okt 04 | 33.73 | 33.20 | 0.52 | 1.55 | 3500 | 2077.1 |
| Fte. Grande | 06 Feb 04 | 4.40 | 4.59 | 0.19 | 4.20 | 415 | 220.2 |
| Fte. Grande | 07 Okt 04 | 4.55 | 4.74 | 0.19 | 4.15 | 446 | 225.9 |
| Fte. de Nivar | 07 Okt 04 | 5.10 | 5.33 | 0.23 | 4.49 | 505 | 271.8 |
| Fte. Cerro Negro | 07 Okt 04 | 4.29 | 4.21 | 0.07 | 1.74 | 412 | 206.8 |
| Nacimiento Rio Darro | 07 Okt 04 | 4.44 | 4.42 | 0.01 | 0.27 | 438 | 215.3 |
| Rio Genil | 07 Okt 04 | 1.22 | 1.25 | 0.03 | 2.57 | 136 | 68.5 |
| Rio Genil 2 | 10 Nov 04 | 1.75 | 1.70 | 0.05 | 2.60 | 130 | 92.6 |
| Rio Genil 3 | 10 Nov 04 | 5.27 | 4.95 | 0.32 | 6.09 | 380 | 266.3 |
| Fte. de Vita | 08 Nov 04 | 8.04 | 7.73 | 0.31 | 3.90 | 854 | 376.6 |
| Fte. Teja | 08 Nov 04 | 7.64 | 7.29 | 0.35 | 4.54 | 722 | 351.5 |
| Fte. Savina | 09 Nov 04 | 7.91 | 7.55 | 0.35 | 4.47 | 755 | 401.2 |
| Fte. Agostinos | 09 Nov 04 | 4.28 | 4.14 | 0.14 | 3.23 | 436 | 197.7 |
| Fte. Carcabal | 09 Nov 04 | 2.73 | 2.64 | 0.09 | 3.32 | 276 | 130.0 |
| Fte. Nabugal | 09 Nov 04 | 2.97 | 2.98 | 0.01 | 0.46 | 309 | 146.9 |
| Fte. 7 ojos | 22 Nov 04 | 5.19 | 5.36 | 0.17 | 3.27 | 507 | 252.5 |
| Rio Darro 2 | 25 Nov 04 | 5.84 | 5.63 | 0.22 | 3.69 | 540 | 282.3 |
| Arroyo Caballo | 13 Feb 05 | 1.34 | 1.30 | 0.03 | 2.58 | 125 | 67.8 |
| Pico de Caballo | 13 Feb 05 | 0.16 | 0.16 | 0.00 | 0.95 | 13 | 8.4 |
| Armilla Vivero Dip | 18 Feb 05 | 8.52 | 8.76 | 0.23 | 2.72 | 735 | 428.4 |
| Cullar Vega | 18 Feb 05 | 11.25 | 11.35 | 0.09 | 0.82 | 828 | 608.8 |
| Alhencira | 18 Feb 05 | 6.23 | 6.26 | 0.02 | 0.38 | 575 | 307.9 |
| Terrazos Terragran | 18 Feb 05 | 21.56 | 21.47 | 0.09 | 0.43 | 1701 | 1268.0 |
| Cort. Santa Ana | 18 Feb 05 | 10.61 | 10.27 | 0.34 | 3.19 | 941 | 547.2 |
| Banos de Sierra Elvira | 18 Feb 05 | 30.69 | 31.93 | 1.24 | 4.04 | 2650 | 1908.7 |
| Manantial de la Reina | 18 Feb 05 | 12.45 | 12.18 | 0.28 | 2.21 | 1125 | 646.3 |
| Arroyo de salado | 18 Feb 05 | 170.22 | 161.78 | 8.44 | 4.96 | 15620 | 9899.2 |
| Banos Santa Fe | 18 Feb 05 | 53.42 | 55.89 | 2.47 | 4.62 | 3700 | 3528.3 |

• Table a4.1 continued

| site | date | cations meq/l | anions meq/l | balance meq/l | balance % | EC μS/cm | TDS |
|---|---|---|---|---|---|---|---|
| Rio Cubillas | 18 Feb 05 | 17.46 | 18.16 | 0.70 | 4.00 | 1501 | 1023.7 |
| Genil 4 | 18 Feb 05 | 16.49 | 16.01 | 0.48 | 2.91 | 1443 | 910.3 |
| Callejon del Angel | 28 Feb 05 | 0.31 | 0.31 | 0.00 | 0.09 | 22 | 16.8 |
| Callejon del Angel | 02 Mrz 05 | 0.24 | 0.23 | 0.01 | 4.12 | 20 | 11.8 |
| Callejon del Angel | 05 Mrz 05 | 0.14 | 0.14 | 0.00 | 1.02 | 45 | 7.1 |
| Los Fagailos | 18 Feb 05 | 11.64 | 11.46 | 0.18 | 1.56 | 1042 | 603.9 |

• Table a4.2 PHREEQC input file for molar Ca:Mg ratio calculation.

```
TITLE --Rainwater (Callejon del Angel) plus co2 soil
SOLUTION 1  rainwater
    units   ppm
    pH      5.31
    density 1.0
    Ca          2.8
    Mg          1.1
    Na          1.4
    K           0.7
    Cl          3
    Alkalinity      7.6 as HCO3
    S(6)        4
EQUILIBRIUM_PHASES
    CO2(g)      -2.0
save solution 1
END


TITLE --Equilibrate mixture with calcite and dolomite.
USE solution 1
EQUILIBRIUM_PHASES
    Calcite     0.0
    Dolomite        0.0

SELECTED_OUTPUT
-file Cc_Do_ratios_equilibrium.sel
-user_punch true
-high_precision
-reset true
-solution true
-si calcite dolomite aragonite co2(g)
-pH true
-temperature true
-ionic_strength true
-percent_error true
-charge_balance true
-molalities H+ Ca+2 CO2 HCO3- CO3-2 Mg+2
END
```

```
TITLE --Equilibrate mixture with calcite only.
USE solution 1
EQUILIBRIUM_PHASES
    Calcite     0.0
SELECTED_OUTPUT (…)
END


TITLE --Equilibrate mixture with dolomite only.
USE solution 1
EQUILIBRIUM_PHASES 3
    Dolomite        0.0
SELECTED_OUTPUT (…)
END
```

• Table a4.4 Field parameters, water type, saturation indices and molar Ca:Mg ratios of group 2 members.

| Site | Date | Water type | pH | T (°C) | EC (µS/cm) | SI Calcite | SI Dolomite | SI Gypsum | SI Anhydrite | rCa/Mg |
|---|---|---|---|---|---|---|---|---|---|---|
| Fte. la Cortijuela | 07-Okt-04 | Mg-Ca-HCO3 | 8.18 | 8.4 | 440 | 0.60 | 1.11 | -3.17 | -3.42 | 0.9 |
| Fte. Cerro Negro | 07-Okt-04 | Ca-Mg-HCO3 | 7.18 | 11.7 | 412 | -0.34 | -1.03 | -2.58 | -2.84 | 1.9 |
| Fte. de Nivar | 07-Okt-04 | Ca-Mg-HCO3-SO4 | 7.44 | 12.2 | 505 | -0.02 | -0.37 | -1.82 | -2.07 | 1.9 |
| Fte. Grande | 07-Okt-04 | HCO3 | 7.68 | 12.1 | 446 | 0.19 | 0.13 | -2.51 | -2.76 | 1.6 |
| Nacimiento Rio Darro | 07-Okt-04 | Ca-Mg-HCO3 | 7.7 | 12.5 | 438 | 0.18 | 0.13 | -2.48 | -2.73 | 1.5 |
| Fte. de los 16 canos | 07-Okt-04 | | 7.8 | 10.7 | 242 | -0.26 | -0.78 | -2.70 | -2.95 | 1.5 |
| Fte. del Hervidero | 07-Okt-04 | | 7.11 | 10.5 | 289 | -0.73 | -1.95 | -2.58 | -2.84 | 2.6 |
| Fte. las Viboras | 07-Okt-04 | | 7.06 | 10.7 | 288 | -0.75 | -1.88 | -3.00 | -3.26 | 2.0 |
| Fte. Alta | 07-Okt-04 | Ca-Mg-Cl-HCO3 | 7.76 | 8.4 | 77 | -1.61 | -3.45 | -4.03 | -4.29 | 1.3 |
| Rio Genil | 07-Okt-04 | Ca-Mg-HCO3-SO4 | 8.15 | 8.8 | 136 | -0.64 | -1.72 | -2.66 | -2.91 | 2.1 |
| Fte. los Molinos | 16-Okt-04 | Ca-Mg-HCO3 | 7.45 | 17.1 | 630 | 0.09 | 0.17 | -2.16 | -2.40 | 1.1 |
| Fte. y Alberca de Palmones | 16-Okt-04 | | 7.65 | 15.9 | 505 | 0.19 | 0.32 | -2.11 | -2.36 | 1.2 |
| Fte. Teja | 08-Nov-04 | | 7.04 | 12.7 | 722 | -0.09 | -0.30 | -2.72 | -2.97 | 1.2 |
| Fte. de Vita | 08-Nov-04 | | 7.02 | 14.3 | 854 | -0.05 | -0.44 | -1.88 | -2.13 | 2.0 |
| Fte. Nabugal | 09-Nov-04 | Ca-HCO3 | 8.15 | 10.1 | 309 | 0.45 | -0.05 | -3.05 | -3.31 | 7.0 |
| Fte. Savina | 09-Nov-04 | Ca-Mg-HCO3-SO4 | 7.34 | 13.1 | 755 | 0.10 | 0.02 | -1.52 | -1.77 | 1.4 |
| Fte. Agostinos | 09-Nov-04 | Ca-Mg-HCO3 | 7.67 | 11.1 | 436 | 0.11 | -0.04 | -3.00 | -3.26 | 1.5 |
| Fte. Carcabal | 09-Nov-04 | | 7.84 | 9.8 | 276 | -0.08 | -0.54 | -2.87 | -3.12 | 1.9 |
| Rio Genil 2 | 10-Nov-04 | Ca-Mg-HCO3-SO4 | 7.32 | 11.3 | 130 | -1.16 | -2.60 | -2.49 | -2.75 | 1.6 |
| Fte. 7 ojos | 22-Nov-04 | Ca-Mg-HCO3 | 7.91 | 9 | 507 | 0.47 | 0.71 | -2.79 | -3.04 | 1.3 |
| Rio Darro 2 | 25-Nov-04 | | 8.16 | 8.9 | 540 | 0.76 | 1.16 | -2.11 | -2.37 | 1.8 |
| Alhencira | 18-Feb-05 | | 7.49 | 15 | 575 | 0.18 | 0.16 | -2.02 | -2.27 | 1.6 |
| **min** | | | **7.02** | **8.4** | **77** | **-1.61** | **-3.45** | **-4.03** | **-4.29** | **0.9** |
| **max** | | | **8.18** | **17.1** | **854** | **0.76** | **1.16** | **-1.52** | **-1.77** | **7.0** |
| **average** | | | | **11.4** | **427** | **-0.09** | **-0.49** | **-2.58** | **-2.83** | **2.1** |

• Table a4.5 Field parameters, water type, saturation indices and molar Ca:Mg ratios of group 3 members.

| Site | Date | Water type | pH | T (°C) | EC (µS/cm) | SI Calcite | SI Dolomite | SI Gypsum | SI Anhydrite | rCa/Mg |
|---|---|---|---|---|---|---|---|---|---|---|
| Rio Genil 3 | 18-Feb-05 | Ca-Mg-HCO3-SO4 | 8.1 | 11.5 | 380 | 0.54 | 0.82 | -1.82 | -2.07 | 1.57 |
| Armilla Vivero Dip | 10-Nov-04 | | 7.31 | 15 | 735 | 0.08 | 0.09 | -1.62 | -1.87 | 1.16 |
| Cullar Vega | 18-Feb-05 | | 7.37 | 14.4 | 828 | 0.25 | 0.16 | -1.18 | -1.43 | 2.09 |
| Terrazos Terragran | 18-Feb-05 | | 7.03 | 15 | 1701 | 0.05 | -0.04 | -0.57 | -0.82 | 1.39 |
| Cort. Santa Ana | 18-Feb-05 | | 7.3 | 15.7 | 941 | 0.11 | 0.18 | -1.30 | -1.55 | 1.10 |
| Meson El Guerro | 18-Feb-05 | | 7.54 | 14.1 | 824 | 0.36 | 0.61 | -1.54 | -1.80 | 1.23 |
| Manantial de la Reina | 18-Feb-05 | | 7.12 | 15 | 1125 | 0.18 | 0.05 | -1.29 | -1.54 | 1.95 |

• Table a4.5 –continued-

| Site | Date | Water type | pH | T (°C) | EC (µS/cm) | SI Calcite | SI Dolomite | SI Gypsum | SI Anhydrite | rCa/Mg |
|------|------|-----------|-----|--------|-----------|-----------|------------|----------|-------------|--------|
| Los Fagailos | 18-Feb-05 | Ca-Mg-SO4-HCO3 | 7.29 | 14.5 | 1042 | 0.20 | 0.27 | -1.28 | -1.53 | 1.28 |
| Rio Cubillas | 18-Feb-05 | | 7.77 | 12.4 | 1443 | 0.26 | 0.21 | -0.80 | -1.05 | 1.75 |
| Puente Rio Genil | 18-Feb-05 | Ca-Mg-HCO3-Cl-SO4 | 7.22 | 13.7 | 1501 | 0.72 | 1.14 | -0.91 | -1.16 | 1.89 |
| min | | | | 11.50 | 380 | 0.05 | -0.04 | -1.82 | -2.07 | 1.10 |
| max | | | | 15.70 | 1701 | 0.72 | 1.14 | -0.57 | -0.82 | 2.09 |
| average | | | | 14.13 | 1052 | 0.27 | 0.35 | -1.23 | -1.48 | 1.54 |

• Table a4.6 Group4 saturation indices and main characteristics.

| Site | Date | Water type | pH | T (°C) | EC (µS/cm) | SI Calcite | SI Dolomite | SI Gypsum | SI Anhydrite |
|------|------|-----------|-----|--------|-----------|-----------|------------|----------|-------------|
| Fte. de Urquiza | 16. Okt 04 | Ca-Mg-SO4-HCO3 | 7.6 | 22.5 | 754 | 0.39 | 0.73 | 1.23 | 1.46 |
| Fte. de Urquiza left | 16. Okt 04 | | 7.0 | 22.6 | 785 | 0.27 | 0.58 | 1.27 | 1.50 |
| Banos de la Malah | 16. Okt 04 | Ca-Na-Mg-Cl-SO4 | 7.2 | 25.5 | 3090 | 0.19 | 0.18 | 0.42 | 0.64 |
| Banos Sierra Elvira | 18. Feb 05 | Na-Ca-Mg-Cl-SO4 | 7.3 | 32 | 2650 | 0.55 | 1.10 | 0.53 | 0.72 |
| Banos Santa Fe | 18. Feb 05 | Ca-Mg-SO4 | 7.0 | 36.6 | 3700 | 0.23 | 0.37 | 0.02 | 0.18 |
| min | | | 7.0 | 22.5 | 754 | 0.27 | 0.58 | 1.27 | 1.50 |
| max | | | 7.6 | 36.6 | 3700 | 0.55 | 1.10 | 0.02 | 0.18 |
| average | | | | 27.8 | 2195 | 0.22 | 0.36 | 0.69 | 0.90 |

• Table a4.7 PHREEQC input file for carbonate chemistry calculations, line of saturation

```
# Calculating the saturation line
SOLUTION 1  dest water in equilibration with calcite
    temp   10
EQUILIBRIUM_PHASES
CO2(g)   2
Calcite   0

SELECTED_OUTPUT
 file Cc_si0_t10_p 2.sel
 user_punch true
 high_precision
 reset true
 solution true
 si halite calcite dolomite gypsum anhydrite aragonite co2(g)
 pH true
 temperature true
 ionic_strength true
 percent_error true
 charge_balance true
 molalities Fe+2 H+ Ca+2 CO2 HCO3  CO3 2 SO4 2 Cl  NO3   Mg+2 Na+ K+ Fe+3
END
```

• Table a4.8 PHREEQC input file for carbonate chemistry calculations, open vs. closed system

```
SOLUTION 1  Rainwater (Granada city) plus soil co2 ( 2) at 10 degree.
     units   ppm
     pH      5.31
     density 1.0
     temp    10
     Ca          2.8
     Mg          1.1
     Na          1.4
     K           0.7
     Cl          3
     Alkalinity      7.6 as HCO3
     S(6)        4
EQUILIBRIUM_PHASES 1
     CO2(g)      2.0
save solution 1
end

SOLUTION 2  Rainwater (Granada city) plus soil co2 ( 3.5) at 10 degree.
     units   ppm
     pH      5.31
     density 1.0
     temp    10
     Ca          2.8
     Mg          1.1
     Na          1.4
     K           0.7
     Cl          3
     Alkalinity      7.6 as HCO3
     S(6)        4
EQUILIBRIUM_PHASES 2
     CO2(g)      3.5
save solution 2
end
# water encounters carbonate minerals
# under open system conditions with
# with pCO2  2
use solution 1
EQUILIBRIUM_PHASES 1
 CO2(g)      2.0
Reaction
 Calcite
 0.002 mole in 10 steps
SELECTED_OUTPUT
 file kinetic_10degree_open_p2.sel
 user_punch true
 high_precision
 reset true
 solution true
 si halite calcite dolomite gypsum anhydrite aragonite co2(g)
 pH true
 temperature true
 ionic_strength true
 percent_error true
 charge_balance true
 molalities  H+ Ca+2 CO2 HCO3  CO3 2 SO4 2 Cl  NO3  HSO4  Mg+2 Na+ K+
END

# water encounters carbonate minerals
# under open system conditions
# with pCO2  3.5
use solution 1
EQUILIBRIUM_PHASES 1
 CO2(g)      3.5
Reaction
 Calcite
 0.0005 mole in 5 steps
SELECTED_OUTPUT
 file kinetic_10degree_open_p3.5.sel
 user_punch true
 high_precision
 reset true
 solution true
 si halite calcite dolomite gypsum anhydrite aragonite co2(g)
 pH true
 temperature true
```

• Table a4.8 (continued)

```
ionic_strength true
percent_error true
charge_balance true
molalities  H+ Ca+2 CO2 HCO3  CO3 2 SO4 2 Cl  NO3  HSO4  Mg+2 Na+ K+
END

# water encounters carbonate minerals
# under closed system conditions with initial pCO2= 2
use solution 1
Reaction
 Calcite
 0.00053 mole in 5 steps
SELECTED_OUTPUT
 file kinetic_10degree_closed.sel
 user_punch true
 high_precision
 reset true
 solution true
 si halite calcite dolomite gypsum anhydrite aragonite co2(g)
 pH true
 temperature true
 ionic_strength true
 percent_error true
 charge_balance true
 molalities  H+ Ca+2 CO2 HCO3  CO3 2 SO4 2 Cl  NO3  HSO4  Mg+2 Na+ K+
END
```

## Stable isotopes in precipitation

• Table a4.8 Stable isotopes (rain event 1)

| Date | $\delta^{18}O$ (‰) | StD | $\delta D$ (‰) | StD | d-excess (‰) |
|---|---|---|---|---|---|
| 2.Feb.04 | -7.83 | 0.02 | -59.2 | 0.3 | 1.84 |

• Table a4.9 Stable isotopes (rain event 2)

| Altitude (masl) | $\delta^{18}O$ (‰) | StD | $\delta D$ (‰) | StD | d-excess (‰) |
|---|---|---|---|---|---|
| 670 | -7.08 | 0.02 | -36.9 | 0.3 | 19.7 |
| 975 | -6.08 | 0.02 | -24.3 | 0.2 | 24.3 |
| 1310 | -6.96 | 0.03 | -29.5 | 0.2 | 26.2 |
| 1500 | -6.70 | 0.03 | -28.9 | 0.2 | 24.7 |
| 1550 | -6.87 | 0.02 | -29.7 | 0.3 | 25.3 |
| mean | -6.74 | | -29.9 | | 24.0 |
| StD | 0.39 | | 2.6 | | 0.8 |

• Table a4.10 Stable isotopes (rain event 3)

| date | $d^{18}O$ (‰) | StD | dD (‰) | StD | d-excess (‰) |
|---|---|---|---|---|---|
| 28-Feb-05 | -12.54 | 0.08 | -91.21 | 0.28 | 9.11 |
| 2-Mar-05 | -18.63 | 0.01 | -142.83 | 0.27 | 6.21 |
| 5-Mar-05 | -13.7 | 0.01 | -100.79 | 0.05 | 8.81 |
| mean | -16.17 | | -121.81 | | 7.51 |
| StD | 3.49 | | 29.73 | | 1.84 |

• Table a4.11 Stable isotopes (rain event 4)

| Altitude (masl) | $\delta^{18}O$ (‰) | StD | $\delta D$ (‰) | StD | d-excess (‰) |
|---|---|---|---|---|---|
| 1295 | -4.29 | 0.0 | -25.2 | 0.1 | 9.13 |
| 650 | -2.06 | 0.0 | -13.3 | 0.3 | 3.19 |
| mean | -3.18 | | -19.24 | | 6.16 |
| StD | 1.58 | | 8.41 | | 4.20 |

• Table a4.12 Date, Altitude (masl), $\delta^{18}O$, $\delta D$ and evaporative-enrichment-corrected $\delta^{18}O$-values of snowmelt samples.

| site ID | Altitude (masl) | X (UTM) | Y (UTM) | $\delta^{18}O$ (‰) | $\delta^{18}O$ (‰) error | $\delta D$ (‰) | $\delta D$ (‰) error | $\delta^{18}O$ (‰) corrected | $\delta D$ (‰) corrected |
|---|---|---|---|---|---|---|---|---|---|
| SP-GR-180 | 3192 | 467216 | 4100692 | -11.55 | 0.06 | -76.9 | 0.3 | -11.32 | -75.7 |
| SP-GR-182 | 2919 | 468241 | 4100417 | -10.28 | 0.06 | -68.8 | 0.4 | -10.58 | -70.3 |
| SP-GR-184 | 3018 | 469256 | 4100752 | -9.98 | 0.1 | -66.5 | 0.2 | -10.25 | -67.8 |
| SP-GR-224 | 3039 | 467010 | 4100073 | -8.78 | 0.01 | -61.1 | 0.3 | -10.48 | -69.5 |
| SP-GR-232 | 2917 | 474283 | 4103394 | -8.27 | 0.09 | -59.9 | 0.1 | -11.03 | -73.6 |
| SP-GR-038 | 2889 | 471254 | 4100231 | -10.58 | 0.02 | -70.1 | 0.3 | -10.50 | -69.7 |
| SP-GR-039 | 2589 | 472401 | 4102774 | -10.33 | 0.05 | -68.6 | 0.4 | -10.40 | -68.9 |
| SP-GR-041 | 2983 | 471254 | 4100231 | -10.54 | 0.05 | -71.1 | 0.2 | -10.99 | -73.4 |
| SP-GR-042 | 3211 | 472401 | 4102774 | -9.31 | 0.05 | -61.2 | 0.3 | -9.44 | -61.8 |
| SP-GR-043 | 3473 | 472450 | 4101088 | -8.61 | 0.02 | -58.2 | 0.1 | -9.63 | -63.3 |
| SP-GR-044 | 2860 | 468831 | 4102567 | -10.24 | 0.05 | -68.3 | 0.3 | -10.46 | -69.4 |
| SP-GR-045 | 2790 | 470268 | 4101727 | -9.37 | 0.05 | -63.7 | 0.3 | -10.34 | -68.5 |
| SP-GR-046 | 2787 | 470131 | 4101794 | -9.5 | 0.06 | -62.9 | 0.2 | -9.75 | -64.1 |
| SP-GR-047 | | | | -9.64 | 0.03 | -64.4 | 0.1 | -10.08 | -66.6 |
| SP-GR-049 | | - | | -9.5 | 0.04 | -62.4 | 0.4 | -9.54 | -62.6 |
| SP-GR-050 | | | | -9.5 | 0.08 | -63.7 | 0.4 | -10.08 | -66.6 |
| SP-GR-055 | 2689 | 473109 | 4096441 | -10.53 | 0.04 | -68.6 | 0.4 | -9.99 | -65.9 |
| SP-GR-056 | 2958 | 471216 | 4100676 | -10.32 | 0.03 | -69.8 | 0.2 | -10.91 | -72.7 |
| **min** | | | | **-11.55** | **0.01** | **-76.9** | **0.1** | **-11.32** | **-75.7** |
| **max** | | | | **-8.27** | **0.1** | **-58.2** | **0.4** | **-9.44** | **-61.8** |
| **average** | | | | **-9.82** | **0.05** | **-65.9** | **0.27** | **-10.32** | **-68.4** |

• Table a4.13: Date, Altitude (masl), $\delta^{18}O$, $\delta D$ and evaporative-enrichment-corrected $\delta^{18}O$-values of *laguna* samples.

| site ID | Altitude (masl) | X / Y (UTM) | | $\delta^{18}O$ (‰) | $\delta^{18}O$ (‰) error | $\delta D$ (‰) | $\delta D$ (‰) error | $\delta^{18}O$ (‰) corrected | $\delta D$ (‰) corrected |
|---|---|---|---|---|---|---|---|---|---|
| SP-GR-211 | 2921 | 463544 | 4098485 | -7.18 | 0.01 | -51.4 | 0.3 | -9.76 | -64.2 |
| SP-GR-212 | 2909 | 462902 | 4098129 | -8.91 | 0.04 | -62.6 | 0.3 | -10.83 | -72.1 |
| SP-GR-213 | 2736 | 461866 | 4097054 | -9.26 | 0.03 | -63.1 | 0.4 | -10.32 | -68.4 |
| SP-GR-215 | 2851 | 461190 | 4096807 | -7.89 | 0.04 | -57.2 | 0.5 | -10.69 | -71.1 |
| SP-GR-216 | 2685 | 461997 | 4099165 | -10.35 | 0.02 | -69.1 | 0.2 | -10.56 | -70.1 |
| SP-GR-217 | 2687 | 464634 | 4100593 | -10.38 | 0.03 | -68.5 | 0.3 | -10.25 | -67.9 |
| SP-GR-218 | 2874 | 469068 | 4100148 | -8.72 | 0.05 | -62.8 | 0.3 | -11.30 | -75.6 |
| SP-GR-219 | 2823 | 469717 | 4100056 | -10.23 | 0.04 | -68.8 | 0.3 | -10.68 | -71.0 |
| SP-GR-220 | 3125 | 467696 | 4100981 | -10.17 | 0.04 | -67.4 | 0.4 | -10.23 | -67.7 |
| SP-GR-221 | 3068 | 467505 | 4101855 | -9.67 | 0.02 | -64 | 0.1 | -9.85 | -64.9 |
| SP-GR-222 | 3093 | 467548 | 4101787 | -9.3 | 0.08 | -61.6 | 0.2 | -9.62 | -63.2 |
| SP-GR-181 | 3059 | 467372 | 4100518 | -10.41 | 0.05 | -69.4 | 0.3 | -10.56 | -70.1 |
| SP-GR-183 | 2881 | 468470 | 4100336 | -10.48 | 0.06 | -70.1 | 0.2 | -10.71 | -71.2 |
| SP-GR-185 | 3023 | 469405 | 4100928 | -9.62 | 0.06 | -64.1 | 0.3 | -10.00 | -66.0 |
| SP-GR-187 | 2868 | 471745 | 4101956 | -8.72 | 0.08 | -58.3 | 0.2 | -9.45 | -61.9 |
| SP-GR-189 | 2936 | 466354 | 4101019 | -9.53 | 0.07 | -64.1 | 0.2 | -10.18 | -67.3 |
| SP-GR-190 | 2950 | 466428 | 4100907 | -9.94 | 0.02 | -66.2 | 0.1 | -10.21 | -67.5 |
| SP-GR-191 | 2928 | 466340 | 4100792 | -10.38 | 0.05 | -68.6 | 0.2 | -10.29 | -68.2 |
| SP-GR-192 | 2899 | 465883 | 4100683 | -10.26 | 0.04 | -68.2 | 0.1 | -10.37 | -68.8 |
| SP-GR-195 | 2421 | 463080 | 4102087 | -9.84 | 0.05 | -66.7 | 0.4 | -10.62 | -70.6 |
| SP-GR-196 | 2495 | 463052 | 4101813 | 3.82 | 0.05 | -5.3 | 0.2 | -13.29 | -90.3 |
| SP-GR-202 | 2982 | 464525 | 4099331 | -8.93 | 0.04 | -61 | 0.2 | -10.13 | -67.0 |
| SP-GR-203 | 2975 | 464393 | 4099293 | -9.55 | 0.03 | -65 | 0.2 | -10.51 | -69.8 |
| SP-GR-204 | 3027 | 473494 | 4101370 | -8.98 | 0.06 | -63.3 | 0.1 | -10.98 | -73.2 |
| SP-GR-205 | 2995 | 473724 | 4101153 | -9.75 | 0.07 | -66.7 | 0.2 | -10.80 | -71.9 |
| SP-GR-206 | 2987 | 473465 | 4100967 | -10.63 | 0.02 | -69 | 0.3 | -9.95 | -65.6 |
| SP-GR-207 | 2942 | 473513 | 4100647 | -10.69 | 0.03 | -70.7 | 0.3 | -10.52 | -69.9 |
| SP-GR-208 | 2897 | 473917 | 4100421 | -10.54 | 0.06 | -70.7 | 0.4 | -10.83 | -72.1 |
| SP-GR-209 | 2796 | 479054 | 4106645 | -10.52 | 0.04 | -71.2 | 0.1 | -11.08 | -74.0 |
| SP-GR-223 | 3084 | 467622 | 4101666 | -9.8 | 0.07 | -64.9 | 0.4 | -9.96 | -65.7 |
| SP-GR-227 | 3073 | 467593 | 4101655 | -9.18 | 0.03 | -60.9 | 0.1 | -9.58 | -62.9 |
| SP-GR-228 | 2866 | 469355 | 4101575 | -10.13 | 0.06 | -68.2 | 0.1 | -10.64 | -70.7 |
| SP-GR-229 | 2784 | 470141 | 4101803 | -10.54 | 0.12 | -70.6 | 0.1 | -10.79 | -71.8 |
| SP-GR-230 | 2787 | 470272 | 4101728 | -8.35 | 0.05 | -60.4 | 0.2 | -11.07 | -73.9 |
| SP-GR-231 | 2894 | 472135 | 4101784 | -10.32 | 0.03 | -68.8 | 0.3 | -10.50 | -69.7 |
| SP-GR-040 | 2895 | 472144 | 4101759 | -10.53 | 0.04 | -70.5 | 0.3 | -10.77 | -71.7 |
| SP-GR-225 | 2707 | 463599 | 4100546 | 3.18 | 0.04 | -5.9 | 0.1 | -12.22 | -82.5 |
| SP-GR-233 | 2891 | 474383 | 4103269 | -6.39 | 0.1 | -50.8 | 0.2 | -11.13 | -74.3 |
| SP-GR-234 | 2880 | 474564 | 4103379 | -4.16 | 0.03 | -38.8 | 0.3 | -10.75 | -71.6 |
| **min** | | | | **-10.69** | **0.02** | **-71.2** | **0.1** | **-12.22** | **-82.5** |
| **max** | | | | **3.18** | **0.12** | **-5.9** | **0.4** | **-9.58** | **-62.9** |
| **average** | | | | **-8.66** | **0.05** | **-61.0** | **0.2** | **-10.68** | **-71.0** |

# Stable isotopes in springs
# Time series

### • Table a4.14 Fte.Cortijuela (X 458341 Y 4104600 Z 1695)

| Sampling date | $\delta^{18}O$ (‰) | $\delta^{18}O$ (‰) error | $\delta D$ (‰) | $\delta D$ (‰) error | d excess (‰) |
|---|---|---|---|---|---|
| 22 Nov 04 | -8.86 | 0.03 | -58.2 | 0.3 | 12.7 |
| 22 Mar 05 | -8.96 | 0.02 | -58.5 | 0.4 | 13.2 |
| 7 Oct 04 | -8.72 | 0.07 | -56.1 | 0.3 | 13.7 |
| 23 Mar 05 | -8.96 | 0.01 | -58.8 | 0.4 | 12.9 |
| 5 Feb 04 | -8.69 | | -56.3 | | 13.2 |
| σ | 0.11 | 0.02 | 1.1 | 0.0 | 0.3 |
| Ø | -8.84 | 0.03 | -57.6 | 0.3 | 13.1 |

### • Table a4.15 Fte.Cerro Negro (X 451504 Y 4125682 Z 1115)

| Sampling date | $\delta^{18}O$ (‰) | $\delta^{18}O$ (‰) error | $\delta D$ (‰) | $\delta D$ (‰) error | d excess (‰) |
|---|---|---|---|---|---|
| 19 Feb 05 | -8.14 | 0.02 | -53.2 | 0.2 | 11.9 |
| 08 Nov 04 | -8.10 | 0.08 | -52.5 | 0.4 | 12.3 |
| 25 Mrz 05 | -8.12 | 0.02 | -53.0 | 0.1 | 12.0 |
| 07 Okt 04 | -8.11 | 0.04 | -53.2 | 0.1 | 11.7 |
| σ | 0.01 | 0.02 | 0.3 | 0.1 | 0.2 |
| Ø | -8.12 | 0.04 | -53.0 | 0.2 | 12.0 |

### • Table a4.16 Fte.Alta (X 463724 Y 4106755 Z 2156)

| Sampling date | $\delta^{18}O$ (‰) | $\delta^{18}O$ (‰) error | $\delta D$ (‰) | $\delta D$ (‰) error | d excess (‰) |
|---|---|---|---|---|---|
| 05 Feb 04 | -9.46 | | -63.0 | | 12.6 |
| 07 Okt 04 | -9.41 | 0.04 | -62.5 | 0.1 | 12.8 |
| 15 Nov 04 | -9.43 | 0.02 | -63.2 | 0.1 | 12.2 |
| 19 Feb 05 | -9.52 | 0.02 | -62.7 | 0.2 | 13.5 |
| σ | 0.04 | 0.01 | 0.28 | 0.02 | 0.46 |
| Ø | -9.46 | 0.03 | -62.85 | 0.12 | 12.79 |

### • Table a4.17 Fte.de 16 Canos (X 460592 Y 4113364 Z 1222)

| Sampling date | $\delta^{18}O$ (‰) | $\delta^{18}O$ (‰) error | $\delta D$ (‰) | $\delta D$ (‰) error | d excess (‰) |
|---|---|---|---|---|---|
| 19 Feb 05 | -8.84 | 0.02 | -58.1 | 0.2 | 12.6 |
| 07 Okt 04 | -8.83 | 0.04 | -58.8 | 0.3 | 11.8 |
| 15 Nov 04 | -8.87 | 0.06 | -58.5 | 0.2 | 12.5 |
| 05 Mrz 05 | -8.97 | 0.01 | -59.3 | 0.3 | 12.5 |
| 05 Feb 04 | -8.86 | | -58.8 | | 12.1 |
| σ | 0.05 | 0.02 | 0.4 | 0.1 | 0.3 |
| Ø | -8.87 | 0.03 | -58.7 | 0.3 | 12.3 |

### • Table a4.18 Banos de la Malah (X 435500 Y 4106901 Z 752)

| Sampling date | $\delta^{18}O$ (‰) | $\delta^{18}O$ (‰) error | $\delta D$ (‰) | $\delta D$ (‰) error | d excess (‰) |
|---|---|---|---|---|---|
| 22 Nov 04 | -8.57 | 0.02 | -57.3 | 0.1 | 11.3 |
| 06 Feb 04 | -8.26 | | -55.4 | | 10.7 |
| 05 Mrz 05 | -8.58 | 0.01 | -57.1 | 0.1 | 11.5 |
| 16 Okt 04 | -8.47 | 0.03 | -56.0 | 0.2 | 11.8 |
| σ | 0.13 | 0.01 | 0.8 | 0.0 | 0.4 |
| Ø | -8.47 | 0.02 | -56.4 | 0.1 | 11.3 |

• Table a4.19 Fte.de Hervidero (X 452680 Y 4104908 Z 1292)

| Sampling date | $\delta^{18}O$ (‰) | $\delta^{18}O$ (‰) error | $\delta D$ (‰) | $\delta D$ (‰) error | d excess (‰) |
|---|---|---|---|---|---|
| 5 Feb 05 | -8.90 | 0.02 | -59.0 | 0.1 | 12.2 |
| 23 Mar 05 | -8.91 | 0.01 | -59.2 | 0.1 | 12.1 |
| 26 Feb 05 | -8.90 | 0.01 | -53.7 | 0.2 | 17.5 |
| 22 Nov 04 | -8.93 | 0.02 | -61.0 | 0.3 | 10.4 |
| 7 Oct 04 | -8.77 | 0.05 | -59.9 | 0.3 | 10.3 |
| 5 Feb 04 | -8.81 | | -59.0 | | 11.5 |
| **σ** | **0.06** | **0.01** | **2.3** | **0.1** | **2.4** |
| **Ø** | **-8.87** | **0.02** | **-58.6** | **0.2** | **12.3** |

• Table a4.20 Fte.de Teja (X 462038 Y 4115147 Z 1278)

| Sampling date | $\delta^{18}O$ (‰) | $\delta^{18}O$ (‰) error | $\delta D$ (‰) | $\delta D$ (‰) error | d excess (‰) |
|---|---|---|---|---|---|
| 05 Feb 04 | -8.19 | | -53.2 | | 12.3 |
| 19 Feb 05 | -8.17 | 0.02 | -53.3 | 0.3 | 12.1 |
| 15 Nov 04 | -8.00 | 0.03 | -53.7 | 0.3 | 10.3 |
| **σ** | **0.09** | **0.00** | **0.2** | **0.0** | **0.9** |
| **Ø** | **-8.12** | **0.03** | **-53.4** | **0.3** | **11.6** |

• Table a4.21 Fte.Grande (X 450942 Y 4122562 Z 1114)

| Sampling date | $\delta^{18}O$ (‰) | $\delta^{18}O$ (‰) error | $\delta D$ (‰) | $\delta D$ (‰) error | d excess (‰) |
|---|---|---|---|---|---|
| 8 Nov 04 | 8.38 | 0.02 | 53.8 | 0.3 | 13.2 |
| 8 Mar 05 | 8.40 | 0.02 | 54.0 | 0.2 | 13.2 |
| 24 Mar 05 | 8.45 | 0.01 | 54.0 | 0.2 | 13.6 |
| 6 Feb 04 | 8.38 | | 54.2 | | 12.9 |
| 7 Oct 04 | 8.35 | 0.02 | 53.2 | 0.3 | 13.6 |
| 19 Feb 05 | 8.41 | 0.01 | 53.4 | 0.2 | 13.9 |
| **σ** | **0.03** | **0.00** | **0.4** | **0.0** | **0.3** |
| **Ø** | **8.40** | **0.02** | **53.8** | **0.2** | **13.4** |

• Table a4.22 Fte.las Viboras (X 460619 Y 4109365 Z 1629)

| Sampling date | $\delta^{18}O$ (‰) | $\delta^{18}O$ (‰) error | $\delta D$ (‰) | $\delta D$ (‰) error | d excess (‰) |
|---|---|---|---|---|---|
| 05 Feb 04 | -8.99 | | -59.0 | | 12.9 |
| 07 Okt 04 | -8.92 | 0.06 | -58.5 | 0.2 | 12.9 |
| 15 Nov 04 | -8.99 | 0.01 | -58.6 | 0.3 | 13.3 |
| **σ** | **0.03** | **0.03** | **0.2** | **0.1** | **0.2** |
| **Ø** | **-8.97** | **0.04** | **-58.7** | **0.3** | **13.0** |

• Table a4.23 Fte.Molinos (X 444626 Y 4096002 Z 730)

| Sampling date | $\delta^{18}O$ (‰) | $\delta^{18}O$ (‰) error | $\delta D$ (‰) | $\delta D$ (‰) error | d excess (‰) |
|---|---|---|---|---|---|
| 06 Feb 04 | 8.07 | | 52.5 | | 12.1 |
| 22 Nov 04 | 8.16 | 0.02 | 53.6 | 0.3 | 11.7 |
| 16 Okt 04 | 8.05 | 0.06 | 54.7 | 0.3 | 9.7 |
| **σ** | **0.05** | **0.02** | **0.9** | **0.0** | **1.1** |
| **Ø** | **8.09** | **0.04** | **53.6** | **0.3** | **11.2** |

• Table a4.24 Nacimiento Rio Darro (X 454448 Y 4121644 Z 1106)

| Sampling date | $\delta^{18}O$ (‰) | $\delta^{18}O$ (‰) error | $\delta D$ (‰) | $\delta D$ (‰) error | d excess (‰) |
|---|---|---|---|---|---|
| 07 Okt 04 | 8.40 | 0.06 | 54.8 | 0.3 | 12.4 |
| 24 Mrz 05 | 8.49 | 0.01 | 54.1 | 0.2 | 13.8 |
| 08 Nov 04 | 8.37 | 0.04 | 53.7 | 0.2 | 13.3 |
| σ | **0.05** | **0.02** | **0.5** | **0.0** | **0.6** |
| Ø | **8.42** | **0.04** | **54.2** | **0.2** | **13.2** |

• Table a4.25 Fte. de Nivar (X 449618 Y 4124631 Z 1108)

| Sampling date | $\delta^{18}O$ (‰) | $\delta^{18}O$ (‰) error | $\delta D$ (‰) | $\delta D$ (‰) error | d excess (‰) |
|---|---|---|---|---|---|
| 24 Mrz 05 | 8.41 | 0.01 | 53.6 | 0.3 | 13.7 |
| 07 Okt 04 | 8.40 | 0.03 | 53.8 | 0.2 | 13.4 |
| 19 Feb 05 | 8.42 | 0.02 | 54.2 | 0.2 | 13.2 |
| 08 Nov 04 | 8.39 | 0.04 | 54.2 | 0.3 | 12.9 |
| σ | **0.01** | **0.01** | **0.2** | **0.0** | **0.3** |
| Ø | **8.41** | **0.03** | **53.9** | **0.2** | **13.3** |

• Table a4.26 Fte. Palmones (X 446488 Y 4097321 Z 745)

| Sampling date | $\delta^{18}O$ (‰) | $\delta^{18}O$ (‰) error | $\delta D$ (‰) | $\delta D$ (‰) error | d excess (‰) |
|---|---|---|---|---|---|
| 05 Mrz 05 | -8.55 | 0.03 | -55.9 | 0.4 | 12.5 |
| 16 Okt 04 | -8.49 | 0.04 | -56.1 | 0.1 | 11.8 |
| 06 Feb 04 | -8.55 | | -56.0 | | 12.4 |
| 22 Nov 04 | -8.63 | 0.01 | -57.1 | 0.2 | 11.9 |
| σ | **0.05** | **0.01** | **0.5** | **0.1** | **0.3** |
| Ø | **-8.56** | **0.03** | **-56.3** | **0.2** | **12.1** |

• Table a4.27 Fte.Urquiza (X 448212 Y 4092451 Z 650)

| Sampling date | $\delta^{18}O$ (‰) | $\delta^{18}O$ (‰) error | $\delta D$ (‰) | $\delta D$ (‰) error | d excess (‰) | |
|---|---|---|---|---|---|---|
| 16 Okt 04 | -8.81 | 0.03 | -57.9 | 0.2 | 12.6 | |
| 05 Feb 04 | -8.79 | | -57.9 | | 12.4 | right tube |
| 10 Mrz 05 | -8.92 | 0.02 | -58.2 | 0.3 | 13.1 | |
| 10 Mrz 05 | -8.85 | 0.01 | -58.2 | 0.2 | 12.6 | |
| 05 Feb 04 | -8.88 | | -58.1 | | 12.9 | left tube |
| 16.Okt.04 | -8.78 | 0.03 | -58.1 | 0.1 | 12.1 | |
| σ | **0.05** | **0.01** | **0.1** | **0.1** | **0.3** | |
| Ø | **-8.84** | **0.02** | **58.1** | **0.2** | **12.7** | |

# Stable isotopes in surface water
# Time series

• Table a4.28 Darro 1 (X 453614 Y 4116883 Z 453614)

| Sampling date | $\delta^{18}O$ (‰) | $\delta^{18}O$ (‰) error | $\delta D$ (‰) | $\delta D$ (‰) error | d excess (‰) |
|---|---|---|---|---|---|
| 10 Jan 05 | -8.13 | 0.0 | -52.0 | 0.2 | 13.01 |
| 25 Nov 04 | -8.22 | 0.0 | -54.3 | 0.4 | 11.46 |
| 7 Dec 04 | -8.20 | 0.0 | -51.8 | 0.5 | 13.80 |
| 4 Feb 05 | -8.06 | 0.0 | -51.6 | 0.3 | 12.86 |
| σ | **0.06** | **0.0** | **1.1** | **0.1** | **0.84** |
| Ø | **-8.15** | **0.0** | **-52.4** | **0.4** | **12.78** |

APPENDIX – Results and discussion

• Table a4.29 Darro 2 (X 452134 Y 4114769 Z 820)

| Sampling date | $\delta^{18}O$ (‰) | $\delta^{18}O$ (‰) error | $\delta D$ (‰) | $\delta D$ (‰) error | d excess (‰) |
|---|---|---|---|---|---|
| 02 Apr 05 | 8.10 | 0.02 | 52.5 | 0.1 | 12.3 |
| 04 Feb 05 | 7.98 | 0.02 | 51.8 | 0.5 | 12.1 |
| 16 Nov 04 | 8.01 | 0.07 | 51.4 | 0.3 | 12.7 |
| 38328 | 8.21 | 0.01 | 52.9 | 0.3 | 12.8 |
| 38362 | 8.07 | 0.01 | 52.3 | 0.2 | 12.3 |
| 25 Nov 04 | 8.18 | 0.03 | 54.1 | 0.3 | 11.3 |
| 28 Okt 04 | 7.98 | 0.04 | 51.3 | 0.2 | 12.5 |
| **σ** | **0.09** | **0.02** | **0.9** | **0.1** | **0.4** |
| **Ø** | **8.08** | **0.03** | **52.3** | **0.3** | **12.3** |

• Table a4.30 Genil 1 (X 465504 Y 4110023 Z 1179)

| Sampling date | $\delta^{18}O$ (‰) | $\delta^{18}O$ (‰) error | $\delta D$ (‰) | $\delta D$ (‰) error | d excess (‰) |
|---|---|---|---|---|---|
| 07 Okt 04 | -9.51 | 0.03 | -65.2 | 0.3 | 10.9 |
| 23 Okt 04 | -9.41 | 0.04 | -64.3 | 0.2 | 11.0 |
| 15 Nov 04 | -9.63 | 0.03 | -64.9 | 0.2 | 12.1 |
| 19 Jan 05 | -9.68 | 0.02 | -65.5 | 0.3 | 11.9 |
| 27 Jan 05 | -9.65 | 0.03 | -66.0 | 0.2 | 11.2 |
| 38416 | -10.27 | 0.01 | -70.8 | 0.2 | 11.4 |
| **σ** | **0.27** | **0.01** | **2.2** | **0.0** | **0.5** |
| **Ø** | **-9.69** | **0.03** | **-66.1** | **0.2** | **11.4** |

• Table a4.31 Genil 2 (X 457130Y 4112948 Z 820)

| Sampling date | $\delta^{18}O$ (‰) | $\delta^{18}O$ (‰) error | $\delta D$ (‰) | $\delta D$ (‰) error | d excess (‰) |
|---|---|---|---|---|---|
| 23 Okt 04 | -9.53 | 0.04 | -64.10 | 0.40 | 12.14 |
| 10 Nov 04 | -9.29 | 0.05 | -63.00 | 0.40 | 11.32 |
| 04 Dez 04 | -9.24 | 0.02 | -63.10 | 0.20 | 10.82 |
| 09 Jan 05 | -9.07 | 0.02 | -61.84 | 0.09 | 10.72 |
| 25 Jan 05 | -9.07 | 0.03 | -61.68 | 0.37 | 10.88 |
| 06 Mrz 05 | -9.01 | 0.02 | -61.29 | 0.15 | 10.79 |
| σ | 0.18 | 0.01 | 0.98 | 0.13 | 0.50 |
| Ø | -9.20 | 0.03 | -62.50 | 0.27 | 11.11 |

• Table a4.32 Genil 3 (X 452810 Y 4112390 Z 725)

| Sampling date | $\delta^{18}O$ (‰) | $\delta^{18}O$ (‰) error | $\delta D$ (‰) | $\delta D$ (‰) error | d excess (‰) |
|---|---|---|---|---|---|
| 09 Jan 05 | -8.52 | 0.02 | -57.1 | 0.1 | 11.0 |
| 23 Okt 04 | -8.49 | 0.04 | -56.7 | 0.3 | 11.2 |
| 04 Dez 04 | -8.71 | 0.02 | -57.7 | 0.4 | 12.0 |
| 10 Nov 04 | -8.35 | 0.04 | -56.3 | 0.2 | 10.5 |
| 25 Jan 05 | -8.61 | 0.02 | -58.6 | 0.2 | 10.3 |
| **σ** | **0.12** | **0.01** | **0.8** | **0.1** | **0.6** |
| **Ø** | **-8.54** | **0.03** | **-57.3** | **0.2** | **11.0** |

• Table a4.33 Embalse Canales (X 457810 Y 4112776 Z 950)

| Sampling date | $\delta^{18}O$ (‰) | $\delta^{18}O$ (‰) error | $\delta D$ (‰) | $\delta D$ (‰) error | d excess (‰) |
|---|---|---|---|---|---|
| 04 Dez 04 | -9.16 | 0.02 | -63.3 | 0.3 | 10.0 |
| 19 Feb 05 | -9.01 | 0.01 | -61.4 | 0.2 | 10.7 |
| 05 Mrz 05 | -9.01 | 0.02 | -61.4 | 0.3 | 10.7 |
| **σ** | **0.07** | **0.00** | **0.9** | **0.0** | **0.3** |
| **Ø** | **-9.06** | **0.02** | **-62.0** | **0.3** | **10.5** |

• Table a4.34 Arr.Huenes (X 455420 Y 4104565 Z 1420)

| Sampling date | $\delta^{18}O$ (‰) | $\delta^{18}O$ (‰) error | $\delta D$ (‰) | $\delta D$ (‰) error | d excess (‰) |
|---|---|---|---|---|---|
| 23 Mrz 05 | -8.93 | 0.01 | -59.0 | 0.2 | 12.5 |
| 05 Feb 05 | -8.89 | 0.01 | -58.8 | 0.2 | 12.3 |
| **σ** | **0.02** | **0.00** | **0.1** | **0.0** | **0.1** |
| **Ø** | **-8.91** | **0.01** | **-58.9** | **0.2** | **12.4** |

## Stable isotopes in single measurements

• Table a4.35 Stable isotopes in single measurements

| Site Name | Type | Sampling date | Altitude (masl) | X/Y (UTM) | | $\delta^{18}O$ (‰) | $\delta^{18}O$ (‰) error | $\delta D$ (‰) | $\delta D$ (‰) error |
|---|---|---|---|---|---|---|---|---|---|
| Camino frente Puleva | Piezometer | 16-Nov-04 | 619 | 442540 | 4115200 | -8.84 | 0.01 | -59.30 | 0.20 |
| Romilla | Piezometer | 05-Nov-04 | 540 | 430100 | 4117700 | -6.92 | 0.02 | -48.40 | 0.40 |
| Atarfe | Piezometer | 17-Nov-04 | 550 | 432480 | 4122400 | -8.52 | 0.03 | -57.90 | 0.30 |
| Pedro Ruiz | Piezometer | 12-Nov-04 | 554 | 432940 | 4119520 | -8.13 | 0.02 | -56.80 | 0.40 |
| Aeropuerto | Piezometer | 25-Nov-04 | 584 | 433530 | 4115090 | -6.33 | 0.04 | -44.70 | 0.20 |
| Alhendin | Piezometer | 08-Nov-04 | 728 | 442560 | 4108020 | -8.82 | 0.03 | -60.30 | 0.30 |
| Cullar Vega | Piezometer | 09-Nov-04 | 647 | 441238 | 4112140 | -8.96 | 0.01 | -59.70 | 0.20 |
| Cort. Trevijano | Piezometer | 26-Nov-04 | 615 | 442229 | 4116375 | -8.27 | 0.03 | -56.60 | 0.30 |
| Instituto del agua | Rain | 20-Feb-04 | 650 | 447015 | 4116550 | -7.63 | 0.05 | -59.20 | 0.20 |
| Rain 975m | Rain | 02-Dez-04 | 975 | 461294 | 4111763 | -6.08 | 0.02 | -24.30 | 0.20 |
| Rain 1310m | Rain | 02-Dez-04 | 1310 | 466974 | 4122957 | -6.96 | 0.03 | -29.50 | 0.20 |
| Rain 1500m | Rain | 02-Dez-04 | 1500 | 469738 | 4123212 | -6.70 | 0.03 | -28.90 | 0.20 |
| Rain 1550m | Rain | 02-Dez-04 | 1550 | 471369 | 4121606 | -6.87 | 0.02 | -29.70 | 0.30 |
| Rain 670m | Rain | 02-Dez-04 | 670 | 447148 | 4114717 | -7.08 | 0.02 | -36.90 | 0.30 |
| Rain at Fte. del Hervidero | Rain | 23-Mrz-05 | 1295 | 452681 | 4104907 | -4.29 | 0.02 | -25.19 | 0.14 |
| Fte. de Vita | Spring | 08-Nov-04 | 944 | 448211 | 4126823 | -7.48 | 0.04 | -48.70 | 0.20 |
| Fte. Teja | Spring | 08-Nov-04 | 1262 | 455011 | 4124238 | -8.35 | 0.02 | -52.30 | 0.20 |
| Fte. Savina | Spring | 09-Nov-04 | 1113 | 463808 | 4120518 | -8.10 | 0.10 | -52.50 | 0.30 |
| Fte. Agostinos | Spring | 09-Nov-04 | 1362 | 469515 | 4119592 | -8.55 | 0.05 | -56.70 | 0.30 |
| Fte. Carcabal | Spring | 09-Nov-04 | 1605 | 471406 | 4120195 | -8.79 | 0.07 | -57.80 | 0.10 |
| Fte. Nabugal | Spring | 09-Nov-04 | 1471 | 472835 | 4121540 | -8.69 | 0.04 | -56.70 | 0.30 |
| Fte. 7 ojos | Spring | 22-Nov-04 | 1411 | 455151 | 4104428 | -8.97 | 0.02 | -59.20 | 0.40 |
| Banos de Sierra Elvira | Spring | 18-Feb-05 | 571 | 436043 | 4120641 | -7.82 | 0.02 | -51.82 | 0.14 |
| Manantial de la Reina | Spring | 18-Feb-05 | 563 | 434096 | 4118218 | -8.39 | 0.01 | -57.45 | 0.25 |

• Table a4.35 -continued-

| Site Name | Type | Sampling date | Altitude (masl) | X/Y (UTM) | | $\delta^{18}O$ (‰) | $\delta^{18}O$ (‰) error | $\delta D$ (‰) | $\delta D$ (‰) error |
|---|---|---|---|---|---|---|---|---|---|
| Banos Santa Fe | Spring | 18-Feb-05 | 840 | 433992 | 4112505 | -8.41 | 0.02 | -55.31 | 0.43 |
| Los Fagailos | Spring | 18-Feb-05 | 542 | 429477 | 4111979 | -8.44 | 0.02 | -57.07 | 0.35 |
| Banos Alhama de Granada | Spring | 10-Mrz-05 | 760 | 413097 | 4098439 | -8.26 | 0.02 | -53.82 | 0.36 |
| Rio Durcal | Surface water | 16-Okt-04 | 647 | 448197 | 4092470 | -8.42 | 0.02 | -56.90 | 0.40 |
| Arroyo Caballo | Surface water | 13-Feb-05 | 2500 | 459726 | 4096646 | -9.78 | 0.02 | -65.30 | 0.38 |
| Arroyo de salado | Surface water | 18-Feb-05 | 740 | 435667 | 4112891 | -6.53 | 0.01 | -48.24 | 0.30 |
| Rio Cubillas | Surface water | 18-Feb-05 | 549 | 430629 | 4122035 | -6.55 | 0.01 | -45.89 | 0.28 |
| Puente Rio Genil | Surface water | 18-Feb-05 | 560 | 426281 | 4117770 | -7.43 | 0.02 | -51.48 | 0.12 |
| Embalse Bermejales | Surface water | 10-Mrz-05 | 800 | 421546 | 4093626 | -5.62 | 0.02 | -38.88 | 0.41 |
| Zulauf Hotel Alhama de Granada | Surface water | 10-Mrz-05 | 760 | 413112 | 4098400 | -7.88 | 0.02 | -50.02 | 0.08 |
| Oberlauf Alhama de Granada | Surface water | 10-Mrz-05 | 761 | 413016 | 4098208 | -7.92 | 0.01 | -50.17 | 0.27 |
| Unterlauf Alhama de Granada | Surface water | 10-Mrz-05 | 758 | 413134 | 4098444 | -7.96 | 0.03 | -50.73 | 0.36 |
| Rio Cubillas | Surface water | 08-Mrz-05 | 693 | 447838 | 4131886 | -7.66 | 0.01 | -52.25 | 0.23 |
| Embalse de Cubillas | Surface water | 08-Mrz-05 | 640 | 440820 | 4126377 | -6.18 | 0.01 | -44.42 | 0.30 |
| Casa Nuevas | Well | 22-Nov-04 | 552 | 430138 | 4123195 | -6.13 | 0.02 | -42.50 | 0.20 |
| Santa Rosa | Well | 10-Nov-04 | 555 | 427396 | 4122063 | -6.64 | 0.02 | -46.70 | 0.20 |
| Armilla Vivero Dip | Well | 18-Feb-05 | 694 | 444801 | 4109716 | -8.98 | 0.01 | -60.22 | 0.25 |
| Cullar Vega | Well | 18-Feb-05 | 654 | 441457 | 4111726 | -9.16 | 0.00 | -62.33 | 0.33 |
| Alhencira | Well | 18-Feb-05 | 814 | 444185 | 4106797 | -9.15 | 0.02 | -60.50 | 0.20 |
| Terrazos Terragran | Well | 18-Feb-05 | 724 | 446535 | 4119370 | -7.81 | 0.01 | -50.90 | 0.20 |
| Cort. Santa Ana | Well | 18-Feb-05 | 574 | 437121 | 4119131 | -8.52 | 0.01 | -57.53 | 0.36 |
| Meson El Guerro | Well | 18-Feb-05 | 719 | 449190 | 4111289 | -8.91 | 0.03 | -60.40 | 0.09 |
| UGR, Facultad de Ciencias | Well | 09-Mrz-05 | 650 | 446075 | 4115214 | -8.19 | 0.01 | -55.07 | 0.10 |